DATA-DRIVEN SINGLE-/MULTI-DOMAIN SPECTRAL METHODS FOR STOCHASTIC FRACTIONAL PDES

By

Ehsan Kharazmi

A DISSERTATION

Submitted to
Michigan State University
in partial fulfillment of the requirements
for the degree of

Mechanical Engineering – Doctor of Philosophy
Computational Mathematics, Science and Engineering – Dual Major

2018

ABSTRACT

DATA-DRIVEN SINGLE-/MULTI-DOMAIN SPECTRAL METHODS FOR STOCHASTIC FRACTIONAL PDES

By

Ehsan Kharazmi

Fractional derivatives are integro-differential convolution type operators with power law kernels, which seamlessly generalize the notion of standard integer order differentiation to their fractional counter parts. In such operators, the order of differentiation is a non-integer number, which in the limiting cases of integer numbers recovers the standard derivatives. The fractional differential equations (FDEs) particularly, have been shown in the literature to provide a rigorous mathematical tool that can be used to describe the anomalous behavior in a wide range of physical phenomenon. They introduce however, the order of fractional derivatives as an additional set of model parameter, whose values are essentially obtained from experimental observations. The inherent randomness in measurements, incomplete sets of data, significant approximations and assumptions upon which the model is built, and the random nature of quantities being modeled pervade uncertainty in the corresponding mathematical formulations. This renders the model parameters, including the fractional orders, random and thus, the fractional model stochastic. We develop proper data-driven mathematical frameworks to efficiently infuse experimental observations/data into the corresponding mathematical models in the context of stochastic fractional partial differential equations.

We extend the fractional order derivatives to the distributed order ones, where the differential orders are distributed over a range of values rather than being just a fixed integer/fraction as it is in standard/fractional ODEs/PDEs. Such distributed operators can also be considered as expectation of fractional derivative with random orders in the context of stochastic modeling. We develop two spectrally-accurate schemes, namely a Petrov-Galerkin spectral method and a spectral collocation method for distributed order fractional differential equations. In both methods, we employ the fractional (non-polynomial) functions, called *Jacobi poly-fractonomials*, which are the analytical eigenfunctions of the fractional Strum-Liouville eigenvalue problem of first and second kind. We

also define the underlying *distributed Sobolev space* and the associated norms, where we carry out the corresponding discrete stability and error analyses of the proposed scheme.

We develop a *fractional sensitivity equation method*, where we obtain the new set of adjoint *fractional sensitivity equations*, in which we introduce another fractional integor-differential operator, associated with logarithmic-power law kernel, for the first time in the context of fractional sensitivity analysis. We show that the developed sensitivity analysis provides a machine learning tool, which build a bridge between experiments and mathematical models to gear observable data via proper optimization techniques. We also develop an operator-based uncertainty quantification framework in the context of stochastic fractional partial differential equations, in which we characterize different sources of uncertainties and further propagate the associated randomness to the fractional model output quantity of interest.

We further apply the developed mathematical tools to investigate the nonlinear vibration of a viscoelastic cantilever beam. In the absence of external excitation, the response amplitude of free vibration reveals a super-sensitivity with respect to the fractional order. Primary resonance of the beam subject to base excitation also discloses a softening behavior in the frequency response of the beam. These unique features can be used further to build a vibration-based health monitoring platform.

To my wife, Fatemeh

ACKNOWLEDGEMENTS

I would like to thank my dear adviser, Professor Mohsen Zayernouri, who has been a great mentor and a dear friend to me over the course of my PhD program at MSU. His patient guidance, enthusiastic encouragement, passion in learning, trust, and very constructive critiques were endless sources of motivation to me. I am indebted to Mohsen for many great opportunities he gave me and also for sharing valuable experiences with me.

I would like to thank Professor Brian Feeny for his support and help during my study at MSU. I have the honor of taking all of Brian's classes and learning from him. His positive and considerate attitude will remain as a valuable reference for me in the rest of my career. I was also fortunate to learn from Professor Chang Wang and am very grateful for his precious inputs to my research too. I would like to acknowledge Professor Shanker Balasubramaniam for his supportive comments and questions that helped improve my work by thinking out of the box.

I have learned a lot about the nonlinear mechanics in the context of dynamics, vibration, and control from the excellent lectures, given by Professor Steve Shaw and Professor Hassan Khalil, to whom my gratitude goes. I would also like to thank Professor Mark M Meerschaert for the great conversation during his class and group meeting. Moreover, many thanks due to our previous and current wonderful staff both in ME and CMSE departments, especially Aida Montalvo, Stacy Hollon, Suzanne Kroll, Jamie Lake, Lindsay Burns, Heather Johnson, Melinda McEwan, and Lisa Roy for being always there to willingly help.

I would like to express my gratitude to my dear peers and friends in the FMATH group, Mehdi Samiee, Dr. Jorge L Suzuki, Eduardo Barros Demoraes, Ali Akhavan Safayi, Pegah Varghaei, Hadis Nouri, and Yongtao Zhou. Thank you all for the very interesting discussions, being so supportive, and open to share ideas.

I would love to especially thank my dear wife, Fatemeh Afzali, to whom this work is dedicated. Her unconditional love, emotional support, and encouragement made me much stronger and more faithful throughout my study at MSU. At last but certainly not the least, I would like to express my

gratitude to my dear parents, lovely brothers, and wonderful friends for their constant love, support, and friendship.

This work was supported by the department of mechanical engineering and department of computational mathematics, science and engineering in the college of engineering at Michigan State University.

TABLE OF CONTENTS

LIST OF TABLES

LIST OF FIGURES

CHAPTER 1

INTRODUCTION

The scientist does not study nature because it is useful;

he studies it because he delights in it, and he delights in it because it is beautiful.

HENRI POINCARÉ

1.1 Fractional Models

Understanding and predicting behavior of natural phenomena, and innovative design intentions have always been an encouraging motivation for scientists progress. Physical phenomena, in general, are characterized as a system, whose behavior is understood via couple of state variables, such as position/velocity of particles that collectively constitute the system. Mathematical models construct proper tools to study time/space evolution of the states of system-of-interest, where the validity range of such models are essentially investigated by comparison of their output (simulations) with observed experiments. A vast range of experimental observations, conducted on complex systems, however, demonstrates the discrepancy of existing mathematical models in properly describing and predicting the ubiquitous anomalies in behavior of such systems, raising the demand to accrete more capable models. Fractional partial differential equations (FPDEs), as a seamless extension of their standard integer order counterparts [90, 134, 146], open up new possibilities for developing robust mathematical tools with the ability to more accurately predict the anomalous behaviors. They put the existing PDEs into a subset of this larger family of mathematical models, and are recently being extensively studied and recognized as most tractable mathematical framework for description of anomalous processes with nonlocal interactions, self-similar structures, long memory dependence, and power-law behavior. These critical interpretative features of complex physical systems are consolidated in the order of fractional derivatives, resulting in a more compliant simulations with experimental tests. Examples of employing fractional modeling stretch over the range of applications including: viscoelasticity in structural vibrations [8], tissue

mechanics and biological phenomena [72, 113], non-Newtonian fluids and rheology [74, 126], non-Brownian transport phenomena in porous and disordered materials [19, 120], non-Markovian processes in multi-scale complex fluids and multi-phase applications [76], non-Gaussian (Lévy flights) processes in turbulent flows [36, 78, 153], and earth system dynamics [198].

1.1.1 Fractional Rheology: Viscoelastic Modeling

Viscoelastic bodies is a class of materials with properties that exhibits both viscous and elastic characteristics when undergoing deformation or loading. The energy dissipation feature of viscous part results in non fully-responsive behavior of such material. In general, the response characteristics of viscoelastic bodies are understood by studying their response to stress and strain inputs in "creep" and "relaxation" test. We denote by $J(t)$, creep compliance, i.e. the strain response to the unit step of stress, and by $G(t)$, relaxation modulus, i.e. the stress response to a unit step of strain. The two functions $J(t)$ and $G(t)$ are usually referred to as the material functions of the body. The constitutive relation of linear viscoelastic models, i.e. stress-strain relation, can be represented by a Volterra equation through Boltzmann superposition principle [116]. When the specimen is under loading, the material instantaneously react elastically and then, immediately starts to relax, where dissipation takes place [59]. Thus, as a step increase in elongation (from the stretch $\lambda = 1$ to some λ) is imposed, the developed stress in the material will be a function of time and the stretch:

$$K(\lambda, t) = G(t)\,\sigma^{(e)}(\lambda), \tag{1.1}$$

where $G(t)$ is the reduced relaxation function and $\sigma^{(e)}$ is the elastic response (in absence of any viscosity). $\sigma^{(e)}$ can be also interpreted as tensile stress response in a sufficiently high rate loading experiment. The Boltzmann superposition principle states that the stresses from different small deformations are additive, meaning that the total tensile stress of the specimen at time t is obtained from the superposition of infinitesimal changes in stretch at some prior time τ_j, given as

$G(t-\tau_j)\frac{\partial\sigma^{(e)}[\lambda(\tau_j)]}{\partial\lambda}\delta\lambda(\tau_j)$. Therefore,

$$\sigma(t) = \sum_{\tau_j<t} G(t-\tau_j)\frac{\partial\sigma^{(e)}[\lambda(\tau_j)]}{\partial\lambda}\frac{\delta\lambda(\tau_j)}{\delta\tau_j}\delta\tau_j, \tag{1.2}$$

where in the limiting case $\delta\tau_j \to 0$ gives the integral form of the equation as

$$\sigma(t) = \int_{-\infty}^{t} G(t-\tau)\,\frac{\partial\sigma^{(e)}[\lambda(\tau)]}{\partial\lambda}\,\frac{\partial\lambda}{\partial\tau}\,d\tau = \int_{-\infty}^{t} G(t-\tau)\,\dot{\sigma}^{(e)}\,d\tau. \tag{1.3}$$

• **Exponential Relaxation, Classical Models:** The relaxation function $G(t)$ is traditionally analyzed into the summation of exponential functions with different exponents and constants as

$$G(t) = \frac{\sum C_i e^{-t/\tau_i}}{\sum C_i}. \tag{1.4}$$

For the simple case of single exponential term (Maxwell model), we have $G(t) = e^{-t/\tau}$. Thus, in the case of zero initial strain we have

$$\sigma(t) = \int_{0}^{t} e^{-(t-\tilde{t})/\tau}\,E\dot{\varepsilon}\,d\tilde{t}, \tag{1.5}$$

which solves the integer-order differential equation $\dot{\varepsilon} = \frac{1}{E}\dot{\sigma} + \frac{1}{\eta}\sigma$, where relaxation time constant $\tau = \eta/E$, obtained from experimental observations. The Maxwell model is in fact a combination of pure elastic and viscous element in series, see Fig. 8.4. Other different combinations of pure elastic and viscous elements in series and parallel give rise to various rheological models with distinctive properties, each of which can be used to model different types of material. The key issue is that the complex hereditary behavior of material requires complicated combinations of elastic and viscous elements, yet they can not be fully captured as the building block elements do not reflect any memory dependence in the material response. Moreover, the complicated combinations introduce relatively big number of model parameter, which adverse the condition of ill-posed inverse problem of model fitting (parameter estimation).

• **Power-Law Relaxation, Fractional Models:** The mechanical stress appeared at the deformation of viscoelastic materials decreases as power-type functions in time, suggesting that relaxation of stress obeys a power law behavior and the relaxation time can not be described with single time

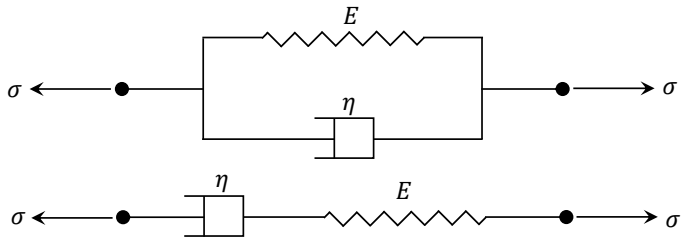

Figure 1.1: Classical visco-elastic models as combination of a spring (pure elastic) and a dash-pot (pure viscous) elements. Kelvin-Voigt (top) and Maxwell (bottom) rheological model.

scale anymore [116]. Therefore, by letting the kernel in (8.13) to have power-type form, the tensile stress takes the form of

$$\sigma(t) = \int_{-\infty}^{t} \frac{g(\alpha)}{(t-\tau)^{\alpha}} E\dot{\varepsilon}\, d\tau = E\, g(\alpha) \int_{-\infty}^{t} \frac{\dot{\varepsilon}}{(t-\tau)^{\alpha}}\, d\tau, \tag{1.6}$$

where the elastic response $\sigma^{(e)} = E\varepsilon$. If we choose $g(\alpha) = \frac{1}{\Gamma(1-\alpha)}$, then the integro-differential operator (8.16) gives the Liouville-Weyl fractional derivative. Under the hypothesis of causal histories, stating that the viscoelastic body is quiescent for all time prior to some starting instant $t = 0$, the equation (8.16) can be written as

$$\begin{aligned} \sigma(t) &= \varepsilon(0^{+}) \frac{E\, g(\alpha)}{t^{\alpha}} + E\, g(\alpha) \int_{0}^{t} \frac{\dot{\varepsilon}}{(t-\tau)^{\alpha}}\, d\tau, \\ &= \varepsilon(0^{+}) \frac{E\, g(\alpha)}{t^{\alpha}} + E\ {}_{0}^{C}\mathcal{D}_{t}^{\alpha}\, \varepsilon, \\ &= {}_{0}^{RL}\mathcal{D}_{t}^{\alpha}\, \varepsilon, \end{aligned} \tag{1.7}$$

where ${}_{0}^{C}\mathcal{D}_{t}^{\alpha}$ and ${}_{0}^{RL}\mathcal{D}_{t}^{\alpha}$ are the Caputo and Riemann-Liouville fractional derivatives, defined later. The constitutive equation (8.17) is the Scott Blair element [75, 138], which can be though of as an interpolation between a pure elastic (spring) and a pure viscous (dash pot) elements [115, 116, 160], see Fig. 1.2.

• **Distributed-Order Fractional Models:** In a more general sense, where the material contain a spectrum of power-type relaxation, the single order fractional constitutive model can be extended to the distributed-order one [8, 87]. Thus, we let the relaxation function $G(t)$ in (8.13) not be only a single order power-law as in (8.16), but rather be distributed over a range. This leads to a distributed

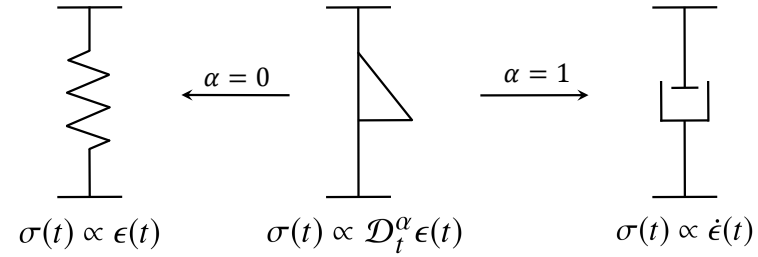

Figure 1.2: Schematic of a fractional model element (Scott Blair element): in the limiting cases of $\alpha = 0$ and $\alpha = 1$, converges to spring and dash-pot element, respectively.

form of constitutive equations expressed as

$$\int_{\beta_{min}}^{\beta_{max}} \Phi(\beta)\ {}_0\mathcal{D}_t^\beta \sigma(t)\, d\beta = \int_{\alpha_{min}}^{\alpha_{max}} \Psi(\alpha)\ {}_0\mathcal{D}_t^\alpha \varepsilon(t)\, d\alpha, \tag{1.8}$$

where $\Phi(\beta)$ and $\Psi(\alpha)$ are distribution functions that can confine the theoretical terminals β_{min}, β_{max}, α_{min}, and α_{max} according to the physical realization of problem (see [87] and the references therein). We see that in distributed order fractional operators, the differential order is distributed over a range of values rather than being just a fixed fraction as it is in standard/fractional ODEs/PDEs. Thus, they offer a rigorous tool for mathematical modeling of multi-rates multi-physics phenomena, such as ultra slow to super diffusive processes [85, 114, 143], and distributed order form of viscoelastic models [7, 20, 21, 34].

If we let the distribution functions be delta functions, the distributed order model becomes the following multi-term model:

$$\left(1 + \sum_{k=1}^{p_\sigma} a_k\ {}_0\mathcal{D}_t^{\beta_k}\right) \sigma(t) = \left(c + \sum_{k=1}^{p_\varepsilon} b_k\ {}_0\mathcal{D}_t^{\alpha_k}\right) \varepsilon(t). \tag{1.9}$$

We note that in viscoelastic modeling, one can design distinctive rheological model (constitutive equations) to get different types of behavior by choosing different distribution functions $\Phi(\beta)$ and $\Psi(\alpha)$. For example, by considering $\Phi(\beta) = \delta(\beta)$ and $\Psi(\alpha) = E_\infty \delta(\alpha) + E_\alpha \delta(\alpha - \alpha_0)$, we show that we recover the fractional Kelvin-Voigt model as

$$\sigma(t) = E_\infty\, \varepsilon(t) + E_{\alpha_0}\ {}^{RL}_{0}\mathcal{D}_t^{\alpha_0}\, \varepsilon(t), \tag{1.10}$$

where $\alpha_0 \in (0,1)$. Other fractional viscoelastic models such as standard linear solid model and generalized Maxwell model, shown in (1.11) can also be obtained by choosing different distribution functions in the distributed-order models [10, 22, 23, 97, 140, 164, 195].

$$J_0(\sigma + \tau_\epsilon^\alpha \, \mathcal{D}^\alpha \sigma) = \epsilon + \tau_\sigma^\alpha \, \mathcal{D}^\alpha \epsilon, \qquad (1.11)$$
$$J_\infty(\sigma + \tau_\epsilon^\alpha \, \mathcal{D}^\alpha \sigma) = \tau_\sigma^\alpha \, \mathcal{D}^\alpha \epsilon.$$

• **Structural Dissipation:** The internal dissipative mechanisms in structural deformations are usually modeled by viscoelasticity. The interaction of systems with an energy sink (e.g. non-Newtonian viscous friction and robber made foundations) also induces a dissipative behavior in the overall response of interactive system. A common example is the problem of fluid solid interaction, which mainly happen in structures immersed in viscous media such as wind turbine blades [1–3] and pipe conveying fluids [182]. In the case of viscoelastic materials in non-Newtonian fluid media, the internal and external dissipation mechanisms can be modeled by fractional constitutive equations. Thus, the corresponding governing equation takes the general form of

$$\left(\frac{\partial^2}{\partial t^2} + L_{t,\mathbf{x}}^q\right) u(t,\mathbf{x}) = \mathrm{f}(t,\mathbf{x}), \quad t,\mathbf{x} \in \Omega, \qquad (1.12)$$

where $u(t,\mathbf{x}) : \Omega \to \mathbb{R}$ denotes the displacement, Ω is the physical domain, $L_{t,\mathbf{x}}^q$ is a (nonlinear) operator with set of parameters q, and $\mathrm{f}(t,\mathbf{x})$ is the external force, which includes the dissipative coupling terms. Extensive derivation and investigation of nonlinear vibration of a viscoelastic cantilever beam is given in the following chapters.

1.1.2 Anomalous Diffusion

Several experimental observations have revealed that the standard diffusion process, in which the mean square displacement of the particles is proportional to elapsed time, is only a subset of a lager classification of phenomena, called anomalous diffusion. In this case, the mean square displacement changes nonlinearly in time (see Fig. 1.3) and thus, the anomalous diffusive process

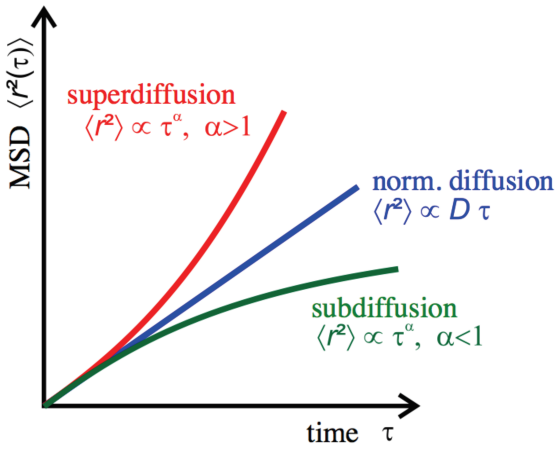

Figure 1.3: Normal and anomalous diffusion process: the means square displacement of particles in a diffusive process is nonlinearly proportional to time, i.e. $r^2 \propto D\tau^\alpha$. $\alpha = 1$: standard diffusion (blue line), $\alpha > 1$: super-diffusion (red curve), and $\alpha < 1$: sub-diffusion (green curve).

is described by a power law, i.e. $r^2 \propto D\tau^\alpha$, where D is the diffusion coefficient and τ is the elapsed time. The normal diffusion process takes place for $\alpha = 1$. If $\alpha > 1$ ($\alpha < 1$), the rate of diffusion increases (decreases), resulting in a super- (sub-) diffusive process (see e.g., [91] and references therein). For such anomalous processes, the non-Markovian and/or non-Gaussian jump distribution of the particles, is modeled by continuous time random walk (CTRW), where the continuous limit for such models leads to a temporal and/or spatial fractional diffusion equation [89, 123, 135], given as follows. Let $\Omega = [0,T] \times [a_1, b_1] \times [a_2, b_2] \times \cdots \times [a_d, b_d]$ be the computational domain for some positive integer d, and $u(t, \mathbf{x}; \mathbf{q}) : Q \times \Omega \to \mathbb{R}$, where $\mathbf{q}$ is the vector of model parameters containing the fractional indices and model coefficients. Then, the linear two-sided FPDE, subject to Dirichlet initial and boundary conditions, takes the form

$$ {}_0\mathcal{D}_t^\alpha u(t,\mathbf{x};\mathbf{q}) - \sum_{j=1}^{d} k_j \left[{}_{a_j}\mathcal{D}_{x_j}^{\beta_j} + {}_{x_j}\mathcal{D}_{b_j}^{\beta_j} \right] u(t,\mathbf{x};\mathbf{q}) = f(t,\mathbf{x};\mathbf{q}), \tag{1.13} $$

in which $\mathcal{D}$ is a fractional operator, $\alpha \in (0,1)$, $\beta_j \in (1,2)$, k_j are real positive constant coefficients.

1.1.3 Fractional Calculus: Definitions and Useful Properties

We briefly give definition of fractional integral and derivative of different senses and some of their useful properties. Let $\xi \in [-1,1]$. Then, the left-sided and right-sided Riemann-Liouville integral

of order σ, $n-1<\sigma\leq n$, $n\in\mathbb{N}$, are defined (see e.g., [122, 134]) respectively as

$$({}^{RL}_{-1}\mathcal{I}^{\sigma}_{\xi})u(\xi)=\frac{1}{\Gamma(\sigma)}\int_{-1}^{\xi}\frac{u(s)ds}{(\xi-s)^{n-\sigma}},\quad \xi>-1, \tag{1.14}$$

$$({}^{RL}_{\xi}\mathcal{I}^{\sigma}_{1})u(\xi)=\frac{1}{\Gamma(\sigma)}\int_{\xi}^{1}\frac{u(s)ds}{(s-\xi)^{n-\sigma}},\quad \xi<1. \tag{1.15}$$

The corresponding left-sided and right-sided fractional derivative of order σ are then defined, as

$$({}^{RL}_{-1}\mathcal{D}^{\sigma}_{\xi})u(\xi)=\frac{d^n}{d\xi^n}({}^{RL}_{-1}\mathcal{I}^{n-\sigma}_{\xi}u)(\xi)=\frac{1}{\Gamma(n-\sigma)}\frac{d^n}{d\xi^n}\int_{-1}^{\xi}\frac{u(s)ds}{(\xi-s)^{\sigma+1-n}},\quad \xi>-1, \tag{1.16}$$

$$({}^{RL}_{\xi}\mathcal{D}^{\sigma}_{1})u(\xi)=\frac{(-d)^n}{d\xi^n}({}^{RL}_{\xi}\mathcal{I}^{n-\sigma}_{1}u)(\xi)=\frac{1}{\Gamma(n-\sigma)}\frac{(-d)^n}{d\xi^n}\int_{\xi}^{1}\frac{u(s)ds}{(s-\xi)^{\sigma+1-n}},\quad \xi<1, \tag{1.17}$$

respectively. We recall a useful property of the Riemann-Liouville fractional derivatives [134]. Assume that $0<p<1$ and $0<q<1$ and $g(x_L)=0\ \ x>x_L$, then

$${}_{x_L}\mathcal{D}^{p+q}_{x}g(x)=\left({}_{x_L}\mathcal{D}^{p}_{x}\ {}_{x_L}\mathcal{D}^{q}_{x}\ g\right)(x)=\left({}_{x_L}\mathcal{D}^{q}_{x}\ {}_{x_L}\mathcal{D}^{p}_{x}\ g\right)(x). \tag{1.18}$$

An alternative approach in defining the fractional derivatives is to begin with the left-sided Caputo derivatives of order σ, $n-1<\sigma\leq n$, $n\in\mathbb{N}$, defined, as

$$({}^{C}_{-1}\mathcal{D}^{\sigma}_{\xi}u)(\xi)=({}_{-1}\mathcal{I}^{n-\sigma}_{\xi}\frac{d^nu}{d\xi^n})(\xi)=\frac{1}{\Gamma(n-\sigma)}\int_{-1}^{\xi}\frac{u^{(n)}(s)ds}{(\xi-s)^{\sigma+1-n}},\quad \xi>-1, \tag{1.19}$$

$$({}^{C}_{\xi}\mathcal{D}^{\sigma}_{1}u)(\xi)=({}_{\xi}\mathcal{I}^{n-\sigma}_{1}\frac{d^nu}{d\xi^n})(\xi)=\frac{1}{\Gamma(n-\sigma)}\int_{\xi}^{1}\frac{u^{(n)}(s)ds}{(s-\xi)^{\sigma+1-n}},\quad \xi<1. \tag{1.20}$$

By performing an affine mapping from the standard domain $[-1,1]$ to the interval $t\in[a,b]$, we obtain

$${}^{RL}_{a}\mathcal{D}^{\sigma}_{t}u=(\frac{2}{b-a})^{\sigma}({}^{RL}_{-1}\mathcal{D}^{\sigma}_{\xi}u)(\xi),\quad {}^{C}_{a}\mathcal{D}^{\sigma}_{t}u=(\frac{2}{b-a})^{\sigma}({}^{C}_{-1}\mathcal{D}^{\sigma}_{\xi}u)(\xi). \tag{1.21}$$

Hence, in developing numerical methods, we can perform the operations in the standard domain only once for any given σ and efficiently utilize them on any arbitrary interval without resorting to repeating the calculations. Moreover, the corresponding relationship between the Riemann-Liouville and Caputo fractional derivatives in $[a,b]$ for any $\sigma\in(0,1)$ is given by

$$({}^{RL}_{a}\mathcal{D}^{\sigma}_{t}\ u)(t)=\frac{u(a)}{\Gamma(1-\sigma)(t-a)^{\sigma}}+({}^{C}_{a}\mathcal{D}^{\sigma}_{t}\ u)(t). \tag{1.22}$$

1.2 Data-Driven Fractional Modeling

The inherent non-local nature of fractional operators makes them excellent choice in accurately predicting the non-locality and memory effect in anomalous behavior of complex physical systems. The exponent of singular power-law kernel in these operators defines the fractional derivative order or fractional index, which is an essential parameter in characterizing the underlying anomaly (e.g., the region of sub-/super-diffusion in an anomalous transport process is characterized by the orders of fractional derivatives, see Fig. 1.3). The values of fractional orders are introduced as new set of parameters in physical systems modeled by fractional operators, and their values are strongly tied to the experimental data in practice. The sensitivity assessment of fractional models with respect to the fractional indecis can build a bridge between experiments and mathematical models to gear observable data via proper optimization techniques. The sensitivity analysis provides a machine learning tool which exploit given experimental/synthetic data to iteratively estimate the parameters and thus construct the fractional model. However, the inherent randomness in measured experimental data, lack of information about true values of parameters (incomplete data), significant approximations as part of assumptions upon which the model is built, and random nature of quantities being modeled pervade uncertainty in the corresponding mathematical formulations. This renders the model parameters, including the fractional indices, random and thus, the fractional model stochastic, in which the novelty is to introduce the order of fractional derivative as random variable.

We consider stochastic fractional PDEs and develop the following useful mathematical and computational frameworks for them. They are mainly listed as follows (see also Fig. 1.4) and are briefly introduced afterwards:

- Distributed-Order fractional differential equations
- Fractional sensitivity analysis with application to fractional model construction
- Forward uncertainty quantification of stochastic fractional PDEs subject to additive noise

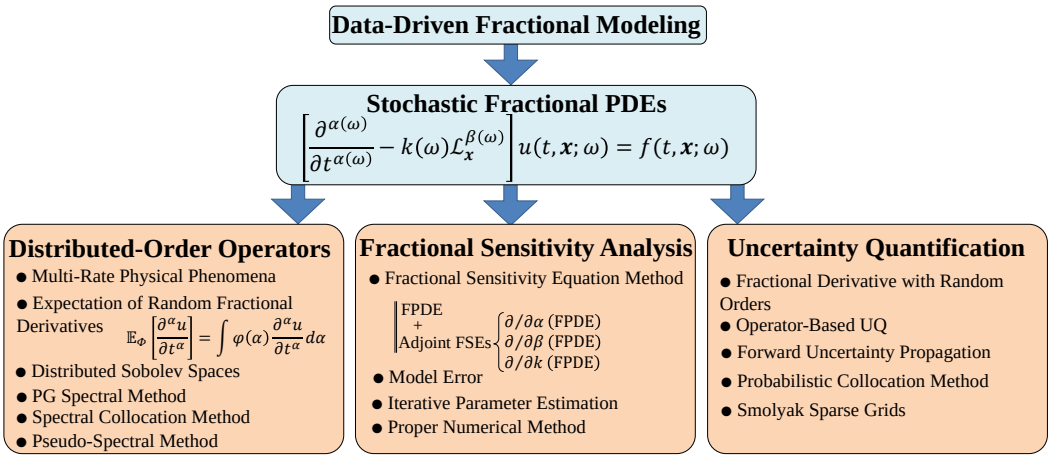

Figure 1.4: Schematic outline of this thesis with main focus on developing proper data-driven computational frameworks for stochastic fractional PDEs. Distributed-Order operators are considered as an extension of fractional operators to the case where the kernel is comprised of a distribution of power-laws; also as expectation of fractional derivative with random orders. Fractional sensitivity analysis provides a tool to study the sensitivity of model output with respect to fractional derivative orders; thus, leads to a machine learning tool to construct the fractional models from available sets of data. They also introduce new type of operators with logarithmic-power law kernels in this context. The randomness of fractional orders is propagated to model output via an operator-based UQ framework. Fast numerical methods with spectral rate of convergence are developed to back up the simulations in each case, where the stability and convergence are mathematically proven in the discrete function spaces.

- Application to nonlinear vibration of viscoelastic cantilever beams

The extensive discussion on developing and implementation of each framework is given later in the corresponding chapters.

1.2.1 Distributed Order Differential Equations

There is a rapidly growing interest in the use of fractional derivatives in the construction of mathematical models, which contain distributed order terms of the form

$$\int_{\alpha_1}^{\alpha_2} \phi(\alpha)\, {}_a\mathcal{D}_t^{\alpha} u(t) d\alpha = f(t), \quad t > a, \tag{1.23}$$

in the field of uncertainty quantification as the inherent uncertainty of experimental data can be directly incorporated into the differential operators. In this setting, distributed order derivative is considered as the expectation of fractional derivate of random order $\alpha(\omega)$ with respect to the

probability density function $\phi(\alpha)$, where ω is the notion of randomness in the parameter α. This provides a new operator in assessing the uncertainties associated with the randomness of derivative order in the context of stochastic fractional modeling; see [6, 12, 47, 87, 114, 154] for some work on numerical methods. We note that while numerical treatment of fractional operator are costly due to non-local kernel, the distributed order operators will excessively increase the computational expense by requiring additional discretization of integral in the distributed order. Most of the numerical studies have followed a two-stages approach, where in the first stage, the distributed order differentiation term was approximated using a quadrature rule, and in the second stage, a suitable multi-term numerical method was employed. We develop two spectrally-accurate schemes to treat linear/nonlinear distributed order fractional differential equations, which are constructed based on the recently developed spectral theory for fractional Sturm-Liouville problems in [186]. The list of main contributions are listed below:

- Introducing distributed sobolev spaces for the first time in the literature
- Developing spectrally/exponentially accurate quadrature rule for distributed-order derivatives
- Developing Petrov-Galerking spectral method and fractional collocation method
- Performing stability and error analysis of PG scheme
- Extension to temporally-distributed order PDEs

1.2.2 Fractional Sensitivity Equation Method: Application to Model Construction

We extend the continuum derivative technique to develop a fractional sensitivity equation method (FSEM) in the context of fractional partial differential equations (FPDEs). We then, construct an iterative algorithm in order to exploit the obtained sensitivity field in parameter estimation. In this setting, we introduce a new fractional operator, associated with the logarithmic-power law kernel, which to best of our knowledge has been presented for the first time here in the context of fractional sensitivity analysis. The key property of derived fractional sensitivity equations (FSEs) is that they

preserve the structure of original FPDE. Thus, similar discretization scheme and forward solver can be readily applied with minimal required changes. By extending the mathematical framework in [145] and accommodating extra required regularity in the underlying function spaces, we formulate a numerical scheme in solving coupled system of FPDE and adjoint FSEs. We prove that the coupled system is mathematically well-posed, further develop a fast solver to efficiently solve the equations and perform the stability and error analysis of the proposed numerical scheme. Moreover, we build our machine learning tool based on the developed FSEM. We estimate the fractional indices and thus, construct the fractional model from available experimental data in an inverse problem setting. The optimization problem is formulated by defining objective functions as two types of model error that measures the difference in computed output/input of fractional model with true output/input in an L2-norm sense. The parameters are obtained by minimizing the errors via a gradient-based minimizer, which uses the developed FSEM. We note that generally the inverse problem of parameter estimation is an ill-posed problem [25]. By numerical evaluation of introduced model errors on a coarse grid over the parameter space, we show that there exists a unique minimum in the objective function, which leads to unique values of fractional orders α and β. The list of main contributions are listed below:

- Sensitivity analysis of fractional models with respect to derivative orders
- A new fractional operator with logarithmic-power law kernel
- Accommodating extra regularity in function spaces due to new operator
- PG spectral method to solve coupled system of FPDE and adjoint FSEs
- Model errors as objective functions in parameter estimation
- Fractional model construction

1.2.3 Operator Based Uncertainty Quantification (UQ) in Stochastic FPDEs

In order to assess the uncertainty in output of fractional model associated with the randomness of model parameters including fractional order derivatives, we develop an operator-based computational forward UQ framework in the context of stochastic fractional PDEs. Assuming the mathematical model under consideration is well-posed and accounts in principle for all features of underlying phenomena, we identify three main sources of uncertainty, i) parametric uncertainty, including fractional indices as new set of random parameters appeared in the operator, ii) additive noises, which incorporates all intrinsic/extrinsic unknown forcing sources as lumped random inputs, and iii) numerical approximations (see also Fig. 1.5). Unlike the classical approach in modeling random inputs, which considers them as some idealized uncorrelated processes (white noises), we model the random inputs as more/fully correlated random processes (colored noises), and parametrize them via Karhunen-Loève (KL) expansion by finite-dimensional noise assumption. This yields the problem in finite dimensional random space. To propagate the parametric uncertainties into the system response, we employ Monte Carlo sampling (MCS) and a high-order probabilistic collocation methods (PCM). MCS enjoys from being embarrassingly parallelizable and can be implement quite readily on high dimensional random spaces but has slow rate of convergence. PCM uses the idea of interpolation/collocation in the random spaces and limits the sample points to an efficient subset of random space. Compare to MCS, PCM has the benefit of easily sampling at nodal points and the rate of convergence is relatively higher. In each simulation of stochastic model, we need to solve the deterministic counterpart in the physical domain, for which we formulate a fast and stable forward solver by developing a high-order Petrov-Galerkin (PG) spectral method. The list of main contributions are listed below:

- Rendering the fractional derivatives as random operator
- Operator-Based UQ framework
- Probabilistic collocation method and Monte Carlo simulation

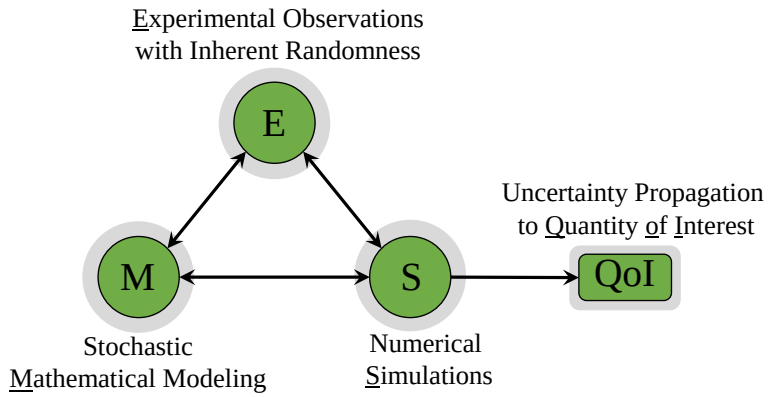

Figure 1.5: Uncertainty propagation toward the model output quantity of interest due to inherent randomness of measurements, incomplete sets of data, significant approximation in models, and numerical errors. The gray clouds show the associate uncertainties with each source and arrows show flow of information between them. Experimental observations feed into the construction of form of mathematical model and estimation of its parameters. The mathematical models are then numerically solved and the simulation results are verified and validated again by the experimental observation, making the two-way flow back to the experiments.

- PG spectral method as deterministic forward solver

1.3 Single/Multi-Domain Numerical Methods

The analytical solution of fractional models are mainly limited to very specific cases, and thus, in almost all practical problems, we need to formulate a proper numerical scheme. A key challenge in developing such scheme, however, is the inherent non-locality of fractional operators, which imposes extra computational costs. This becomes even more important as data-infused inverse problem of model construction and uncertainty frameworks usually instruct several numerical simulation of fractional models, predominating the urge of efficient numerical methods for fractional differential equations (FDEs). The immanent power-law singularity of the kernel, which essentially transmits to the output of model, also demand a numerical method that can capture the existing singularity of solution while yielding a fast, accurate, and stable scheme. Over the past two decades, an extensive amount of work has been done developing numerical schemes for fractional differential equations such as variational iteration method [71], homotopy perturbation method [162], Adomian's decomposition method [73], homotopy analysis method [68] and collocation

method [136]. While most of the attention has been devoted to the finite difference methods (FDMs), [33, 48, 65, 70, 93, 103, 111, 112, 121, 148, 158, 159, 167, 172, 192, 196] with fixed algebraic accuracy and significant memory allocation and history calculation, less effort has been put in developing global methods such as spectral schemes for discretizing FPDEs, see e.g., [28, 39, 83, 84, 99, 100, 103, 136, 158, 170].

1.3.1 Petrov-Galerkin Spectral Method and Spectral Collocation Method

Two new spectral theories on fractional Sturm-Liouville problems (FSLPs) have been recently developed by Zayernouri et al. in [183, 186]. This approach fractionalizes the well-known theory of Sturm-Liouville eigen-problems, where the explicit eigenfunctions of FSLPs are analytically obtained in terms of *Jacobi poly-fractonomials*. Recently, in [185, 187, 188], Jacobi poly-fractonomials are successfully employed in developing a series of high-order and efficient Petrov-Galerkin spectral and discontinuous spectral element methods of Galerkin and Petrov-Galerkin projection type for fractional ODEs.

We develop different high-order accurate spectral schemes to numerically solve linear/non-linear single-order and distributed order FPDEs. Petrov-Galerkin (PG) spectral methods approximate the solution by using a modal expansion in the weak form of problem, where the modes are called basis/trial functions and weak form is obtained via inner production by proper test functions. We develop a PG spectral method by following [186] and employing Jacobi poly-fractonomials of first and second kind as temporal basis and test functions, given in the standard domain $[-1, 1]$ as

$$ {}^{(1)}\mathcal{P}_n^{\mu}(x) = (1+x)^{\mu} P_{n-1}^{-\mu,+\mu}(x), \quad n = 1, 2, \cdots \tag{1.24} $$

$$ {}^{(2)}\mathcal{P}_k^{\mu}(x) = (1-x)^{\mu} P_{k-1}^{\mu,-\mu}(x), \quad k = 1, 2, \cdots \tag{1.25} $$

respectively, where $\mu > 0$, and $P_{n-1}^{-\mu,\mu}(x)$ and $P_{k-1}^{\mu,-\mu}(x)$ denote Jacobi polynomials. We see that they have the property to vanish at the left and right boundaries, respectively, i.e. ${}^{(1)}\mathcal{P}_n^{\mu}(-1) =$

${}^{(2)}\mathcal{P}_k^{\ \mu}(1) = 0$. We later prove that their RL-fractional derivatives preserve structure, i.e.

$$\begin{aligned} {}^{RL}_{x}\mathcal{D}_1^{\sigma}\ {}^{(2)}\mathcal{P}_n^{\mu}(x) &= \frac{\Gamma(n+\mu)}{\Gamma(n+\mu-\sigma)}\,{}^{(2)}\mathcal{P}_n^{\mu-\sigma}(x), \\ {}^{RL}_{-1}\mathcal{D}_x^{\sigma}\ {}^{(1)}\mathcal{P}_n^{\mu}(x) &= \frac{\Gamma(n+\mu)}{\Gamma(n+\mu-\sigma)}\,{}^{(1)}\mathcal{P}_n^{\mu-\sigma}(x) \end{aligned} \tag{1.26}$$

where $\sigma > 0$. Extensive properties of Jacobi poly-fractonomials can be found in [186]. We also note that Jacobi poly-fractonomials are non-polynomial functions, comprised of a fractional part multiplied by a polynomial, where the fractional exponent in the former can play the role of a tunning knob to accurately capture the solution singularity, while the latter approximates smooth part of solution. In developing PG spectral method for problems involving derivatives in space direction, we additionally consider Legendre polynomials as spatial basis/test functions. While the nonlocal nature of the fractional operators generally leads to non-symmetric full linear system, we symmetrize the corresponding mass/stiffness matrices in our method by embedding smart choices of coefficients in the constructions of function spaces. This further helps us formulate a fast solver to obtain the solution of resulting linear system. The excellence of developed PG method become more pronounced when used in inverse problem of data-driven model construction and also uncertainty quantification frameworks. The numerical analysis and computer implementation of each PG spectral method is discussed in detail in the corresponding chapter.

Spectral methods generally lead to high arithmetic complexity in treating nonlinearity due to cross terms of modal expansion. For fast treatment of nonlinear and multi-term fractional PDEs, a new spectral method, called *fractional spectral collocation method*, is developed in [189]. This new class of collocation schemes introduces a new family of fractional Lagrange interpolants, mimicking the structure of Jacobi poly-fractonomials. They are given as

$$h_j^{\mu}(\xi) = \Big(\frac{\xi - x_1}{x_j - x_1}\Big)^{\mu} \prod_{\substack{k=1 \\ k\neq j}}^{N} \Big(\frac{\xi - x_k}{x_j - x_k}\Big), \qquad j = 2, 3, \cdots, N, \tag{1.27}$$

where x_j's are the interpolation points and μ is the parameter to be adjusted to capture solution singularity. We note that fractional Lagrange interpolants satisfy the Kronecker delta property, i.e., $h_j^{\mu}(\xi_k) = \delta_{jk}$, at interpolation points, however they vary as a poly-fractonomial between interpola-

tion points. This makes it possible to efficiently treat the algebraic and differential nonlinearities such as in nonlinear reaction diffusion and Burger's equations. We extend the existing setting in [189] to develop a spectral collocation method for distributed-order differential equations. We properly modify the number of interpolation points in construction of interpolants to accommodate enough regularity in the approximation solution and derive the fractional differentiation matrices for different ranges of derivative order.

To relax the required high regularity of solution in the strong form of problem, yet preserving spectral rate of convergence, we combine the two modal and nodal expansion methods, i.e. PG spectral and collocation methods and thus, develop a pseudo-spectral method. We construct two separate sets of fractional Lagrange interpolants of first and second kind as basis and test functions, respectively, and plug into the weak form of the problem to obtain the corresponding *weak distributed differentiation matrices*. We further study the effect of distribution function and interpolation points on the condition number of the resulting linear system and also design distributed pre-conditioners, based on the distribution function. We show the better conditioning of the resulting linear system compare to the case that we solely use fractional spectral collocation method, which employs similar expansions but in the strong form of problem.

1.3.2 Petrov-Galerkin Spectral Element Method

Almost all numerical time integrators that march in time (e.g. finite difference method) instruct solving the resulting boundary value problem in each time step. The overall convergence of time integration and computational cost are then bounded by the spatial solver, requiring accurate and fast schemes in spatial directions. The existing complexity in geometry of spatial domain over which high-dimensional boundary value problems are defined usually imposes specific regularity/property over the underlying function spaces, which makes expansion over single domain approximation impractical to use. A common example is the effect of shock singularities in three dimensional fluid flows. Such complexity can be overcome via domain decomposition into sub-domains with simpler geometries, and thus less regularities, where the use of high-order accurate methods such as spectral

element method (SEM) is feasible. The SEM discretization has the benefit of domain decomposition into non-overlapping elements, where high-order approximations within each element yield a fast rate of convergence even in the cases of non-smooth and/or rapid transients in the solution. Therefore, a tractable computational cost of the method can be achieved by a successful combination of *h-refinement*, where the solution is rough, and *p-refinement*, where the solution is smooth. We note that the approximate solution inside each element in SEM is expanded using locally defined basis functions. This locality becomes a serious challenge in developing SEM for fractional operators as their non-local kernel requires a globally definition of solution approximation. This leads to construction of extra *history* matrices, which do not happen to be needed in integer-order problems. We develop a new high-order C^0-continuous Petrov–Galerkin spectral element method for a one-dimensional space-fractional Helmholtz equation of fractional order ($1 < \alpha \leq 2$), subject to homogeneous boundary conditions. We can use the standard polynomial modal basis functions in the weak formulation of problem by transferring the fractional portion of derivative order onto some proper non-polynomial test functions. We compute all elemental matrices, and then formulate a new non-local assembling procedure to construct the global linear system from the elemental mass, stiffness, and history matrices. We show that the proposed schemes can accurately capture boundary and interior singularities of solution by minimal number of domain decompositions.

CHAPTER 2

A PETROV-GALERKIN SPECTRAL ELEMENT METHOD FOR FRACTIONAL ELLIPTIC PROBLEMS

2.1 Background

A number of local numerical methods, prominently finite difference methods (FDMs), have been developed for solving fractional partial differential equations (FPDEs) [33, 48, 65, 70, 93, 103, 111, 112, 121, 148, 158, 159, 167, 172, 191, 196]. Fix and Roop [55] developed the first theoretical framework for the least-square finite element method (FEM) approximation of a fractional-order differential equation, where optimal error estimates are proven for piecewise linear elements. However, Roop [139] later showed that the main hurdle to overcome in the FEM is the non-local nature of the fractional operator, which leads to large dense matrices; he showed that even the construction of such matrices presents difficulties. Ervin and Roop [52] presented a theoretical framework for the variational solution of the steady state fractional advection dispersion equation based on FEM and proved the existence and uniqueness of the results. Jin et al. [80] proved the existence and uniqueness of a weak solution to the space-fractional parabolic equation using FEM; they showed an enhanced regularity of the solution and derived the error estimate for both semidiscrete and fully discrete solution. Well-posedness, regularity of the weak solution, stability of the discrete variational formulation and error estimate of the FEM approximation were investigated for fractional elliptic problems in [79]. Wang and Yang [168] generalized the analysis to the case of fractional elliptic problems with variable coefficient, analyzed the regularity of the solution in Hölder spaces, and established the well-posedness of proposed Petrov-Galerkin formulation. Wang and Zhang [170] developed a high-accuracy preserving spectral Galerkin method for the Dirichlet boundary-value problem of one-sided variable-coefficient conservative fractional diffusion equations. Wang et al. [171] later used the discontinuous Petrov-Galerkin framework to develop a Petrov-Galerkin FEM for a class of variable-coefficient conservative one-

dimensional FPDEs, where they also proved the error estimates of the scheme. Moreover, Wang et al. [169] developed an indirect FEM for the Dirichlet boundary-value problems of Caputo FPDEs showing the reduction in the computational work for numerical solution and memory requirements.

There has been recently more attention and effort put on developing global and high-order approximations, which are capable of efficiently capturing the inherent non-local effects. A Chebyshev spectral element method (SEM) for fractional-order transport was adopted by Hanert [67] and later on, the idea of least-square FEM was extended to SEM by Carella [35]. More recently, Deng and Hesthevan [44] and Xu and Hesthaven [178] developed local discontinuous Galerkin (DG) methods for solving space-fractional diffusion and convection-diffusion problems.

Two new spectral theories on fractional and tempered fractional Sturm-Liouville problems (TFSLPs) have been developed by Zayernouri et al. in [183, 186]. This approach first fractionalizes and then tempers the well-known theory of Sturm-Liouville eigen-problems. The explicit eigenfunctions of TFSLPs are analytically obtained in terms of *tempered Jacobi poly-fractonomials*. These poly-fractonomials have been successfully employed in developing a series of high-order and efficient Petrov-Galerkin spectral and discontinuous spectral element methods [184, 187, 190]. In [188], Zayernouri and Karniadakis developed a spectral and spectral element method for FODEs with an exponential accuracy. They also developed a highly accurate discontinuous SEM for time- and space- fractional advection equation in [187]. Dehghan et al. [42] considered Legendre SEM in space and FDM in time for solving time-fractional sub-diffusion equation. Su [157] provided a parallel spectral element method for the fractional Lorenz system and a comparison of the method with FEM and FDM.

The SEM discretization has the benefit of domain decomposition into non-overlapping elements, which potentially provide a geometrical flexibility, especially for adaptivity as well as complex domains. Moreover, high-order approximations within each element yield a fast rate of convergence even in the cases of non-smooth and/or rapid transients in the solution. Therefore, a tractable computational cost of the method can be achieved by a successful combination of *h-refinement*, where the solution is rough, and *p-refinement*, where the solution is smooth.

In this chapter, we consider the one-dimensional space-fractional Helmholtz equation of order $\alpha \in (1,2]$, subject to homogeneous boundary conditions. We formulate a weak form, in which the fractional portion $\mu \in (0,1]$ is transfered onto some proper fractional order test functions via integration-by-parts. This setting enables us to employ the standard polynomial modal basis functions, used in SEM [81]. Subsequently, we develop a new C^0-continuous Petrov-Galerkin SEM, following the recent spectral theory of fractional Sturm-Liouville problem, where the test functions are of Jacobi poly-fractonomials of second kind [186]. We investigate two distinct choices of basis/test functions: i) *local* basis/test functions, and ii) *local* basis with *global* test functions, which enables the construction of elemental mass/stiffness matrices in the standard domain $[-1,1]$. We explicitly compute the elemental stiffness matrices using the orthogonality of Jacobi polynomials. Moreover, we efficiently obtain the non-local (history) stiffness matrices, in which the non-locality is presented *analytically*. On one hand, we formulate a new *non-local assembling procedure* in order to construct the global linear system from the local (elemental) mass/stiffness matrices and history matrices. On the other hand, we formulate a procedure for *non-local scattering* to obtain the elemental expansion coefficients from the global degrees of freedom. We demonstrate the efficiency of the Petrov-Galerkin methods and show that the choice of local bases/test functions leads to a better accuracy and conditioning. Moreover, for uniform grids, we compute the history matrices off-line. The stored history matrices can be retrieved later in the construction of the global linear system. We show the great improvement in the computational cost by performing the retrieval procedure compared to on-line computation. We also introduce a non-uniform *kernel-based* grid generation in addition to *geometrically progressive* grid generation approaches. Furthermore, we investigate the performance of the developed schemes by considering two cases of smooth and singular solutions, where the singularity can occur at boundary points or the interior domain. Finally, we study the effect of history fading via a systematic analysis, where we consider the history up to some specific element and let the rest fade. This results in less computational cost, while we show that the accuracy is still preserved. The main contributions of this work are listed in the following:

- Development of a new fast and accurate C^0-continuous Petrov-Galerkin spectral element method, employing local basis/test functions, where the test functions are Jacobi poly-fractonomials.
- Reducing the number of history matrix calculation from $\frac{N_{el}(N_{el}-1)}{2}$ to $(N_{el}-1)$ for a uniformly partitioned domain.
- Analytical expressions of non-local effects in uniform grids leading to fast computation of the history matrices.
- A new procedure for the assembly of the global linear system.
- Performing off-line computation of history matrices and on-line retrieval of the stored matrices.
- Non-uniform “kernel-based" grid generation for resolving steep gradients and singularities.

The organization of this chapter is as follows: section 2.2 provides problem definition, derivation of the weak form and expressions for the local basis and local/global test functions. In section 2.3, we present a Petrov-Galerkin method, employing the local basis/test functions in addition to formulating the non-local assembling and non-local scattering procedures, followed by a discussion on how to compute the history matrices *off-line*. We also present the two non-uniform grid generation approaches. In section 2.4, we present a Petrov-Galerkin method, employing the local basis with global test functions. In section 2.5, we demonstrate the computational efficiency of the two proposed schemes by considering several numerical examples of smooth and singular solutions. Finally, we perform the off-line computation and retrieval procedure of history matrices and a systematic history fading analysis.

2.2 Definitions

2.2.1 Problem Definition

We study the following fractional Helmholtz equation of order $\alpha = 1 + \mu$, $\mu \in (0, 1]$:

$$
\begin{aligned}
{}^{RL}_{0}\mathcal{D}^{\alpha}_{x} u(x) - \lambda u(x) &= f(x), \quad \forall x \in \Omega && (2.1)\\
u(0) &= u(L) = 0, \quad \forall x \in \partial\Omega, && (2.2)
\end{aligned}
$$

where $\Omega = [0, L]$. We multiply both sides of (2.1) by some proper test function $v(x)$ and transfer the fractional portion, μ, of derivative onto the test function by taking the fractional integration-by-parts, following the proof of Lemma 2.4 in [87]. Therefore, we obtain the following bilinear form:

$$
a(u, v) = l(v), \tag{2.3}
$$

in which

$$
\begin{aligned}
a(u, v) &= \left(\frac{du}{dx}, {}^{RL}_{x}\mathcal{D}^{\mu}_{L} v\right)_{\Omega} - \lambda\left(u, v\right)_{\Omega}, && (2.4)\\
l(v) &= \left(f, v\right)_{\Omega}, && (2.5)
\end{aligned}
$$

where $(\cdot, \cdot)_{\Omega}$ denotes the usual L^2 inner product.

2.2.2 Local Basis Functions

We partition the computational domain into N_{el} non-overlapping elements $\Omega_e = [x_{e-1}, x_e]$ such that $\Omega = \cup_{e=1}^{Nel}\Omega_e$, see Fig. 2.1. Therefore, the bilinear form (2.4) can be written as

$$
a(u, v) \approx a(u^{\delta}, v^{\delta}) = \sum_{e=1}^{N_{el}} \left(\frac{du_N^{(e)}}{dx}, {}^{RL}_{x}\mathcal{D}^{\mu}_{L} v^{\delta}\right)_{\Omega_e} - \lambda \sum_{e=1}^{N_{el}} \left(u_N^{(e)}, v^{\delta}\right)_{\Omega_e}, \tag{2.6}
$$

where $u_N^{(e)}$ is the approximation solution in each element, which is given by

$$
u_N^{(e)}(x) = \sum_{p=0}^{P} \hat{u}_p^{(e)} \psi_p(x), \quad x \in \Omega_e, \tag{2.7}
$$

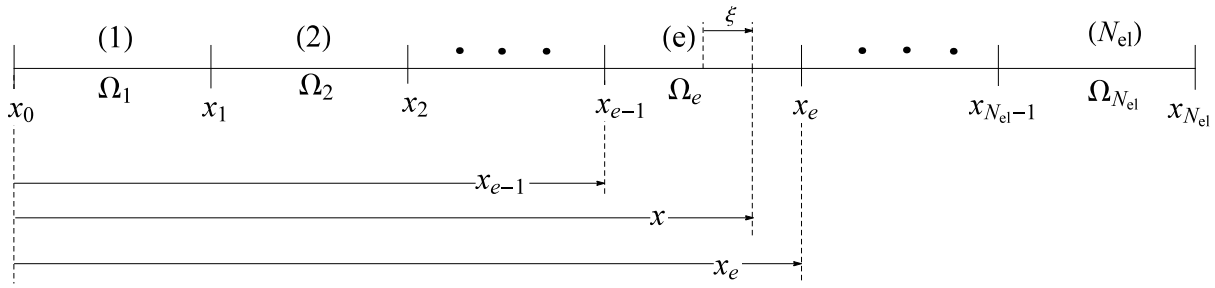

Figure 2.1: Domain partitioning

using the basis functions $\psi_p(x)$'s in the element. Thus, the approximated solution over the whole domain can be written as

$$u \approx u^{\delta}(x) = \sum_{e=1}^{N_{el}} \sum_{p=0}^{P} \hat{u}_p^{(e)} \psi_p(x). \tag{2.8}$$

The modal bases $\psi_p(x)$ are defined in the standard (reference) domain [-1,1] as:

$$\psi_p(x(\zeta)) = \begin{cases} \frac{1-\zeta}{2}, & p = 0, \\ (\frac{1-\zeta}{2})(\frac{1+\zeta}{2}) P_{p-1}^{1,1}(\zeta), & p = 1, 2, \cdots, P-1, \\ \frac{1+\zeta}{2}, & p = P. \end{cases} \tag{2.9}$$

The choice of basis functions is the same as in standard spectral element methods for integer-order PDEs (see e.g., [81]).

2.2.3 Test Functions: Local vs. Global

We choose two types of test functions v^{δ}: i) *local* test functions, and ii) *global* test functions, given for $\varepsilon = 1, 2, \cdots, N_{el}$ as follows:

$$v_k^{local}(x) = v_k^{\varepsilon}(x) = \begin{cases} {}^{(2)}\mathcal{P}_{k+1}^{\mu}(x^{\varepsilon}), & \forall x \in \Omega_{\varepsilon}, \\ 0, & otherwise, \end{cases}, \quad k = 0, 1, \cdots, P, \tag{2.10}$$

in which ${}^{(2)}\mathcal{P}^{\mu}_{k+1}(x^{\varepsilon})$ represents the Jacobi *poly-fractonomial* of second kind, defined in the corresponding intervals $\Omega_{\varepsilon} = [x_{\varepsilon-1}, x_{\varepsilon}]$; and

$$v_k^{global}(x) = v_k^{\varepsilon}(x) = \begin{cases} {}^{(2)}\mathcal{P}^{\mu}_{k+1}(x^{1\sim\varepsilon}), & \forall x \in [0, x_{\varepsilon}], \\ 0, & otherwise \end{cases}, \quad k = 0, 1, \cdots, P, \tag{2.11}$$

where ${}^{(2)}\mathcal{P}^{\mu}_{k+1}(x^{1\sim\varepsilon})$ represents the Jacobi *poly-fractonomial* of second kind, defined in the corresponding intervals $[0, x_{\varepsilon}]$. The structure of Jacobi poly-fractonomial are given in (1.25). It should be noted that for each element ε, the corresponding local test function has nonzero value only in the element and vanishes elsewhere, unlike the corresponding global test function, which vanishes only where $x > x_{\varepsilon}$.

2.3 Petrov-Galerkin Method with Local Test Functions

We develop the Petrov-Galerkin scheme by substituting (2.7) and (2.10) into (2.6) to obtain:

$$\begin{aligned} &\sum_{e=1}^{N_{el}} \Big(\sum_{p=0}^{P} \hat{u}_p^{(e)} \, \frac{d\psi_p(x)}{dx}, \, {}^{RL}_{x}\mathcal{D}^{\mu}_{L} \, v_k^{\varepsilon}(x) \Big)_{\Omega_e} - \lambda \sum_{e=1}^{N_{el}} \Big(\sum_{p=0}^{P} \hat{u}_p^{(e)} \, \psi_p(x), \, v_k^{\varepsilon}(x) \Big)_{\Omega_e} \\ = \; & \Big(f \, , \, v_k^{\varepsilon}(x) \Big)_{\Omega}, \quad \varepsilon = 1, 2, \cdots, N_{el}, \quad k = 0, 1, \cdots, P. \end{aligned} \tag{2.12}$$

Since the local test function vanishes $\forall x \in \Omega_e \neq \Omega_{\varepsilon}$, we have

$$\begin{aligned} \lambda \sum_{e=1}^{N_{el}} \Big(\sum_{p=0}^{P} \hat{u}_p^{(e)} \psi_p(x), \, v_k^{\varepsilon}(x) \Big)_{\Omega_e} &= \lambda \Big(\sum_{p=0}^{P} \hat{u}_p^{(\varepsilon)} \psi_p(x), \, v_k^{\varepsilon}(x) \Big)_{\Omega_{\varepsilon}}, \\ \Big(f \, , \, v_k^{\varepsilon}(x) \Big)_{\Omega} &= \Big(f \, , \, v_k^{\varepsilon}(x) \Big)_{\Omega_{\varepsilon}}. \end{aligned}$$

Moreover, for every ε, the right-sided fractional derivative,

$${}^{RL}_{x}\mathcal{D}^{\mu}_{L} \, v_k^{\varepsilon}(x) = \frac{-1}{\Gamma(1-\mu)} \frac{d}{dx} \int_x^L \frac{v_k^{\varepsilon}(s)}{(s-x)^{\mu}} ds, \quad x \in \Omega_e,$$

is taken from $x \in \Omega_e$ to $x = L$, where $e = 1, 2, \cdots, N_{el}$ through the summation over the elements and s varies from $x \in \Omega_e$ to L. The local test function vanishes $\forall x \in \Omega_e \neq \Omega_{\varepsilon}$, thus if $e > \varepsilon$ ($x > x_{\varepsilon}$, see Fig. 2.2 top), then

$${}^{RL}_{x}\mathcal{D}^{\mu}_{L} \, v_k^{\varepsilon}(x) = \frac{-1}{\Gamma(1-\mu)} \frac{d}{dx} \int_x^L \frac{0}{(s-x)^{\mu}} ds = 0, \tag{2.13}$$

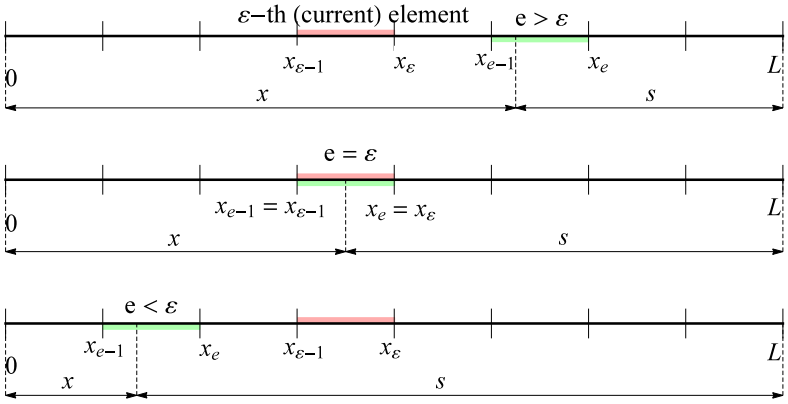

Figure 2.2: Location of the (dummy) element number, e, with respect to the current element, ε. If $e > \varepsilon$, (top), then ${}^{RL}_{x}\mathcal{D}^{\mu}_{L}\, v^{\varepsilon}_{k}(x) = 0$. If $e = \varepsilon$, (middle), then ${}^{RL}_{x}\mathcal{D}^{\mu}_{L}\, v^{\varepsilon}_{k}(x) = {}^{RL}_{x}\mathcal{D}^{\mu}_{x_\varepsilon}\left[\, {}^{(2)}\mathcal{P}^{\mu}_{k+1}(x)\,\right]$. If $e < \varepsilon$, (bottom), then ${}^{RL}_{x}\mathcal{D}^{\mu}_{L}\, v^{\varepsilon}_{k}(x) = H^{(\varepsilon)}_{k}(x)$.

and if $e < \varepsilon$ ($x < x_{\varepsilon-1}$, see Fig. 2.2 bottom), then

$$ {}^{RL}_{x}\mathcal{D}^{\mu}_{L}\, v^{\varepsilon}_{k}(x) = \frac{-1}{\Gamma(1-\mu)}\frac{d}{dx}\int_{x_{\varepsilon-1}}^{x_\varepsilon} \frac{{}^{(2)}\mathcal{P}^{\mu}_{k+1}(s)}{(s-x)^{\mu}}ds \equiv H^{(\varepsilon)}_{k}(x), \tag{2.14} $$

and if $e = \varepsilon$, ($x_{\varepsilon-1} < x < x_\varepsilon$, see Fig. 2.2 middle), then

$$ {}^{RL}_{x}\mathcal{D}^{\mu}_{L}\, v^{\varepsilon}_{k}(x) = \frac{-1}{\Gamma(1-\mu)}\frac{d}{dx}\int_{x}^{x_\varepsilon} \frac{{}^{(2)}\mathcal{P}^{\mu}_{k+1}(s)}{(s-x)^{\mu}}ds = {}^{RL}_{x}\mathcal{D}^{\mu}_{x_\varepsilon}\left[\, {}^{(2)}\mathcal{P}^{\mu}_{k+1}(x)\,\right]. \tag{2.15} $$

Hence, for $\varepsilon = 1, 2, \cdots, N_{el}$ and $k = 0, 1, \cdots, P$,

$$ {}^{RL}_{x}\mathcal{D}^{\mu}_{L}\, v^{\varepsilon}_{k}(x) = \begin{cases} 0, & \forall x \in \Omega_e,\ e > \varepsilon, \\ {}^{RL}_{x}\mathcal{D}^{\mu}_{x_\varepsilon}\left[\, {}^{(2)}\mathcal{P}^{\mu}_{k+1}(x)\,\right], & \forall x \in \Omega_e,\ e = \varepsilon, \\ H^{(\varepsilon)}_{k}(x), & \forall x \in \Omega_e,\ e < \varepsilon. \end{cases} \tag{2.16} $$

Therefore, the bilinear form (2.12) can be written as

$$ \begin{aligned} &\sum_{e=1}^{\varepsilon-1}\sum_{p=0}^{P} \hat{u}^{(e)}_{p}\left(\frac{d\psi_p(x)}{dx}, H^{(\varepsilon)}_{k}(x)\right)_{\Omega_e} + \sum_{p=0}^{P} \hat{u}^{(\varepsilon)}_{p}\left(\frac{d\psi_p(x)}{dx}, {}^{RL}_{x}\mathcal{D}^{\mu}_{x_\varepsilon}\left[\, {}^{(2)}\mathcal{P}^{\mu}_{k+1}(x)\,\right]\right)_{\Omega_\varepsilon} \\ &-\lambda\sum_{p=0}^{P} \hat{u}^{(\varepsilon)}_{p}\left(\psi_p(x),\ {}^{(2)}\mathcal{P}^{\mu}_{k+1}(x)\right)_{\Omega_\varepsilon} = \left(f,\ {}^{(2)}\mathcal{P}^{\mu}_{k+1}(x)\right)_{\Omega_\varepsilon}, \end{aligned} \tag{2.17} $$

and the weak form is obtained as

$$\sum_{e=1}^{\varepsilon-1}\sum_{p=0}^{P}\hat{u}_p^{(e)}\ \hat{\mathbf{S}}_{kp}^{(e,\varepsilon)}+\sum_{p=0}^{P}\hat{u}_p^{(\varepsilon)}\Big[\ \mathbf{S}_{kp}^{(\varepsilon)}-\lambda\ \mathbf{M}_{kp}^{(\varepsilon)}\Big]=\mathbf{f}_k^{(\varepsilon)},\quad \begin{cases}\varepsilon=1,2,\cdots,N_{el},\\ k=0,1,\cdots,P,\end{cases} \tag{2.18}$$

in which

$$\begin{aligned}
\hat{\mathbf{S}}_{kp}^{(e,\varepsilon)} &= \Big(\frac{d\psi_p}{dx},H_k^{(\varepsilon)}(x)\Big)_{\Omega_e},\quad e=1,2,\cdots,\varepsilon-1, \\
\mathbf{S}_{kp}^{(\varepsilon)} &= \Big(\frac{d\psi_p}{dx},\ {}^{RL}_{x}\mathcal{D}^{\mu}_{x_\varepsilon}\Big[\ {}^{(2)}\mathcal{P}^{\mu}_{k+1}(x)\ \Big]\Big)_{\Omega_\varepsilon}, \\
\mathbf{M}_{kp}^{(\varepsilon)} &= \Big(\psi_p(x),\ {}^{(2)}\mathcal{P}^{\mu}_{k+1}(x)\Big)_{\Omega_\varepsilon}, \\
\mathbf{f}_k^{(\varepsilon)} &= \Big(f,\ {}^{(2)}\mathcal{P}^{\mu}_{k+1}(x)\Big)_{\Omega_\varepsilon},
\end{aligned} \tag{2.19}$$

are respectively the *history*, local stiffness, local mass matrices, and local force vector.

2.3.1 Elemental (Local) Operations: the construction of local matrices $\mathbf{S}^{(\varepsilon)}$ and $\mathbf{M}^{(\varepsilon)}$, and vector $\mathbf{f}^{(\varepsilon)}$

Here, we provide the analytically obtained expressions of the local stiffness matrix as well as the proper quadrature rules to construct the local mass matrix and force vector for all elements $\varepsilon=1,2,\cdots,N_{el}$.

Elemental (Local) Stiffness Matrix $\mathbf{S}^{(\varepsilon)}$: given the structure of the basis functions and using (1.26), we first obtain the first ($p=0$) and last column ($p=P$) of the the local stiffness matrix $\mathbf{S}^{(\varepsilon)}$, and then, the rest of entries corresponding to the interior modes. Hence,

$$\begin{aligned}
\mathbf{S}_{k0}^{(\varepsilon)} &= \int_{x_{\varepsilon-1}}^{x_\varepsilon}\frac{d\psi_0}{dx}\ {}^{RL}_{x}\mathcal{D}^{\mu}_{x_\varepsilon}\Big[\ {}^{(2)}\mathcal{P}^{\mu}_{k+1}(x)\ \Big]dx, \\
&= Jac(\varepsilon,\mu)\int_{-1}^{1}(\frac{-1}{2})(\frac{d\zeta}{dx})\frac{\Gamma[1+k+\mu]}{\Gamma[1+k]}P_k(\zeta)(\frac{dx}{d\zeta})d\zeta, \\
&= -Jac(\varepsilon,\mu)\frac{\Gamma(1+k+\mu)}{2\ \Gamma(1+k)}\int_{-1}^{1}P_k(\zeta)d\zeta, \\
&= -Jac(\varepsilon,\mu)\frac{\Gamma(1+k+\mu)}{\Gamma(1+k)}\delta_{k,0},\quad (\textit{by the orthogonality})
\end{aligned} \tag{2.20}$$

in which the Jacobian constant, associated with the element ε and the fractional order μ, is $Jac(\varepsilon,\mu) = (\frac{2}{x_\varepsilon - x_{\varepsilon-1}})^\mu$. Thus, the first column of the local stiffness matrix is obtained as

$$\boxed{\mathbf{S}^{(\varepsilon)}_{k0} = -(\frac{2}{x_\varepsilon - x_{\varepsilon-1}})^\mu \frac{\Gamma(1+k+\mu)}{\Gamma(1+k)}\delta_{k,0}, \quad k = 0,1,\cdots,P.} \tag{2.21}$$

Similarly, we can obtain the last column of the local stiffness matrix $\mathbf{S}^{(\varepsilon)}_{kP}$ as

$$\boxed{\mathbf{S}^{(\varepsilon)}_{kP} = (\frac{2}{x_\varepsilon - x_{\varepsilon-1}})^\mu \frac{\Gamma(1+k+\mu)}{\Gamma(1+k)}\delta_{k,0} = -\mathbf{S}^{(\varepsilon)}_{k0}, \quad k = 0,1,\cdots,P.} \tag{2.22}$$

In order to obtain the rest of entries of $\mathbf{S}^{(\varepsilon)}_{kp}$ ($k = 0,1,\cdots,P$ and $p = 1,2,\cdots,P-1$), we carry out the integration-by-parts and transfer another derivative onto the test function, taking into account that the interior modes vanish at the boundary points x_ε and $x_{\varepsilon-1}$. Therefore,

$$\begin{aligned}
\mathbf{S}^{(\varepsilon)}_{kp} &= \int_{x_{\varepsilon-1}}^{x_\varepsilon} \frac{d\psi_p}{dx}\ {}^{RL}_{x}\mathcal{D}^{\mu}_{x_\varepsilon}\left[{}^{(2)}\mathcal{P}^{\mu}_{k+1}(x)\right]dx, \\
&= -\int_{x_{\varepsilon-1}}^{x_\varepsilon} \psi_p(x)\ \frac{d}{dx}\ {}^{RL}_{x}\mathcal{D}^{\mu}_{x_\varepsilon}\left[{}^{(2)}\mathcal{P}^{\mu}_{k+1}(x)\right]dx, \\
&= -\int_{-1}^{1} \psi_p(\zeta)\ \frac{d}{d\zeta}\frac{d\zeta}{dx}\ Jac(\varepsilon,\mu)\ {}^{RL}_{\zeta}\mathcal{D}^{\mu}_{1}\left[{}^{(2)}\mathcal{P}^{\mu}_{k+1}(\zeta)\right]\frac{dx}{d\zeta}d\zeta, \\
&= -Jac(\varepsilon,\mu)\frac{\Gamma(1+k+\mu)}{4\ \Gamma(1+k)}\int_{-1}^{1}(1-\zeta)(1+\zeta)P^{1,1}_{p-1}(\zeta)\ \frac{d}{d\zeta}\Big[P_k(\zeta)\Big]d\zeta, \\
&= -Jac(\varepsilon,\mu)\frac{\Gamma(1+k+\mu)}{4\ \Gamma(1+k)}\frac{k+1}{2}\int_{-1}^{1}(1-\zeta)(1+\zeta)P^{1,1}_{p-1}(\zeta)\ P^{1,1}_{k-1}(\zeta)d\zeta.
\end{aligned} \tag{2.23}$$

Hence, for $\varepsilon = 1,2,\cdots,N_{el}$,

$$\boxed{\mathbf{S}^{(\varepsilon)}_{kp} = -(\frac{2}{x_\varepsilon - x_{\varepsilon-1}})^\mu \frac{\Gamma(1+k+\mu)(k+1)}{8\ \Gamma(1+k)}C^{1,1}_{k-1}\delta_{k,p}, \quad \begin{array}{l} k = 0,\cdots,P, \\ p = 1,\cdots,P-1, \end{array}} \tag{2.24}$$

where $C^{1,1}_{k-1}$ represents the corresponding orthogonality constant of Jacobi polynomials of order $k-1$ with parameters $\alpha = \beta = 1$. We note that the entries of $\mathbf{S}^{(\varepsilon)}_{kp}$ are obtained analytically, using the orthogonality of Jacobi polynomial. Also, the interior modes lead to a *diagonal* matrix due to $\delta_{k,p}$. Fig. 2.3 shows the sparsity of the local stiffness matrix.

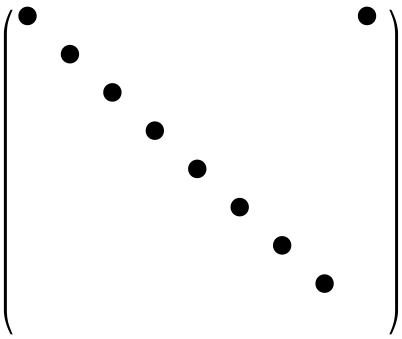

Figure 2.3: Sparsity of local stiffness matrix

Elemental (Local) Mass Matrix $\mathbf{M}^{(\varepsilon)}$: given the structure of basis functions and definition (2.19), we first obtain the corresponding first ($p = 0$) and last column ($p = P$) of the local mass matrix $\mathbf{M}^{(\varepsilon)}$, and then, we compute the rest of entries associated with the interior modes, using proper quadrature rules. Therefore,

$$\mathbf{M}^{(\varepsilon)}_{k0} = (\frac{x_\varepsilon - x_{\varepsilon-1}}{4}) \sum_{q=1}^{Q} w_q^{1+\mu,0} \; P_k^{\mu,-\mu}(\, z_q^{1+\mu,0}\,),$$

$$\mathbf{M}^{(\varepsilon)}_{kP} = (\frac{x_\varepsilon - x_{\varepsilon-1}}{4}) \sum_{q=1}^{Q} w_q^{\mu,1} \; P_k^{\mu,-\mu}(\, z_q^{\mu,1}\,),$$

$$\mathbf{M}^{(\varepsilon)}_{kp} = (\frac{x_\varepsilon - x_{\varepsilon-1}}{8}) \sum_{q=1}^{Q} w_q^{1+\mu,1} \; P_k^{\mu,-\mu}(\, z_q^{1+\mu,1}\,),$$

where $k = 0, 1, \cdots, P$ and $\{w_q^{\alpha,\beta}, z_q^{\alpha,\beta}\}_{q=1}^{Q}$ are the Gauss-Lobatto-Jacobi weights and points corresponding to the parameters α and β.

Elemental (Local) Load Vector $\mathbf{f}^{(\varepsilon)}$: the local load vector is obtained as:

$$\mathbf{f}_k^{(\varepsilon)} = \int_{x_{\varepsilon-1}}^{x^\varepsilon} f(x) \; {}^{(2)}\mathcal{P}^{\mu}_{k+1}(x)dx = (\frac{x_\varepsilon - x_{\varepsilon-1}}{2}) \int_{-1}^{1} (1-\zeta)^\mu \; f(x(\zeta)) \; P_k^{\mu,-\mu}(\zeta) \; d\zeta.$$

Hence, for $\varepsilon = 1, 2, \cdots, N_{el}$,

$$\mathbf{f}_k^{(\varepsilon)} = (\frac{x_\varepsilon - x_{\varepsilon-1}}{2}) \sum_{q=1}^{Q} w_q^{\mu,0} \; f(\, x^\varepsilon(\zeta_q)\,) \, P_k^{\mu,-\mu}(\, z_q^{\mu,0}\,), \quad k = 0, 1, \cdots, P,$$

where $\{w_q^{\mu,0}, z_q^{\mu,0}\}_{q=1}^{Q}$ are the Gauss-Lobatto-Jacobi weights and points corresponding to the parameters $\alpha = \mu$ and $\beta = 0$.

2.3.2 Non-Local Operation: the construction of history matrix $\hat{\mathbf{S}}^{(e,\varepsilon)}$

The most challenging part of constructing the linear system is to compute the global history matrix $\hat{\mathbf{S}}^{(e,\varepsilon)}$. The history matrix relates the current element $\varepsilon = 1, 2, \cdots, N_{el}$ to its past elements $e = 1, 2, \cdots, \varepsilon - 1$ by

$$\hat{\mathbf{S}}_{kp}^{(e,\varepsilon)} = \int_{x_{e-1}}^{x_e} \frac{d\psi_p}{dx} H_k^{(\varepsilon)}(x)\, dx, \quad k = 0, \cdots, P, \quad p = 1, \cdots, P-1, \tag{2.25}$$

where $H_k^{(\varepsilon)}(x)$ is given in (2.14) as

$$\begin{aligned} H_k^{(\varepsilon)}(x) &= \frac{-1}{\Gamma(1-\mu)} \frac{d}{dx} \int_{x_{\varepsilon-1}}^{x^\varepsilon} \frac{{}^{(2)}\mathcal{P}_{k+1}^{\mu}(s)}{(s-x)^{\mu}} ds, \\ &= \frac{-\mu}{\Gamma(1-\mu)} \int_{x_{\varepsilon-1}}^{x^\varepsilon} \frac{{}^{(2)}\mathcal{P}_{k+1}^{\mu}(s)}{(s-x)^{1+\mu}} ds, \end{aligned}$$

in which, $x \in \Omega_e = [x_{e-1}, x_e]$ and $s \in \Omega_\varepsilon = [x_{\varepsilon-1}, x_\varepsilon]$. By performing the following affine mappings

$$\begin{aligned} s &= \frac{x_\varepsilon + x_{\varepsilon-1}}{2} + \frac{x_\varepsilon - x_{\varepsilon-1}}{2}\zeta, \\ x &= \frac{x_e + x_{e-1}}{2} + \frac{x_e - x_{e-1}}{2}\xi, \end{aligned}$$

from Ω_e and Ω_ε to the standard domain $[-1, 1]$, the history function $H_k^{(\varepsilon,e)}(\xi) = H_k^{(\varepsilon)}(x)$ is obtained as

$$\begin{aligned} &H_k^{(\varepsilon,e)}(\xi) \\ &= \left(\frac{x_\varepsilon - x_{\varepsilon-1}}{2}\right) \frac{-\mu}{\Gamma(1-\mu)} \int_{-1}^{1} \frac{{}^{(2)}\mathcal{P}_{k+1}^{\mu}(\zeta) d\zeta}{\left[\frac{(x_\varepsilon + x_{\varepsilon-1}) - (x_e + x_{e-1})}{2} + \frac{x_\varepsilon - x_{\varepsilon-1}}{2}\zeta - \frac{x_e - x_{e-1}}{2}\xi\right]^{1+\mu}}. \end{aligned} \tag{2.26}$$

If the mesh is "uniform", then

$$\begin{aligned} &\frac{x_\varepsilon + x_{\varepsilon-1}}{2} = \frac{2\varepsilon - 1}{2}\Delta x, \quad \frac{x_e + x_{e-1}}{2} = \frac{2e-1}{2}\Delta x, \\ &\frac{x_\varepsilon - x_{\varepsilon-1}}{2} = \frac{x_e - x_{e-1}}{2} = \frac{\Delta x}{2}, \end{aligned} \tag{2.27}$$

and thus,

$$
\begin{aligned}
H_k^{(\varepsilon,e)}(\xi) &= \frac{\Delta x}{2}\frac{-\mu}{\Gamma(1-\mu)}\int_{-1}^{1}\frac{{}^{(2)}\mathcal{P}_{k+1}^{\mu}(\zeta)}{\left[\frac{(2\varepsilon-1)-(2e-1)}{2}\Delta x+\frac{\Delta x}{2}(\zeta-\xi)\right]^{1+\mu}}d\zeta,\\
&= \frac{-\mu}{\Gamma(1-\mu)}(\frac{2}{\Delta x})^{\mu}\int_{-1}^{1}\frac{{}^{(2)}\mathcal{P}_{k+1}^{\mu}(\zeta)}{\left[2(\varepsilon-e)+\zeta-\xi\right]^{1+\mu}}d\zeta,\\
&= \frac{-\mu}{\Gamma(1-\mu)}(\frac{2}{\Delta x})^{\mu}\int_{-1}^{1}\frac{{}^{(2)}\mathcal{P}_{k+1}^{\mu}(\zeta)}{\left[2\,\Delta\varepsilon+\zeta-\xi\right]^{1+\mu}}d\zeta,
\end{aligned}
\tag{2.28}
$$

where $\Delta\varepsilon=\varepsilon-e>0$, denotes the element difference between the current element ε and the e-th element. Next, we expand the poly-fractonomials ${}^{(2)}\mathcal{P}_{k+1}^{\mu}(\zeta)$ in terms of fractonomials $(1-\zeta)^{\mu+m}$ as

$$
{}^{(2)}\mathcal{P}_{k+1}^{\mu}(\zeta)=(1-\zeta)^{\mu}P_k^{\mu,-\mu}(\zeta)=\sum_{m=0}^{k}C_{km}(1-\zeta)^{\mu+m},
\tag{2.29}
$$

in which $C_{km}=\binom{k+m}{m}\binom{k+\mu}{k-m}(-\frac{1}{2})^m$ is a lower-triangle matrix. Therefore, (2.28) can be written as

$$
H_k^{(\varepsilon,e)}(\xi)=\frac{-\mu}{\Gamma(1-\mu)}(\frac{2}{\Delta x})^{\mu}\sum_{m=0}^{k}C_{km}h_m^{(\varepsilon,e)}(\xi),
\tag{2.30}
$$

where we call

$$
h_m^{(\varepsilon,e)}(\xi)\equiv\int_{-1}^{1}\frac{(1-\zeta)^{\mu+m}}{[2\,\Delta\varepsilon+\zeta-\xi]^{1+\mu}}d\zeta,\quad m=0,1,\cdots,k,
\tag{2.31}
$$

the *(modal) memory mode*. Also, $h_m^{(\varepsilon,e)}(\xi)$ can be obtained analytically as

$$
h_m^{(\varepsilon,e)}(\xi)=\frac{2^{-\mu}(\Delta\varepsilon-\xi/2)^{-\mu}}{1+m+\mu}\Big[h_{m,I}(\xi,\Delta\varepsilon)+h_{m,II}(\xi,\Delta\varepsilon)+h_{m,III}(\xi,\Delta\varepsilon)\Big],
\tag{2.32}
$$

in which

$$
\begin{aligned}
h_{m,I}(\xi,\Delta\varepsilon)&=-Z_I(\xi,\Delta\varepsilon)\;{}_2F_1\Big(1,\,1+m,\,2+m+\mu,\,Z_I(\xi,\Delta\varepsilon)\Big),\\
h_{m,II}(\xi,\Delta\varepsilon)&=\Big(\frac{1-2\Delta\varepsilon+\xi}{-2\Delta\varepsilon+\xi}\Big)^{-\mu}(2^{m+\mu})\;Z_{II}(\xi,\Delta\varepsilon){}_2F_1\Big(1,\,1+m,\,2+m+\mu,\,Z_{II}(\xi,\Delta\varepsilon)\Big),\\
h_{m,III}(\xi,\Delta\varepsilon)&=-Z_{III}(\xi,\Delta\varepsilon){}_2F_1\Big(1,\,1+m,\,2+m+\mu,\,Z_{III}(\xi,\Delta\varepsilon)\Big),
\end{aligned}
\tag{2.33}
$$

and the group variables are $Z_I(\xi,\Delta\varepsilon) = \frac{1}{1+2\Delta\varepsilon-\xi}$, $Z_{II}(\xi,\Delta\varepsilon) = \frac{-2}{-1-2\Delta\varepsilon+\xi}$, and $Z_{III}(\xi,\Delta\varepsilon) = \frac{1}{-2\Delta\varepsilon+\xi}$. Therefore, by (2.30) and obtaining the derivative of basis function in the standard domain, the entries of the history matrix can be efficiently computed, using a Gauss quadrature. Hence:

$$\boxed{\hat{\mathbf{S}}_{kp}^{(\varepsilon,e)} \equiv \hat{\mathbf{S}}_{kp}^{(\Delta\varepsilon)} = \int_{-1}^{1} \frac{d\psi_p}{d\xi} H_k(\xi,\Delta\varepsilon)d\xi, \quad k,p = 0,1,\cdots,P.} \tag{2.34}$$

Remark 2.3.1. *We note that when a uniform mesh is employed, the history function* $H_k^{(\varepsilon,e)}(\xi) \equiv H_k(\xi,\Delta\varepsilon)$*, defined in the standard domain, only depends on the "element difference",* $\Delta\varepsilon = \varepsilon - e$*. This is significant since one only needs to construct* $N_{el} - 1$ *history function, and thus, history matrices* $\hat{\mathbf{S}}^{(e,\varepsilon)}$*.*

2.3.3 Assembling the Global System with Local Test Functions

We generalize the notion of global linear system assembly by taking into account the presence of the history stiffness matrices and recalling that the corresponding local mass matrix $\mathbf{M}^{(\varepsilon)}$ or the local load vector $\mathbf{f}^{(\varepsilon)}$ do not contribute to any history calculations. We impose the $C^0 - continuity$ by employing the "mapping arrays", map[e][p], defined as

$$map[e][p] = P(e-1) + p, \quad p = 1,2,\cdots,P, \quad e = 1,2,\cdots,N_{el}, \tag{2.35}$$

as for instance in Mathematica, the first entry of a vector is labelled by 1 rather than 0 as in C++. Then, the corresponding $(P+1)\times(P+1)$ "local" linear system, which is associated with the element Ω_ε, is obtained as

$$\mathcal{M}^{(\varepsilon)} = \mathbf{S}^{(\varepsilon)} - \lambda\mathbf{M}^{(\varepsilon)}. \tag{2.36}$$

We assemble the corresponding global linear matrix $\mathbb{M}_G$ and the global load vector $\mathbb{F}_G$ as follows:

$do\ \varepsilon = 1, N_{el}$

$do\ k = 1, P+1$

$\mathbb{F}_G\Big[\ map[\varepsilon][k]\ \Big] = \mathbf{f}^{(\varepsilon)}[k]$

$do\ p = 1, P+1$

$\mathbb{M}_G\Big[\ map[\varepsilon][k]\ \Big]\Big[\ map[\varepsilon][p]\ \Big] = \mathbb{M}_G\Big[\ map[\varepsilon][k]\ \Big]\Big[\ map[\varepsilon][p]\ \Big] + \mathcal{M}^{(\varepsilon)}[k][p]$

$do\ e = 1, \varepsilon - 1$

$\mathbb{M}_G\Big[\ map[\varepsilon][k]\ \Big]\Big[\ map[e][p]\ \Big] = \mathbb{M}_G\Big[\ map[\varepsilon][k]\ \Big]\Big[\ map[e][p]\ \Big] + \hat{\mathbf{S}}^{(\Delta\varepsilon)}[k][p]$

End

This global operation leads to the following linear system:

$$\boxed{\mathbb{M}_G\ \hat{u}_G = \mathbb{F}_G,} \tag{2.37}$$

in which $\hat{u}_G$ denotes the global degrees of freedom. The homogeneous Dirichlet boundary conditions require the first and last entries of the global degree of freedom to be zero, i.e. $\hat{u}_0^1 = \hat{u}_P^{N_{el}} = 0$. This is enforced by removing the first and last rows as well as the first and last columns of the global matrix, in addition to removing the first and last entries of the load vector. We also note that the C^0-continuity and decomposition of basis functions into boundary and interior modes lead to the standard scattering process from the global to local degrees of freedom (see e.g., [81]).

2.3.4 Off-Line Computation of History Matrices and History Retrieval

As mentioned in remark 2.3.1 (on uniform grid generation), the history matrices solely depend on the element difference, $\Delta\varepsilon = \varepsilon - e$. Thus, for all local elements ε, where $\varepsilon = 1, 2, \cdots, N_{el}$, the history matrices corresponding to the past element e with similar element difference, are the same. See Fig. 2.4, where similarly-colored blocks represent the same history matrix and one can see that, for example, all the history matrices adjacent to the local stiffness matrices have the same element difference, $\Delta\varepsilon = 1$, and thus are in the same color. Therefore, given number of element N_{el}, we only need to construct the total number of $N_{el} - 1$ history matrices.

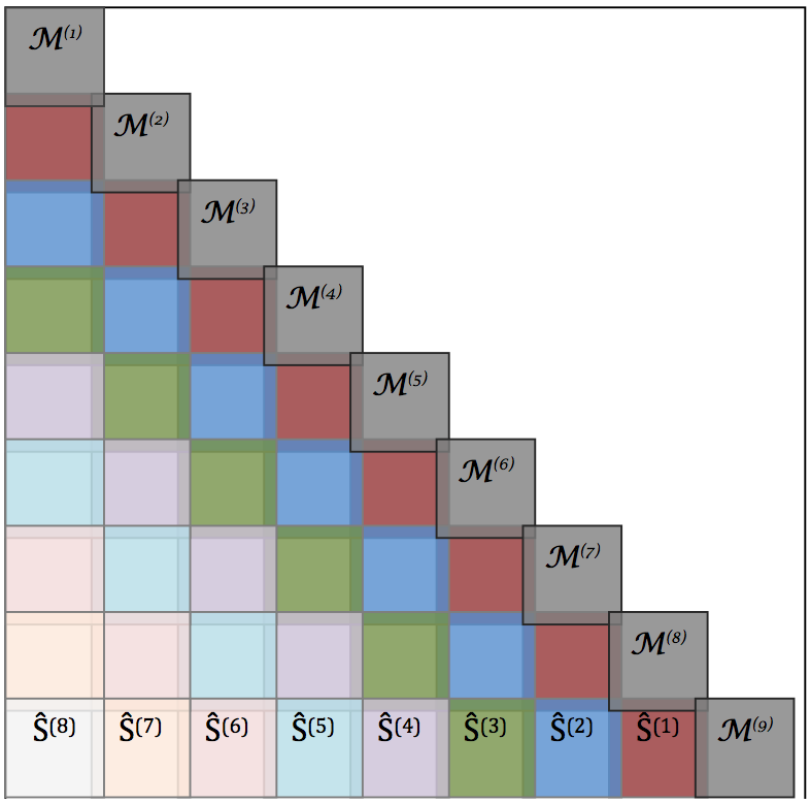

Figure 2.4: The assembled global matrix corresponding to a uniform grid with $N_{el} = 9$. In this global matrix, $\mathcal{M}^{(\varepsilon)} = \mathbf{S}^{(\varepsilon)} - \lambda \mathbf{M}^{(\varepsilon)}$, $\varepsilon = 1, 2, \cdots, N_{el}$, represents the local matrix, associated with the element Ω_ε. To fill the lower-triangular block matrices, we construct only $(N_{el} - 1)$ history matrices $\hat{\mathbf{S}}^{(\Delta\varepsilon)}$, where $\Delta\varepsilon = 1, 2, .., N_{el} - 1$, rather than $\frac{N_{el}(N_{el}-1)}{2}$ matrices.

For a maximum number of elements, $N_{el}|_{max}$, and a maximum number of modes, $P|_{max}$, we can compute off-line and store the total $N_{el}|_{max} - 1$ history matrices of size $(P|_{max}+1)\times(P|_{max}+1)$, which we can fetch later for any specific $N_{el} \leq N_{el}|_{max}$ and $P \leq P|_{max}$.

2.3.5 Non-Uniform Kernel-Based Grids

We present a non-uniform grid generation based on the power-law kernel in the definition of fractional derivative. There are different sources of singularity in the proposed problem that can be caused mainly due to the force function $f(x)$. However, even if the force term is smooth the underlying kernel of a fractional derivative leads to formation of singularities at the boundaries. Herein, we propose a new kernel-based grid generation method that considers a sufficiently small boundary layer at the vicinity of singular point and partitions that particular region non-uniformly. In

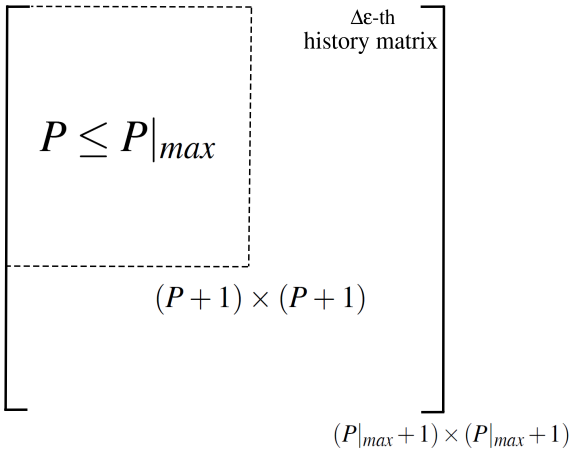

Figure 2.5: History computation and retrieval.

this approach, we treat the kernel of the form $\frac{1}{x^\sigma}$ as a density function and then, we construct the grid such that the integral of kernel function over each element $\Omega_e \in [x_{e-1}, x_e]$ (in the boundary layer) is constant. Since the operator is a left sided fractional derivative, we represent the non-uniform grid

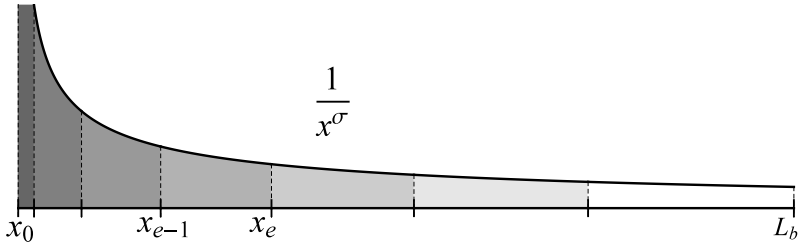

Figure 2.6: Kernel-based non-uniform grid in the boundary layer; L_b and N_b are the length of and the number of elements in the boundary layer, respectively.

refinement at the left boundary. Let L_b be the length of boundary layer and $\int_0^{L_b} \frac{1}{x^\sigma}\, dx = \frac{L_b^{1-\sigma}}{1-\sigma} = A$. Then, the integral over each element is

$$\frac{1}{A} \int_{x_{e-1}}^{x_e} \frac{1}{x^\sigma}\, dx = \frac{1}{L_b^{1-\sigma}} \left[(x_{e-1} + \Delta x_e)^{1-\sigma} - x_{e-1}^{1-\sigma} \right] = C,$$

where $\Delta x_e = x_e - x_{e-1}$ and C is a constant. Thus,

$$\Delta x_e = \left[x_{e-1}^{1-\sigma} + C\, L_b^{1-\sigma} \right]^{\frac{1}{1-\sigma}} - x_{e-1}.$$

Starting from $x_0 = 0$ and calculating the rest of grid locations successively, we obtain

$$x_e = \delta\ e^{\frac{1}{1-\sigma}}, \quad e = 1, 2, \cdots, N_b, \quad \text{element numbers,} \tag{2.38}$$

in which $\delta = L_b\ C^{\frac{1}{1-\sigma}}$ and N_b is the number of elements in the boundary layer. The constant C is obtained by the constraint $\sum_{e=1}^{N_b} \Delta x_e = L_b$ and hence,

$$C = \left(\sum_{e=1}^{N_b} \left[e^{\frac{1}{1-\sigma}} - (e-1)^{\frac{1}{1-\sigma}} \right] \right)^{\sigma-1}.$$

We consider $\sigma = 1 - \mu$ and thus when $\mu = 1$, we recover the uniform grid $x_e = \frac{L_b}{N_b}\, e$, where the kernel is 1, $C = \frac{1}{N_b}$, $\delta = \frac{L_b}{N_b}$. We note that in the boundary layer, where the grid is non-uniform, equations (2.27)-(2.31) no longer hold. Thus, using (2.38), we obtain

$$H_k^{(\varepsilon,e)}(\xi) = \frac{-\mu}{\Gamma(1-\mu)} \frac{\delta}{2} \left(\varepsilon^{\frac{1}{\mu}} - (\varepsilon-1)^{\frac{1}{\mu}} \right) \int_{-1}^{1} \frac{{}^{(2)}\mathcal{P}_{k+1}^{\mu}(\zeta) d\zeta}{\mathcal{Z}}, \tag{2.39}$$

in which,

$$\mathcal{Z} = \left(\frac{\delta}{2} \right)^{1+\mu} \Big[\left(\varepsilon^{\frac{1}{\mu}} + (\varepsilon-1)^{\frac{1}{\mu}} \right) - \left(e^{\frac{1}{\mu}} + (e-1)^{\frac{1}{\mu}} \right) + \left(\varepsilon^{\frac{1}{\mu}} - (\varepsilon-1)^{\frac{1}{\mu}} \right) \zeta - \left(e^{\frac{1}{\mu}} - (e-1)^{\frac{1}{\mu}} \right) \xi \Big]^{1+\mu}.$$

Therefore, by (2.25), the entries of the history matrix for the boundary layer elements, where $\varepsilon = 1, 2, \cdots, N_b$ and $e = 1, 2, \cdots, \varepsilon - 1$, can be numerically obtained as

$$\boxed{\hat{\mathbf{S}}_{kp}^{(\varepsilon,e)} = \int_{-1}^{1} \frac{d\psi_p}{d\xi} H_k^{(\varepsilon,e)}(\xi)\ d\xi, \quad k, p = 0, 1, \cdots, P,} \tag{2.40}$$

These matrices are the small squares in the upper left corner of Fig. 2.7 (interaction of boundary layer elements e and ϵ). For the interior elements, $\varepsilon = N_b + 1, N_b + 2, \cdots, N_{el}$, when $N_b + 1 \le e \le \epsilon - 1$, the grid is uniform and therefore, we use (2.34) to obtain the history matrices. These matrices are shown as the big squares in Fig. 2.7 (interaction of interior elements e and ϵ). However, when $1 \le e \le N_b$, the grid is non-uniform and we use (2.40) to obtain the history matrices. These matrices are shown as skinny rectangles in Fig. 2.7 (interaction of interior elements with boundary layer elements).

In uniform grid generation, the history function (2.28) only depends on element difference $\Delta\epsilon$, which leads to a fast and efficient construction of history matrices (see Remark 2.3.1). However, in

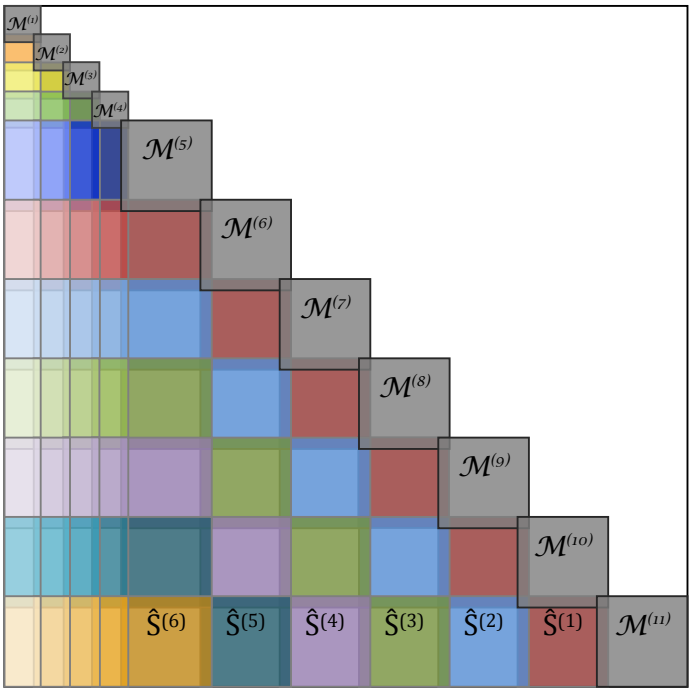

Figure 2.7: The assembled global matrix corresponding to $N_{el} = 11$ with $N_b = 4$ non-uniform boundary elements and 7 uniform interior elements. In this global matrix, $\mathcal{M}^{(\varepsilon)} = \mathbf{S}^{(\varepsilon)} - \lambda \mathbf{M}^{(\varepsilon)}$, $\varepsilon = 1, 2, \cdots, N_{el}$, represents the local matrix, associated with the element Ω_ε. The lower-triangle consists of three parts: 1) The small square $\frac{N_b(N_b-1)}{2}$ history matrices (interaction of boundary elements, $\varepsilon = 1, 2, \cdots, N_b$). 2) The big square history matrices (interaction of interior elements, $\varepsilon = N_b + 1, \cdots, N_{el}$). 3) The skinny rectangular $(N_{el} - N_b)N_b$ history matrices (interaction of boundary elements with interior elements).

non-uniform kernel-based grid generation, this is not the case anymore and construction of history matrices is computationally expensive. Improving the history construction on non-uniform grids requires further investigations, to be done in our future works.

2.3.6 Non-Uniform Geometrically Progressive Grids

In addition to the non-uniform grid generation based on the kernel of fractional derivative, we consider a non-uniform grid using geometrically progressive series [4, 15]. In this case, the length of elements are increased by a constant factor r (see Fig. 2.8). By considering the length of first element to be δ, we construct the grid as $x_0 = 0,\ x_1 = \delta,\ x_2 = \delta(1 + r),\ x_3 = \delta(1 + r + r^2)$ and so

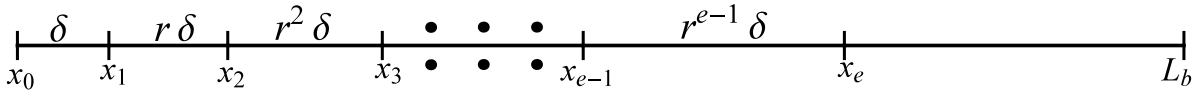

Figure 2.8: Non-uniform geometrically progressive grid.

on. Hence,

$$x_e = \delta \sum_{i=0}^{e-1} r^i = \delta \frac{r^e - 1}{r - 1}, \quad e = 1, 2, \cdots, N_b. \tag{2.41}$$

Choosing r and N_b, the constant δ is obtained by the constraint $x_{N_b} = L_b$, which gives $\delta = L_b \frac{r-1}{r^{N_b}-1}$. Since the grid is non-uniform, equations (2.27)-(2.31) do not hold anymore. Thus, using (2.41), we obtain

$$H_k^{(\varepsilon,e)}(\xi) = \frac{-\mu}{\Gamma(1-\mu)} (\frac{2}{\delta})^{\mu} r^{\Delta\varepsilon - \mu(e-1)} \int_{-1}^{1} \frac{{}^{(2)}\mathcal{P}_{k+1}^{\mu}(\zeta) d\zeta}{\left[\frac{r+1}{r-1}(r^{\Delta\varepsilon} - 1) + (\zeta - r^{\Delta\varepsilon}\xi)\right]^{1+\mu}}, \tag{2.42}$$

where $\Delta\varepsilon = \varepsilon - e > 0$, denotes the *element difference* between the current element ε and the e-th element. Using the same expansion as in (2.29), we can write (2.42) as

$$H_k^{(\varepsilon,e)}(\xi) = \frac{-\mu}{\Gamma(1-\mu)} (\frac{2}{\delta})^{\mu} r^{\Delta\varepsilon - \mu(e-1)} \sum_{m=0}^{k} C_{km} \tilde{h}_m^{(\varepsilon,e)}(\xi), \tag{2.43}$$

where the (modal) memory mode

$$\tilde{h}_m^{(\varepsilon,e)}(\xi) = \int_{-1}^{1} \frac{(1-\zeta)^{\mu+m}}{[\frac{r+1}{r-1}(r^{\Delta\varepsilon} - 1) + (\zeta - r^{\Delta\varepsilon}\xi)]^{1+\mu}} d\zeta, \quad m = 0, 1, \cdots, k, \tag{2.44}$$

can be obtained analytically using hypergeometric functions. Therefore, by (2.43), the entries of the history matrix can be efficiently computed using the Gauss quadrature in (2.34). The construction of the assembled global linear system is the same as kernel-based grid generation approach. We note that similar to uniform grid, in the non-uniform grid generation using the geometrical progression, the history functions depend on the element difference $\Delta\varepsilon = \varepsilon - e$, leading to a fast and efficient construction of history matrices.

2.4 Petrov-Galerkin Method with Global Test Functions

In this section, similar to the case of local test functions, we develop the Petrov-Galerkin scheme by substituting (2.7) into (2.6) and considering the global test function, given in (2.11) to obtain:

$$\begin{aligned}
&\sum_{e=1}^{N_{el}} \Big(\sum_{p=0}^{P} \hat{u}_p^{(e)} \ \frac{d\psi_p(x)}{dx}, \ {}^{RL}_{x}\mathcal{D}^{\mu}_{L} \ v_k^{\varepsilon}(x) \Big)_{\Omega_e} - \lambda \sum_{e=1}^{N_{el}} \Big(\sum_{p=0}^{P} \hat{u}_p^{(e)} \ \psi_p(x), \ v_k^{\varepsilon}(x) \Big)_{\Omega_e} \\
&= \sum_{e=1}^{N_{el}} \Big(f \, , \, v_k^{\varepsilon}(x) \Big)_{\Omega_e}, \quad \varepsilon = 1, 2, \cdots, N_{el}, \quad k = 0, 1, \cdots, P. \qquad (2.45)
\end{aligned}$$

Since the test function vanishes only $\forall x \in \Omega_e \neq \Omega_\varepsilon$ and $e > \varepsilon$, (2.45) reduces to

$$\begin{aligned}
&\sum_{e=1}^{\varepsilon} \sum_{p=0}^{P} \hat{u}_p^{(e)} \Big(\frac{d\psi_p}{dx}, \ {}^{RL}_{x}\mathcal{D}^{\mu}_{x_\varepsilon} \ v_k^{\varepsilon}(x) \Big)_{\Omega_e} - \lambda \sum_{e=1}^{\varepsilon} \sum_{p=0}^{P} \hat{u}_p^{(e)} \Big(\psi_p(x), \ v_k^{\varepsilon}(x) \Big)_{\Omega_e} \\
&= \sum_{e=1}^{\varepsilon} \Big(f \, , \, v_k^{\varepsilon}(x) \Big)_{\Omega_e}.
\end{aligned}$$

By substituting (2.11), we obtain

$$\begin{aligned}
&\sum_{e=1}^{\varepsilon} \sum_{p=0}^{P} \hat{u}_p^{(e)} \Big(\frac{d\psi_p}{dx}, \ {}^{RL}_{x}\mathcal{D}^{\mu}_{x_\varepsilon} \ {}^{(2)}\mathcal{P}^{\mu}_{k+1}(x^{1\sim\varepsilon}) \Big)_{\Omega_e} - \lambda \sum_{e=1}^{\varepsilon} \sum_{p=0}^{P} \hat{u}_p^{(e)} \Big(\psi_p(x), \ {}^{(2)}\mathcal{P}^{\mu}_{k+1}(x^{1\sim\varepsilon}) \Big)_{\Omega_e} \\
&= \int_0^{x_\varepsilon} f(x) \ {}^{(2)}\mathcal{P}^{\mu}_{k+1}(x^{1\sim\varepsilon}) dx, \quad \varepsilon = 1, 2, \cdots, N_{el}, \quad k = 0, 1, \cdots, P,
\end{aligned}$$

which can be written in the matrix form as

$$\sum_{e=1}^{\varepsilon} \sum_{p=0}^{P} \hat{u}_p^{(e)} \ \Big[\hat{\mathbf{S}}_{kp}^{(\varepsilon,e)} - \lambda \ \hat{\mathbf{M}}_{kp}^{(\varepsilon,e)} \Big] = \mathbf{f}_k^{(\varepsilon)}, \quad \varepsilon = 1, 2, \cdots, N_{el}, \quad k = 0, 1, \cdots, P, \qquad (2.46)$$

where

$$\hat{\mathbf{S}}_{kp}^{(\varepsilon,e)} = \Big(\frac{d\psi_p^{\varepsilon}}{dx}, \ {}^{RL}_{x}\mathcal{D}^{\mu}_{x_\varepsilon} \Big[{}^{(2)}\mathcal{P}^{\mu}_{k+1}(x^{1\sim\varepsilon}) \Big] \Big)_{\Omega_\varepsilon}, \qquad (2.47)$$

$$\hat{\mathbf{M}}_{kp}^{(\varepsilon,e)} = \Big(\psi_p^{\varepsilon}(x), \ {}^{(2)}\mathcal{P}^{\mu}_{k+1}(x^{1\sim\varepsilon}) \Big)_{\Omega_\varepsilon}, \qquad (2.48)$$

$$\mathbf{f}_k^{(\varepsilon)} = \int_0^{x_\varepsilon} f \ {}^{(2)}\mathcal{P}^{\mu}_{k+1}(x^{1\sim\varepsilon}) dx. \qquad (2.49)$$

Remark 2.4.1. *The benefit of choosing such global test functions is now clear since we can analytically evaluate* ${}^{RL}_{x}\mathcal{D}^{\mu}_{x_\varepsilon}\ {}^{(2)}\mathcal{P}^{\mu}_{k+1}(x^{1\sim\varepsilon})$. *However, we note that this choice of test functions introduces "extra" work associated with the construction of the "history mass matrix"* $\hat{\boldsymbol{M}}^{(\varepsilon,e)}$, $\forall e = 1, 2, \cdots, \varepsilon - 1$, *when* $\lambda \neq 0$.

Remark 2.4.2. *The choice of global test functions leads to extra cost of quadrature carried out over the increasing-in-length domains of integration in* (2.49). *Depending on the behaviour of the force-term* $f(x)$*, this approach might require adaptive/multi-element quadrature rules to obtain the corresponding entries of the desired precision.*

2.4.1 Elemental (Local) Operations: the construction of $\mathbf{f}^{(\varepsilon)}$

Here, the construction of the load vector is the only operation that could be regarded as "local operations". Hence,

$$\begin{aligned}\mathbf{f}^{(\varepsilon)}_{k} &= \int_0^{x_\varepsilon} f(x)\ {}^{(2)}\mathcal{P}^{\mu}_{k+1}(x^{1\sim\varepsilon})dx \\ &= (\frac{x_\varepsilon}{2})\int_{-1}^{1}(1-\zeta)^{\mu} f(\,x^{1\sim\varepsilon}(\zeta)\,)\,P^{\mu,-\mu}_{k}(\zeta)d\zeta,\end{aligned}$$

and thus,

$$\boxed{\mathbf{f}^{(\varepsilon)}_{k} = (\frac{x_\varepsilon}{2})\sum_{q=1}^{Q} w^{\mu,0}_{q}\ f(\,x^{1\sim\varepsilon}(\zeta_q)\,)\,P^{\mu,-\mu}_{k}(\,z^{\mu,0}_{q}\,),}$$

where $\{w^{\mu,0}_{q}\,,\, z^{\mu,0}_{q}\}^{Q}_{q=1}$ are the Gauss-Lobatto-Jacobi weights and points corresponding to the parameters $\alpha = \mu$ and $\beta = 0$.

2.4.2 Global Operations: the construction of $\hat{\mathbf{S}}^{(\varepsilon,e)}$ and $\hat{\mathbf{M}}^{(\varepsilon,e)}$

The corresponding stiffness and mass matrices are global in nature and we obtain their entries using proper Gauss quadrature rules.

2.4.3 Assembling the Global System with Global Test Functions

We extend the notion of global linear system assembly by taking into account the presence of the history stiffness and mass matrices. We similarly impose the $C^0 - continuity$ by employing the same "mapping arrays", $map[e][p]$, defined in (2.35). Let us define the $(P+1)\times(P+1)$ matrix

$$\hat{\mathcal{M}}^{(\varepsilon,e)} = \hat{\mathbf{S}}^{(\varepsilon,e)} - \lambda\hat{\mathbf{M}}^{(\varepsilon,e)}, \tag{2.50}$$

$\forall\varepsilon$, e fixed. Then, we assemble the corresponding global linear matrix $\mathbb{M}_G$ and the global load vector $\mathbb{F}_G$ as follows:

$do\ \varepsilon = 1, N_{el}$

$do\ k = 1, P+1$

$\mathbb{F}_G\Big[\ map[\varepsilon][k]\ \Big] = \mathbf{f}^{(\varepsilon)}[k]$

$do\ p = 1, P+1$

$do\ e = 1, \varepsilon$

$\mathbb{M}_G\Big[\ map[\varepsilon][k]\ \Big]\Big[\ map[e][p]\ \Big] = \mathbb{M}_G\Big[\ map[\varepsilon][k]\ \Big]\Big[\ map[e][p]\ \Big] + \hat{\mathcal{M}}^{(\varepsilon,e)}[k][p]$

End

This leads to a linear system similar to that in (2.37), shown in Fig. 2.9, where the homogeneous Dirichlet boundary conditions are enforced in a similar fashion as before. We note that the scattering operation from global to local degrees of freedom is similar to the standard scattering process.

2.5 Numerical Examples

We consider numerical examples of the two PG schemes we have proposed. We provide examples of smooth and singular solutions with singularities at boundary points and in the interior domain, where we show the efficiency of developed schemes in capturing the singularities. We also perform the off-line computation of history matrices and show the improvement of computational cost. Moreover, we construct non-uniform kernel-based and geometrically progressive grids and present the success of the two approaches in capturing singular solutions. Furthermore, we

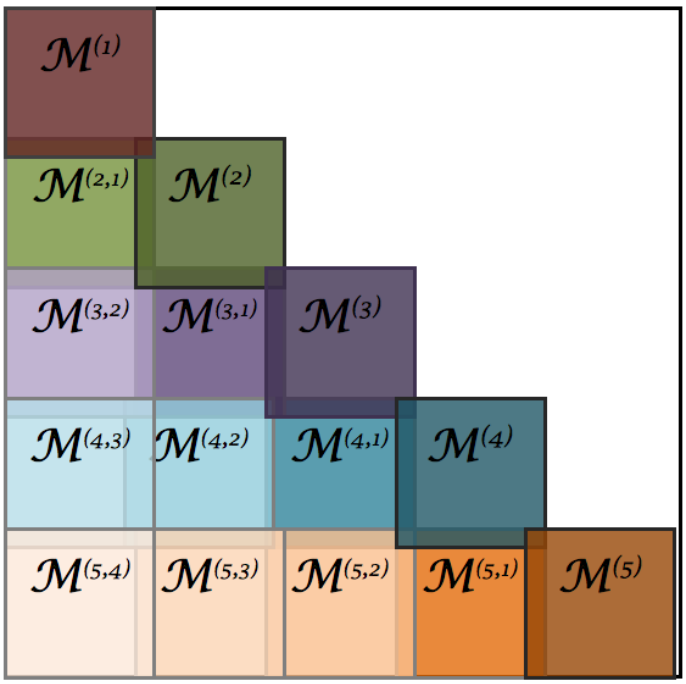

Figure 2.9: The assembled global matrix corresponding to $N_{el} = 5$ elements when global test functions are employed. In this global matrix, $\mathcal{M}^{(\varepsilon)} = \hat{\mathbf{S}}^{(\varepsilon)} - \lambda\hat{\mathbf{M}}^{(\varepsilon)}$, $\varepsilon = 1, 2, \cdots, N_{el}$, represents the local matrix, associated with the element Ω_ε. To fill the lower-triangular block matrices, we must construct $\frac{N_{el}(N_{el}-1)}{2}$ history matrices $\hat{\mathbf{S}}^{(\varepsilon,e)}$.

investigate the non-local effects for different cases of history fading. In this section, we consider the computational domain $L = 1$.

2.5.1 Smooth Problems

In the proposed schemes, the choice of basis functions are polynomials, enabling the scheme to accurately and efficiently approximate the smooth solutions over the whole domain. We consider two smooth solutions of the form $u^{ext} = x^7 - x^6$ and $u^{ext} = x^6 \sin(2\pi x)$. The corresponding force functions are obtained by substituting the exact solutions into (2.1) (with $\lambda = 0$). By employing PG SEM, using local basis/test functions and local basis with global test functions (developed in Sec. 2.3 and Sec. 2.4, respectively), we observe that the former leads to a better approximability and condition number. Fig. 2.10 presents the L_2-norm error of the PG SEM, employing local basis/test functions, where we show the exponential convergence of the scheme in approximating the two

smooth solutions. The condition number of the resulting assembled global matrix, using the two developed schemes are also presented in Table 2.1. We show that the choice of local bases/test functions leads to a better conditioning for different number of elements and modes.

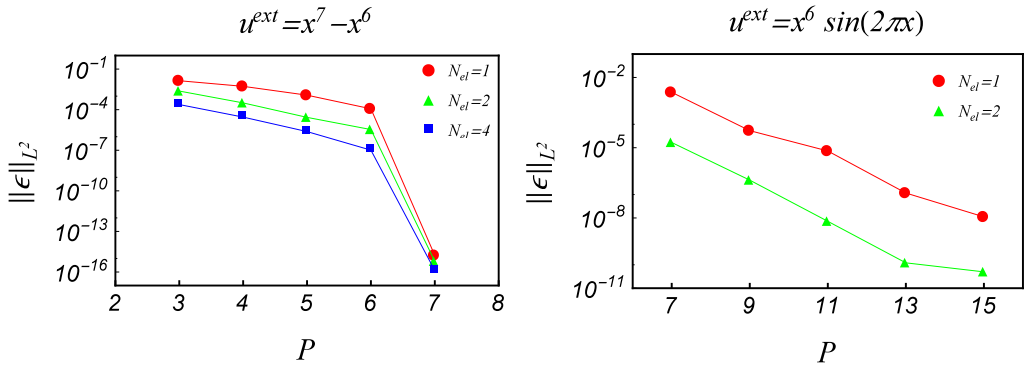

Figure 2.10: PG SEM with local basis/test functions. Plotted is the error with respect to the polynomial degree of each element (spectral order).

Table 2.1: Condition number of the resulting assembled global matrix for the two choices of local bases/test functions (left) and local bases with global test functions (right) for different number of elements and modes.

(Local Test Functions)			(Global Test Function)		
P	$N_{el}=2$	$N_{el}=10$	P	$N_{el}=2$	$N_{el}=10$
3	7.13	86.13	3	3.46×10^{4}	1.84×10^{16}
5	13.21	153.86	5	4.3×10^{7}	7.2×10^{16}
10	35.39	420.24	10	2.73×10^{15}	5.1×10^{17}

2.5.2 History Retrieval

As discussed in Sec. 2.3.4, a large number of history matrices can be computed off-line, stored, and retrieved for later use. The retrieval process, compared to on-line construction of the history matrices, leads to higher computational efficiency. In this section, by considering 1000 elements, we compute and store 999 history matrices for different number of modes, $P = 2, 3$, and 4 (here $\mu = \frac{1}{2}$). Then, for different number of elements, we compute the CPU time required for constructing and solving the linear system, obtained by retrieving the stored history matrices from hard drive.

We also compute the CPU time required for constructing and solving the linear system, obtained by on-line computation of the history matrices. Table 2.2 shows that in the case of $p = 4$ and for $N_{el} = 10$, $N_{el} = 100$, $N_{el} = 500$, and $N_{el} = 1000$, the retrieval process is almost 4, 5, and 10 times faster, respectively. Thus, the higher p is, the faster and more efficient the retrieval becomes.

Table 2.2: CPU time of constructing and solving the linear system based on off-line retrieval and on-line calculation of history matrices.

CPU Time

	$N_{el} = 10$		$N_{el} = 100$		$N_{el} = 500$		$N_{el} = 1000$	
P	Off-line retrieval	On-line computation	Off-line retrieval	On-line computation	Off-line retrieval	On-line computation	Off-line retrieval	On-line computation
2	2.6520	7.2540	24.7105	83.5229	141.3525	429.3147	370.6895	790.3478
3	4.7580	18.9073	46.0826	161.8042	266.0441	1308.8327	746.4959	4423.7671
4	8.8140	32.2922	84.8645	499.9988	485.7715	5599.4062	1392.8705	14709.4902

2.5.3 Singular Problems

The developed PG spectral element method, compared to single-domain spectral methods, further leads to accurate solutions even in the presence of singularities via *hp*-refinements at the vicinity of singularities, while still employing smooth polynomial bases. The error in the boundary layer is controlled by considering sufficient number of modes in the boundary layer elements. The error in the interior domain is then improved by performing p-refinement in those elements. In order to investigate the performance of the scheme in capturing a singularity, we consider three types of singularities, including: i) single-boundary singularity, ii) full-boundary singularity, and iii) interior singularity (when discontinuous force functions are applied).

I) Single-Boundary Singularity: we consider two singular solutions of the form $u^{ext} = (1 - x)x^{2+\mu}$ and $u^{ext} = (1 - x)x^{5+\mu}$ with left boundary singularity. We partition the domain into two non-overlapping elements, including one boundary element of length L_b at the vicinity of singular point in addition to an interior element for the rest of computational domain. The schematic of corresponding global system is shown in Fig. 2.11 (left). Table 2.3 shows the exponential convergence of L_2-norm error in the interior domain. The error in the boundary layer

element is then controlled by choosing sufficient number of modes in the boundary element. The results are obtained for the two cases of $L_b = 10^{-2}L$ and $L_b = 10^{-4}L$.

Table 2.3: Single-Boundary Singularity: L_2-norm error in the boundary and interior elements using PG SEM with local basis/test functions. Here, L_b represents the size of left boundary element, P_b and P_I denote the number of modes in the boundary and interior elements respectively.

$u^{ext} = (1-x)x^{2+\mu}, \quad \mu = 1/2$

Boundary Element Error			
P_b	$L_b = 10^{-1}L$	$L_b = 10^{-2}L$	$L_b = 10^{-4}L$
6	1.29387×10^{-7}	1.29634×10^{-10}	1.19525×10^{-16}
10	1.46601×10^{-8}	1.4193×10^{-11}	4.07955×10^{-18}
Interior Element Error, $P_b = 10$			
P_I	$L_b = 10^{-1}L$	$L_b = 10^{-2}L$	$L_b = 10^{-4}L$
6	5.49133×10^{-6}	2.6893×10^{-5}	3.38957×10^{-5}
10	9.39045×10^{-8}	1.08594×10^{-6}	1.91087×10^{-6}
14	8.27224×10^{-8}	1.13249×10^{-7}	3.02065×10^{-7}

$u^{ext} = (1-x)x^{5+\mu}, \quad \mu = 1/2$

Boundary Element Error			
P_b	$L_b = 10^{-1}L$	$L_b = 10^{-2}L$	$L_b = 10^{-4}L$
6	3.94221×10^{-11}	2.96862×10^{-17}	4.8243×10^{-29}
10	7.07024×10^{-13}	2.54089×10^{-18}	2.26939×10^{-29}
Interior Element Error, $P_b = 10$			
P_I	$L_b = 10^{-1}L$	$L_b = 10^{-2}L$	$L_b = 10^{-4}L$
6	1.73622×10^{-5}	3.80264×10^{-5}	4.13249×10^{-5}
10	1.3122×10^{-9}	8.76951×10^{-9}	1.10139×10^{-8}
14	4.39611×10^{-12}	1.07775×10^{-10}	1.66044×10^{-10}

II) Full-Boundary Singularity: we consider the solution of the form $u^{ext} = (1-x)^{3+\mu_1}x^{3+\mu_2}$ with singular points at two ends, i.e. $x = 0$ and $x = 1$. Herein, we partition the domain into three non-overlapping elements including two boundary elements of length L_b in the vicinity of singular points, and one interior element for the rest of domain. The schematic of corresponding global system is shown in Fig. 2.11 (right). Similar to previous example, the PG SEM can accurately capture the singularities at both ends, where increasing the number of modes in the interior element results in exponential convergence. Table 2.4 shows the L_2-norm error in the boundary layers and interior elements with two choices of $P_b = 6$, 10 and $L_b = 10^{-2}L$, $10^{-4}L$.

Table 2.4: Full-Boundary Singularity: L_2-norm error in the boundary element (BE) and interior element (IE) by PG SEM with local basis/test functions. Here, $u^{ext} = (1-x)^{3+\mu_1} x^{3+\mu_2}$ with $\mu_1 = \frac{1}{4}$, $\mu_2 = \frac{2}{3}$, L_b represents the size of left and right boundary elements, P_b and P_I denote the number of modes in the boundary and interior elements respectively.

$L_b = 10^{-2}L$

$P_b = 6$

P_I	Left BE Error	IE Error	Right BE Error
6	2.73893×10^{-7}	6.52605×10^{-5}	3.51075×10^{-6}
10	2.46964×10^{-11}	1.52215×10^{-7}	2.2902×10^{-9}
14	3.08719×10^{-12}	9.30483×10^{-9}	2.69541×10^{-10}

$P_b = 10$

P_I	Left BE Error	IE Error	Right BE Error
6	2.73892×10^{-7}	6.52605×10^{-5}	3.51075×10^{-6}
10	2.48058×10^{-11}	1.52215×10^{-7}	2.29003×10^{-9}
14	3.19684×10^{-12}	9.30511×10^{-9}	2.69506×10^{-10}

$L_b = 10^{-4}L$

$P_b = 6$

P_I	Left BE Error	IE Error	Right BE Error
6	3.61679×10^{-10}	5.85397×10^{-5}	4.60538×10^{-8}
10	1.2676×10^{-10}	2.43295×10^{-7}	1.62151×10^{-10}
14	1.53993×10^{-13}	2.09933×10^{-8}	1.97677×10^{-11}

$P_b = 10$

P_I	Left BE Error	IE Error	Right BE Error
6	3.61679×10^{-10}	5.85397×10^{-5}	4.60538×10^{-8}
10	1.2676×10^{-12}	2.43295×10^{-7}	1.62151×10^{-10}
14	1.53993×10^{-13}	2.09933×10^{-8}	1.97677×10^{-11}

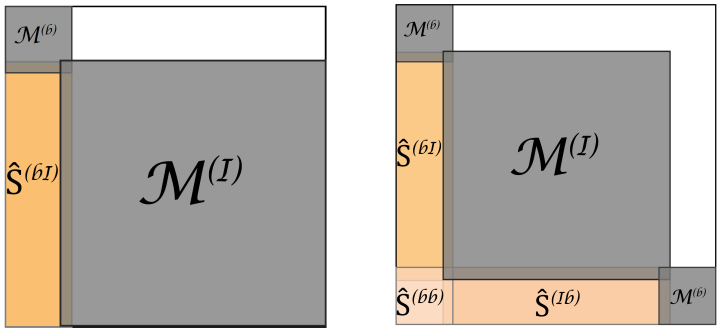

Figure 2.11: Schematic of global matrices corresponding to the case of singular solutions. (left): left boundary singularity, (right): left and right boundary singularities. $\hat{S}^{(bI)}$, $\hat{S}^{(Ib)}$, and $\hat{S}^{(bb)}$ denote the interaction of boundary/interior, interior/boundary and boundary/boundary elements, respectively.

III) Interior Singularity (Discontinuous Force Function)**:** we consider the solutions with singularity in the middle of domain. The force function, obtained by substituting the solution into (2.1), is considered to be discontinuous at the point of singularity. Fig. 2.12 shows the two exact solutions of the form $u_1^{ext} = x^2\,(1-x)^2\,|x-\frac{1}{2}|$ (top) and $u_2^{ext} = sin(3\pi\,x)\,x\,(1-x)\,|x-\frac{1}{2}|$ (bottom) and their corresponding force functions. We partition the domain at the vicinity of singular point using two non-overlapping interior elements, in which the solution is smooth. The PG scheme with local basis/test functions is shown to be able to accurately capture the singularity in the middle of the domain. In the case of u_1^{ext}, we approximate the solution in the range of machine precision with

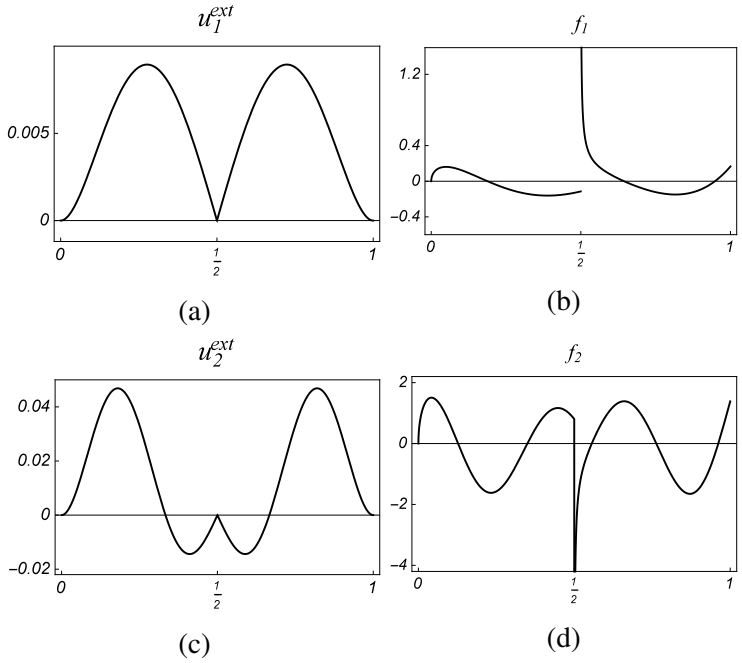

Figure 2.12: Interior Singularity. (left): exact solutions, (right): the corresponding force functions.

$P = 5$ within each element. We also show the exponential rate of convergence in the case of u_2^{ext} by increasing the number of modes, P, in each element. The results are shown in Fig. 2.13.

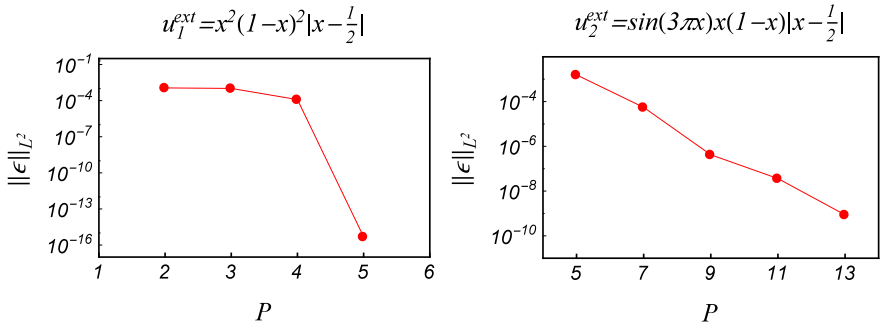

Figure 2.13: Interior Singularity: PG SEM with local basis/test functions. Plotted is the error with respect to spectral order in each element.

2.5.4 Non-Uniform Grids

We consider a singular solution of the form $u^{ext} = (1 - x)x^{1+\mu}$ (here $\mu = \frac{1}{10}$ and $\lambda = 0$) with singularity at the left boundary. In order to solve the problem, we consider three grid generation approaches with similar degrees of freedom, including one uniform and two non-uniform grids

over the computational domain. The non-uniform grids are generated based on the power-law kernel in the definition of fractional derivative and the geometric progression series (discussed in Sec.2.3.5 and Sec.2.3.6, respectively). Here, we choose $L_b = L$. Table 2.5 shows the L_2-norm error considering the uniform and non-uniform grids. We keep the total degrees of freedom fixed, but we increase the polynomial order P in each simulation. The success of the non-uniform grid in providing more accurate results is observed, where fewer number of elements are used, while higher order polynomial are employed. We recall that the size of boundary layer has been set to its maximum possible length, i.e. $L_b = L$. Clearly, one can obtain even more accurate results when L_b is set to much smaller length (e.g. $10^{-1}L$, $10^{-3}L$, *etc.*).

Table 2.5: L_2-norm error, using uniform and non-uniform grids. The exact singular solution is $u^{ext} = (1-x)x^{1+\mu}$ with $\mu = 1/10$.

	Uniform Grid	Kernel-Based Non-Uniform Grid	Geometrically Progressive Non-Uniform Grid
$N_{el} = 50$, $P = 2$	5.83943×10^{-4}	2.33461×10^{-5}	3.93956×10^{-4}
$N_{el} = 25$, $P = 4$	3.04739×10^{-5}	1.77458×10^{-7}	1.38755×10^{-6}
$N_{el} = 10$, $P = 10$	1.39586×10^{-5}	2.10813×10^{-9}	1.45695×10^{-9}

2.5.5 A Systematic Memory Fading Analysis

In order to investigate the effect of truncating the history matrices, we perform a systematic memory fading analysis.

In *full* memory fading, we fade the memory by truncating the history matrices, i.e., we consider the full history matrices up to some specific number and then truncate the rest of history. For instance, we consider up to the first 4 history matrices for each element and thus compute $\hat{\mathbf{S}}^1$, $\hat{\mathbf{S}}^2$, $\hat{\mathbf{S}}^3$ and $\hat{\mathbf{S}}^4$, and truncate the rest $N_{el} - 1 - 4$ matrices; see Fig. 2.4 for better visualization.

In *partial* memory fading, we fade the memory by partially computing the history matrices. Similar to the *full* memory fading, we consider the full history matrices up to some specific number, however, for the rest of history matrices we partially compute the entries of matrices. In partial memory fading, we consider three different cases as follows.

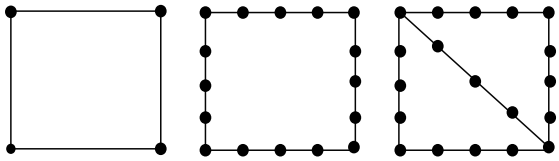

(a) : Case I (b) : Case II (c) : Case III

Figure 2.14: Memory fading: (a) B-B interaction, the corner entries (b) B-B and B-I interaction, the boundary entries (c) B-B, B-I and S-I interaction, boundary and diagonal entries

- **Case I:** Boundary-Boundary (B-B) interaction. In this case, we only consider the interactions of boundary mode and boundary test functions, i.e., $p = 0, P$ and $k = 0, P$, and thus, only compute the corner entries (See Fig. 2.14a).

- **Case II:** Boundary-Boundary (B-B) and Boundary-Interior (B-I) interaction. In addition to the corner entries, here we also consider the interaction of boundary mode/test functions with the interior test/mode functions, i.e.,

$$\begin{cases} k = 0, \quad p = 0, 1, \cdots, P, \quad \text{and} \quad k = P, \quad p = 0, 1, \cdots, P \\ p = 0, \quad k = 0, 1, \cdots, P, \quad \text{and} \quad p = P, \quad k = 0, 1, \cdots, P, \end{cases}$$

  and thus, we compute the boundary entries (See Fig. 2.14b).

- **Case III:** Boundary-Boundary (B-B), Boundary-Interior (B-I), Self-Interior (S-I) interaction. In addition to the last two cases, we consider the interaction of each mode with its corresponding test function and thus, we compute the boundaries as well as the diagonal entries (See Fig. 2.14c).

Tables 2.6 and 2.7 show the L_2-norm error for cases of full and partial memory fading. It is clear from the computed norms that even in the case of fading memory, we can still accurately obtain the approximation solution, however with a proportional loss of accuracy depending on the lack of modal interaction.

Table 2.6: Full history fading: L_2-norm error using PG SEM with local basis/test functions, where $u^{ext} = x^7 - x^6$, $N_{el} = 19$, $P = 6$. The first column in the table shows the number of fully faded history matrices.

Full fading

# faded history matrices	$\mu = 1/10$	$\mu = 1/2$	$\mu = 9/10$
0	9.26034×10^{-12}	2.31391×10^{-11}	4.24903×10^{-9}
2	7.8905×10^{-11}	1.26365×10^{-10}	4.25456×10^{-9}
5	1.42423×10^{-8}	6.39474×10^{-8}	1.95976×10^{-8}
8	2.69431×10^{-7}	2.47423×10^{-6}	8.45001×10^{-7}
11	2.09737×10^{-6}	3.19995×10^{-5}	1.37959×10^{-5}
14	9.07427×10^{-6}	2.44911×10^{-4}	1.40684×10^{-4}
17	2.94001×10^{-5}	1.39043×10^{-3}	1.6001×10^{-3}

Table 2.7: Partial history fading: L_2-norm error using PG SEM with local basis/test functions, where $u^{ext} = x^7 - x^6$, $N_{el} = 19$, $P = 6$. The first column in the tables shows number of partially faded history matrices.

Partial fading case I

# faded history matrices	$\mu = 1/10$	$\mu = 1/2$	$\mu = 9/10$
0	9.26034×10^{-12}	2.31391×10^{-11}	4.24903×10^{-9}
2	7.8905×10^{-11}	1.26365×10^{-10}	4.25456×10^{-9}
5	1.42423×10^{-8}	6.39474×10^{-8}	1.95976×10^{-8}
8	2.69431×10^{-7}	2.47423×10^{-6}	8.45001×10^{-7}
11	2.09737×10^{-6}	3.19995×10^{-5}	1.37959×10^{-5}
14	9.07427×10^{-6}	2.44911×10^{-4}	1.40684×10^{-4}
17	2.94001×10^{-5}	1.39043×10^{-3}	1.6001×10^{-3}

Partial fading case II

# faded history matrices	$\mu = 1/10$	$\mu = 1/2$	$\mu = 9/10$
0	9.26034×10^{-12}	2.31391×10^{-11}	4.24903×10^{-9}
2	9.27241×10^{-12}	2.34361×10^{-11}	4.2491×10^{-9}
5	3.37716×10^{-11}	6.6476×10^{-10}	4.44832×10^{-9}
8	3.8092×10^{-10}	1.99961×10^{-8}	1.36941×10^{-8}
11	1.47228×10^{-9}	2.2715×10^{-7}	1.47786×10^{-7}
14	1.15821×10^{-8}	1.64103×10^{-6}	1.47098×10^{-6}
17	5.06103×10^{-7}	7.87929×10^{-6}	1.85274×10^{-5}

Partial fading case III

# faded history matrices	$\mu = 1/10$	$\mu = 1/2$	$\mu = 9/10$
0	9.26034×10^{-12}	2.31391×10^{-11}	4.24903×10^{-9}
2	9.26023×10^{-12}	2.3113×10^{-11}	4.24903×10^{-9}
5	1.18462×10^{-11}	7.7854×10^{-11}	4.23683×10^{-9}
8	1.60656×10^{-10}	3.38055×10^{-9}	3.65689×10^{-9}
11	1.32413×10^{-9}	4.35421×10^{-8}	8.84638×10^{-9}
14	7.10271×10^{-9}	3.87096×10^{-7}	1.7226×10^{-7}
17	2.87023×10^{-8}	3.71057×10^{-6}	5.12104×10^{-6}

CHAPTER 3

DISTRIBUTED-ORDER FRACTIONAL ODES: PETROV-GALERKIN AND SPECTRAL COLLOCATION METHOD

3.1 Background

Distributed order fractional operators offer a rigorous tool for mathematical modeling of multi-physics phenomena. In this case, the differential order is distributed over a range of values rather than being just a fixed fraction as it is in standard/fractional ODEs/PDEs. There is a rapidly growing interest in the use of fractional derivatives in the construction of mathematical models, which contain distributed order terms of the form

$$\int_{\sigma_1}^{\sigma_2} \phi(\sigma)\, {}_a^*\mathcal{D}_t^{\sigma} u(t) d\sigma = f(t), \quad t > a,$$

in the field of uncertainty quantification as the inherent uncertainty of experimental data can be directly incorporated into the differential operators; see [6, 12, 47, 114, 154], for some work on numerical methods. Almost all of the numerical schemes developed for such models are finite-difference methods. While the treatment of fractional differential equations with a fixed fractional order could be memory demanding due to the locality of these methods and their low-accuracy, the main challenge remains the additional effect of the discretization of the distributed order model, which may lead to exceeding computational cost of numerical simulations.

To the best of our knowledge, the first numerical study of distributed order differential equations (DODEs) was performed by Diethelm and Ford in [46], where a two-stage basic framework was developed. In the first stage, the distributed order differentiation term was approximated using a quadrature rule, and in the second stage, a suitable multi-term numerical method was employed. They later performed the corresponding error analysis of the method in [49]. Subsequently, most of the numerical studies have followed the same approach yet they vary in the discretization method in the second stage. The distributed order time-fractional diffusion equation was numerically studied in [57] and the corresponding stability and convergence study of the scheme was provided in

[58]. Adding a nonlinear source, [124] studied the distributed order reaction diffusion equation following the same scheme. In [98], the second stage of the distributed order diffusion equation was established using a reproducing kernel method. The distributed order time fractional diffusion-wave equation was investigated by developing a compact difference scheme in [179]. Other numerical studies include: an implicit numerical method of a temporal distributed order and two-sided space-fractional advection-dispersion equation in [69], high-order difference schemes in [60], alternating direction implicit (ADI) difference schemes with the extrapolation method for one-dimensional case in [62] and two-dimensional problem in [61], and an operational matrix technique in [50].

Two new spectral theories on fractional and tempered fractional Sturm-Liouville problems (TFSLPs) have been recently developed by Zayernouri et al. in [183, 186]. This approach first fractionalizes and then tempers the well-known theory of Sturm-Liouville eigen-problems. The explicit eigenfunctions of TFSLPs are analytically obtained in terms of *tempered Jacobi poly-fractonomials*. Recently, in [185, 187, 188], Jacobi poly-fractonomials were successfully employed in developing a series of high-order and efficient Petrov-Galerkin spectral and discontinuous spectral element methods of Galerkin and Petrov-Galerkin projection type for fractional ODEs. To treat nonlinear problems the *collocation* schemes are relatively easy to implement. Khader in [83] presented a Chebyshev collocation method for the discretization of the space-fractional diffusion equation. More recently, Khader and Hendy [84] developed a Legendre pseudospectral method for fractional-order delay differential equations. For fast treatment of nonlinear and multi-term fractional PDEs such as the fractional Burgers' equation, a new spectral method, called *fractional spectral collocation method*, was developed in [189]. This new class of collocation schemes introduces a new family of fractional Lagrange interpolants, mimicking the structure of the Jacobi poly-fractonomials. For variable-order fractional PDEs, a fast and spectrally accurate collocation method was developed and implemented in [190].

In this chapter, we first introduce the *distributed Sobolev spaces* and their associated norms. We show their equivalence to the defined left-side and right-side norms as well. By employing Riemann-Liouville derivatives, we define the distributed order differential equation and then obtain

its variational form. We develop a Petrov-Galerkin (PG) spectral method following the recent theory of fractional Sturm-Liouville eigen-problems (FSLP) in [186] and employ the corresponding eigenfunctions, namely the *Jacobi Poly-fractonomial*s of first kind as the bases and the *Jacobi Poly-fractonomial*s of second kind as test functions. We develop a spectrally accurate Gauss-Legendre quadrature rule in the construction of the linear system, where we investigate the stability and error analysis of the scheme. In addition, we construct a spectrally-accurate fractional spectral collocation scheme, where we employ fractional Lagrange interpolants satisfying the Kronecker delta property at the collocation points, and then, we obtain the corresponding fractional differentiation matrices. We demonstrate the computational efficiency of both schemes considering several numerical examples and distribution functions.

The organization of this chapter is as follows: section 3.2 provides preliminary definitions along with useful lemmas. We recall fractional Sobolev spaces, and then, introduce their generalization to so called *distributed Sobolev space* and associated norms, which provides the natural setting of our problem in this study. We furthermore obtain some equivalent norms to facilitate the corresponding analysis of our methods. In section 3.3, we derive and discretize the corresponding variational form of the problem and subsequently we prove the stability and convergence rate of the scheme. In addition, we develop a fractional collocation method in section 3.5 and test the performance of the two methods in section 3.6.

3.2 Preliminaries

Lemma 3.2.1. *Let $\sigma, \mu > 0$. The fractional derivative of the Jacobi poly-fractonomials, [186], of first ($i = 1$) and second kind ($i = 2$) are given by*

$$ {}^{RL}\mathcal{D}^{\sigma}\left\{ {}^{(i)}\mathcal{P}_n^{\mu}(\xi)\right\} = \frac{\Gamma(n+\mu)}{\Gamma(n+\mu-\sigma)}\, {}^{(i)}\mathcal{P}_n^{\mu-\sigma}(\xi), \tag{3.1} $$

and are also of Jacobi poly-fractonomial type, where ${}^{RL}\mathcal{D}^{\sigma} \equiv {}^{RL}_{-1}\mathcal{D}^{\sigma}_{x}$ when $i = 1$, ${}^{RL}\mathcal{D}^{\sigma} \equiv {}^{RL}_{x}\mathcal{D}^{\sigma}_{1}$ when $i = 2$.

Proof. See section (3.7.1).

□

Remark 3.2.2. *Lemma 3.2.1 shows that the structure of Jacobi poly-fractonomials is preserved under the action of fractional derivatives. Moreover, we note that when $\sigma = \mu$ in Lemma 3.2.1, the fractional derivatives of Jacobi poly-fractonomials are obtained in terms of Legendre polynomials, which has been reported in [186].*

3.2.1 Fractional Sobolev Spaces

By $H^s(\mathbb{R})$, $s \geq 0$, we denote the fractional Sobolev space on $\mathbb{R}$, defined as

$$H^s(\mathbb{R}) = \{v \in L^2(\mathbb{R}) |\ (1 + |\omega|^2)^{\frac{s}{2}} \mathcal{F}(v)(\omega) \in L^2(\mathbb{R})\}, \tag{3.2}$$

which is endowed with the norm

$$\|\cdot\|_{s,\mathbb{R}} = \|(1 + |\omega|^2)^{\frac{s}{2}} \mathcal{F}(\cdot)(\omega)\|_{L^2(\mathbb{R})}, \tag{3.3}$$

where $\mathcal{F}(v)$ represents the Fourier transform of v. Subsequently, we denote by $H^s(I)$, $s \geq 0$ the fractional Sobolev space on any finite closed interval I, defined as

$$H^s(I) = \{v \in L^2(I) |\ \exists \tilde{v} \in H^s(\mathbb{R})\ \ s.t.\ \ \tilde{v}|_I = v\}, \tag{3.4}$$

with the norm

$$\|\cdot\|_{s,I} = \inf_{\tilde{v} \in H^s(\mathbb{R}), \tilde{v}|_I = (\cdot)} \|\tilde{v}\|_{s,\mathbb{R}}. \tag{3.5}$$

We note that the definition of $H^s(I)$ and the corresponding norm relies on the Fourier transformation of the function. Other useful norms associated with $H^s(I)$, e.g., when $I = [x_L, x_R]$, have been also introduced in [99],

$$\|\cdot\|_{l,s,I} = \left(\|\cdot\|^2_{L^2(I)} + \|\, {}^{RL}_{x_L}\mathcal{D}^{\mu}_{x}(\cdot)\|^2_{L^2(I)}\right)^{\frac{1}{2}}, \tag{3.6}$$

$$\|\cdot\|_{r,s,I} = \left(\|\cdot\|^2_{L^2(I)} + \|\, {}^{RL}_{x}\mathcal{D}^{\mu}_{x_R}(\cdot)\|^2_{L^2(I)}\right)^{\frac{1}{2}}, \tag{3.7}$$

such that the left-side $\|\cdot\|_{l,s,I}$, the right-sided $\|\cdot\|_{r,s,I}$, and $\|\cdot\|_{s,I}$ are shown to be equivalent.

Next, let $\phi \in L^1([\alpha_{min}, \alpha_{max}])$, $0 \leq \alpha_{min} < \alpha_{max}$, be nonnegative. By ${}^{\phi}\mathcal{H}(\mathbb{R})$, we denote the *distributed* fractional Sobolev space on $\mathbb{R}$, defined as

$$ {}^{\phi}\mathcal{H}(\mathbb{R}) = \{v \in L^2(\mathbb{R}) | \int_{\alpha_{min}}^{\alpha_{max}} \left[\phi(\alpha)(1+|\omega|^2)^{\alpha}\right]^{\frac{1}{2}} \mathcal{F}(v)(\omega)\, d\alpha \in L^2(\mathbb{R})\}, \tag{3.8} $$

which is endowed with the norm

$$ \|\cdot\|_{\phi,\mathbb{R}} = \left(\int_{\alpha_{min}}^{\alpha_{max}} \phi(\alpha) \left\| (1+|\omega|^2)^{\frac{\alpha}{2}} \mathcal{F}(\cdot)(\omega) \right\|_{L^2(\mathbb{R})}^2 d\alpha\right)^{\frac{1}{2}}. \tag{3.9} $$

3.2.2 Distributed Fractional Sobolev Spaces

We denote by ${}^{\phi}\mathcal{H}(I)$ the *distributed* fractional Sobolev space on the finite closed interval I, defined as

$$ {}^{\phi}\mathcal{H}(I) = \{v \in L^2(I) | \ \exists \tilde{v} \in {}^{\phi}\mathcal{H}(\mathbb{R}) \ \ s.t. \ \ \tilde{v}|_I = v\}, \tag{3.10} $$

with the norm

$$ \|\cdot\|_{\phi,I} = \inf_{\tilde{v} \in {}^{\phi}\mathcal{H}(\mathbb{R}), \tilde{v}|_I = (\cdot)} \|\tilde{v}\|_{\phi,\mathbb{R}}. \tag{3.11} $$

Moreover, we introduce the following useful norms, associated with ${}^{\phi}\mathcal{H}(I)$:

$$ \|\cdot\|_{l,\phi,I} = \left(\|\cdot\|_{L^2(I)}^2 + \int_{\alpha_{min}}^{\alpha_{max}} \phi(\alpha) \left\| {}^{RL}_{x_L}\mathcal{D}_x^{\alpha}(\cdot) \right\|_{L^2(I)}^2 d\alpha\right)^{\frac{1}{2}}, \tag{3.12} $$

and

$$ \|\cdot\|_{r,\phi,I} = \left(\|\cdot\|_{L^2(I)}^2 + \int_{\alpha_{min}}^{\alpha_{max}} \phi(\alpha) \left\| {}^{RL}_{x_L}\mathcal{D}_x^{\alpha}(\cdot) \right\|_{L^2(I)}^2 d\alpha\right)^{\frac{1}{2}}. \tag{3.13} $$

We note that when $\phi > 0$ is continuous in I, ${}^{\phi}\mathcal{H}(\mathbb{R})$ is equivalent to $H^{\alpha_{max}}(\mathbb{R})$. However, in general, the choice of ϕ can arbitrarily confine the domain of integration in practice. In other words, α_{min} and α_{max} are only the theoretical lower and upper terminals in the definition of distributed order fractional derivative. For instance, in a distributed sub-diffusion problem, the temporal derivative is associated with $\alpha_{min} = 0$ and $\alpha_{max} = 1$, and in a super-diffusion problem, the theoretical upper terminal $\alpha_{max} = 2$. In this study we particularly aim to let ϕ be defined in any possible subset of the interval $[\alpha_{min}, \alpha_{max}]$. Hence, in each realization of a physical process (e.g.

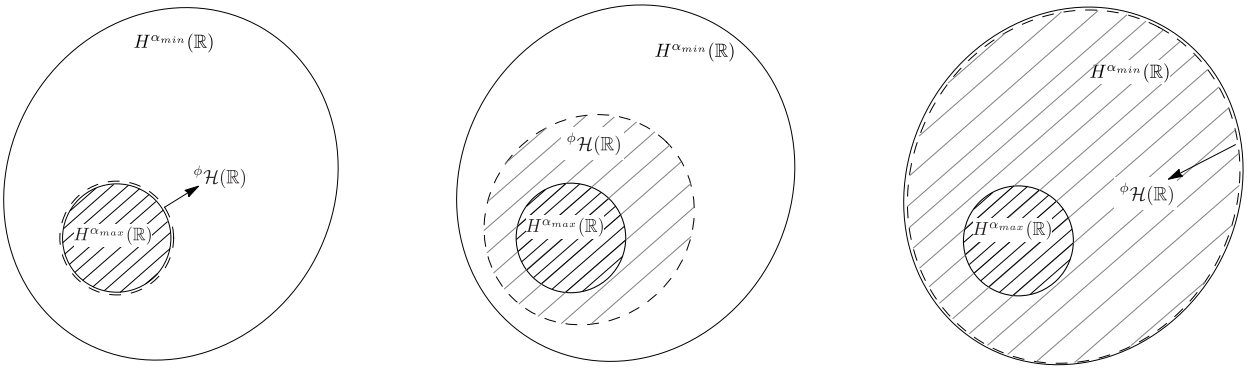

Figure 3.1: Schematic of distributed fractional Sobolev space ${}^{\phi}\mathcal{H}(\mathbb{R})$: (left) $\phi = \delta(\alpha - \alpha_{max})$ hence ${}^{\phi}\mathcal{H}(\mathbb{R}) = H^{\alpha max}(\mathbb{R})$; (middle) ϕ defined on a compact support in $[\alpha_{min}, \alpha_{max}]$, hence, ${}^{\phi}\mathcal{H}(\mathbb{R}) \supset H^{\alpha max}(\mathbb{R})$; (right) $\phi = \delta(\alpha - \alpha_{min})$, where ${}^{\phi}\mathcal{H}(\mathbb{R}) = H^{\alpha min}(\mathbb{R})$.

sub- or super-diffusion) ϕ can be obtained from data, where the theoretical setting of the problem remains invariant yet requiring the solution to have less regularity (since ${}^{\phi}\mathcal{H}(\mathbb{R}) \supset H^{\alpha max}(\mathbb{R})$ in general, see Fig.3.1).

In the following theorem, we prove the equivalence (shown by the notation $\sim$) of the aforementioned norms.

Theorem 3.2.3. *Let $\phi \in L^1([\alpha_{min}, \alpha_{max}])$ be non-negative. Then, the norms $\|\cdot\|_{\phi,I}$, $\|\cdot\|_{l,\phi,I}$, and $\|\cdot\|_{r,\phi,I}$ are equivalent.*

Proof. See section (3.7.2). □

Lemma 3.2.4. *[99]: For all $0 < \alpha \leq 1$, if $u \in H^1([a,b])$ such that $u(a) = 0$, and $w \in H^{\alpha/2}([a,b])$, then*

$$({}_a\mathcal{D}_s^{\alpha} u, w)_{\Omega} = ({}_a\mathcal{D}_s^{\alpha/2} u\,,\, {}_s\mathcal{D}_b^{\alpha/2} w)_{\Omega}, \tag{3.14}$$

where $(\cdot,\cdot)_{\Omega}$ represents the standard inner product in $\Omega = [a,b]$.

Lemma 3.2.5. *Let $1/2 < \mu < 1$, a and b be arbitrary finite or infinite real numbers. Assume $u \in H^{2\mu}(a,b)$ such that $u(a) = 0$, also ${}_x\mathcal{D}_b^{\mu} v$ is integrable in (a,b) such that $v(b) = 0$. Then*

$$({}_a\mathcal{D}_x^{2\mu} u\,,\, v) = ({}_a\mathcal{D}_x^{\mu} u\,,\, {}_x\mathcal{D}_b^{\mu} v). \tag{3.15}$$

Proof. See section (3.7.3). □

Remark 3.2.6. *Unlike other existing proofs (e.g., see Proposition 1 in [197]), our proof requires $v(x)$ to only vanish at the right boundary (note that $v(a)$ can be non-zero), moreover, we only require the μ-th derivative (rather than the first derivative) of $v(x)$ to be integrable in (a, b).*

3.3 Distributed-Order Differential Equations: Problem Definition

Following [11], let $\alpha \mapsto \phi(\alpha)$ be a continuous mapping in $[\alpha_{min}, \alpha_{max}]$. Then, we define the distributed order fractional derivative as

$$ {}^{D}\mathcal{D}_{\phi} u(t) = \int_{\alpha_{min}}^{\alpha_{max}} \phi(\alpha)\, {}_{a}^{*}\mathcal{D}_{t}^{\alpha} u(t) d\alpha, \quad t > a, \tag{3.16} $$

where ${}_{a}^{*}\mathcal{D}_{t}^{\alpha}$ denotes Riemann-Liouville fractional derivative of order α. Next, we aim to solve the following differential equation of distributed order:

$$ {}^{D}\mathcal{D}_{\phi} u(t) = f(t; u), \quad \forall t \in (0, T], \tag{3.17} $$

$$ u(0) = 0, \quad (\alpha_{max}) \in (0, 1], \tag{3.18} $$

$$ u(0) = \frac{du}{dt}|_{t=0} = 0, \quad (\alpha_{max}) \in (1, 2]. \tag{3.19} $$

In the sequel, we present different approaches to discretize the aforementioned differential operator. Due to (1.22), the Caputo and Riemann-Liouville fractional derivatives of order $\alpha \in (0, 1)$ coincide with each other when $u(a) = 0$. Therefore, in this study, we employ the definition of the distributed fractional derivatives of Riemann-Liouville sense and remove the pre-superscript *RL* for simplicity.

3.3.1 Variational Formulation

In order to obtain the variational form we multiply (4.6) by a proper test function v (defined later) and integrate over the computational domain:

$$ \int_{\Omega} {}^{D}\mathcal{D}_{\phi} u(t)\, v(t)\, d\Omega = \int_{\Omega} f(t; u)\, v(t)\, d\Omega. \tag{3.20} $$

Using the definition of distributed order fractional derivatives defined in (5.7) we get

$$\int_{\alpha_{min}}^{\alpha_{max}} \phi(\alpha) \int_{\Omega} {}_0\mathcal{D}_t^{\alpha} u(t)\, v(t)\, d\Omega\, d\alpha = \int_{\Omega} f(t;u)\, v(t)\, d\Omega, \tag{3.21}$$

where

$$\forall \alpha \in (\alpha_{min}, \alpha_{max}), \quad \int_{\Omega} {}_0\mathcal{D}_t^{\alpha} u\, v\, d\Omega = \left({}_0\mathcal{D}_t^{\alpha} u, v\right)_{\Omega}$$

denotes the well-known L^2-inner product. Given the initial conditions (4.7) and/or (4.8) and by Lemmas (7.3.3), we define the bilinear form associated with $\alpha \in (\alpha_{min}, \alpha_{max})$ as

$$a^{(\alpha)}(u, v) = \left({}_0\mathcal{D}_t^{\alpha} u, v\right)_{\Omega} = ({}_0\mathcal{D}_t^{\alpha/2} u, {}_t\mathcal{D}_T^{\alpha/2} v)_{\Omega}. \tag{3.22}$$

We choose v such that $v(T) = 0$ and ${}_t\mathcal{D}_T^{\alpha/2} v$ is integrable in $\Omega \;\; \forall \alpha \in (\alpha_{min}, \alpha_{max})$. Moreover, let U be the solution space, defined as

$$U = \{u \in L^2(\Omega) : \quad \sqrt{\int_{\alpha_{min}}^{\alpha_{max}} \phi(\alpha) \left\| {}_0\mathcal{D}_t^{\alpha/2} u \right\|_{L^2(\Omega)}^2 d\alpha} < \infty \tag{3.23}$$

$$s.t. \quad \begin{array}{ll} u(0) = 0 & \text{if } \alpha_{max} \in (0, 1] \\ u(0) = \frac{du}{dt}|_{t=0} = 0 & \text{if } \alpha_{max} \in (1, 2] \end{array} \Bigg\}$$

and let V be the test function space given by

$$V = \{v \in L^2(\Omega) : \sqrt{\int_{\alpha_{min}}^{\alpha_{max}} \phi(\alpha) \left\| {}_t\mathcal{D}_T^{\alpha/2} v \right\|_{L^2(\Omega)}^2 d\alpha} < \infty \quad s.t. \quad v(T) = 0\}. \tag{3.24}$$

The problem thus reads as: find $u \in U$ such that $a(u, v) = l(v), \quad \forall v \in V$ where

$$a(u, v) := \int_{\alpha_{min}}^{\alpha_{max}} \phi(\alpha)\; a^{(\alpha)}(u, v)\, d\alpha \tag{3.25}$$

denotes the *distributed* bilinear form and $l(v) := (f, v)_{\Omega}$.

3.4 Petrov-Galerkin Method: Modal Expansion

In the Petrov-Galerkin (PG) method, we follow the recent theory of fractional Sturm-Liouville eigen-problems (FSLP) in [186] and employ the corresponding eigenfunctions, known as the *Jacobi Poly-fractonomial*s (of first kind) given in the standard domain $[-1, 1]$ by

$$ {}^{(1)}\mathcal{P}_n^{\mu}(\xi) = (1+\xi)^{\mu} P_{n-1}^{-\mu,\mu}(\xi), \quad \xi \in [-1, 1], \tag{3.26} $$

as *non-polynomial* basis functions consisting of a fractional term multiplied by the Jacobi polynomial $P_{n-1}^{-\mu,\mu}(\xi)$, hence we employ (3.26) in construction of a basis to formulate a projection type scheme, namely *modal* expansion. We represent the solution in terms of the elements of the basis space U_N given as follows

$$ U_N = span\big\{ {}^{(1)}\mathcal{P}_n^{\mu}(\xi), \quad \xi \in [-1, 1], \quad n = 1, 2, \cdots, N\big\}, \tag{3.27} $$

via the poly-fractonomial *modal* expansion as

$$ u_N(\xi) = \sum_{n=1}^{N} c_n \, {}^{(1)}\mathcal{P}_n^{\mu}(\xi), \tag{3.28} $$

in which μ is to be fixed as a fractional parameter *a priori* depending on the range of distribution order interval, i.e. $\mu \in (0, 1)$ if $\alpha_{max} \in (0, 1]$ and $\mu \in (1, 2)$ if $\alpha_{max} \in (1, 2]$. It can also be tunned to capture possible singularities in the exact solution if some knowledge about that is available.

Moreover, in the PG scheme, we employ another space of test functions V_N, however of the same dimension, given by

$$ V_N = span\big\{ {}^{(2)}\mathcal{P}_k^{\mu}(\xi), \quad \xi \in [-1, 1], \quad k = 1, 2, \cdots, N\big\}, \tag{3.29} $$

in which ${}^{(2)}\mathcal{P}_k^{\mu}(\xi) = (1-\xi)^{\mu} P_{k-1}^{\mu,-\mu}(\xi)$ denotes the Jacobi poly-fractonomial of second kind, which is the explicit eigenfunction of fractional Sturm-Liouville problem of second kind in [186].

It should be noted that since $\phi(\alpha) \geq 0$ and $\int_{\alpha_{min}}^{\alpha_{max}} \phi(\alpha)\, d\alpha = 1$ it is not difficult to see that $U_N \subset U$ and $V_N \subset V$ when μ is chosen properly. Therefore, the bilinear form (7.28) reduces to the *discrete* bilinear form

$$a_h^{\alpha}(u_N, v_N) = ({}_0\mathcal{D}_t^{\alpha/2} u_N, {}_t\mathcal{D}_T^{\alpha/2} v_N)_{\Omega} \tag{3.30}$$

and thus the problem reads as: find $u_N \in U_N$ such that

$$a_h(u_N, v_N) = l_h(v_N), \quad \forall v_N \in V_N, \tag{3.31}$$

where $a_h(u_N, v_N) := \int_{\alpha_{min}}^{\alpha_{max}} \phi(\alpha)\ a_h^{\alpha}(u_N, v_N)\, d\alpha$ denotes the *discrete* distributed bilinear form and $l_h(v_N) := (f, v_N)_{\Omega}$ represents the load vector.

By substituting the expansion (3.28), choosing $v_N = {}^{(2)}\mathcal{P}_k^{\mu}(\xi) \in V_N$, $k = 1, 2, \cdots, N$ and using (1.21), the discrete distributed bilinear form in (4.23) can be written as

$$\int_{\alpha_{min}}^{\alpha_{max}} \phi(\alpha)\ \sum_{n=1}^{N} c_n (\frac{2}{T})^{\alpha} \Big({}_{-1}\mathcal{D}_{\xi}^{\alpha/2} [{}^{(1)}\mathcal{P}_n^{\mu}(\xi)],\ {}_{\xi}\mathcal{D}_1^{\alpha/2} [{}^{(2)}\mathcal{P}_k^{\mu}(\xi)] \Big)_{\Omega} d\alpha. \tag{3.32}$$

From Lemma 3.2.1, we have

$$\begin{aligned} {}_{-1}\mathcal{D}_{\xi}^{\alpha/2} [{}^{(1)}\mathcal{P}_n^{\mu}(\xi)] &= \frac{\Gamma(n+\mu)}{\Gamma(n+\eta)}\, {}^{(1)}\mathcal{P}_n^{\eta}(\xi) && (3.33) \\ {}^{RL}_{\xi}\mathcal{D}_1^{\alpha/2} [{}^{(2)}\mathcal{P}_k^{\mu}(\xi)], &= \frac{\Gamma(k+\mu)}{\Gamma(k+\eta)}\, {}^{(2)}\mathcal{P}_k^{\eta}(\xi), && (3.34) \end{aligned}$$

where $\eta = \mu - \alpha/2$. Thus, by changing the order of summation, the integral (3.32) takes the form

$$\begin{aligned} &\sum_{n=1}^{N} c_n \int_{\alpha_{min}}^{\alpha_{max}} \phi(\alpha)\ (\frac{2}{T})^{\alpha} \frac{\Gamma(n+\mu)}{\Gamma(n+\eta)} \frac{\Gamma(k+\mu)}{\Gamma(k+\eta)} \Big({}^{(1)}\mathcal{P}_n^{\eta}(\xi), {}^{(2)}\mathcal{P}_k^{\eta}(\xi) \Big)_{\Omega} d\alpha && (3.35) \\ &= \sum_{n=1}^{N} c_n \int_{\alpha_{min}}^{\alpha_{max}} \phi(\alpha) (\frac{2}{T})^{\alpha} \frac{\Gamma(n+\mu)}{\Gamma(n+\eta)} \frac{\Gamma(k+\mu)}{\Gamma(k+\eta)} \int_{-1}^{1} {}^{(1)}\mathcal{P}_n^{\eta}(\xi)\ {}^{(2)}\mathcal{P}_k^{\eta}(\xi)\ d\xi\, d\alpha, \end{aligned}$$

where by changing the order of integrations we get

$$\begin{aligned} &a_h(u_N, v_N) && (3.36) \\ &= \sum_{n=1}^{N} c_n \int_{-1}^{1} \left[\int_{\alpha_{min}}^{\alpha_{max}} \phi(\alpha) (\frac{2}{T})^{\alpha} \frac{\Gamma(n+\mu)}{\Gamma(n+\eta)} \frac{\Gamma(k+\mu)}{\Gamma(k+\eta)}\, {}^{(1)}\mathcal{P}_n^{\eta}(\xi)\ {}^{(2)}\mathcal{P}_k^{\eta}(\xi)\ d\alpha \right] d\xi. \end{aligned}$$

Theorem 3.4.1 (Spectrally/Exponentially Accurate Quadrature Rule in α-Dimension)**.** *Part A:* $\forall \xi = \xi_0 \in [-1,1]$ *fixed, and* $\forall n \in \mathbb{N} \cup \{0\}$*, the Jacobi polynomial* $P_n^{\pm\alpha,\mp\alpha}(\xi_0)$ *is a polynomial of order n in* α*.*

Part B: Let $\phi \in H^r([\alpha_{min}, \alpha_{max}])$*,* $r > 0$*. Then* $\forall \mu \geq \alpha_{max}/2$

$$\left| \int_{\alpha_{min}}^{\alpha_{max}} \phi(\alpha) \left(\frac{2}{T}\right)^{\alpha} \frac{\Gamma(n+\mu)}{\Gamma(n+\eta)} \frac{\Gamma(k+\mu)}{\Gamma(k+\eta)} \, {}^{(1)}\mathcal{P}_n^{\eta}(\xi) \; {}^{(2)}\mathcal{P}_k^{\eta}(\xi) \; d\alpha - \right.$$
$$\left. \sum_{q=1}^{Q} \widetilde{w}_q \, \phi(\alpha_q) \left(\frac{2}{T}\right)^{\alpha q} \frac{\Gamma(n+\mu)}{\Gamma(n+\eta_q)} \frac{\Gamma(k+\mu)}{\Gamma(k+\eta_q)} \, {}^{(1)}\mathcal{P}_n^{\eta q}(\xi) \; {}^{(2)}\mathcal{P}_k^{\eta q}(\xi) \right| \leq \mathscr{C} \, Q^{-r} \, \|\phi\|_{H^r([\alpha_{min},\alpha_{max}])},$$

where $\mathscr{C} > 0$*,* $\phi_N(\alpha) = \sum_{n=0}^{N} \widetilde{\rho}_n \, P_n(\alpha)$ *denotes the polynomial expansion of* $\phi(\alpha)$*, and* $\{\alpha_q, \widetilde{w}_q\}\Big|_{q=1}^{Q}$ *represents the set of Gauss-Legendre quadrature points and weights.*

Part C: If $\phi(\alpha)$ *is smooth, the quadrature rule in* α*-dimension becomes exponentially accurate in* Q*.*

Proof. See section (3.7.4).

□

By theorem (4.3.2) and performing an affine mapping from $[\alpha \in \alpha_{min}, \alpha_{max}]$ to the standard domain $\alpha_{st} \in [-1,1]$, the inner integral in (3.36) can be evaluated with spectral accuracy by employing a Gauss-Legendre quadrature rule. Then by changing the order of summation and integral $a_h(u_N, v_N) = l_h(v_N)$ can be written as:

$$\sum_{n=1}^{N} \sum_{j=1}^{Q} c_n \, J_\alpha \, w_j \, \phi_j \left(\frac{2}{T}\right)^{\alpha_j} \frac{\Gamma(n+\mu)}{\Gamma(n+\eta_j)} \frac{\Gamma(k+\mu)}{\Gamma(k+\eta_j)} \int_{-1}^{1} {}^{(1)}\mathcal{P}_n^{\eta_j}(\xi) \; {}^{(2)}\mathcal{P}_k^{\eta_j}(\xi) \; d\xi \tag{3.37}$$
$$= \left(f \, , \, {}^{(2)}\mathcal{P}_k^{\mu}(\xi) \right)_{\Omega}, \qquad k = 1, 2, ..., N,$$

where $J_\alpha = \frac{d\alpha}{d\alpha_{st}} = \frac{(\alpha_{max} - \alpha_{min})}{2}$ is constant and $\alpha_j = \alpha(\alpha_{st_j})$, $\phi_j = \phi(\alpha(\alpha_{st_j}))$, $\eta_j = \mu - \alpha_j/2$ and α_{st_j} and w_j are the quadrature points and weights respectively. The linear system is then constructed as

$$\mathcal{S}\vec{c} = \vec{\mathcal{F}}, \tag{3.38}$$

in which the entries of the stiffness matrix $\mathcal{S}$ and force vector $\vec{\mathcal{F}}$ are given by

$$\mathcal{S}_{kn} = \sum_{j=0}^{Q-1} J_\alpha \, w_j \, \phi_j \, (\frac{2}{T})^{\alpha_j} \; C_{kn} \int_{-1}^{1} {}^{(1)}\mathcal{P}_n^{\eta_j}(\xi) \, {}^{(2)}\mathcal{P}_k^{\eta_j}(\xi) d\xi \tag{3.39}$$

and

$$\mathcal{F}_k = \int_{-1}^{1} f(\xi) \, {}^{(2)}\mathcal{P}_k^{\mu}(\xi) \; d\xi \tag{3.40}$$

respectively, where

$$C_{kn} \equiv \frac{\Gamma(n+\mu)}{\Gamma(n+\eta_j)} \frac{\Gamma(k+\mu)}{\Gamma(k+\eta_j)}.$$

Remark 3.4.2. *For each fixed j and given the structure of ${}^{(1)}\mathcal{P}_n^{\eta_j}(\xi)$ and ${}^{(2)}\mathcal{P}_k^{\eta_j}(\xi)$, the above integrations take the form*

$$\begin{aligned} \int_{-1}^{1} {}^{(1)}\mathcal{P}_n^{\eta_j}(\xi) \, {}^{(2)}\mathcal{P}_k^{\eta_j}(\xi) d\xi &= \int_{-1}^{1} (1-\xi)^{\eta_j} (1+\xi)^{\eta_j} \; P_{k-1}^{\eta_j,-\eta_j}(\xi) \; P_{n-1}^{-\eta_j,\eta_j}(\xi) \; d\xi, \\ \int_{-1}^{1} f(\xi) \, {}^{(2)}\mathcal{P}_k^{\mu}(\xi) \; d\xi &= \int_{-1}^{1} (1-\xi)^{\mu} \; f(\xi) \; P_{k-1}^{\mu,-\mu}(\xi) \; d\xi, \end{aligned}$$

and therefore, the full stiffness matrix $\mathcal{S}$ and vector $\vec{\mathcal{F}}$ can be constructed accurately using a proper Gauss-Lobatto-Jacobi rule corresponding to the weight function $(1-\xi)^{\eta_j}(1+\xi)^{\eta_j}$ and $(1-\xi)^{\mu}$ respectively.

3.4.1 Discrete Stability Analysis

In this section, we investigate the stability of the numerical scheme, developed based on the aforementioned choice of solution and test function space considering the bilinear form in (4.23).

Theorem 3.4.3. *The scheme* (4.23) *is stable and the following inequality holds*

$$\inf_{u_N \in U_N} \sup_{v_N \in V_N} \frac{a_h(u_N, v_N)}{\|u_N\|_{U_N} \; \|v_N\|_{V_N}} \geq \beta.$$

Proof. Recalling from (4.15)

$$a_h(u_N, v_N) = \int_{\alpha_{min}}^{\alpha_{max}} \phi(\alpha) a_h^{\alpha}(u_N, v_N) \; d\alpha,$$

where, by lemma (3.2.1),

$$a_h^\alpha(u_N, v_N) = a_h^\alpha(\sum_{n=1}^{N} a_n\, {}^{(1)}\mathcal{P}_n^\mu(\xi), \sum_{k=1}^{N} a_k\, {}^{(2)}\mathcal{P}_k^\mu(\xi)), \quad \forall \alpha \in (\alpha_{min}, \alpha_{max}),$$
$$= \sum_{n=1}^{N}\sum_{k=1}^{N} a_n a_k C_{n,k}^{\mu,\alpha} \int_{-1}^{1} (1-\xi)^{\tilde{\mu}}(1+\xi)^{-\tilde{\mu}}(1+\xi)^{2\tilde{\mu}} P_{k-1}^{\tilde{\mu},-\tilde{\mu}}(\xi)\; P_{n-1}^{-\tilde{\mu},\tilde{\mu}}(\xi)\; d\xi,$$

in which, $\tilde{\mu} = \mu - \alpha/2$, $C_{n,k}^{\mu,\alpha} = \frac{\Gamma(n+\mu)}{\Gamma(n+\tilde{\mu})}\frac{\Gamma(k+\mu)}{\Gamma(k+\tilde{\mu})}$ and $(1+\xi)^{\tilde{\mu}}$ is replaced by $(1+\xi)^{-\tilde{\mu}}(1+\xi)^{2\tilde{\mu}}$. We let $\tilde{\mu} > -1/2$, hence the function $(1+\xi)^{2\tilde{\mu}}$ is nonnegative, nondecreasing, continuous and integrable in the integration domain. Therefore,

$$a_h^\alpha(u_N, v_N) \geq \sum_{n=1}^{N}\sum_{k=1}^{N} a_n a_k C_{n,k}^{\mu,\alpha} C_0 \int_{-1}^{1} (1-\xi)^{\tilde{\mu}}(1+\xi)^{-\tilde{\mu}} P_{k-1}^{\tilde{\mu},-\tilde{\mu}}(\xi) P_{n-1}^{-\tilde{\mu},\tilde{\mu}}(\xi)\; d\xi.$$

Moreover, the Jacobi polynomial $P_{n-1}^{-\tilde{\mu},\tilde{\mu}}(\xi)$ can be expanded as:

$$P_{n-1}^{-\tilde{\mu},\tilde{\mu}}(\xi) = \sum_{j=0}^{n-1} \binom{n-1+j}{j}\binom{n-1+\tilde{\mu}}{n-1-j}(-1)^{j-n+1}(\frac{1}{2})^j(1+\xi)^j.$$

By multiplying and dividing each term within the summation by $\binom{n-1-\tilde{\mu}}{n-1-j}$ we get

$$P_{n-1}^{-\tilde{\mu},\tilde{\mu}}(\xi) = \sum_{j=0}^{n-1} \mathcal{A}_{n,j}^{\tilde{\mu}} \binom{n-1+j}{j}\binom{n-1-\tilde{\mu}}{n-1-j}(-1)^{j-n+1}(\frac{1}{2})^j(1+\xi)^j,$$

where $\mathcal{A}_{n,j}^{\tilde{\mu}} = \binom{n-1+\tilde{\mu}}{n-1-j}/\binom{n-1-\tilde{\mu}}{n-1-j}$ is nondecreasing, positive and bounded $\forall n, j, \tilde{\mu}$. Therefore, there exists $C_1 = C_1(n) > 0$ such that

$$a_h^\alpha(u_N, v_N) \geq \sum_{n=1}^{N}\sum_{k=1}^{N} a_n a_k\, C_{n,k}^{\mu,\alpha}\, C_0\, C_1(n) \int_{-1}^{1} (1-\xi)^{\tilde{\mu}}(1+\xi)^{-\tilde{\mu}} P_{k-1}^{\tilde{\mu},-\tilde{\mu}}(\xi) P_{n-1}^{\tilde{\mu},-\tilde{\mu}}(\xi)\; d\xi$$
$$\geq C_0 \sum_{k=1}^{N} a_k^2\; C_{k,k}^{\mu,\alpha}\, C_1(n)\, \epsilon_{k-1}^{\tilde{\mu},-\tilde{\mu}},$$

in which $\epsilon_{k-1}^{\tilde{\mu},-\tilde{\mu}} = \frac{2}{2k-1}\frac{\Gamma(k+\mu)\,\Gamma(k-\mu)}{(k-1)!\,\Gamma(k)}$. Hence,

$$a_h(u_N, v_N) \geq C_0 \int_{\alpha_{min}}^{\alpha_{max}} \phi(\alpha)\; \sum_{k=1}^{N} a_k^2\, C_{k,k}^{\mu,\alpha}\, C_1(n)\, \epsilon_{k-1}^{\tilde{\mu},-\tilde{\mu}}\; d\alpha. \tag{3.41}$$

Moreover, we have

$$\|v_N\|^2_{V_N} = \int_{\alpha_{min}}^{\alpha_{max}} \phi(\alpha) \ \left\| {}_{-1}\mathcal{D}_x^{\alpha/2} v_N \right\|^2_{L^2(\Omega)} d\alpha,$$

where by considering $v_n = \sum_{k=1}^{N} a_k \ {}^{(2)}\mathcal{P}_k^{\mu}(\xi)$, we can write $\forall \alpha \in (\alpha_{min}, \alpha_{max})$,

$$\begin{aligned}
\left\| {}_{-1}\mathcal{D}_x^{\alpha/2} v_N \right\|^2_{L^2(\Omega)} &= \int_{-1}^{1} \Big(\sum_{k=1}^{N} a_k \ \frac{\Gamma(k+\mu)}{\Gamma(k+\tilde{\mu})} (1-\xi)^{\tilde{\mu}} P_{k-1}^{\tilde{\mu},-\tilde{\mu}}(\xi) \Big)^2 d\xi, \\
&\leq \int_{-1}^{1} \sum_{k=1}^{N} a_k^2 \ \left(\frac{\Gamma(k+\mu)}{\Gamma(k+\tilde{\mu})} \right)^2 (1-\xi)^{2\tilde{\mu}} (P_{k-1}^{\tilde{\mu},-\tilde{\mu}}(\xi))^2 d\xi, \\
&\quad \text{(By Jensen Inequality).}
\end{aligned}$$

By multiplying the integrand by $(1+\xi)^{-\tilde{\mu}}(1+\xi)^{\tilde{\mu}}$ and changing the order of summation and integration, we obtain

$$\begin{aligned}
\left\| {}_{-1}\mathcal{D}_x^{\alpha/2} v_N \right\|^2_{L^2(\Omega)} &\leq \sum_{k=1}^{N} a_k^2 \ \left(\frac{\Gamma(k+\mu)}{\Gamma(k+\tilde{\mu})} \right)^2 \int_{-1}^{1} (1-\xi)^{\tilde{\mu}} (1+\xi)^{-\tilde{\mu}} (1-\xi^2)^{\tilde{\mu}} P_{k-1}^{\tilde{\mu},-\tilde{\mu}}(\xi) \ P_{k-1}^{\tilde{\mu},-\tilde{\mu}}(\xi) \ d\xi, \\
&\leq \sum_{k=1}^{N} a_k^2 \ \left(\frac{\Gamma(k+\mu)}{\Gamma(k+\tilde{\mu})} \right)^2 C_2 \int_{-1}^{1} (1-\xi)^{\tilde{\mu}} (1+\xi)^{-\tilde{\mu}} P_{k-1}^{\tilde{\mu},-\tilde{\mu}}(\xi) \ P_{k-1}^{\tilde{\mu},-\tilde{\mu}}(\xi) \ d\xi,
\end{aligned}$$

since $\tilde{\mu} > -1/2$ and consequently $(1-\xi^2)^{\tilde{\mu}}$ is a nonnegative and integrable in the domain of integration. By the orthogonality of Jacobi polynomials, we get

$$\left\| {}_{-1}\mathcal{D}_x^{\alpha/2} v_N \right\|^2_{L^2(\Omega)} \leq C_2 \sum_{k=1}^{N} a_k^2 \ \left(\frac{\Gamma(k+\mu)}{\Gamma(k+\tilde{\mu})} \right)^2 \epsilon_{k-1}^{\tilde{\mu},-\tilde{\mu}},$$

and thus

$$\|v_N\|_{V_N} \leq \sqrt{C_2 \int_{\alpha_{min}}^{\alpha_{max}} \phi(\alpha) \ \sum_{k=1}^{N} a_k^2 \ \left(\frac{\Gamma(k+\mu)}{\Gamma(k+\tilde{\mu})} \right)^2 \epsilon_{k-1}^{\tilde{\mu},-\tilde{\mu}} \ d\alpha}. \tag{3.42}$$

Similarly for $\|u_N\|^2_{U_N}$:

$$\|u_N\|^2_{U_N} = \int_{\alpha_{min}}^{\alpha_{max}} \phi(\alpha) \ \left\| {}_{-1}\mathcal{D}_x^{\alpha/2} u_N \right\|^2_{L^2(\Omega)} d\alpha,$$

where $\forall \alpha \in (\alpha_{min}, \alpha_{max})$:

$$\begin{aligned}
\left\| {}_{-1}\mathcal{D}_x^{\alpha/2} u_N \right\|^2_{L^2(\Omega)} &= \int_{-1}^{1} \Big(\sum_{n=1}^{N} a_n \ \frac{\Gamma(n+\mu)}{\Gamma(n+\tilde{\mu})} (1+\xi)^{\tilde{\mu}} P_{n-1}^{-\tilde{\mu},\tilde{\mu}}(\xi) \Big)^2 d\xi, \\
&\leq \int_{-1}^{1} \sum_{n=1}^{N} a_n^2 \ \left(\frac{\Gamma(n+\mu)}{\Gamma(n+\tilde{\mu})} \right)^2 (1+\xi)^{2\tilde{\mu}} (P_{n-1}^{-\tilde{\mu},\tilde{\mu}}(\xi))^2 d\xi, \\
&\quad \text{By Jensen Inequality.}
\end{aligned}$$

Following similar steps, and by multiplying the integrand by $(1-\xi)^{-\tilde{\mu}}(1-\xi)^{\tilde{\mu}}$ and changing the order of summation and integration, we obtain

$$\begin{aligned}
&\left\| {}_{-1}\mathcal{D}_x^{\alpha/2} u_N \right\|^2_{L^2(\Omega)}, \\
\leq\ & \sum_{n=1}^{N} a_n^2 \left(\frac{\Gamma(n+\mu)}{\Gamma(n+\tilde{\mu})}\right)^2 \int_{-1}^{1} (1-\xi)^{-\tilde{\mu}}(1+\xi)^{\tilde{\mu}}(1-\xi^2)^{\tilde{\mu}} P_{n-1}^{-\tilde{\mu},\tilde{\mu}}(\xi)\ P_{n-1}^{-\tilde{\mu},\tilde{\mu}}(\xi)\ d\xi, \\
\leq\ & \sum_{n=1}^{N} a_n^2 \left(\frac{\Gamma(n+\mu)}{\Gamma(n+\tilde{\mu})}\right)^2 C_3 \int_{-1}^{1} (1-\xi)^{-\tilde{\mu}}(1+\xi)^{\tilde{\mu}} P_{n-1}^{-\tilde{\mu},\tilde{\mu}}(\xi)\ P_{n-1}^{-\tilde{\mu},\tilde{\mu}}(\xi)\ d\xi,
\end{aligned}$$

since $(1-\xi^2)^{\tilde{\mu}}$ is a nonnegative and integrable in the domain of integral. Next, by the orthogonality of Jacobi polynomials,

$$\left\| {}_{-1}\mathcal{D}_x^{\alpha/2} u_N \right\|^2_{L^2(\Omega)} \leq C_3 \sum_{n=1}^{N} a_n^2 \left(\frac{\Gamma(n+\mu)}{\Gamma(n+\tilde{\mu})}\right)^2 \epsilon_{n-1}^{-\tilde{\mu},\tilde{\mu}}.$$

Therefore,

$$\|u_N\|_{U_N} \leq \sqrt{C_3 \int_{\alpha_{min}}^{\alpha_{max}} \phi(\alpha) \sum_{n=1}^{N} a_n^2 \left(\frac{\Gamma(n+\mu)}{\Gamma(n+\tilde{\mu})}\right)^2 \epsilon_{n-1}^{\tilde{\mu},-\tilde{\mu}}\ d\alpha}, \tag{3.43}$$

where $\epsilon_{n-1}^{-\tilde{\mu},\tilde{\mu}} = \epsilon_{n-1}^{\tilde{\mu},-\tilde{\mu}}$.

Therefore, using (3.41), (3.42) and (3.43),

$$\inf_{u_N \in U_N} \sup_{v_N \in V_N} \frac{a_h(u_N, v_N)}{\|u_N\|_{U_N}\ \|v_N\|_{V_N}} \geq \frac{C_0\ {C_1}_{min}}{\sqrt{C_2\ C_3}} = \beta.$$

□

3.4.2 Projection Error Analysis

In this section, we investigate the error due to the projection of the true solution onto the defined set of basis functions.

Theorem 3.4.4. *Let $\frac{d^r u}{dt^r} \in U$, that is, $\int_{\alpha_{min}}^{\alpha_{max}} \phi(\alpha) \left\| {}_0\mathcal{D}_t^{r+\alpha/2} u \right\|^2_{L^2(\Omega)}\ d\alpha < \infty$ and u_N denotes the projection of the exact solution u. Then,*

$$\|u - u_N\|_U^2 \leq C\, N^{-2r} \int_{\alpha_{min}}^{\alpha_{max}} \phi(\alpha) \left\| {}_0\mathcal{D}_t^{r+\alpha/2} u \right\|^2_{L^2(\Omega)} d\alpha. \tag{3.44}$$

Proof. By performing an affine mapping from $t \in [0,T]$ to the standard domain $\xi \in [-1,1]$, we expand the exact solution u in terms of the following infinite series of Jacobi poly-fractonomials

$$u(\xi) = \sum_{n=1}^{\infty} c_n \, {}^{(1)}\mathcal{P}_n^{\mu}(\xi). \tag{3.45}$$

Then, we note that by using (3.2.1) and (1.21),

$$\begin{aligned} {}_0\mathcal{D}_t^{r+\alpha/2} \; u(\xi(t)) &= (\frac{2}{T})^{r+\alpha/2} \; {}_{-1}\mathcal{I}_{\xi}^{\mu-\alpha/2} \; \frac{d^r}{d\xi^r} \; {}_{-1}\mathcal{D}_{\xi}^{\mu} \; u(\xi), \\ &= (\frac{2}{T})^{r+\alpha/2} \; \sum_{n=1}^{\infty} c_n \left(\frac{\Gamma(n+\mu)}{\Gamma(n)} \right) {}_{-1}\mathcal{I}_{\xi}^{\mu-\alpha/2} \; \frac{d^r}{d\xi^r}[P_{n-1}(\xi)], \end{aligned}$$

where,

$$\frac{d^r}{d\xi^r}[P_{n-1}(\xi)] = \begin{cases} \frac{(n-1+r)!}{2r(n-1)!} P^{r,r}_{n-1-r}(\xi) & r < n, \\ 0 & r \geq n. \end{cases}$$

Thus, by multiplying with a proper weight function, $w(\xi) = (1+\xi)^{r/2-\mu+\alpha/2} \; (1-\xi)^{r/2}$, the right-hand-side of (3.44) takes the form

$$\begin{aligned} \int_{\alpha_{min}}^{\alpha_{max}} \phi(\alpha) (\frac{2}{T})^{2r+\alpha/2} \Bigg\| &(1+\xi)^{r/2-\mu+\alpha/2} \; (1-\xi)^{r/2} \\ &\sum_{n=r+1}^{\infty} c_n \left(\frac{\Gamma(n+\mu)}{\Gamma(n)} \right) \frac{(n-1+r)!}{2r(n-1)!} \; {}_{-1}\mathcal{I}_{\xi}^{\mu-\alpha/2} \; P^{r,r}_{n-1-r}(\xi) \Bigg\|^2_{L^2(\Omega)} d\alpha. \end{aligned} \tag{3.46}$$

By expanding the Jacobi polynomial as

$$P^{r,r}_{n-1-r}(\xi) = (-1)^{n-1-r} \sum_{j=0}^{n-1-r} \binom{n-1+r+j}{j} \binom{n-1}{n-1-r-j} (\frac{-1}{2})^j \; (1+\xi)^j,$$

and changing the order of summation and the integration, we obtain the fractional integral as

$$\begin{aligned} &{}_{-1}\mathcal{I}_{\xi}^{\mu-\alpha/2} \; P^{r,r}_{n-1-r}(\xi), \\ &= (-1)^{n-1-r} \, (1+\xi)^{\mu-\alpha/2} \sum_{j=0}^{n-1-r} \binom{n-1+r+j}{j} \binom{n-1}{n-1-r-j} (\frac{-1}{2})^j \; \frac{\Gamma(1+j)}{\Gamma(1+j+\mu-\alpha/2)} \, (1+\xi)^j, \\ &= (-1)^{n-1-r} \, (1+\xi)^{\mu-\alpha/2} \sum_{q=0}^{n-1-r} \tilde{c}_q(\alpha) \; P_q^{r,r}(\xi), \end{aligned} \tag{3.47}$$

where, the coefficient, $\tilde{c}_q(\alpha)$, can be obtained using the orthogonality of Jacobi polynomials. Hence, by taking $C_n = c_n\,(-1)^{n-1}\,\frac{\Gamma(n+\mu)}{\Gamma(n)}$, (3.46) takes the form

$$\int_{\alpha_{min}}^{\alpha_{max}} \phi(\alpha)(\frac{2}{T})^{2r+\alpha} \left\| (1+\xi)^{r/2}(1-\xi)^{r/2} \sum_{n=r+1}^{\infty} C_n \frac{(n-1+r)!}{2r(n-1)!}(-1)^{-r} \sum_{q=0}^{n-1-r} \tilde{c}_q(\alpha) P_q^{r,r}(\xi) \right\|_{L^2(\Omega)}^2 d\alpha, \tag{3.48}$$

$$= \int_{\alpha_{min}}^{\alpha_{max}} \phi(\alpha)(\frac{2}{T})^{2r+\alpha} \left[\int_{-1}^{1} (1+\xi)^r (1-\xi)^r \left(\sum_{n=r+1}^{\infty} C_n \frac{(n-1+r)!}{2r(n-1)!} \sum_{q=0}^{n-1-r} \tilde{c}_q(\alpha) P_q^{r,r}(\xi) \right)^2 d\xi \right] d\alpha.$$

Then, we change the order of two summations in order to use the orthogonality of Jacobi polynomials and obtain

$$\int_{\alpha_{min}}^{\alpha_{max}} \phi(\alpha)(\frac{2}{T})^{2r+\alpha} \left[\int_{-1}^{1} (1+\xi)^r (1-\xi)^r \left(\sum_{q=0}^{\infty} \sum_{n=r+1+q}^{\infty} C_n \frac{(n-1+r)!}{2r(n-1)!} \tilde{c}_q(\alpha) P_q^{r,r}(\xi) \right)^2 d\xi \right] d\alpha, \tag{3.49}$$

$$= \int_{\alpha_{min}}^{\alpha_{max}} \phi(\alpha)(\frac{2}{T})^{2r+\alpha} \left[\int_{-1}^{1} (1+\xi)^r (1-\xi)^r \sum_{q=0}^{\infty} \left(\sum_{n=r+1+q}^{\infty} C_n \frac{(n-1+r)!}{2r(n-1)!} \right)^2 \tilde{c}_q^2(\alpha) (P_q^{r,r}(\xi))^2 d\xi \right] d\alpha,$$

$$= \sum_{q=0}^{\infty} \left(\sum_{n=r+1+q}^{\infty} C_n \frac{(n-1+r)!}{2r(n-1)!} \right)^2 \int_{-1}^{1} (1+\xi)^r (1-\xi)^r (P_q^{r,r}(\xi))^2 d\xi \int_{\alpha_{min}}^{\alpha_{max}} \phi(\alpha)(\frac{2}{T})^{2r+\alpha} \tilde{c}_q^2(\alpha) d\alpha,$$

$$= \sum_{q=0}^{\infty} \left(\sum_{n=r+1+q}^{\infty} C_n \frac{(n-1+r)!}{2r(n-1)!} \right)^2 \frac{2^{2r+1}}{2q+2r+1} \frac{((q+1)!)^2}{q!(q+2r)!} \int_{\alpha_{min}}^{\alpha_{max}} \phi(\alpha)(\frac{2}{T})^{2r+\alpha} \tilde{c}_q^2(\alpha) d\alpha,$$

$$= \frac{2^{2r+1}(\frac{2}{T})^{2r}}{(2r)^2} \sum_{q=0}^{\infty} \left(\sum_{n=r+1+q}^{\infty} C_n \frac{(n-1+r)!}{(n-1)!} \right)^2 \frac{(q+1)^2\, q!}{(2q+2r+1)(q+2r)!} \int_{\alpha_{min}}^{\alpha_{max}} \phi(\alpha)(\frac{2}{T})^{\alpha} \tilde{c}_q^2(\alpha) d\alpha.$$

Moreover, using the approximation of the solution given in (3.28) and by multiplying with the proper weight functions, the left-hand-side of (3.44) takes the form

$$\left\| (1+\xi)^{-\mu+\alpha/2} (u - u_N) \right\|_U^2, \tag{3.50}$$

$$= \int_{\alpha_{min}}^{\alpha_{max}} \phi(\alpha) (\frac{2}{T})^{\alpha} \left\| (1+\xi)^{-\mu+\alpha/2} \sum_{n=N+1}^{\infty} c_n \left(\frac{\Gamma(n+\mu)}{\Gamma(n)} \right)_{-1} \mathcal{I}_{\xi}^{\mu-\alpha/2} P_{n-1}(\xi) \right\|_{L^2(\Omega)}^2 d\alpha,$$

in which, ${}_{-1}\mathcal{D}_{\xi}^{\alpha/2} = {}_{-1}\mathcal{D}_{\xi}^{\alpha/2-\mu+\mu} = {}_{-1}\mathcal{I}_{\xi}^{\mu-\alpha/2}\ {}_{-1}\mathcal{D}_{\xi}^{\mu}$ and the fractional derivative is taken using (3.2.1). By expanding the Legendre polynomial as

$$P_{n-1}(\xi) = (-1)^{n-1} \sum_{j=0}^{n-1} \binom{n-1+j}{j} \binom{n-1}{n-1-j} (\frac{-1}{2})^j \, (1+\xi)^j,$$

and following similar steps as in (3.47), we obtain the fractional integral as

$${}_{-1}\mathcal{I}_{\xi}^{\mu-\alpha/2} P_{n-1}(\xi) = (-1)^{n-1} \, (1+\xi)^{\mu-\alpha/2} \sum_{q=0}^{n-1} \tilde{a}_q(\alpha) \, P_q(\xi), \tag{3.51}$$

where the coefficient, $\tilde{a}_q(\alpha)$, can be obtained using the orthogonality of Legendre polynomials. Hence, (3.50) takes the form

$$\left\| (1+\xi)^{-\mu+\alpha/2} \, (u - u_N) \right\|_U^2 = \int_{\alpha_{min}}^{\alpha_{max}} \phi(\alpha) \, (\frac{2}{T})^{\alpha} \ \int_{-1}^{1} \left(\sum_{n=N+1}^{\infty} C_n \ \sum_{q=0}^{n-1} \tilde{a}_q(\alpha) \, P_q(\xi) \right)^2 d\xi \, d\alpha, \tag{3.52}$$

in which, $C_n = c_n \, (-1)^{n-1} \, \frac{\Gamma(n+\mu)}{\Gamma(n)}$. We change the order of two summations to use the orthogonality of Legendre polynomials and obtain

$$\begin{aligned}
&\int_{\alpha_{min}}^{\alpha_{max}} \phi(\alpha) \, (\frac{2}{T})^{\alpha} \ \int_{-1}^{1} \left(\sum_{q=0}^{N} \sum_{n=q+1}^{\infty} C_n \ \tilde{a}_q(\alpha) \, P_q(\xi) \ + \ \sum_{q=N+1}^{\infty} \sum_{n=q+1}^{\infty} C_n \ \tilde{a}_q(\alpha) \, P_q(\xi) \right)^2 d\xi \, d\alpha, \\
&= \int_{\alpha_{min}}^{\alpha_{max}} \phi(\alpha) \, (\frac{2}{T})^{\alpha} \ \left(\sum_{q=0}^{N} \left(\sum_{n=q+1}^{\infty} C_n \right)^2 \tilde{a}_q^2(\alpha) \ \int_{-1}^{1} (P_q(\xi))^2 \, d\xi \right. \\
&\qquad \left. + \ \sum_{q=N+1}^{\infty} \left(\sum_{n=q+1}^{\infty} C_n \right)^2 \tilde{a}_q^2(\alpha) \ \int_{-1}^{1} (P_q(\xi))^2 \, d\xi \right) d\alpha, \\
&\leq \sum_{q=N+1}^{\infty} \left(\sum_{n=q+1}^{\infty} C_n \right)^2 \frac{2}{2q+1} \ \int_{\alpha_{min}}^{\alpha_{max}} \phi(\alpha) \, (\frac{2}{T})^{\alpha} \, \tilde{a}_q^2(\alpha) \, d\alpha, \\
&\leq \left(\frac{N!}{(N-r)!} \right)^2 \sum_{q=N+1}^{\infty} \left(\sum_{n=q+1}^{\infty} C_n \, \frac{(n-1+r)!}{(n-1)!} \right)^2 \frac{2}{2q+1} \, \frac{(q+1)^2 \, q!}{(2q+2r+1)(q+2r)!} \ \int_{\alpha_{min}}^{\alpha_{max}} \phi(\alpha) \, (\frac{2}{T})^{\alpha} \, \tilde{a}_q^2(\alpha) \, d\alpha, \\
&\leq \left(\frac{N!}{(N-r)!} \right)^2 \int_{\alpha_{min}}^{\alpha_{max}} \phi(\alpha) \, (\frac{2}{T})^{2r+\alpha} \ \left\| (1+\xi)^{r/2-\mu+\alpha/2} \ (1-\xi)^{r/2} \ {}_{-1}\mathcal{D}_{\xi}^{r+\alpha/2} u \right\|_{L^2(\Omega)}^2 d\alpha, \\
&\leq \left(\frac{N!}{(N-r)!} \right)^2 \int_{\alpha_{min}}^{\alpha_{max}} \phi(\alpha) \ \left\| {}_{0}\mathcal{D}_{t}^{r+\alpha/2} u \right\|_{L^2(\Omega)}^2 d\alpha.
\end{aligned} \tag{3.53}$$

Therefore,

$$\|u-u_N\|_U^2 \leq \left\|(1+\xi)^{-\mu+\alpha/2}\,(u-u_N)\right\|_U^2 \leq C\,N^{-2r}\int_{\alpha_{min}}^{\alpha_{max}}\phi(\alpha)\left\|{}_0\mathcal{D}_t^{r+\alpha/2}u\right\|_{L^2(\Omega)}^2 d\alpha.$$

□

Remark 3.4.5. *Since the inf-sup condition holds (see Theorem* (3.4.3)*), by the Banach-Nečas-Babuška theorem [51], the error in the numerical scheme is less that or equal to a constant times the projection error. Choosing the projection u_N in Theorem* (3.4.4)*, we infer the spectral accuracy of the scheme.*

3.5 Fractional Collocation Method: Nodal Expansion

Next, we represent the solution via the following poly-fractonomial *nodal* expansion as

$$u_N(\xi) = \sum_{j=1}^{N} u_N(\xi_j)\,h_j^{\mu}(\xi), \tag{3.54}$$

where $h_j^{\mu}(\xi)$ represent *fractional Lagrange interpolants* FLIs, which are all of fractional order $(N+\mu-1)$ and constructed using the aforementioned interpolations points $-1=\xi_1<\xi_2<\cdots<\xi_N=1$ as:

$$h_j^{\mu}(\xi) = \left(\frac{\xi-x_1}{x_j-x_1}\right)^{\mu}\prod_{\substack{k=1\\k\neq j}}^{N}\left(\frac{\xi-x_k}{x_j-x_k}\right), \qquad j=2,3,\cdots,N. \tag{3.55}$$

Because of the homogeneous Dirichlet boundary condition(s) in (4.7) and (4.8), $u_N(-1)=0$, and thus we only construct $h_j^{\mu}(\xi)$ for $j=2,3,\cdots,N$. We note that FLIs satisfy the Kronecker delta property, i.e., $h_j^{\mu}(\xi_k)=\delta_{jk}$, at interpolation points, however they vary as a poly-fractonomial between ξ_k's.

3.5.1 Differentiation Matrices $\mathbf{D}^{\alpha}$ and $\mathbf{D}^{1+\alpha}$, $\alpha\in(0,1)$

By breaking the domain of integration in α, (5.7) takes the form

$$\int_{\alpha_{min}}^{1}\phi(\alpha)\,{}_0\mathcal{D}_t^{\alpha}u(t)d\alpha + \int_{1}^{\alpha_{max}}\phi(\alpha)\,{}_0\mathcal{D}_t^{\alpha}u(t)d\alpha = f(t;u), \quad \forall t\in(0,T]. \tag{3.56}$$

Following [189], we obtain the corresponding fractional differentiation matrices $\mathbf{D}^{\alpha}$ and $\mathbf{D}^{1+\alpha}$, $\alpha \in (0,1)$ by substituting (3.55) in (3.54) and taking the α-th order fractional derivative. These matrices are given as:

$$\mathbf{D}_{ij}^{\alpha} = \frac{1}{(\xi_j+1)^{\mu}} \sum_{n=1}^{N} \beta_n^j \sum_{q=\lceil \alpha-\mu \rceil}^{n-1} b_{nq}\,(\xi_i+1)^{q+\mu-\alpha}, \tag{3.57}$$

and

$$\mathbf{D}_{ij}^{1+\alpha} = \frac{1}{(\xi_j+1)^{\mu}} \Big[\sum_{n=1}^{N} \beta_n^j \sum_{q=\lceil \alpha-\mu \rceil}^{n-1} b_{nq}(q+\mu-\alpha)\,(\xi_i+1)^{q+\mu-\alpha-1} \Big], \tag{3.58}$$

in which $\lceil \alpha-\mu \rceil$ denotes the ceiling of $\alpha-\mu$ and

$$b_{nq} = (-1)^{n+q-1} (\frac{1}{2})^{q} \binom{n-1+q}{q} \binom{n-1+\mu}{n-1-q} \frac{\Gamma(q+\mu+1)}{\Gamma(q+\mu-\alpha+1)}. \tag{3.59}$$

The coefficients, β_n^j, are the coefficients in expansion of the polynomial $p_j(\xi) = \prod_{\substack{k=1 \\ k\neq j}}^{N} \left(\frac{\xi-\xi_k}{\xi_j-\xi_k}\right)$ in terms of Jacobi polynomials as

$$\prod_{\substack{k=1 \\ k\neq j}}^{N} \left(\frac{\xi-\xi_k}{x_j-x_k}\right) = \sum_{n=1}^{N} \beta_n^j P_{n-1}^{-\mu,\mu}(\xi). \tag{3.60}$$

Due to the orthogonality of the Jacobi poly-fractonomials $P_{n-1}^{-\mu,\mu}(\xi)$ with respect to the weight function $w(\xi) = (1-\xi)^{-\mu}(1+\xi)^{-\mu}$, these coefficients can be computed efficiently only *once* by employing a proper Guass-Lobatto-Jacobi quadrature rule.

Therefore, by substituting the nodal expansion (3.55) into (3.56), performing an affine mapping from $[\alpha_{min}, \alpha_{max}]$ to the standard domain $[-1,1]$, and employing a proper quadrature rule in α-domain, (3.56) can be written as

$$\begin{aligned} &\sum_{j=2}^{N} \left[\sum_{q}^{Q} w_q\, \phi(\alpha_q)\, (\frac{2}{T})^{\alpha q} \left(\mathbf{D}_{ij}^{\alpha q} + \mathbf{D}_{ij}^{1+\alpha q} \right) \right] u_N(\xi_j) = f(\xi_i), \\ &\sum_{j=2}^{N} \mathscr{D}_{i,j}\; u_N(\xi_j) = f(\xi_i), \quad i = 2,3,\cdots,N. \end{aligned} \tag{3.61}$$

Remark 3.5.1. *Multi-term problems can be generalized to the distributed order counterparts through the definition of distribution function $\phi(\alpha)$. For instance, if the operator consists of multiple fractional orders $0 < \alpha_1 < \alpha_2 < \cdots < \alpha_P \leq 2$, the corresponding multi-term problem*

$$\sum_{p=1}^{p=P} {}_0\mathcal{D}_t^{\alpha_p} u(t) = f(t)$$

can be represented as a distributed order problem of the form (5.7)*, in which $\phi(\alpha) = \sum_{p=1}^{p=P} \delta(\alpha - \alpha_p)$. We note that in this case, the distributed fractional Sobolev space, ${}^{\phi}\mathcal{H}(\mathbb{R})$, coincides with the fractional Sobolev space ,$H^{\alpha_P}(\mathbb{R})$. The choice of collocation/interpolation points is the key to construct well-conditioned linear systems with optimal approximability. In the present work, we leave μ in expansion* (3.54) *as a free interpolation parameter to capture possible singularities and employ the zeros of Legendre polynomials as the interpolation collocation/interpolation points.*

3.6 Numerical Simulations

In order to examine the convergence of the schemes with *modal* and *nodal* expansions, we consider problems with smooth and non-smooth solutions.

3.6.1 Smooth Solutions

Let $\alpha \in [0, 2]$ and consider the following two cases:

- Case I: $u^{ext} = t^5$, $\phi(\alpha) = \Gamma(6-\alpha)/5!$, $f(t) = \frac{(t^5 - t^3)}{\log(t)}$
- Case II: $u^{ext} = t^3$, $\phi(\alpha) = \Gamma(4-\alpha)\sinh(\alpha)$, $f(t) = \frac{6t(t^2 - \cosh(2) - \sinh(2)\log(t))}{(\log(t)^2 - 1)}$.

By taking the simulation time $T = 2$ and for different choices of μ, we provide the convergence study in L^∞-norm, L^2-norm, H^{μ_1}-norm and ${}^{\phi}\mathcal{H}$-norm using the PG scheme and in L^∞-norm using the collocation scheme. It is observed that the choice of μ has an important effect on the convergence behaviour of the scheme. For instance, since the exact solution is a polynomial, as $\mu \to 1$, we recover the exponential convergence in capturing the exact solution.

Table 3.1: Case-I; PG scheme convergence study in L^∞-norm, L^2-norm, H^{μ_1}-norm and ${}^{\phi}\mathcal{H}$-norm, where $T = 2$.

$\mu_1 = 1 + 10^{-4}$

N	L^∞-Error	L^2-Error	H^{μ_1}-Error	${}^{\phi}\mathcal{H}$-Error
2	9.49784	3.38063	20.604	6.52507
4	0.163486	0.0823368	0.802757	0.187176
6	9.71043×10^{-8}	6.7433×10^{-8}	8.37613×10^{-7}	1.70551×10^{-7}
8	2.9053×10^{-9}	2.32457×10^{-9}	3.53574×10^{-8}	6.59486×10^{-9}
10	2.27748×10^{-10}	2.01002×10^{-10}	3.67074×10^{-9}	6.38469×10^{-10}

$\mu_1 = 1.1$

N	L^∞-Error	L^2-Error	H^{μ_1}-Error	${}^{\phi}\mathcal{H}$-Error
2	9.6776	3.2898	23.3004	6.38693
4	0.160434	0.0661304	0.872809	0.157957
6	0.0000947942	0.0000589784	0.00107458	0.00015822
8	3.10668×10^{-6}	2.19939×10^{-6}	0.0000507737	6.59429×10^{-6}
10	2.48519×10^{-7}	1.9822×10^{-7}	5.5753×10^{-6}	6.61409×10^{-7}

$\mu_1 = 1.5$

N	L^∞-Error	L^2-Error	H^{μ_1}-Error	${}^{\phi}\mathcal{H}$-Error
2	9.8476	3.10681	35.8457	5.96161
4	0.102534	0.0264974	0.949183	0.0718496
6	0.000584995	0.00015106	0.0117235	0.000524729
8	0.0000272655	7.37649×10^{-6}	0.000989158	0.0000306404
10	2.75271×10^{-6}	7.75346×10^{-7}	0.000158823	3.72512×10^{-6}

Tables 3.1 and 3.2 show the convergence behaviour of the simulation results based on the PG scheme for the two case-I and II respectively. Tables 3.3 shows the convergence behaviour of the simulation results based on the collocation scheme for the two cases I and II. Table 3.4 shows the convergence behaviour of the simulation results based on the collocation scheme for the case where the exact solution is the same as case-I but the distribution function is $\phi(\alpha) = \sum_{p=1}^{4} \delta(\alpha - \alpha_p)$ with the fractional orders $\{1/10, 1/2, 13/10, 19/10\}$ and the forcing function is $f(t) = \sum_{p=1}^{4} \frac{120}{\Gamma(6-\alpha_p)} t^{5-\alpha_p}$.

3.6.2 Non-Smooth Solutions

Since the exact solution is not always known and in contrast to the standard fractional ODEs where the forcing term gives some regularity information about the exact solution, in distributed order problems such a prediction is rather difficult to make. Hence, the fractional parameter μ can play the role of a *fine-tuning knob* giving the possibility of searching for the best/optimal case, where the highest rate can be achieved with minimal degrees of freedom. Here, we let $\alpha \in [0, 1]$ and consider

Table 3.2: Case-II; PG scheme convergence study in L^∞-norm, L^2-norm, H^{μ_1}-norm and ${}^{\phi}\mathcal{H}$-norm, where $T = 2$.

$\mu_1 = 1 + 10^{-4}$

N	L^∞-Error	L^2-Error	H^{μ_1}-Error	${}^{\phi}\mathcal{H}$-Error
2	0.379134	0.325253	1.44392	1.86897
4	6.80222×10^{-7}	6.33141×10^{-7}	4.61395×10^{-6}	5.29606×10^{-6}
6	5.22608×10^{-8}	4.52071×10^{-8}	4.80236×10^{-7}	5.08899×10^{-7}
8	1.27547×10^{-8}	9.98313×10^{-9}	1.0532×10^{-7}	1.049×10^{-7}
10	7.31142×10^{-9}	7.21402×10^{-9}	3.44882×10^{-8}	3.39574×10^{-8}

$\mu_1 = 1.1$

N	L^∞-Error	L^2-Error	H^{μ_1}-Error	${}^{\phi}\mathcal{H}$-Error
2	0.369682	0.263829	1.45384	1.62458
4	0.000646557	0.000569995	0.00548608	0.00499413
6	0.0000458334	0.0000438926	0.000636023	0.000511403
8	7.74333×10^{-6}	7.36329×10^{-6}	0.000147177	0.000107932
10	2.02013×10^{-6}	1.84714×10^{-6}	0.000048212	0.0000327428

$\mu_1 = 1.5$

N	L^∞-Error	L^2-Error	H^{μ_1}-Error	${}^{\phi}\mathcal{H}$-Error
2	0.288508	0.114871	1.25471	0.848595
4	0.00403916	0.00163979	0.0511667	0.0190804
6	0.000406095	0.000169817	0.0106909	0.00268063
8	0.0000789352	0.0000336939	0.00358698	0.000671243
10	0.0000219275	9.49574×10^{-6}	0.00153771	0.000228446

Table 3.3: Case-I and II; collocation scheme convergence study in L^∞-norm, where $T = 2$.

	$\mu = 1 - 10^{-10}$		$\mu = 7/10$		$\mu = 1/10$	
N	Case-I	Case-II	Case-I	Case-II	Case-I	Case-II
2	$2.59 \times 10^{+1}$	5.74	$3.0 \times 10^{+1}$	8.84	$4.3 \times 10^{+1}$	19.91
4	6.81×10^{-1}	5.30×10^{-12}	$1.10 \times 10^{+1}$	2.58×10^{-1}	$2.51 \times 10^{+1}$	1.01×10^{-1}
6	3.87×10^{-13}	2.15×10^{-13}	1.43×10^{-3}	1.52×10^{-3}	3.48×10^{-3}	8.03×10^{-3}
8	1.10×10^{-14}	2.68×10^{-14}	3.10×10^{-5}	3.34×10^{-4}	8.38×10^{-5}	1.83×10^{-3}
10	8.75×10^{-15}	7.01×10^{-15}	2.12×10^{-6}	1.12×10^{-4}	1.0×10^{-5}	6.25×10^{-4}

Table 3.4: Multi-term case; collocation scheme convergence study in L^∞-norm, where $T = 2$.

N	$\mu = 1 - 10^{-10}$	$\mu = 7/10$	$\mu = 1/10$
6	2.99596×10^{-4}	1.93088×10^{3}	7.10859×10^{-2}
10	4.40056×10^{-7}	7.90916×10^{-6}	1.95735×10^{-4}
14	9.35031×10^{-9}	3.39228×10^{-7}	7.99603×10^{-6}
18	9.15918×10^{-10}	3.53369×10^{-8}	8.27226×10^{-7}

the following two cases of singular solution, where by the proper choice of μ we can easily capture the singularity of the solution.

- Case III: $u^{ext} = t^{\mu_0}$, $\phi(\alpha) = \Gamma(1 + \mu_0 - \alpha)/(\mu_0)!$, $\mu_0 = 1/10, 9/10,$
- Case IV: $u^{ext} = t^{\mu_0}\, sin(t)$, $\phi(\alpha)$, $\mu_0 = 75/100, 25/100.$

In case-III, we are able to obtain the exact solution only with one term by choosing $\mu = \mu_0$. In

case-IV, we take $\mu = \mu_0$ and expand $sin(t)$ using Taylor series. Table 3.5 shows the L^2-norm convergence of the PG scheme for two different distribution functions.

Table 3.5: Case-IV; PG scheme convergence study in L^2-norm, where $T = 2$.

	$\mu = 75/100$		$\mu = 25/100$	
N	$\phi(\alpha) = 1$	$\phi(\alpha) =$ Normal	$\phi(\alpha) = 1$	$\phi(\alpha) =$ Normal
2	1.56682×10^{-1}	1.62765×10^{-1}	1.5773×10^{-1}	1.548×10^{-1}
4	3.13043×10^{-3}	3.3898×10^{-3}	3.4228×10^{-3}	3.28626×10^{-3}
6	2.55359×10^{-5}	2.81522×10^{-5}	2.8956×10^{-5}	2.76729×10^{-5}
8	1.13562×10^{-7}	1.2512×10^{-7}	4.24126×10^{-7}	1.40114×10^{-7}
10	2.60471×10^{-9}	7.84647×10^{-10}	3.9524×10^{-7}	5.49882×10^{-8}

3.6.3 Condition Number

The condition number of the constructed linear system is obtained for different distribution functions, $\phi(\alpha)$. Tables 3.6 and 3.7 show, respectively, the condition number of the constructed linear system for case-I and II based on PG and collocation scheme for the aforementioned distribution functions.

Table 3.6: Case-I and II; PG scheme condition number of the constructed linear system, where $T = 2$.

	$\mu = 2 - 10^{-8}$		$\mu = 2 - 10^{-1}$		$\mu = 1 + 1/2$		$\mu = 1 + 1/10$	
N	Case-I	Case-II	Case-I	Case-II	Case-I	Case-II	Case-I	Case-II
6	29706.682	4863.50	14319.465	2168.87	661.70145	70.1081	51.928935	7.19267
10	240000.55	33494.8	90197.388	11817.9	1339.2855	130.925	42.754111	9.35597
14	882010.62	118283	279501.78	35395.6	1941.9838	190.309	47.335770	13.0337
18	2.2811229×10^6	301479	633307.06	79324.0	2505.5107	247.627	50.713428	16.7944

Table 3.7: Case-I and II; collocation scheme condition number of the constructed linear system, where $T = 2$.

	$\mu = 1 - 10^{-8}$		$\mu = 1 - 10^{-1}$		$\mu = 1/2$		$\mu = 1/10$	
N	Case-I	Case-II	Case-I	Case-II	Case-I	Case-II	Case-I	Case-II
6	67.5606	345.045	60.3467	302.74	43.6649	191.058	36.0056	340.539
10	386.339	2781.51	325.037	2309.25	214.935	1515.11	202.826	3554.95
14	1330.11	10646.1	1076.14	8518.56	685.166	5435.91	713.002	16539.5
18	3388.95	28619.5	2665.32	22290.4	1661.16	13964.9	3397.2	50911.1

Moreover, three cases for the distribution function are considered: 1) the distribution is more biased toward the left of domain, 2) the distribution is symmetric and 3) the distribution is more biased toward the right of domain, namely *left biased*, *symmetric* and *right biased* respectively. The distribution functions are well-known normal, exponential, log-normal, Cauchy, Laplace, Beta

and Maxwell distributions, however, they are truncated and normalized, see Fig.4.5. For these distributions, the condition number of the constructed linear system based on the two methods is computed and provided in Tables 3.8, 3.9 and 3.10.

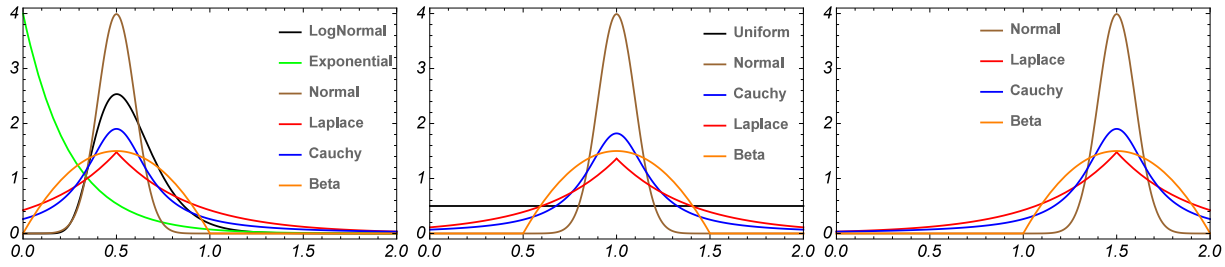

(a) (b) (c)

Figure 3.2: Distribution functions: (a) *Left biased* (b) *Symmetric* (c) *Right biased*

Table 3.8: Left biased distribution function; PG (top) and collocation (bottom) scheme condition number of the constructed linear system, where $T = 2$.

N	LogNormal	Exponential	Normal	Laplace	Cauchy	Beta
			$\mu = 2 - 1/10$			
6	62101.5	130227	85410.4	21714.7	31361	70458.4
10	1.28119×10^6	2.62266×10^6	2.15167×10^6	186527	294630	1.51681×10^6
14	9.84911×10^6	1.61563×10^7	1.98724×10^7	668178	1.04066×10^6	1.22216×10^6
18	4.48721×10^7	5.34428×10^7	1.0748×10^8	1.62018×10^6	2.41399×10^6	5.86944×10^6
			$\mu = 1 + 1/10$			
6	200.626	505.679	300.643	71.5348	100.504	233.849
10	654.259	1397.74	1309.12	91.8644	140.467	816.254
14	1322.63	1969.15	3437.72	64.4093	98.4193	1780.96
18	2145.61	2178	7037.99	70.7541	91.8767	3134.64

N	LogNormal	Exponential	Normal	Laplace	Cauchy	Beta
			$\mu = 1 - 1/10$			
6	20.1001	9.42989	13.3574	51.9103	39.5064	16.8765
10	48.3364	25.6229	26.2852	237.89	169.114	38.3283
14	91.0866	55.5712	46.5097	714.563	503.229	65.4666
18	143.171	126.19	73.3388	1672.61	1185.15	97.5852
			$\mu = 1/10$			
6	15.7319	5.67323	11.4277	33.4341	26.3924	13.3573
10	40.2359	18.0958	22.8619	150.375	102.285	30.7949
14	71.0054	37.1664	35.1324	435.867	309.089	52.9303
18	110.725	80.9506	48.0051	1032.88	742.025	81.7202

Table 3.9: Symmetric distribution function; PG (left) and collocation (right) scheme condition number of the constructed linear system, where $T = 2$.

N	Uniform	Normal	Cauchy	Laplace	Beta
		$\mu = 2 - 1/10$			
6	3104.6331	16261.6	9328.53	6969.22	13404.7
10	17244.219	220205	80110.2	51304.3	157767
14	52095.460	1.28827×10^6	308549	179737	817268
18	117338.89	4.86517×10^6	803362	441628	2.77821×10^6
		$\mu = 1 + 1/10$			
6	9.5451677	44.0857	27.6858	17.9872	37.4224
10	11.211269	85.3822	30.0092	21.361	64.2331
14	12.360897	127.844	30.9343	20.1997	87.2794
18	15.900925	172.888	34.2126	22.1982	107.403

N	Uniform	Normal	Cauchy	Laplace	Beta
		$\mu = 1 - 1/10$			
6	219.733	81.9543	118.433	140.922	95.0983
10	1592.05	284.171	598.247	798.174	375.673
14	5769.24	620.056	1788.85	2549.17	905.972
18	14944.9	1097.37	4122.7	6115.65	1737.18
		$\mu = 1/10$			
6	183.984	55.8908	72.0876	78.4252	62.069
10	1854.46	198.226	360.943	506.994	248.186
14	8678.37	439.316	1113.83	1595.84	589.611
18	26873.1	786.655	2600.56	3954.72	1171.64

Table 3.10: Right biased distribution function; PG (left) and collocation (right) scheme condition number of the constructed linear system, where $T = 2$.

N	Normal	Laplace	Cauchy	Beta
	$\mu = 2 - 1/10$			
6	2985.08	2274.39	2368.82	2105.03
10	23439.3	13948.9	15471.9	13474.7
14	92925.7	45201.4	52626.9	45325.7
18	259993	107082	129454	110813
	$\mu = 1 + 1/10$			
6	6.99801	6.60933	6.54308	6.18762
10	10.8049	9.81523	10.0861	10.1067
14	15.1563	14.2958	14.0265	14.6423
18	19.4415	18.4003	18.8445	18.8791

N	Normal	Laplace	Cauchy	Beta
	$\mu = 1 - 1/10$			
6	329.01	328.433	333.499	360.053
10	2022.09	2330.68	2275.43	2501.41
14	6299.73	8170.64	7736.87	8579.48
18	14429.7	20615.9	19067.6	21250
	$\mu = 1/10$			
6	278.525	333.384	322.187	378.704
10	1539.25	2647.09	2246.71	2727.03
14	4701.38	10365.3	8041.12	9884.8
18	10622.6	28764.7	20895.4	25800.8

3.7 Proof of Lemmas and Theorems

3.7.1 Proof of Lemma (3.2.1)

Proof. Following [5] and for $\sigma > 0$, $\alpha > -1$, $\beta > -1$, and $\forall x \in [-1, 1]$ we have

$$(1+x)^{\beta+\sigma} \frac{P_n^{\alpha-\sigma,\beta+\sigma}(x)}{P_n^{\alpha-\sigma,\beta+\sigma}(-1)} = \frac{\Gamma(\beta+\sigma+1)}{\Gamma(\beta+1)\Gamma(\sigma)P_n^{\alpha,\beta}(-1)} \int_{-1}^{x} \frac{(1+s)^{\beta}\ P_n^{\alpha,\beta}(s)}{(x-s)^{1-\sigma}} ds, \tag{3.62}$$

and

$$(1-x)^{\alpha+\sigma} \frac{P_n^{\alpha+\sigma,\beta-\sigma}(x)}{P_n^{\alpha+\sigma,\beta-\sigma}(+1)} = \frac{\Gamma(\alpha+\sigma+1)}{\Gamma(\alpha+1)\Gamma(\sigma)P_n^{\alpha,\beta}(+1)} \int_{x}^{1} \frac{(1-s)^{\alpha}\ P_n^{\alpha,\beta}(s)}{(s-x)^{1-\sigma}} ds. \tag{3.63}$$

By the definition of the left-sided Riemann-Liouville integral ${}^{RL}_{-1}\mathcal{I}_x^{\sigma}$ and evaluating the special end-values $P_n^{\alpha-\sigma,\beta+\sigma}(-1)$ and $P_n^{\alpha,\beta}(-1)$, we can re-write (3.62) as

$${}^{RL}_{-1}\mathcal{I}_x^{\sigma}\left\{(1+x)^{\beta} P_n^{\alpha,\beta}(x)\right\} = \frac{\Gamma(n+\beta+1)}{\Gamma(n+\beta+\sigma+1)}(1+x)^{\beta+\sigma}\ P_n^{\alpha-\sigma,\beta+\sigma}(x),$$

where, by taking the fractional derivative ${}^{RL}_{-1}\mathcal{D}_x^{\sigma}$ on the both sides, we obtain

$${}^{RL}_{-1}\mathcal{D}_x^{\sigma}\left\{(1+x)^{\beta+\sigma} P_n^{\alpha-\sigma,\beta+\sigma}(x)\right\} = \frac{\Gamma(n+\beta+\sigma+1)}{\Gamma(n+\beta+1)}(1+x)^{\beta} P_n^{\alpha,\beta}(x). \tag{3.64}$$

Hence, taking $\beta + \sigma = \mu$, $\alpha - \sigma = -\mu$ in (3.64), and shifting from n to $n-1$, we obtain

$$\begin{aligned} {}^{RL}_{-1}\mathcal{D}^{\sigma}_{x}\left\{ {}^{(1)}\mathcal{P}^{\mu}_{n}(x)\right\} &= \frac{\Gamma(n+\mu)}{\Gamma(n+\mu-\sigma)}(1+x)^{\mu-\sigma}P^{\sigma-\mu,\mu-\sigma}_{n-1}(x), \\ &= \frac{\Gamma(n+\mu)}{\Gamma(n+\mu-\sigma)}(1+x)^{\eta}P^{-\eta,\eta}_{n-1}(x), \\ &= \frac{\Gamma(n+\mu)}{\Gamma(n+\mu-\sigma)}\,{}^{(1)}\mathcal{P}^{\eta}_{n}(x), \end{aligned} \tag{3.65}$$

where $\eta = \mu - \sigma$. Moreover, by the definition of the right-sided Riemann-Liouville integral ${}^{RL}_{x}\mathcal{I}^{\sigma}_{1}$ and evaluating the special end-values $P^{\alpha-\sigma,\beta+\sigma}_{n}(+1)$ and $P^{\alpha,\beta}_{n}(+1)$, we can re-write (3.63) as

$${}^{RL}_{x}\mathcal{I}^{\sigma}_{1}\left\{(1-x)^{\alpha}P^{\alpha,\beta}_{n}(x)\right\} = \frac{\Gamma(n+\alpha+1)}{\Gamma(n+\alpha+\sigma+1)}(1-x)^{\alpha+\sigma}P^{\alpha+\sigma,\beta-\sigma}_{n}(x).$$

In a similar fashion, by taking the fractional derivative ${}^{RL}_{x}\mathcal{D}^{\sigma}_{-1}$ on the both sides, we obtain

$${}^{RL}_{x}\mathcal{D}^{\sigma}_{1}\left\{(1-x)^{\alpha+\sigma}P^{\alpha+\sigma,\beta-\sigma}_{n}(x)\right\} = \frac{\Gamma(n+\alpha+\sigma+1)}{\Gamma(n+\alpha+1)}(1-x)^{\alpha}P^{\alpha,\beta}_{n}(x). \tag{3.66}$$

Next, by taking $\alpha + \sigma = \mu$, $\beta - \sigma = -\mu$ in (3.66), and again shifting from n to $n-1$ we have

$$\begin{aligned} {}^{RL}_{x}\mathcal{D}^{\sigma}_{1}\left\{ {}^{(2)}\mathcal{P}^{\mu}_{n}(x)\right\} &= \frac{\Gamma(n+\mu)}{\Gamma(n+\mu-\sigma)}(1-x)^{\mu-\sigma}P^{\mu-\sigma,\sigma-\mu}_{n-1}(x). \\ &= \frac{\Gamma(n+\mu)}{\Gamma(n+\mu-\sigma)}(1-x)^{\eta}P^{\eta,-\eta}_{n-1}(x), \\ &= \frac{\Gamma(n+\mu)}{\Gamma(n+\mu-\sigma)}\,{}^{(2)}\mathcal{P}^{\eta}_{n}(x), \end{aligned} \tag{3.67}$$

and that completes the proof. □

3.7.2 Proof of Theorem (3.2.3)

Proof. Let ϕ be bounded in $(\alpha_{min}, \alpha_{max})$. Then,

$$\begin{aligned} C_1\phi_{min}A \;\leq\; \|\cdot\|^2_{l,\phi,I} \;\leq\; C_2\phi_{max}A, \\ C_3\phi_{min}B \;\leq\; \|\cdot\|^2_{r,\phi,I} \;\leq C_4\phi_{max}B, \end{aligned} \tag{3.68}$$

where

$$A = \|\cdot\|^2_{L^2(I)} + \int_{\alpha_{min}}^{\alpha_{max}} \left\| {}^{RL}_{x_L}\mathcal{D}^{\alpha}_{x}(\cdot)\right\|^2_{L^2(I)}\, d\alpha,$$
$$B = \|\cdot\|^2_{L^2(I)} + \int_{\alpha_{min}}^{\alpha_{max}} \left\| {}^{RL}_{x}\mathcal{D}^{\alpha}_{x_R}(\cdot)\right\|^2_{L^2(I)}\, d\alpha,$$

and C_1, C_2, C_3, and C_4 are positive constants. From [99], we know that $\forall\alpha = s$ fixed, $\|\cdot\|_{l,s,I} \sim \|\cdot\|_{r,s,I}$ that is $\left\| {}^{RL}_{x_L}\mathcal{D}^{s}_{x}(\cdot)\right\|^2_{L^2(I)} \sim \left\| {}^{RL}_{x}\mathcal{D}^{s}_{x_R}(\cdot)\right\|^2_{L^2(I)}$, hence let $\vec{s} = \{s_1, s_2, \cdots, s_Q\}$, and similarly $\forall s = s_q$ the aforementioned equivalence holds. Therefore, any linear combination of

$$\sum_{q=1}^{Q} w_q \left\| {}^{RL}_{x_L}\mathcal{D}^{s}_{x}(\cdot)\right\|^2_{L^2(I)} \sim \sum_{q=1}^{Q} w_q \left\| {}^{RL}_{x}\mathcal{D}^{s}_{x_R}(\cdot)\right\|^2_{L^2(I)}.$$

Taking $Q \longrightarrow \infty$ and assuming $\{w_q, s_q\}$ to be Riemann integral weights and points in $[\alpha_{min}, \alpha_{max}]$,

$$\int_{\alpha_{min}}^{\alpha_{max}} \left\| {}^{RL}_{x_L}\mathcal{D}^{s}_{x}(\cdot)\right\|^2_{L^2(I)} \sim \int_{\alpha_{min}}^{\alpha_{max}} \left\| {}^{RL}_{x}\mathcal{D}^{s}_{x_R}(\cdot)\right\|^2_{L^2(I)}.$$

By adding $\|\cdot\|^2_{L^2(I)}$ to the both sides of the above equivalence, we obtain $A \sim B$; and by (3.68), $\|\cdot\|_{l,\phi,I} \sim \|\cdot\|_{r,\phi,I}$.

In addition, from [99], we know that $\forall\alpha = s$ fixed, $\|\cdot\|^2_{s,I} \sim \|\cdot\|^2_{l,s,I}$. Let $\vec{s} = \{s_1, s_2, \cdots, s_Q\}$ thus $\forall s = s_q \in \vec{s},\ \|\cdot\|^2_{s_q,I} \sim \|\cdot\|^2_{l,s_q,I}$. Therefore, for any linear combination of $\sum_{q=1}^{Q} w_q \|\cdot\|^2_{s_q,I} \sim \sum_{q=1}^{Q} w_q \|\cdot\|^2_{l,s_q,I}$. Taking $Q \longrightarrow \infty$, we obtain:

$$\int_{\alpha_{min}}^{\alpha_{max}} \|\cdot\|^2_{\alpha,I}\, d\alpha \ \sim\ \int_{\alpha_{min}}^{\alpha_{max}} \|\cdot\|^2_{l,\alpha,I}\, d\alpha,$$

where the right hand side of the equivalence is

$$\begin{aligned}\int_{\alpha_{min}}^{\alpha_{max}} \left(\|\cdot\|^2_{L^2(I)} + \left\| {}^{RL}_{x_L}\mathcal{D}^{\alpha}_{x}(\cdot)\right\|^2_{L^2(I)}\right) d\alpha \ &= \ (\alpha_{max} - \alpha_{min})\|\cdot\|^2_{L^2(I)} + \int_{\alpha_{min}}^{\alpha_{max}} \left\| {}^{RL}_{x_L}\mathcal{D}^{\alpha}_{x}(\cdot)\right\|^2_{L^2(I)}\, d\alpha, \\ &\sim \ \|\cdot\|^2_{l,\phi,I} \sim \|\cdot\|^2_{r,\phi,I}.\end{aligned}$$

Therefore,

$$\int_{\alpha_{min}}^{\alpha_{max}} \|\cdot\|^2_{\alpha,I}\, d\alpha \ \sim\ \|\cdot\|^2_{l,\phi,I} \sim \|\cdot\|^2_{r,\phi,I}. \tag{3.69}$$

We can also show that

$$\phi_{min}\int_{\alpha_{min}}^{\alpha_{max}} \left\|(1+|\omega|^2)^{\frac{\alpha}{2}}\mathcal{F}(\cdot)(\omega)\right\|^2_{L^2(\mathbb{R})}\, d\alpha \le \|\cdot\|^2_{\phi,\mathbb{R}} \le \phi_{max}\int_{\alpha_{min}}^{\alpha_{max}} \left\|(1+|\omega|^2)^{\frac{\alpha}{2}}\mathcal{F}(\cdot)(\omega)\right\|^2_{L^2(\mathbb{R})}\, d\alpha.$$

Because of the non-negativity of the norms, we have

$$\begin{aligned}
&\phi_{min} \inf_{\tilde{v}\in{}^{\phi}\mathcal{H}(\mathbb{R}),\tilde{v}|_I=(\cdot)} \int_{\alpha_{min}}^{\alpha_{max}} \left\| (1+|\omega|^2)^{\frac{\alpha}{2}} \mathcal{F}(\tilde{v})(\omega) \right\|_{L^2(\mathbb{R})}^2 \, d\alpha \\
&\qquad \leq \inf_{\tilde{v}\in{}^{\phi}\mathcal{H}(\mathbb{R}),\tilde{v}|_I=(\tilde{v})} \|\cdot\|_{\phi,\mathbb{R}}^2 \leq \\
&\phi_{max} \inf_{\tilde{v}\in{}^{\phi}\mathcal{H}(\mathbb{R}),\tilde{v}|_I=(\cdot)} \int_{\alpha_{min}}^{\alpha_{max}} \left\| (1+|\omega|^2)^{\frac{\alpha}{2}} \mathcal{F}(\tilde{v})(\omega) \right\|_{L^2(\mathbb{R})}^2 \, d\alpha.
\end{aligned} \tag{3.70}$$

In general, ${}^{\phi}\mathcal{H}(\mathbb{R}) \subset H^{\alpha_{max}}(\mathbb{R})$, $\forall \alpha \in [\alpha_{min}, \alpha_{max}]$. Therefore, we have:

$$\begin{aligned}
&\inf_{\tilde{v}\in{}^{\phi}\mathcal{H}(\mathbb{R}),\tilde{v}|_I=(\cdot)} \int_{\alpha_{min}}^{\alpha_{max}} \left\| (1+|\omega|^2)^{\frac{\alpha}{2}} \mathcal{F}(\tilde{v})(\omega) \right\|_{L^2(\mathbb{R})}^2 \, d\alpha, \\
= \; & \int_{\alpha_{min}}^{\alpha_{max}} \inf_{\tilde{v}\in{}^{\phi}\mathcal{H}(\mathbb{R}),\tilde{v}|_I=(\cdot)} \left\| (1+|\omega|^2)^{\frac{\alpha}{2}} \mathcal{F}(\tilde{v})(\omega) \right\|_{L^2(\mathbb{R})}^2 \, d\alpha, \\
\leq \; & C \int_{\alpha_{min}}^{\alpha_{max}} \inf_{\tilde{v}\in H^{\alpha}(\mathbb{R}),\tilde{v}|_I=(\cdot)} \left\| (1+|\omega|^2)^{\frac{\alpha}{2}} \mathcal{F}(\tilde{v})(\omega) \right\|_{L^2(\mathbb{R})}^2 \, d\alpha, \\
= \; & C \int_{\alpha_{min}}^{\alpha_{max}} \|\cdot\|_{\alpha,I}^2 \, d\alpha.
\end{aligned}$$

However, for some choices of $\phi = \delta(\alpha - \alpha_{min})$ and thus ${}^{\phi}\mathcal{H}(\mathbb{R}) \supset H^{\alpha_{max}}(\mathbb{R})$, $\forall \alpha \in [\alpha_{min}, \alpha_{max}]$. Therefore,

$$\begin{aligned}
&\int_{\alpha_{min}}^{\alpha_{max}} \inf_{\tilde{v}\in{}^{\phi}\mathcal{H}(\mathbb{R}),\tilde{v}|_I=(\cdot)} \left\| (1+|\omega|^2)^{\frac{\alpha}{2}} \mathcal{F}(\tilde{v})(\omega) \right\|_{L^2(\mathbb{R})}^2 \, d\alpha, \\
\geq \; & \widetilde{C} \int_{\alpha_{min}}^{\alpha_{max}} \inf_{\tilde{v}\in H^{\alpha}(\mathbb{R}),\tilde{v}|_I=(\cdot)} \left\| (1+|\omega|^2)^{\frac{\alpha}{2}} \mathcal{F}(\tilde{v})(\omega) \right\|_{L^2(\mathbb{R})}^2 \, d\alpha, \\
= \; & \widetilde{C} \int_{\alpha_{min}}^{\alpha_{max}} \|\cdot\|_{\alpha,I}^2 \, d\alpha,
\end{aligned}$$

which by (3.70) and (3.5), we get

$$\int_{\alpha_{min}}^{\alpha_{max}} \|\cdot\|_{\alpha,I}^2 \, d\alpha \sim \|\cdot\|_{\phi,I}^2 . \tag{3.71}$$

Comparing (3.69) and (3.71), we have

$$\|\cdot\|_{\phi,I}^2 \sim \|\cdot\|_{l,\phi,I}^2 \sim \|\cdot\|_{r,\phi,I}^2 .$$

□

Remark 3.7.1. *We note that if $\phi = \delta(\alpha - s)$, we recover the standard ${}^{RL}_{x_L}\mathcal{D}^s_x(u) = f$, where the equivalence between the corresponding $\|\cdot\|_{l,s,I}$, $\|\cdot\|_{r,s,I}$, and $\|\cdot\|_{s,I}$ has been already established. Moreover, we note that for the case $\phi \in L^1([\alpha_{min}, \alpha_{max})$ containing finitely many singularities at $\alpha_1, \alpha_2, \cdots, \alpha_m$, the whole interval $[\alpha_{min}, \alpha_{max}]$ and the integration can be written as*

$$\int_{\alpha_{min}}^{\alpha_1} \phi(\alpha)\ {}^{RL}_{x_L}\mathcal{D}^s_x(u)\, d\alpha + \int_{\alpha_1}^{\alpha_2} \phi(\alpha)\ {}^{RL}_{x_L}\mathcal{D}^s_x(u)\, d\alpha + \cdots + \int_{\alpha_m}^{\alpha_{max}} \phi(\alpha)\ {}^{RL}_{x_L}\mathcal{D}^s_x(u)\, d\alpha,$$

where all the previous steps in the proof can apply in each interval.

3.7.3 Proof of Lemma (7.3.4)

Proof. Since $u(a) = 0$, by (1.18) ${}_a\mathcal{D}^{2\mu}_x u = {}_a\mathcal{D}^{\mu}_x({}_a\mathcal{D}^{\mu}_x u)$. Taking $\widetilde{u}(x) = {}_a\mathcal{D}^{\mu}_x u$, we have

$$\begin{aligned}
({}_a\mathcal{D}^{2\mu}_x u\,,\, v) &= ({}_a\mathcal{D}^{\mu}_x \widetilde{u}\,,\, v), \\
&= \frac{1}{\Gamma(1-\mu)} \int_a^b \Big[\frac{d}{dx} \int_a^x \frac{\widetilde{u}(s)ds}{(x-s)^{\mu}} \Big] v(x)dx, \\
&= \Big\{ \frac{v(x)}{\Gamma(1-\mu)} \int_a^x \frac{\widetilde{u}(s)ds}{(x-s)^{\mu}} \Big\}_{x=a}^{x=b} \\
&- \frac{1}{\Gamma(1-\mu)} \int_a^b \Big[\int_a^x \frac{\widetilde{u}(s)ds}{(x-s)^{\mu}} \Big] \frac{dv(x)}{dx} dx, \quad by\ v(b) = 0, \\
&= -v(a) \lim_{x\to a}\, {}_a\mathcal{I}^{1-\mu}_x \widetilde{u} - \frac{1}{\Gamma(1-\mu)} \int_a^b \int_s^b \frac{\frac{dv(x)}{dx}dx}{(x-s)^{\mu}} \widetilde{u}(s)ds, \qquad (3.72)
\end{aligned}$$

which make sense when the interior term $\int_s^b \frac{\frac{dv(x)}{dx}dx}{(x-s)^{\mu}}$ is integrable in (a, b). Taking into account that $v(a)$ is bounded, we can show that the boundary term $v(a)\ \lim_{x\to a}\, {}_a\mathcal{I}^{1-\mu}_x \widetilde{u}$ also vanishes as

$$\begin{aligned}
\lim_{x\to a} \Big| {}_a\mathcal{I}^{1-\mu}_x \widetilde{u} \Big| &= \lim_{x\to a} \frac{1}{\Gamma(1-\mu)} \Big| \int_a^x \frac{\widetilde{u}(s)ds}{(x-s)^{\mu}} \Big|, \qquad (3.73) \\
&\leq \lim_{x\to a} \frac{1}{\Gamma(1-\mu)} \Big| \int_a^x \frac{ds}{(x-s)^{\mu}} \Big| \|\widetilde{u}\|_{L^\infty}, \\
&= \lim_{x\to a} \frac{1}{\Gamma(1-\mu)} \frac{(x-a)^{1-\mu}}{1-\mu} \|\widetilde{u}\|_{L^\infty} = 0.
\end{aligned}$$

Moreover, it is easy to check that

$$\begin{aligned}\frac{d}{ds}\int_s^b \frac{v(x)dx}{(x-s)^{\mu}} &= \frac{d}{ds}\Big\{\frac{v(x)(x-s)^{1-\mu}}{1-\mu}\Big|_{x=s}^{x=b} - \frac{1}{1-\mu}\int_s^b \frac{dv(x)}{dx}(x-s)^{1-\mu}dx\Big\},\\ &= \frac{d}{ds}\Big\{0 - \frac{1}{1-\mu}\int_s^b \frac{dv(x)}{dx}(x-s)^{1-\mu}dx\Big\},\\ &= \int_s^b \frac{\frac{dv(x)}{dx}dx}{(x-s)^{\mu}}. \end{aligned} \tag{3.74}$$

Now, by substituting (3.74) into (3.72), we obtain

$$\begin{aligned}({}_a\mathcal{D}_x^{2\mu}u\,,\,v) &= \int_a^b \widetilde{u}(s)\Big\{\frac{1}{\Gamma(1-\mu)}(\frac{-d}{ds})\int_s^b \frac{v(x)dx}{(x-s)^{\mu}}\Big\}ds,\\ &= (\widetilde{u}\,,\,{}_x\mathcal{D}_b^{\mu}v),\end{aligned}$$

when ${}_x\mathcal{D}_b^{\mu}v$ is well-defined and is integrable in the interval $[a,b]$. □

3.7.4 Proof of Theorem (4.3.2)

Proof. Part A:

The Jacobi polynomials, $P_n^{\alpha,\beta}(\xi)$, can be constructed via the three-term recursion relation. By letting $\beta = -\alpha$, the corresponding tree term recursion reduces to

$$P_{n+1}^{\alpha,-\alpha}(\xi) = \frac{(2n+1)}{(n+1)}\,\xi\;P_n^{\alpha,-\alpha}(\xi) - \frac{(n-\alpha^2)}{n(n+1)}\,\xi\;P_{n-1}^{\alpha,-\alpha}(\xi), \tag{3.75}$$

and therefore, the Jacobi polynomials evaluated at $\xi = \xi_0 \in [-1,1]$ are obtained in the following standard form

$$\begin{aligned}&P_0^{\alpha,-\alpha}(\xi_0) = \mathbb{P}_0(\alpha) = 1, && \text{: zeroth order in } \alpha\\ &P_1^{\alpha,-\alpha}(\xi_0) = \mathbb{P}_1(\alpha) = \alpha + \xi_0, && \text{: linear in } \alpha\\ &P_2^{\alpha,-\alpha}(\xi_0) = \mathbb{P}_2(\alpha) = \frac{1}{2}\,\alpha^2 + \frac{3}{2}\,\xi_0\,\alpha + \frac{3\,\xi_0^2-1}{2}, && \text{: quadratic in } \alpha\\ &P_3^{\alpha,-\alpha}(\xi_0) = \mathbb{P}_3(\alpha) = \frac{1}{6}\,\alpha^3 + \xi_0\,\alpha^2 + \frac{15\,\xi_0^2-4}{6}\,\alpha + \frac{5\,\xi_0^3-3\,\xi_0}{2}. && \text{: cubic in } \alpha\end{aligned} \tag{3.76}$$

Now, let $n = k$, thus, $P_k^{\alpha,-\alpha}(\xi_0)$ and $P_{k-1}^{\alpha,-\alpha}(\xi_0)$ are respectively polynomials of order k and $k-1$ in α. Using (3.75) for $n = k+1$, we get

$$P_{k+1}^{\alpha,-\alpha}(\xi_0) = \frac{(2k+1)}{(k+1)}\,\xi_0\;P_k^{\alpha,-\alpha}(\xi_0) - \frac{(k-\alpha^2)}{k(k+1)}\,\xi_0\;P_{k-1}^{\alpha,-\alpha}(\xi_0),$$

which is a polynomials of order $k+1$ in α due to the second term. Hence, by mathematical induction, $P_n^{\alpha,-\alpha}(\xi_0) = \mathbb{P}_n(\alpha)$ is a polynomial of order n in α $\forall \xi_0 \in [-1,1]$. Similarly with the same argument, we can show that $P_n^{-\alpha,\alpha}(\xi_0) = \mathbb{P}_n(-\alpha)$ is also a polynomial of order n in α $\forall \xi_0 \in [-1,1]$.

Part B:

The inner integral of the discrete distributed bilinear form (3.36) can be written as

$$\int_{\alpha_{min}}^{\alpha_{max}} \phi(\alpha) (\frac{2}{T})^{\alpha} \frac{\Gamma(n+\mu)}{\Gamma(n+\eta)} \frac{\Gamma(k+\mu)}{\Gamma(k+\eta)} {}^{(1)}\mathcal{P}_n^{\eta}(\xi) \ {}^{(2)}\mathcal{P}_k^{\eta}(\xi) \ d\alpha = \tag{3.77}$$
$$\Gamma(n+\mu)\Gamma(k+\mu) \int_{\alpha_{min}}^{\alpha_{max}} \phi(\alpha) \ (\frac{2}{T})^{\alpha} \frac{(1+\xi)^{\eta}}{\Gamma(n+\eta)} \frac{(1-\xi)^{\eta}}{\Gamma(k+\eta)} \ P_{n-1}^{-\eta,\eta}(\xi) \ P_{k-1}^{\eta,-\eta}(\xi) \ d\alpha,$$

in which $\eta = \mu - \alpha/2$. By theorem (4.3.2) part A, $P_{n-1}^{\frac{\alpha}{2}-\mu,\mu-\frac{\alpha}{2}}(\xi)$ and $P_{k-1}^{\mu-\frac{\alpha}{2},\frac{\alpha}{2}-\mu}(\xi)$ are polynomials in α of order $n-1$ and $k-1$, respectively, $\forall \xi \in [-1,1]$, and μ fixed. Thus,

$$P_{n-1}^{\frac{\alpha}{2}-\mu,\mu-\frac{\alpha}{2}}(\xi) \ = \sum_{r=0}^{n-1} \sigma_r \ P_r(\alpha), \tag{3.78}$$

$$P_{k-1}^{\mu-\frac{\alpha}{2},\frac{\alpha}{2}-\mu}(\xi) \ = \sum_{l=0}^{k-1} \widetilde{\sigma}_l \ P_l(\alpha). \tag{3.79}$$

By plugging (3.78) and (3.79) into (3.77), we obtain

$$\int_{\alpha_{min}}^{\alpha_{max}} \phi(\alpha) \ (\frac{2}{T})^{\alpha} \frac{(1+\xi)^{\eta}}{\Gamma(n+\eta)} \frac{(1-\xi)^{\eta}}{\Gamma(k+\eta)} \ P_{n-1}^{-\eta,\eta}(\xi) \ P_{k-1}^{\eta,-\eta}(\xi) \ d\alpha =$$
$$\int_{\alpha_{min}}^{\alpha_{max}} \phi(\alpha) \ \mathcal{W}_{kn}^{\xi,\mu}(\alpha) \ \sum_{r=0}^{n-1} \sigma_r \ P_r(\alpha) \ \sum_{l=0}^{k-1} \widetilde{\sigma}_l \ P_l(\alpha) \ d\alpha, \tag{3.80}$$

in which

$$\mathcal{W}_{kn}^{\xi,\mu}(\alpha) = (\frac{2}{T})^{\alpha} \ \frac{(1-\xi)^{\mu-\alpha}}{\Gamma(n+\mu-\alpha)} \frac{(1+\xi)^{\mu-\alpha}}{\Gamma(k+\mu-\alpha)}$$

is *smooth* in any compact support in $[\alpha_{min}, \alpha_{max}]$ and its polynomial expansion $\mathcal{W}_{kn}^{\xi,\mu}\big|_N(\alpha) = \mathcal{W}_N(\alpha) = \sum_{q=0}^{N} \ \rho_q \ P_q(\alpha)$ converges exponentially i.e.,

$$\left\| \mathcal{W}_{kn}^{\xi,\mu}(\alpha) - \mathcal{W}_N(\alpha) \right\| \leq c_1 \exp(-c_2 N^{c_3}), \tag{3.81}$$

in which $\|.\|$ denotes the L^2-norm in $[\alpha_{min}, \alpha_{max}]$. If the distribution function $\phi \in H^r([\alpha_{min}, \alpha_{max}])$, $r > 0$, we have the following projection error:

$$\|\phi(\alpha) - \phi_N(\alpha)\| \leq c_4 \, N^{-r} \, \|\phi\|_{H^r([\alpha_{min}, \alpha_{max}])}, \tag{3.82}$$

where $\phi_N(\alpha) = \sum_{n=0}^{N} \widetilde{\rho}_n P_n(\alpha)$. Consequently, the integrand in (3.80) can be well-approximated via

$$\phi(\alpha)\, \mathcal{W}_{kn}^{\xi,\mu}(\alpha) \sum_{r=0}^{n-1} \sigma_r P_r(\alpha) \sum_{l=0}^{k-1} \widetilde{\sigma}_l P_l(\alpha) \approx \phi_N(\alpha)\, \mathcal{W}_N(\alpha) \sum_{r=0}^{n-1} \sigma_r P_r(\alpha) \sum_{l=0}^{k-1} \widetilde{\sigma}_l P_l(\alpha). \tag{3.83}$$

Next, let

$$\begin{aligned} \mathcal{I} &= \int_{\alpha_{min}}^{\alpha_{max}} \phi(\alpha)\, \mathcal{W}_{kn}^{\xi,\mu}(\alpha) \sum_{r=0}^{n-1} \sigma_r P_r(\alpha) \sum_{l=0}^{k-1} \widetilde{\sigma}_l P_l(\alpha)\, d\alpha, \\ \mathcal{I}_N &= \int_{\alpha_{min}}^{\alpha_{max}} \phi_N(\alpha)\, \mathcal{W}_N(\alpha) \sum_{r=0}^{n-1} \sigma_r P_r(\alpha) \sum_{l=0}^{k-1} \widetilde{\sigma}_l P_l(\alpha)\, d\alpha, \end{aligned} \tag{3.84}$$

where $\mathcal{I}_N$ can be *accurately* calculated via

$$\mathcal{I}_N = \sum_{q=1}^{Q} \widetilde{w}_q\, \phi_N(\alpha_q) \mathcal{W}_N(\alpha_q) \sum_{r=0}^{n-1} \sigma_r P_r(\alpha_q) \sum_{l=0}^{k-1} \widetilde{\sigma}_l P_l(\alpha_q), \tag{3.85}$$

employing a Gauss-Legendre quadrature rule, provided $Q = 2N$. Thus by Cauchy-schwarz inequality,

$$|\mathcal{I} - \mathcal{I}_N| \leq \sqrt{\alpha_{min} - \alpha_{max}} \left\| \phi\, \mathcal{W}_{kn}^{\xi,\mu} \sum_{r=0}^{n-1} \sigma_r P_r \sum_{l=0}^{k-1} \widetilde{\sigma}_l P_l - \phi_N\, \mathcal{W}_N \sum_{r=0}^{n-1} \sigma_r P_r \sum_{l=0}^{k-1} \widetilde{\sigma}_l P_l \right\|, \tag{3.86}$$

in which

$$\left\|\left(\phi\,\mathcal{W}_{kn}^{\xi,\mu}\,\sum_{r=0}^{n-1}\sigma_r P_r\;\sum_{l=0}^{k-1}\widetilde{\sigma}_l P_l\right)-\left(\phi_N\,\mathcal{W}_N\,\sum_{r=0}^{n-1}\sigma_r P_r\;\sum_{l=0}^{k-1}\widetilde{\sigma}_l P_l\right)\right\|, \tag{3.87}$$

$$\leq \left\|\sum_{r=0}^{n-1}\sigma_r P_r\;\sum_{l=0}^{k-1}\widetilde{\sigma}_l P_l\right\|\left\|\phi\,\mathcal{W}_{kn}^{\xi,\mu}-\phi_N\,\mathcal{W}_N\right\|,\quad \text{(by Hölder inequality)},$$

$$\leq c_5\left\|\phi\,\mathcal{W}_{kn}^{\xi,\mu}-\phi_N\,\mathcal{W}_N\right\|,$$

$$\leq c_5\left\|\left[(\phi-\phi_N)+\phi_N\right]\left[(\mathcal{W}_{kn}^{\xi,\mu}-\mathcal{W}_N)+\mathcal{W}_N\right]\;-\phi_N\,\mathcal{W}_N\right\|,$$

$$\leq c_5\left\|(\phi-\phi_N)(\mathcal{W}_{kn}^{\xi,\mu}-\mathcal{W}_N)+\phi_N(\mathcal{W}_{kn}^{\xi,\mu}-\mathcal{W}_N)+(\phi-\phi_N)\mathcal{W}_N+\phi_N\,\mathcal{W}_N-\phi_N\,\mathcal{W}_N\right\|,$$

$$\leq c_5\left(\left\|(\phi-\phi_N)(\mathcal{W}_{kn}^{\xi,\mu}-\mathcal{W}_N)\right\|+\left\|\phi_N(\mathcal{W}_{kn}^{\xi,\mu}-\mathcal{W}_N)\right\|+\|(\phi-\phi_N)\mathcal{W}_N\|\right),\quad \text{(by triangle inequality)},$$

$$\leq c_5\left(\|(\phi-\phi_N)\|\left\|(\mathcal{W}_{kn}^{\xi,\mu}-\mathcal{W}_N)\right\|+\|\phi_N\|\left\|(\mathcal{W}_{kn}^{\xi,\mu}-\mathcal{W}_N)\right\|+\|(\phi-\phi_N)\|\,\|\mathcal{W}_N\|\right),$$

$$\leq c_5\left(c_4\;N^{-r}\,\|\phi\|_{H^r([\alpha_{min},\alpha_{max}])}\;.\,c_1\exp(-c_2N^{c_3})+\|\phi_N\|\,c_1\exp(-c_2N^{c_3})\right.$$

$$\left.+\,\|\mathcal{W}_N\|\,c_4\;N^{-r}\,\|\phi\|_{H^r([\alpha_{min},\alpha_{max}])}\right),\qquad \text{(by (3.81) and (3.82))},$$

$$\leq c_6\,N^{-r}\,\|\phi\|_{H^r([\alpha_{min},\alpha_{max}])}\,.$$

Hence, by (3.86) and (3.87) we can show

$$|\mathcal{I}-\mathcal{I}_N|\;\leq\;\mathscr{C}\,N^{-r}\,\|\phi\|_{H^r([\alpha_{min},\alpha_{max}])}\,, \tag{3.88}$$

and therefore, by (3.78), (3.79), (3.84) and (3.85), we obtain

$$\left|\int_{\alpha_{min}}^{\alpha_{max}}\phi(\alpha)\,(\frac{2}{T})^{\alpha}\,\frac{\Gamma(n+\mu)}{\Gamma(n+\eta)}\frac{\Gamma(k+\mu)}{\Gamma(k+\eta)}\,{}^{(1)}\mathcal{P}_n^{\eta}(\xi)\;\;{}^{(2)}\mathcal{P}_k^{\eta}(\xi)\;d\alpha\right.$$

$$\left.-\sum_{q=1}^{Q}\widetilde{w}_q\,\phi_N(\alpha_q)\,(\frac{2}{T})^{\alpha_q}\,\frac{\Gamma(n+\mu)}{\Gamma(n+\eta_q)}\frac{\Gamma(k+\mu)}{\Gamma(k+\eta_q)}\,{}^{(1)}\mathcal{P}_n^{\eta q}(\xi)\;\;{}^{(2)}\mathcal{P}_k^{\eta q}(\xi)\;\right|$$

$$\leq\mathscr{C}\,Q^{-r}\,\|\phi\|_{H^r([\alpha_{min},\alpha_{max}])}\,.$$

Part C:

If $\phi(\alpha)$ is smooth, then the approximation $\phi_N(\alpha)$, in (3.82), converges with an exponential accuracy and so does the norm in (3.87). Thus,

$$|\mathcal{I}-\mathcal{I}_N|\;\leq\;\mathscr{C}_1\exp(-\mathscr{C}_2\,N^{\mathscr{C}_3}), \tag{3.89}$$

and therefore, the quadrature rule becomes exponentially accurate in Q.

□

CHAPTER 4

DISTRIBUTED-ORDER FRACTIONAL PDES: FRACTIONAL PSEUDO-SPECTRAL METHODS

4.1 Background

In comparison to single order fractional operator, distributive character of DODEs increases the computational costs due to integration in the domain of derivative order, requiring efficient and accurate numerical schemes. Diethelm and Ford in [46], as one of the first numerical studies of DODEs, developed a two-stage basic frame-work, where in the first stage, the distributed order differentiation term was approximated using a quadrature rule, and in the second stage, a suitable multi-term numerical method was employed. Most of the subsequent numerical studies have followed the same approach yet they vary in the discretization method in the second stage, see e.g., distributed-order time-fractional diffusion equation [57], distributed-order reaction diffusion equation [124], distributed-order diffusion equation using a reproducing kernel method [98], and distributed-order time fractional diffusion-wave equation based on a compact difference scheme [179]. Other numerical studies include: multi-term and distributed order problems in half-line [106], an implicit numerical method of a temporal distributed order and two-sided space-fractional advection-dispersion equation in [69], high-order difference schemes in [60], alternating direction implicit (ADI) difference schemes with the extrapolation method for one-dimensional case in [62] and two-dimensional problem in [61], and an operational matrix technique in [50].

More recently, Kharazmi et al. [87] have developed a Petrov-Galerkin spectral method for DODEs, following the recent theory of FSLP in [186] and by employing Jacobi Poly-fractonomials as the bases and test functions, where they introduced the distributed Sobolev spaces and their associated equivalent norms, and investigated the stability and error analysis of the scheme. More importantly, they have developed a spectrally accurate Gauss-Legendre quadrature rule in the construction of linear system. We extend their developed scheme by proposing a pseudo-spectral

method in order to efficiently treat the nonlinear DODEs.

In this chapter, we propose a Petrov-Galerkin (PG) pseudo-spectral method for DODEs. We construct fractional Lagrange interpolants of first and second kind as basis and test functions, respectively. We obtain the corresponding *weak distributed differentiation matrices* for distributed-order operators with one- and two-sided fractional derivatives. We further study the effect of distribution function and interpolation points on the condition number of the resulting linear system and also design distributed pre-conditioners, based on the distribution function. We show the better conditioning of the resulting linear system by comparing the proposed method with the fractional spectral collocation method, developed in [87], which employs similar expansions but in a strong sense of problem. Moreover, the fractional Lagrange interpolants are comprised of a fractional order term multiplied by standard Lagrange interpolants, where we show that the interpolation parameter in the fractional part can be tunned properly to accurately capture any singularity of the solution. In addition, these fractional interpolants enjoy the property of Kronecker delta at the interpolation points, which makes it possible to efficiently treat the algebraic and differential nonlinearities such as in nonlinear reaction diffusion and Burgers equations. We demonstrate the efficiency of the proposed schemes by considering several numerical examples including nonlinearity, in which we show the spectral convergence of the approximate solution.

The organization of this chapter is as follows: In section (4.2), we provide preliminary definitions along with useful lemmas, and then define the initial and boundary value problems and obtain the weak formulation. In section (4.3), we implement the pseudo-spectral method and derive the weak distributed differentiation matrices. We further study the condition number of the linear system and design the pre-conditioner. We provide numerical examples in section (4.4).

4.2 Definitions

4.2.1 Distributed Fractional Sobolev Spaces

We first recall the fractional Sobolev space. By $H^s(\mathbb{R})$, $s \geq 0$, we denote the Fractional Sobolev space on $\mathbb{R}$, defined as $H^s(\mathbb{R}) = \{v \in L^2(\mathbb{R}) |\ (1 + |\omega|^2)^{\frac{s}{2}} \mathcal{F}(v)(\omega) \in L^2(\mathbb{R})\}$, which is endowed

with the norm $\|\cdot\|_{s,\mathbb{R}} = \|(1+|\omega|^2)^{\frac{s}{2}}\mathcal{F}(\cdot)(\omega)\|_{L^2(\mathbb{R})}$, where $\mathcal{F}(v)$ represents the Fourier transform of v. Subsequently, we denote by $H^s(I)$, $s \geq 0$ the Fractional Sobolev space on the finite closed interval I, defined as $H^s(I) = \{v \in L^2(\mathbb{R}) |\ \exists \tilde{v} \in H^s(\mathbb{R})\ s.t.\ \tilde{v}|_I = v\}$ with the norm $\|\cdot\|_{s,I} = \inf_{\tilde{v}\in H^s(\mathbb{R}),\tilde{v}|_I=(\cdot)} \|\tilde{v}\|_{s,\mathbb{R}}$. We note that the definition of $H^s(I)$ and the corresponding norm relies on the Fourier transformation of the function. Other left-sided $\|\cdot\|_{l,s,I}$ and right-sided $\|\cdot\|_{r,s,I}$ useful norms, associated with $H^s(I)$, e.g., when $I = [x_L, x_R]$, are also given as $\|\cdot\|_{l,s,I} = \left(\|\cdot\|^2_{L^2(I)} + \|\,{}^{RL}_{x_L}\mathcal{D}^{\mu}_{x}(\cdot)\|^2_{L^2(I)}\right)^{\frac{1}{2}}$, and $\|\cdot\|_{r,s,I} = \left(\|\cdot\|^2_{L^2(I)} + \|\,{}^{RL}_{x}\mathcal{D}^{\mu}_{x_R}(\cdot)\|^2_{L^2(I)}\right)^{\frac{1}{2}}$, which are shown in [52, 53] that are equivalent to $\|\cdot\|_{s,I}$.

Definition 4.2.1. *Distributed Fractional Sobolev Space* [87]: Let $\phi \in L^1([\alpha_{min}, \alpha_{max}])$, $0 \leq \alpha_{min} < \alpha_{max}$ be nonnegative. Then, the *distributed* fractional Sobolev space on $\mathbb{R}$ and its associated norm are

$$
{}^{\phi}\mathcal{H}(\mathbb{R}) = \{v \in L^2(\mathbb{R}) |\ \int_{\alpha_{min}}^{\alpha_{max}} \left[\phi(\alpha)(1+|\omega|^2)^{\alpha}\right]^{\frac{1}{2}}\ \mathcal{F}(v)(\omega)\ d\alpha\ \in L^2(\mathbb{R})\}, \tag{4.1}
$$

$$
\|\cdot\|_{\phi,\mathbb{R}} = \left(\int_{\alpha_{min}}^{\alpha_{max}} \phi(\alpha)\ \left\|(1+|\omega|^2)^{\frac{\alpha}{2}}\mathcal{F}(\cdot)(\omega)\right\|^2_{L^2(\mathbb{R})}\ d\alpha\right)^{\frac{1}{2}}. \tag{4.2}
$$

Subsequently, the *distributed* fractional Sobolev space on the finite closed interval I, i.e. ${}^{\phi}\mathcal{H}(I)$, is defined as

$$
{}^{\phi}\mathcal{H}(I) = \{v \in L^2(\mathbb{R}) |\ \exists \tilde{v} \in {}^{\phi}\mathcal{H}(\mathbb{R})\ \ s.t.\ \tilde{v}|_I = v\}, \tag{4.3}
$$

with the norm $\|\cdot\|_{\phi,I} = \inf_{\tilde{v}\in{}^{\phi}\mathcal{H}(\mathbb{R}),\tilde{v}|_I=(\cdot)} \|\tilde{v}\|_{\phi,\mathbb{R}}$. Moreover, the following useful norms, associated with ${}^{\phi}\mathcal{H}(I)$ are introduced as:

$$
\|\cdot\|_{l,\phi,I} = \left(\|\cdot\|^2_{L^2(I)} + \int_{\alpha_{min}}^{\alpha_{max}} \phi(\alpha)\ \left\|\,{}^{RL}_{x_L}\mathcal{D}^{\alpha}_{x}(\cdot)\right\|^2_{L^2(I)}\ d\alpha\right)^{\frac{1}{2}} \tag{4.4}
$$

$$
\|\cdot\|_{r,\phi,I} = \left(\|\cdot\|^2_{L^2(I)} + \int_{\alpha_{min}}^{\alpha_{max}} \phi(\alpha)\ \left\|\,{}^{RL}_{x}\mathcal{D}^{\alpha}_{x_R}(\cdot)\right\|^2_{L^2(I)}\ d\alpha\right)^{\frac{1}{2}}, \tag{4.5}
$$

which are proven in [87] to be equivalent to the norm $\|\cdot\|_{\phi,I}$.

Remark 4.2.2. *The lower and upper limits $\{\alpha_{min}, \alpha_{max}\}$ are only the theoretical terminals. However, for any realization of physical process, the range of derivative orders are not exactly equal*

to the these theoretical terminals. Moreover, the choice of ϕ can arbitrarily confine the domain of integration in practice, see for example Fig. 4.1 in the following sections, and if $\phi > 0$ is continuous in $(\alpha_{min}, \alpha_{max})$, then ${}^{\phi}\mathcal{H}$ is equivalent to $H^{\alpha_{max}-\epsilon}$, for some small ϵ.

Lemma 4.2.3. *[99]: For all $0 < \alpha \leq 1$, if $u \in H^1([a,b])$ such that $u(a) = 0$, and $w \in H^{\alpha/2}([a,b])$, then $({}_a\mathcal{D}_s^{\alpha} u, w)_\Omega = ({}_a\mathcal{D}_s^{\alpha/2} u\,,\, {}_s\mathcal{D}_b^{\alpha/2} w)_\Omega$, where $(\cdot,\cdot)_\Omega$ represents the standard inner product in $\Omega = [a,b]$.*

Lemma 4.2.4. *[87]: Let $1/2 < \mu < 1$, a and b be arbitrary finite or infinite real numbers. Assume $u \in H^{2\mu}(a,b)$ such that $u(a) = 0$, ${}_x\mathcal{D}_b^{\mu} v$ is integrable in (a,b), and $v(b) = 0$. Then $({}_a\mathcal{D}_x^{2\mu} u\,,\, v) = ({}_a\mathcal{D}_x^{\mu} u\,,\, {}_x\mathcal{D}_b^{\mu} v)$.*

4.2.2 Problem Definition: Initial/Boundary Value Problem

We consider the following distributed-order fractional differential equation, subject to the proper initial conditions

$$
\begin{aligned}
{}^{D}\mathcal{D}_{\phi} u(t) &= f(t;u), \quad \forall t \in (0,T], && (4.6)\\
u(0) &= 0, \quad \alpha_{max} \in (0,1], && (4.7)\\
u(0) = \frac{du}{dt}|_{t=0} &= 0, \quad \alpha_{max} \in (1,2], && (4.8)
\end{aligned}
$$

in which the distributed-order fractional derivative is defined in [87], as

$$
{}^{D}\mathcal{D}_{\phi} u(t) = \int_{\alpha_{min}}^{\alpha_{max}} \phi(\alpha)\, {}_a^*\mathcal{D}_t^{\alpha} u(t) d\alpha, \quad t > a, \tag{4.9}
$$

where $\alpha \mapsto \phi(\alpha)$ is a continuous mapping in $[\alpha_{min}, \alpha_{max}]$ and ${}_a^*\mathcal{D}_t^{\alpha}$ denotes Riemann-Liouville fractional derivative of order α. Due to (1.22), the Caputo and Riemann-Liouville fractional derivatives of order $\alpha \in (0,1)$ coincide with each other when $u(0) = 0$. Therefore, in this study, we employ the definition of the distributed fractional derivatives of Riemann-Liouville sense and remove the pre-superscript *RL* for simplicity.

Borrowing the same idea as in definition of distributed-order fractional derivative, we define the following distributed-order fractional derivative in space.

$$ {}^{D}\mathcal{D}_{\phi}u(x) = \int_{\alpha_{min}}^{\alpha_{max}} \phi(\alpha)\, {}_{a}^{*}\mathcal{D}_{x}^{\alpha}u(x)d\alpha, \quad a < x < b. \tag{4.10} $$

By performing an affine mapping from any confined domain $[a, b]$ to the standard domain $[-1, 1]$, we define the boundary value problem, subject to homogeneous Dirichlet boundary conditions as

$$ {}^{D}\mathcal{D}_{\phi}u(x) = f(x; u), \quad \forall x \in (-1, 1), \tag{4.11} $$

$$ u(-1) = u(1) = 0, \quad 1 < \alpha_{min} < \alpha_{max} \leq 2. \tag{4.12} $$

4.2.3 Weak Formulation

In order to obtain the weak form of the IVP (4.6) and BVP (4.11), we multiply the equations with proper test functions, and then integrate over the corresponding computational domain. Here, we show the weak form derivation only for the IVP. However, the formulation is similar for the BVP as well. Thus,

$$ \int_{\Omega} {}^{D}\mathcal{D}_{\phi}u(t)\, v(t)\, d\Omega = \int_{\Omega} f(t; u)\, v(t)\, d\Omega. \tag{4.13} $$

Using the definition of distributed order fractional derivatives defined in (5.7), we get

$$ \int_{\alpha_{min}}^{\alpha_{max}} \phi(\alpha) \left({}_{0}\mathcal{D}_{t}^{\alpha}u, v \right)_{\Omega} d\alpha = \int_{\Omega} f(t; u)\, v(t)\, d\Omega, \tag{4.14} $$

where $\left({}_{0}\mathcal{D}_{t}^{\alpha}u, v \right)_{\Omega} = \int_{\Omega} {}_{0}\mathcal{D}_{t}^{\alpha}u\, v\, d\Omega, \ \forall \alpha \in (\alpha_{min}, \alpha_{max})$, denotes the well-known L^2-inner product. Given the initial conditions (4.7) and/or (4.8) and by Lemmas (7.3.3) and (7.3.4), we define the bilinear form associated with $\alpha \in (\alpha_{min}, \alpha_{max})$ as $a^{(\alpha)}(u, v) = \left({}_{0}\mathcal{D}_{t}^{\alpha}u, v \right)_{\Omega} = ({}_{0}\mathcal{D}_{t}^{\alpha/2}u, {}_{t}\mathcal{D}_{T}^{\alpha/2}v)_{\Omega}$, in which we choose v such that $v(T) = 0$ and ${}_{t}\mathcal{D}_{T}^{\alpha/2}v$ is integrable in $\Omega \ \ \forall \alpha \in (\alpha_{min}, \alpha_{max})$.

Moreover, let U and V be the solution and test spaces, respectively defined as

$$ U = \left\{ u \in {}^{\phi}\mathcal{H}(\Omega) : \quad u(0) = 0 \text{ if } \alpha_{max} \in (0, 1], \quad u(0) = \frac{du}{dt}|_{t=0} = 0 \text{ if } \alpha_{max} \in (1, 2] \right\}, $$

$$ V = \left\{ v \in {}^{\phi}\mathcal{H}(\Omega) : \quad v(T) = 0 \right\}, $$

in which $\phi : (\alpha_{min}, \alpha_{max}) \rightarrow \mathbb{R}$. The problem thus reads as: find $u \in U$ such that $a(u,v) = l(f), \quad \forall v \in V$ where

$$a(u,v) := \int_{\alpha_{min}}^{\alpha_{max}} \phi(\alpha)\ a^{(\alpha)}(u,v)\, d\alpha \tag{4.15}$$

denotes the *distributed* bilinear form and $l(f) := (f,v)_\Omega$.

We note that by defining the following solution and test spaces, we obtain the same *distributed* bilinear form for the BVP as well, where the solution and test spaces are

$$U = \Big\{ u \in {}^{\phi}\mathcal{H}(\Omega) :\ u(-1) = u(1) = 0 \Big\}, \qquad V = \Big\{ v \in {}^{\phi}\mathcal{H}(\Omega) :\ v(1) = 0 \Big\}. \tag{4.16}$$

4.3 Fractional Pseudo-Spectral Method

4.3.1 Initial Value Problem

We consider the weak form $a(u,v) = l(f), \quad \forall v \in V$, associated with the IVP, and perform an affine mapping from $[0,T]$ to the standard domain $[-1,1]$. Following [186], we employ the *fractional Lagrange interpolant*s, given in the standard domain $[-1,1]$ by

$${}^{(1)}h_j^{\mu}(\xi) = \Big(\frac{\xi - x_1}{x_j - x_1}\Big)^{\mu} \prod_{\substack{k=1 \\ k \neq j}}^{N+1} \Big(\frac{\xi - x_k}{x_j - x_k}\Big), \ \ j = 1, 3, \cdots, N+1, \tag{4.17}$$

in which, $\mu \in (0,1)$, the *interpolation parameter*, is used as a tunable parameter for capturing possible singularities in the solution. We construct $N+1$ fractional Lagrange interpolants of order $N+\mu$ by defining $N+1$ " basis interpolating points" ${}^{(1)}\mathbb{W} = \{x_j \mid x_1 = -1,\ x_j \in (-1,1),\ j = 2, 3, \cdots, N+1\}$, of which, we assign the first degree of freedom (the first point, $x_1 = -1$) to the fractional part. Because of homogeneous initial condition, we only need to construct the interpolants, ${}^{(1)}h_j^{\mu}(\xi),\ j = 2, 3, \cdots, N+1$, thus, we seek the solution

$$u_N \in U_N = span\ \Big\{ {}^{(1)}h_j^{\mu}(\xi), \quad \xi \in [-1,1], \quad j = 2, 3, \cdots, N+1 \Big\}, \tag{4.18}$$

of the form

$$u_N(\xi) = \sum_{j=2}^{N+1} u_j\ \ {}^{(1)}h_j^{\mu}(\xi), \tag{4.19}$$

where, $u_j = u_N(\xi_j)$. We note that in the construction of fractional interpolants (4.17), we include the left boundary $x_1 = -1$ and start from $k = 1$. Therefore, we have a regularity of order $1 + \mu$ at $x_1 = -1$, which ensures satisfying the initial conditions, where $\alpha_{max} \in (1, 2)$.

Moreover, we construct another $N+1$ fractional Lagrange interpolants of order $N+\mu$ by defining a new set of $N + 1$ "test interpolating points" ${}^{(2)}\mathbb{W} = \{\tilde{x}_i \mid \tilde{x}_{N+1} = 1, \tilde{x}_i \in (-1, 1), i = 1, 2, \cdots, N\}$, of which, we assign the last degree of freedom (the last point, $x_{N+1} = 1$) to the fractional part. Therefore,

$$ {}^{(2)}h_i^{\mu}(\xi) = \left(\frac{\tilde{x}_{N+1} - \xi}{\tilde{x}_{N+1} - \tilde{x}_i}\right)^{\mu} \prod_{\substack{k=1 \\ k\neq i}}^{N+1} \left(\frac{\xi - \tilde{x}_k}{\tilde{x}_1 - \tilde{x}_k}\right), \quad i = 1, 2, \cdots, N. \tag{4.20} $$

Hence, we define the space of test functions V_N, of same dimension as the solution space, by

$$ V_N = span \left\{ {}^{(2)}h_i^{\mu}(\xi), \quad \xi \in [-1, 1], \quad i = 1, 2, \cdots, N \right\}, \tag{4.21} $$

where including $x_{N+1} = 1$ ensures vanishing test functions at the right boundary.

4.3.2 Boundary Value Problem

In this case due to the boundary conditions, we add one extra interpolation point and consider $N+2$ points. Therefore, we consider the following two sets of interpolation points ${}^{(1)}\mathbb{W} = \{x_j \mid x_1 = -1, x_{N+2} = 1, x_j \in (-1, 1), j = 2, 3, \cdots, N + 1\}$ and ${}^{(2)}\mathbb{W} = \{\tilde{x}_i \mid \tilde{x}_1 = -1, \tilde{x}_{N+2} = 1, \tilde{x}_i \in (-1, 1), i = 2, \cdots, N + 1\}$, and use (4.17) and (4.20) to construct the corresponding interpolants, where $k = 1, 2, \cdots, N + 2$.

Remark 4.3.1. *Such a construction has two benefits: (i) due to the homogeneous Dirichlet boundary conditions, we only need to construct the intrerpolants for $j = 2, 3, \cdots, N + 1$ (and not for $j = 1$ and $j = N + 2$). Therefore, the discrete solution space and the expansion* (4.18) *remain invariant. Moreover, the size of discrete test space does not change neither, however its elements shift from $i = 1, 2, \cdots, N$ for IVP to $i = 2, 3, \cdots, N + 1$ for BVP; (ii) the mathematical framework of the proposed scheme (derivation of the differentiation matrix) also remains invariant. Therefore, one can use the same derivation for the two cases IVP and BVP to construct the linear system, as will*

be discussed later, by properly changing the limits of iterator i on number of test functions. We also should note that inclusion of -1 *and* 1*, in addition to letting* k *to take vales* 1 *and* $N+2$*, imposes extra regularity to the solution at the boundaries, making its first derivative to vanish as well as the solution itself.*

For either case of IVP or BVP, since $\phi(\alpha) \geq 0$ and $\int_{\alpha_{min}}^{\alpha_{max}} \phi(\alpha)\, d\alpha$ is finite, it is straight forward to check that $U_N \subset U$ and $V_N \subset V$ when μ is chosen properly. Therefore, the bilinear form $a^{(\alpha)}(u, v)$ reduces to the *discrete* bilinear form

$$a_h^{\alpha}(u_N, v_N) = ({}_a\mathcal{D}_x^{\alpha/2} u_N, {}_x\mathcal{D}_b^{\alpha/2} v_N)_{\Omega}, \quad \forall x \in [a, b] \tag{4.22}$$

and thus, the problem reads as: find $u_N \in U_N$ such that

$$a_h(u_N, v_N) = l_h(f), \quad \forall v_N \in V_N, \tag{4.23}$$

where $a_h(u_N, v_N) := \int_{\alpha_{min}}^{\alpha_{max}} \phi(\alpha)\ a_h^{\alpha}(u_N, v_N)\, d\alpha$ denotes the *discrete* distributed bilinear form and $l_h(f) := (f, v_N)_{\Omega}$ represents the load vector.

4.3.3 Weak Distributed Differentiation Matrix

Here, we derive the corresponding differentiation matrix for IVP. As mentioned earlier, the same procedure can be readily used for BVP by changing the limits of iterator i, once proper interpolants are constructed (See subsections 4.3.1 and 4.3.2). By substituting (4.19), choosing $v_N = {}^{(2)}h_i^{\mu}(\xi) \in V_N$, $i = 1, 2, \cdots, N$ and using (1.21), the discrete distributed bilinear form (4.23) can be written as

$$\begin{aligned} a_h(u_N, v_N) &= \int_{\alpha_{min}}^{\alpha_{max}} \phi(\alpha)\ (\frac{2}{T})^{\alpha} \sum_{j=2}^{N+1} u_j \left({}_{-1}\mathcal{D}_{\xi}^{\alpha/2}[{}^{(1)}h_j^{\mu}(\xi)],\ {}_{\xi}\mathcal{D}_1^{\alpha/2}[{}^{(2)}h_i^{\mu}(\xi)] \right)_{\Omega} d\alpha, \qquad (4.24) \\ &= \sum_{j=2}^{N+1} u_j \int_{\alpha_{min}}^{\alpha_{max}} \phi(\alpha)\ (\frac{2}{T})^{\alpha} \left({}_{-1}\mathcal{D}_{\xi}^{\alpha/2}[{}^{(1)}h_j^{\mu}(\xi)],\ {}_{\xi}\mathcal{D}_1^{\alpha/2}[{}^{(2)}h_i^{\mu}(\xi)] \right)_{\Omega} d\alpha = \sum_{j=2}^{N+1} \mathscr{D}_{i,j}\ u_j, \end{aligned}$$

where

$$\mathscr{D}_{i,j} = \int_{\alpha_{min}}^{\alpha_{max}} \phi(\alpha)\ (\frac{2}{T})^{\alpha}\ \mathbb{D}_{i,j}^{\alpha}\ d\alpha \tag{4.25}$$

is the *weak distributed differentiation matrix*, and the integrand

$$\mathbb{D}^{\alpha}_{i,j} = \Big({}_{-1}\mathcal{D}^{\alpha/2}_{\xi}[{}^{(1)}h^{\mu}_{j}(\xi)]\,,\, {}_{\xi}\mathcal{D}^{\alpha/2}_{1}[{}^{(2)}h^{\mu}_{i}(\xi)] \Big)_{\Omega}$$

is derived as follows. Given the definition of fractional Lagrange interpolants in (4.17) and (4.20), we have

$$\mathbb{D}^{\alpha}_{i,j} = \Big(a_j \ {}_{-1}\mathcal{D}^{\alpha/2}_{\xi}[(1+\xi)^{\mu}\,\mathcal{G}_j(\xi)]\,,\, \tilde{a}_i \ {}_{\xi}\mathcal{D}^{\alpha/2}_{1}[(1-\xi)^{\mu}\,\tilde{\mathcal{G}}_i(\xi)] \Big)_{\Omega}, \quad \begin{matrix} i = 1,2,\cdots,N, \\ j = 2,3,\cdots,N+1, \end{matrix} \tag{4.26}$$

where, $a_j = \frac{1}{(x_j+1)^{\mu}}$, $\tilde{a}_i = \frac{1}{(1-\tilde{x}_i)^{\mu}}$, and

$$\mathcal{G}_j(\xi) = \prod_{\substack{k=1 \\ k\neq j}}^{N+1} \left(\frac{\xi - x_k}{x_j - x_k} \right), \qquad \tilde{\mathcal{G}}_i(\xi) = \prod_{\substack{k=1 \\ k\neq i}}^{N+1} \left(\frac{\xi - \tilde{x}_k}{\tilde{x}_1 - \tilde{x}_k} \right). \tag{4.27}$$

The functions $\mathcal{G}_j(\xi)$ and $\tilde{\mathcal{G}}_i(\xi)$ are polynomials of order N and thus, can be expanded in terms of Jacobi polynomials as

$$\mathcal{G}_j(\xi) = \sum_{n=1}^{N+1} {}^{(1)}\beta^{j}_{n}\ p^{-\mu,\mu}_{n-1}(\xi), \qquad j = 2,3,\cdots,N+1, \tag{4.28}$$

$$\tilde{\mathcal{G}}_i(\xi) = \sum_{m=1}^{N+1} {}^{(2)}\beta^{i}_{m}\ p^{\mu,-\mu}_{m-1}(\xi), \qquad i = 1,2,\cdots,N, \tag{4.29}$$

for which the coefficients ${}^{(1)}\beta^{j}_{n}$ and ${}^{(2)}\beta^{i}_{m}$ are obtained analytically, using the orthogonality of Jacobi polynomials, see section (4.5.1). Therefore,

$$\mathbb{D}^{\alpha}_{i,j} = \Big(a_j \sum_{n=1}^{N+1} {}^{(1)}\beta^{j}_{n}\ {}_{-1}\mathcal{D}^{\alpha/2}_{\xi}[(1+\xi)^{\mu}\ p^{-\mu,\mu}_{n-1}(\xi)]\,,\, \tilde{a}_i \sum_{m=1}^{N+1} {}^{(2)}\beta^{i}_{m}\ {}_{\xi}\mathcal{D}^{\alpha/2}_{1}[(1-\xi)^{\mu}\ p^{\mu,-\mu}_{m-1}(\xi)] \Big)_{\Omega}, \tag{4.30}$$

$$= \Big(a_j \sum_{n=1}^{N+1} {}^{(1)}\beta^{j}_{n}\ {}_{-1}\mathcal{D}^{\alpha/2}_{\xi}[{}^{(1)}\mathcal{P}^{\mu}_{n}(\xi)]\,,\, \tilde{a}_i \sum_{m=1}^{N+1} {}^{(2)}\beta^{i}_{m}\ {}_{\xi}\mathcal{D}^{\alpha/2}_{1}[{}^{(2)}\mathcal{P}^{\mu}_{m}(\xi)] \Big)_{\Omega},$$

where ${}^{(1)}\mathcal{P}^{\mu}_{n}(\xi)$ and ${}^{(2)}\mathcal{P}^{\mu}_{m}(\xi)$ are Jacobi poly-fractonomials of first and second kind, respectively, of which the fractional derivatives are

$${}_{-1}\mathcal{D}^{\alpha/2}_{\xi}[{}^{(1)}\mathcal{P}^{\mu}_{n}(\xi)] = \frac{\Gamma(n+\mu)}{\Gamma(n+\mu-\alpha/2)}\,{}^{(1)}\mathcal{P}^{\mu-\alpha/2}_{n}(\xi), \tag{4.31}$$

$${}^{RL}_{\xi}\mathcal{D}^{\alpha/2}_{1}[{}^{(2)}\mathcal{P}^{\mu}_{m}(\xi)] = \frac{\Gamma(m+\mu)}{\Gamma(m+\mu-\alpha/2)}\,{}^{(2)}\mathcal{P}^{\mu-\alpha/2}_{m}(\xi), \tag{4.32}$$

using (3.1). Let

$$ {}_L\mathbb{D}^{\alpha/2,\mu}_{\xi,j}(\xi) = a_j \sum_{n=1}^{N+1} {}^{(1)}\beta^j_n \ \frac{\Gamma(n+\mu)}{\Gamma(n+\mu-\alpha/2)} \ p^{-\mu+\alpha/2,\,\mu-\alpha/2}_{n-1}(\xi), \tag{4.33} $$

$$ {}_R\mathbb{D}^{\alpha/2,\mu}_{\xi,i}(\xi) = \tilde{a}_i \sum_{m=1}^{N+1} {}^{(2)}\beta^i_m \ \frac{\Gamma(m+\mu)}{\Gamma(m+\mu-\alpha/2)} \ p^{\mu-\alpha/2,\,-\mu+\alpha/2}_{m-1}(\xi). \tag{4.34} $$

Hence,

$$ \begin{aligned} \mathbb{D}^{\alpha}_{i,j} &= \Big({}_{-1}\mathcal{D}^{\alpha/2}_{\xi}[{}^{(1)}h^{\mu}_j(\xi)] \,,\, {}_{\xi}\mathcal{D}^{\alpha/2}_{1}[{}^{(2)}h^{\mu}_i(\xi)] \Big)_{\Omega}, \\ &= \Big((1+\xi)^{\mu-\alpha/2} \ {}_L\mathbb{D}^{\alpha/2,\mu}_{\xi,j}(\xi) \,,\, (1-\xi)^{\mu-\alpha/2} \ {}_R\mathbb{D}^{\alpha/2,\mu}_{\xi,i}(\xi) \Big)_{\Omega}. \end{aligned} \tag{4.35} $$

The expression in (4.35) is also used later in the section of numerical results to obtain the corresponding system of ODEs in solving Burgers equation.

Theorem 4.3.2. *Spectrally/Exponentially Accurate Quadrature Rule in α-Dimension [87]:*

Part A: $\forall \xi = \xi_0 \in [-1,1]$ fixed, and $\forall n \in \mathbb{N} \cup \{0\}$, the Jacobi polynomial $P_n^{\pm\alpha,\mp\alpha}(\xi_0)$ is a polynomial of order n in α.

Part B: Let $\phi \in H^r([\alpha_{min},\alpha_{max}])$, $r > 0$. Then $\forall \mu \geq \alpha_{max}/2$

$$ \begin{aligned} &\left| \int_{\alpha_{min}}^{\alpha_{max}} \phi(\alpha) \left(\frac{2}{T}\right)^{\alpha} \frac{\Gamma(n+\mu)}{\Gamma(n+\eta)} \frac{\Gamma(k+\mu)}{\Gamma(k+\eta)} \, {}^{(1)}\mathcal{P}^{\eta}_n(\xi) \ {}^{(2)}\mathcal{P}^{\eta}_k(\xi) \, d\alpha \, - \right. \\ &\left. \sum_{q=1}^{Q} \widetilde{w}_q \, \phi(\alpha_q) \left(\frac{2}{T}\right)^{\alpha_q} \frac{\Gamma(n+\mu)}{\Gamma(n+\eta_q)} \frac{\Gamma(k+\mu)}{\Gamma(k+\eta_q)} \, {}^{(1)}\mathcal{P}^{\eta_q}_n(\xi) \ {}^{(2)}\mathcal{P}^{\eta_q}_k(\xi) \right| \leq \mathscr{C} \, Q^{-r} \, \|\phi\|_{H^r([\alpha_{min},\alpha_{max}])}, \end{aligned} $$

where $\mathscr{C} > 0$, $\phi_N(\alpha) = \sum_{n=0}^{N} \widetilde{\rho}_n \, P_n(\alpha)$ denotes the polynomial expansion of $\phi(\alpha)$, and $\{\alpha_q, \widetilde{w}_q\}\big|_{q=1}^{Q}$ represents the set of Gauss-Legendre quadrature points and weights.

Part C: If $\phi(\alpha)$ is smooth, the quadrature rule in α-dimension becomes exponentially accurate in Q.

The construction of weak distributed differentiation matrix $\mathscr{D}_{i,j}$ requires two stages of quadrature rule. The first stage is in the domain of α, following Theorem 4.3.2, where we obtain the quadrature points and corresponding weights $\{\alpha_q, w_q\}\big|_{q=0}^{Q}$ by performing an affine mapping from

$\alpha \in [\alpha_{min}, \alpha_{max}]$ to the standard domain $\alpha_{st} \in [-1, 1]$ with Jacobian $J_\alpha = \frac{(\alpha_{max} - \alpha_{min})}{2}$. Therefore,

$$\mathscr{D}_{i,j} = \sum_{q=0}^{Q} J_\alpha \; w_q \, \phi(\alpha_q) \; (\frac{2}{T})^{\alpha q} \; \mathbb{D}_{i,j}^{\alpha q} \tag{4.36}$$

In the second stage, for each quadrature point α_q, we obtain the proper set of quadrature points in ξ, corresponding to the weight functions $(1+\xi)^{\mu-\alpha q/2}$ and $(1-\xi)^{\mu-\alpha q/2}$ and thus, we carry out the integral (4.35) to compute the entry $\mathbb{D}_{i,j}^{\alpha q}$.

4.3.4 Construction of Linear System

The bilinear form $a_h(u_N, v_N) = l_h(v_N)$ can be recast as:

$$\sum_{j=2}^{N+1} \mathscr{D}_{i,j} \; u_j = f_i \; , \qquad \begin{array}{ll} i = 1, 2, \cdots, N, & \text{IVP} \\ i = 2, 3, \cdots, N+1, & \text{BVP} \end{array} \tag{4.37}$$

where $\mathscr{D}_{i,j}$ are given in (4.36) and

$$f_i = \big(f, {}^{(2)}h_i^\mu(\xi)\big)_\Omega = \tilde{a}_i \int_{-1}^{1} (1-\xi)^\mu f(\xi) \, \tilde{\mathcal{G}}(\xi) \, d\xi, \tag{4.38}$$

are computed by employing a proper quadrature rule based on the regularity of force function f. Thus, the linear system is constructed as

$$\mathscr{D}\vec{u} = \vec{\mathcal{F}}, \tag{4.39}$$

where $\vec{u} = \{u_2, u_3, \cdots, u_{N+1}\}$. In the section of numerical results, we use the obtained differentiation matrix to solve non-linear equations as well, where we provide the corresponding system of ODEs for each problem. We follow the steps below to construct the liner system, and then, perform time integration in time dependent problems (The following interpolation matrix $\mathcal{M}$ and

nonlinear-induced matrix $\mathcal{N}$ are defined later in section 4.4).

(i) *Choose the proper sets of interpolation points* : ${}^{(1)}\mathbb{W}, {}^{(2)}\mathbb{W}$

(ii) *Form the basis and test functions* : ${}^{(1)}h_j^{\mu}(\xi), {}^{(2)}h_i^{\mu}(\xi)$

(iii) *Obtain the quadrature points in* α *domain integal* : α_q, w_q

(iv) *Obtain the quadrature points in space integral*

(v) *Construct the corresponding interpolation, differentiation, and nonlniear-induced matrices* : $\mathcal{M}, \mathscr{D}, \mathcal{N}$

(vi) 2^{nd}*-order Adams Bashforth time integration*

4.3.5 Condition Number of Linear System

We consider different choices of interpolation points and study the condition number of the resulting linear system. Also, based on the distribution function $\phi(\alpha)$, we develop several pre-conditioning matrices, corresponding to the choice of interpolation points, and investigate their efficiency.

4.3.5.1 Interpolation Points

Fractional operators in general lead to full and asymmetric linear systems, of which the condition number significantly grows with the number of modes, thus, requiring developing effective and easy to construct pre-conditioners. In addition, the distribution function $\phi(\alpha)$ and the choice of interpolation points are other major factors affecting the condition number of the resulting linear system. In the distributed order fractional operators, for each realization of a physical process, the distribution function $\phi(\alpha)$ can be obtained from observable data and arbitrarily confine the theoretical lower and upper terminals α_{min} and α_{max} in practice. For example, in a super-diffusive process, the distribution can be more biased toward the upper bound $\alpha_{max} = 2$. Therefore, the choice of $\phi(\alpha)$ has a direct effect on the properties of resulting linear system. To illustrate, we consider $\phi(\alpha)$ to be left- and right-biased normal distribution function with various mean and variance, shown in Fig. 4.1 (left). We construct the corresponding differentiation matrices for interpolation parameters $\mu = \{0.1, 0.9\}$, where we use choice (ii) of interpolation points. The

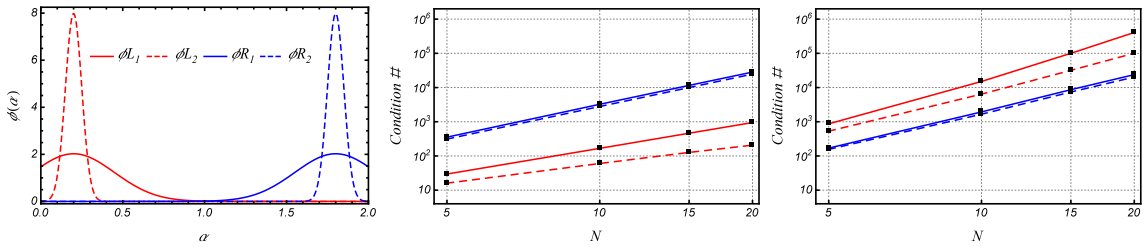

Figure 4.1: Initial/Boundary value problem: condition number of the resulting linear system for left- and right-biased normal distributions (left), where $\mu = 0.1$ (middle), $\mu = 0.9$ (right), and choice (ii) of interpolation points is used.

condition number of resulting linear system is shown in Fig. 4.1 (middle) and (right). We observe that for the right-biased distributions, which have the mean values closer to the upper terminal, the choice of μ does not have a significant effect on the condition number of the linear system. However, this is not the case for left-sided distributions, where we observe that the choice of $\mu = 0.1$, closer to mean value of distribution, results in better condition number. Moreover, the results in Fig. 4.1 suggests that distributions with larger variance, which include a wider range of derivative orders, lead to higher condition number; and this situation becomes even more adverse when the distribution is also left-biased.

The constructed fractional Lagrange interpolants are all of same order and do not form a set of hierarchical basis. Thus, for each set of interpolation points, we need to reconstruct the interpolants as well as the differentiation matrix. Therefore, the corresponding linear system highly depends on the choice of interpolation points. Here, we examine four methods that yield different sets of interpolation/collocation points. In each case, we form two sets of N points in the open range $(-1, 1)$ and append -1 to obtain ${}^{(1)}\mathbb{W}$ as the first set of interpolations points to construct the interpolants, ${}^{(1)}h_j^{\mu}(\xi)$, $j = 2, 3, \cdots, N+1$, and 1 to obtain ${}^{(2)}\mathbb{W}$ as the second set of interpolations points to construct the interpolants, ${}^{(2)}h_i^{\mu}(\xi)$, $1 = 1, 2, \cdots, N$. We refer to the aforementioned points as follows:

(i) *Equidistant points:* this choice is inspired by the well-known Fourier collocation points. We form the two similar set of N points by considering $\xi_q = -1 + \frac{2q}{N+1}$, $q = 1, 2, \cdots, N$, and then, obtain ${}^{(1)}\mathbb{W}$ and ${}^{(2)}\mathbb{W}$.

(ii) *Roots of Jacobi polynomials:* we form the two different set of N points by considering the zeros of $p_N^{-\mu,\mu}(\xi)$ and $p_N^{\mu,-\mu}(\xi)$, which are essentially the *Gauss-Jacobi* points. Then, we obtain ${}^{(1)}\mathbb{W}$ and ${}^{(2)}\mathbb{W}$ by appending -1 and 1 to the first and second set, respectively. Indeed, the obtained interpolation points are the *Gauss-Radau* points as the zeros of Jacobi polyfractonomials ${}^{(1)}\mathcal{P}^{\mu}_{N+1}(\xi)$ and ${}^{(2)}\mathcal{P}^{\mu}_{N+1}(\xi)$.

(iii) *Roots of Chebyshev polynomials:* we form the two similar set of N points by considering $\xi_q = -\cos\left(\frac{2q+1}{N}\frac{\pi}{2}\right),\ q = 0, 1, \cdots, N-1$ as the roots of Chebyshev polynomial $T_N(\xi)$, which are also Gauss points. Hence, we obtain ${}^{(1)}\mathbb{W}$ and ${}^{(2)}\mathbb{W}$ by adding -1 and 1.

(iv) *Roots of derivative of Chebyshev polynomials:* we form the two similar set of N points by considering $\xi_q = -\cos\left(\frac{\pi q}{\text{Ntot}+1}\right),\ q = 1, 2, \cdots, N$ as the roots $\frac{d}{d\xi}T_{N+1}(\xi)$ and then, obtain the two sets.

In order to examine the efficiency of each choice of interpolation points, we consider the linear distributed-order initial value problem (4.6), where we let $u^{ext} = t^5$, $\phi(\alpha) = \frac{\Gamma(6-\alpha)}{\Gamma(6)}$, $\alpha \in (0,2)$, and $f(t) = \frac{t^3\left(t^2-1\right)}{\log(t)}$. We solve the problem, using the developed scheme, in which we consider the aforementioned four choices of interpolation points and then, compute error and condition number of the resulting linear system for $\mu = \{1 - 10^{-4}, 0.1, 0.5, 0.9\}$. Due to the uniqueness of polynomials, we observe that the choice of different points does not affect the rate of convergence, however, has a great effect on the condition number of the constructed linear system. We see in Fig. 4.2 that for the given $\phi(\alpha)$, roots of Jacobi polynomials $p_N^{-\mu,\mu}(\xi)$ and $p_N^{\mu,-\mu}(\xi)$ (choice (ii)) leads to the lowest condition number, and for relatively small and large values of μ, improves the condition number by almost two orders of magnitude. In the next section, we design a set of pre-conditioners, which can further improve the condition number for this choice of interpolation points.

4.3.5.2 Pre-Conditioning

We introduce a distributed pre-conditioner matrix M^{-1}, whose entries are given by:

$$M_{lr}^{-1} = \int_{\sigma_{min}}^{\sigma_{max}} \varphi(\sigma)\ {}^{(2)}\mathcal{P}_r^{\sigma}(\xi_l)\ d\sigma, \quad l, r = 1, 2, \cdots, N, \tag{4.40}$$

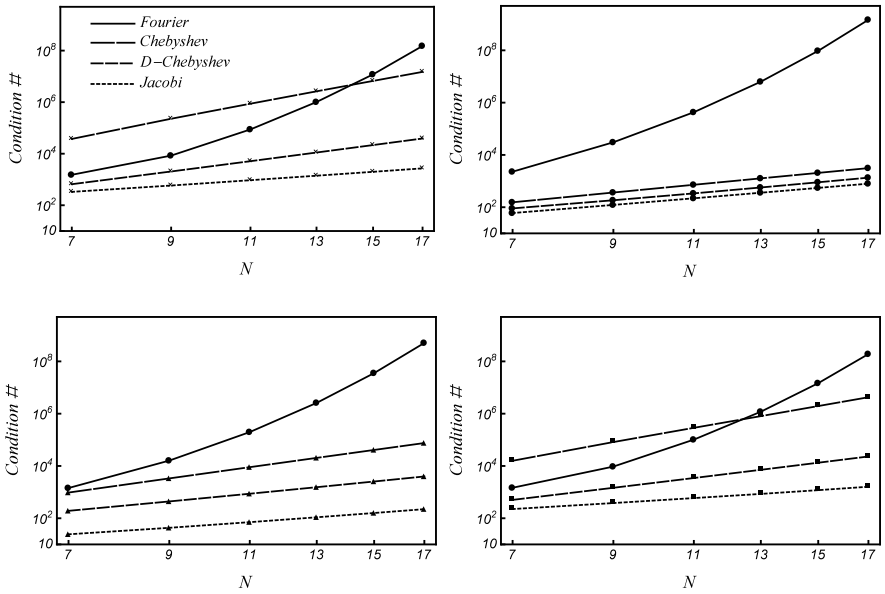

Figure 4.2: Initial/Boundary value problem: condition number of the resulting linear system for different choices of interpolation points for different interpolation parameter, (left to right) $\mu = 1 - 10^{-4}$, 0.1, 0.5, and 0.9, where $\phi(\alpha) = \frac{\Gamma(6-\alpha)}{\Gamma(6)}$ and $\alpha \in (0,2)$.

where we consider $\{\sigma_{min}, \sigma_{max}\} = \{\alpha_{min}, \alpha_{max}\}$ and $\xi_l\big|_{l=1}^{N}$ to be the zeros of $P_N^{\sigma_0,-\sigma_0}$. Different choices of σ_0 and also $\varphi(\sigma)$ result in different matrices M. We consider the following choices to construct the pre-conditioning matrix:

(i) $\varphi = \delta(\sigma - \sigma_0) \quad \sigma_0 = \mu$

(ii) $\varphi = \phi \qquad\qquad \sigma_0 = \mu$

where μ is the interpolation parameter and δ is the kronecker delta function.

In order to investigate the efficiency of introduced pre-conditioner, we apply them to the linear system, obtained in the previous section for choice (ii) of interpolation points. Thus, we let $\phi(\alpha) = \frac{\Gamma(6-\alpha)}{\Gamma(6)}$, $\alpha \in (0,2)$. We show in Fig. 4.3 that the designed pre-conditioner (ii) improves the condition number of the linear system more efficiently and at least. Furthermore, we consider the same problem but with a right-biased distribution function, and show in Fig. 4.4 that the designed pre-conditioner (i) is more effective. We also note that in both cases of $\phi(\alpha)$, either choices of pre-conditioners have almost similar performance.

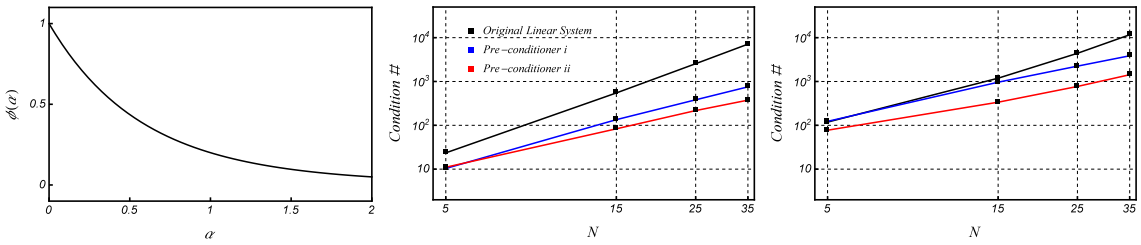

Figure 4.3: Condition number of the original linear system with $\phi(\alpha) = \frac{\Gamma(6-\alpha)}{\Gamma(6)}$ (left), and the pre-conditioned one for $\mu = 1/10$ (middle), and $\mu = 9/10$ (right).

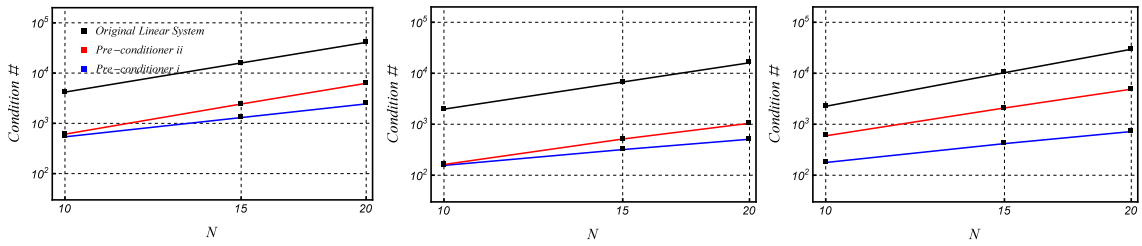

Figure 4.4: Condition number of the linear system for right-biased normal distribution. The original linear system (black lines) and the pre-conditioned one (red and blue lines) for $\mu = 1/10$ (left), $\mu = 5/10$ (middle), and $\mu = 9/10$ (right).

4.3.6 Weak Distributed Differentiation Matrix: Two-Sided Distributed-Order BVPs

We extend our formulation to the two-sided space distributed-order derivative (in Riemann-Liouville sense) in BVPs and consider the following problem

$$
\begin{aligned}
{}^{D}\mathcal{D}_{\phi}u(x) &= \int_{\alpha_{min}}^{\alpha_{max}} \phi(\alpha)\left(\kappa_l\ {}_{-1}\mathcal{D}_x^{\alpha}u(x) + \kappa_r\ {}_{x}\mathcal{D}_1^{\alpha}u(x)\right)d\alpha = f(x;u), \qquad (4.41)\\
u(-1) &= u(1) = 0, \quad 1 < \alpha_{min} < \alpha_{max} \leq 2 \quad \forall x \in (-1,1),
\end{aligned}
$$

for which the discrete bilinear form can be written as: $a_h^{\alpha}(u_N, v_N) = \kappa_l\,({}_{-1}\mathcal{D}_x^{\alpha/2}u_N, {}_{x}\mathcal{D}_1^{\alpha/2}v_N)_{\Omega} + \kappa_r\,({}_{x}\mathcal{D}_1^{\alpha/2}u_N, {}_{-1}\mathcal{D}_x^{\alpha/2}v_N)_{\Omega}$. We follow the derivation in implementing the pseudo-spectral scheme, where we need to construct two sets of fractional interpolants. The challenge in such problem is to consider the interpolation points such that we can take the two sided derivative of the resulting interpolant with no extra cost and thus, respect the formulation of weak distributed differentiation matrix. By picking the interpolation parameter μ to be zero, the two sets of interpolation points coincide. Therefore, the fractional interpolants become the standard Lagrange interpolants, which

can be expanded in terms of Legendre polynomial, and we can readily take their right- and left-sided derivatives. Hence,

$$ {}^{(1)}h_j^{\mu}(\xi)\Big|_{\mu=0} = h_j(\xi) = \prod_{\substack{k=1\\k\neq j}}^{N+2}\left(\frac{\xi - x_k}{x_j - x_k}\right) = \sum_{n=1}^{N+1}\beta_n^j\ P_n(\xi),\ j = 2,3,\cdots,N+1, $$

$$ {}^{(2)}h_i^{\mu}(\xi)\Big|_{\mu=0} = h_i(\xi) = \prod_{\substack{k=1\\k\neq i}}^{N+2}\left(\frac{\xi - x_k}{x_i - x_k}\right) = \sum_{m=1}^{N+1}\beta_m^i\ P_m(\xi),\ i = 2,3,\cdots,N+1, $$

where $P_n(\xi)$ and $P_m(\xi)$ are the Legendre polynomial. We follow similar derivation as in Sec. 4.3.3 and let

$$ \begin{aligned} \mathbb{D}_{i,j}^{\alpha} &= \Big(\sum_{n=1}^{N+1}\beta_{n\ -1}^{j}\mathcal{D}_{\xi}^{\alpha/2}[P_n(\xi)], \sum_{m=1}^{N+1}\beta_{m\ \xi}^{i}\mathcal{D}_{1}^{\alpha/2}[P_m(\xi)]\Big)_{\Omega} \\ &= \Big((1+\xi)^{-\alpha/2}\ {}_L\mathbb{D}_{\xi,j}^{\alpha/2}(\xi),\,(1-\xi)^{-\alpha/2}\ {}_R\mathbb{D}_{\xi,i}^{\alpha/2}(\xi)\Big)_{\Omega}, \end{aligned} $$

which can be taken by a proper quadrature rule with the corresponding weights $(1+\xi)^{-\alpha/2}$ and $(1-\xi)^{-\alpha/2}$, where

$$ {}_L\mathbb{D}_{\xi,j}^{\alpha/2}(\xi) = \sum_{n=1}^{N+1}\beta_n^j\ \frac{\Gamma(n+1)}{\Gamma(n-\alpha/2+1)}P_n^{\alpha/2,-\alpha/2}(\xi)\,(1+\xi)^{-\alpha/2}, $$

$$ {}_R\mathbb{D}_{\xi,i}^{\alpha/2}(\xi) = \sum_{m=1}^{N+1}\beta_m^i\ \frac{\Gamma(m+1)}{\Gamma(m-\alpha/2+1)}P_m^{-\alpha/2,\alpha/2}(\xi)\,(1-\xi)^{-\alpha/2}. $$

Thus, the discrete bilinear can be written as $a_h^{\alpha}(u_N, v_N) = \left(\kappa_l\ \mathbb{D}_{i,j}^{\alpha} + \kappa_r\ \mathbb{D}_{j,i}^{\alpha}\right)$ and the *two-sided weak distributed differentiation matrix* takes the form

$$ \mathscr{D}_{i,j} = \int_{\alpha_{min}}^{\alpha_{max}}\phi(\alpha)\ \left(\kappa_l\ \mathbb{D}_{i,j}^{\alpha} + \kappa_r\ \mathbb{D}_{j,i}^{\alpha}\right)\ d\alpha. \tag{4.42} $$

We note that if $\kappa_l = \kappa_r$, then the obtained differentiation matrix is symmetric.

4.4 Numerical Simulations

In order to examine the efficiency of proposed numerical schemes, we consider several numerical examples as follows.

4.4.1 Distributed-Order IVP

We recall the IVP (4.6) here ${}^{D}\mathcal{D}_{\phi}u(t) = f(t),\ \forall t \in (0,T]$, subject to zero initial conditions, which we solve for two smooth and non-smooth test cases:

- Case I: $u^{ext} = t^5$, $\phi(\alpha) = \frac{\Gamma(6-\alpha)}{\Gamma(6)}$, $f(t) = \frac{t^3\left(t^2-1\right)}{\log(t)}$,
- Case II: $u^{ext} = t^{5+\mu}$, $\phi(\alpha) = \frac{\Gamma(6+\mu-\alpha)}{\Gamma(6+\mu)}$, $f(t) = \frac{t^{3+\mu}\left(t^2-1\right)}{\log(t)}$,

where $\alpha \in (0,2)$. following the procedure, we construct the linear system (4.39). By taking the simulation time $T = 2$ and for different choices of μ, we investigate the convergence of the solution in L^2-norm. It is observed that the choice of μ has an important effect on the accuracy of scheme. But the exact solution is not always known in distributed-order problems. Hence, the fractional parameter μ can play the role of a *fine-tuning knob* giving the possibility of searching for the best/optimal case, where the highest rate can be achieved with minimal degrees of freedom. As shown in Fig. 4.5 (a) for the case of smooth solution, the error reaches machine precision much faster by tunning the parameter μ to be close to 1, where the nodal basis resemble the standard Lagrange behavior and thus, more efficient to capture the smooth solution. Moreover, in the case of singular solution, we can readily capture the singularity by tunning the interpolation parameter such that the singularity is captured by the fractional part of the nodal basis and the smooth part is captured by choosing enough number of interpolation points. In both cases, decreasing the value of μ leads to a better conditioned resulting linear system, see Table. 4.1.

Table 4.1: Pseudo-spectral method: condition number of the resulting linear system, Case-I (left), Case-II (right).

N	$\mu = 1 - 10^{-4}$	$\mu = 9/10$	$\mu = 5/10$	$\mu = 1/10$
5	165.846	118.412	14.519	23.5263
9	582.666	381.589	43.1632	122.499
13	1400.63	853.817	109.051	358.571
17	2701.79	1607.76	222.974	796.262

N	$\mu = 1 - 10^{-4}$	$\mu = 9/10$	$\mu = 5/10$	$\mu = 1/10$
2	28.8334	22.2707	4.61492	3.03315
3	71.0737	56.0664	8.03363	6.21275
4	119.133	92.2287	6.85646	12.7772
5	184.823	136.858	15.935	22.9091

Table 4.2 shows the condition number of the resulting linear system for case-I, constructed by fractional collocation method for distributed-order differential equations, developed in [87] and the current pseudo-spectral method, and we observe that the proposed scheme wins.

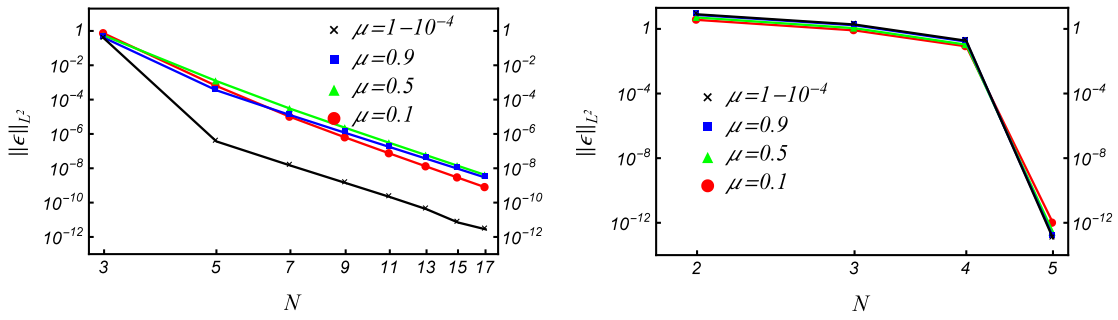

Figure 4.5: Pseudo-spectral method: L^2-norm error of the approximate solution, (left) Case I (right) Case II

Table 4.2: Condition number of the resulting linear system. The comparison between fractional collocation method (employing fractional interpolants in the strong sense [87]), and pseudo-spectral method (employing fractional interpolants in the weak sense).

	μ = 9/10		μ = 5/10		μ = 1/10	
N	Strong	Weak	Strong	Weak	Strong	Weak
6	60.3467	118.412	43.6649	14.519	36.0056	23.5263
10	325.037	381.589	214.935	43.1632	202.826	122.499
14	1076.14	853.817	685.166	109.051	713.002	358.571
18	2665.32	1607.76	1661.16	222.974	3397.2	796.262

4.4.2 (1+1)-Dimensions Space Distributed-Order Burgers Equation

Let $u : \Omega \rightarrow \mathbb{R}$, where $\Omega = [-1,1] \times [0,T]$. We consider the following space distributed-order fractional Burgers equation with nonlinear reaction term

$$\frac{\partial u(x,t)}{\partial t} = \kappa \ {}^{D}\mathcal{D}_{\phi} u(x,t) - \gamma \ u^3(x,t) - \beta \ u \ {}_{-1}\mathcal{D}_x^{\sigma} u(x,t) + f(x,t), \tag{4.43}$$

subject to homogeneous Dirichlet boundary conditions $u(-1,t) = u(1,t) = 0$, and initial condition $u(x,0) = u^{ext}(x,0)$, where $\kappa = 10^{-4}$ is the diffusion coefficient, γ and β are constant coefficients. The distributed-order operator ${}^{D}\mathcal{D}_{\phi}$ is defined in (5.7), in which $\phi(\alpha) : (1,2) \rightarrow \mathbb{R}$. The singular exact solution is $u^{ext}(x,t) = e^{-0.2t}\left((1+x)^{3+\mu} - \frac{1}{2}(1+x)^{4+\mu}\right)$, and the force term $f(x,t)$ is computed by substituting the exact solution in (4.43), in which we take the integral in α-domain using the same quadrature rule as in the weak distributed differentiation matrix. We use the proposed scheme to approximate the solution in space and then, by employing proper time integration method, we march in time. To this end, we first take the weak form of the problem by multiplying test functions and integrate over the spatial computational domain. We form two proper sets of

$N+2$ interpolation points to construct the nodal basis ${}^{(1)}h_j^{\mu}(x)$ and test functions ${}^{(2)}h_i^{\mu}(x)$, as discussed in section 4.3.2. Then, similar to (4.19), we approximate the solution in space as

$$u_N(\xi,t) = \sum_{j=2}^{N+1} u_j(t)\ {}^{(1)}h_j^{\mu}(\xi), \tag{4.44}$$

where $u_j(t) = u(\xi_j, t)$, and we only need to construct N interpolants due to zero boundary conditions. Thus, we obtain the linear system of ODEs

$$\mathbf{M}\,\frac{d}{dt}U(t) = \kappa\ \mathscr{D}\,U(t) - \gamma\ \mathbf{N}(t) - \beta\ \mathbf{D}(t) + \mathbf{f}(t), \tag{4.45}$$

where $U(t)$ is the vector of $u_j(t)$, $j = 2, 3, \cdots, N+1$, $\mathbf{M}_{ij}$ is the interpolation matrix, $\mathscr{D}$ is the weak distributed differentiation matrix in (4.25), $\mathbf{f}(t)$ is the force vector, $\mathbf{N}(t)$ is the vector associated with the cubic non-linear reaction term, and $\mathbf{D}(t)$ is the vector associated with the weak form of non-linear term. For $i, j = 2, 3, \cdots, N+1$, we employ proper quadrature rules by following Remark 4.4.1, and compute the entries of each matrices and vectors, which are defined as:

$$\mathbf{M}_{ij} = \int_{-1}^{1} {}^{(1)}h_j^{\mu}(x)\ {}^{(2)}h_i^{\mu}(x)\,dx, \tag{4.46}$$

$$\mathbf{f}_i(t) = \int_{-1}^{1} f(x,t)\ {}^{(2)}h_i^{\mu}(x)\,dx, \tag{4.47}$$

$$\mathbf{N}_i(t) = \tilde{a}_i \sum_{q=2}^{N+1} W_q\ a_q^3\ \tilde{\mathcal{G}}_i(x_q)\ u_q(t)^3 \tag{4.48}$$

$$\mathbf{D}_i(t) = \tilde{a}_i \sum_{q=2}^{N+1} W_q \left(\sum_{r=2}^{N+1} u_r(t)\ a_r\ {}_L\mathbb{D}_{x,r}^{\sigma,\mu}(x_q)\right) \tilde{\mathcal{G}}_i(x_q)\ u_q(t), \tag{4.49}$$

where $\tilde{a}_i$, a_q, and $\tilde{\mathcal{G}}_i(x)$ are given in section 4.3.3. See also section 4.5.2 on derivation of vectors (4.48) and (4.49) corresponding to the nonlinear terms.

Remark 4.4.1. *The difficulty in obtaining the system of ODEs is to efficiently compute the integral for the non-linear terms* $\mathbf{N}(t)$ *and* $\mathbf{D}(t)$*, which we overcome by using the property of fractional Lagrange interpolants that satisfy the Kronecker delta at the interpolation points. Thus, we let the quadrature points in taking the integral of non-linear terms to coincide with the first set of interpolation points, i.e.* ${}^{(1)}\mathbb{W}$*, which we use to construct the nodal basis. Therefore, for the case*

that we only have cubic non-linearity, i.e. $\beta = 0$, we show that Gauss-Lobatto-Jacobi formula with weights $\{\mu, 3\mu\}$ is the proper quadrature rule in taking the integral of non-linear term. Hence, we choose ${}^{(1)}\mathbb{W}$ to be the zeros of $p_{N+2}^{\mu,3\mu}(\xi)$. In the case that $\gamma = 0$, however, by considering the order of fractional derivative in the non-linear term, we find that Gauss-Lobatto-Jacobi formula with weights $\{\mu, 2\mu - \sigma\}$ is the proper quadrature rule in taking the integral of non-linear term. Thus, we choose ${}^{(1)}\mathbb{W}$ to be the zeros of $p_{N+2}^{\mu,2\mu-\sigma}(\xi)$.

The obtained linear system of ODE (4.45) is then integrated in time, using a 2^{nd}-order Adams Bashforth method with time step $\Delta t = 10^{-4}$ for different values of γ, β, and left- and right-biased distribution functions $\phi(\alpha)$, as shown in Fig. 4.6 (left). We consider $\gamma = 1$ and $\beta = 0$, where we recover the linear system corresponding to the distribute-order diffusion reaction equation, for which we show the convergence of numerical solution in L^∞-norm in Fig. 4.6 (middle). Moreover, we consider $\gamma = 0$ and $\beta = 1$, and recover the linear system corresponding to the distribute-order Burgers equation, where we show the convergence of numerical solution in L^∞-norm in Fig. 4.6 (right). We note that the exact solution in space is a power law type with highest order $4 + \mu$ and singularity of order μ, to which the interpolation parameter is tunned. The exact solution is well-approximated up to the order of 10^{-9} with $N = 4$ in the case of distributed-order diffusion reaction equation. However, in the case of distributed-order Burgers equation, the single order fractional derivative shifts the singularity and thus, postpone convergence to $N = 9$. We also note that in both cases, we observe a plateau in the convergence of solution after reaching error level 10^{-9}, which is due to the inaccuracy in integrations involved with Gamma functions.

4.4.3 (1+2)-Dimensions Two-Sided Space Distributed-Order Diffusion Reaction Equation

Let $u(t, x, y) : \Omega \to \mathbb{R}$, where $\Omega = [0, T] \times [-1, 1] \times [-1, 1]$. We use the definition of two-sided distributed-order derivative, given in (4.41) and consider the following 1 + 2-D two-sided space

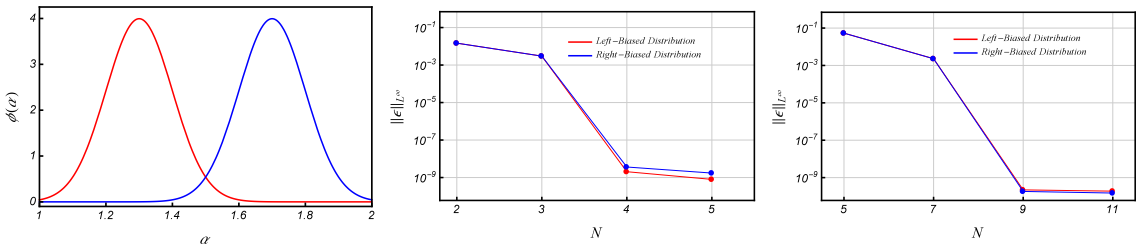

Figure 4.6: (1+1)-D space distributed-order Burgers equation, pseudo-spectral in space and 2^{nd}-order Adams Bashforth in time. (left): The left- and right-biased normal distribution functions (mean 1.3 and 1.7, respectively with variance 0.1) in the distributed-order operator. (middle) : L^{∞}-norm error v.s. N for $\beta = 0$ and $\gamma = 1$. (right):L^{∞}-norm error v.s. N for $\beta = 1$ and $\gamma = 0$.

distributed-order diffusion equation with nonlinear reaction term

$$\begin{aligned}\frac{\partial u}{\partial t} = &\int_{\alpha_{min}}^{\alpha_{max}} \phi_x(\alpha)\left(\kappa_{l_x}\ {}_{-1}\mathcal{D}_x^{\alpha} + \kappa_{r_x}\ {}_{x}\mathcal{D}_1^{\alpha}\right) u\, d\alpha \\ &+ \int_{\alpha_{min}}^{\alpha_{max}} \phi_y(\alpha)\left(\kappa_{l_y}\ {}_{-1}\mathcal{D}_y^{\alpha} + \kappa_{r_y}\ {}_{y}\mathcal{D}_1^{\alpha}\right) u\, d\alpha - u^3 + f\end{aligned} \tag{4.50}$$

subject to proper initial and boundary conditions, in which κ_{l_x}, κ_{r_x}, κ_{l_y}, and κ_{r_y} are the diffusion coefficients. We obtain the weak form of the problem by multiplying proper test functions and integrating over the whole computational domain. As discussed in section 4.3.6 for two-sided operators, we form two sets of $N+2$ interpolation points for each dimension and construct the corresponding interpolants. Then, we approximate the solution using nodal expansion as

$$u_N(t,x,y) = \sum_{j=2}^{N+1}\sum_{j=2}^{N+1} u_{j,s}(t)\ h_j(x)\ h_s(y). \tag{4.51}$$

By considering the test function $v(x,y) = h_i(x)\ h_r(y)$ and substituting (4.51) into (4.50), we obtain the corresponding linear system as

$$\mathcal{M}^x \frac{dU(t)}{dt} \mathcal{M}^{yT} = \mathscr{D}^x\, U(t)\, \mathcal{M}^{yT} + \mathcal{M}^x\, U(t)\, \mathscr{D}^{yT} - \mathcal{N}(t) + \mathcal{F}(t), \tag{4.52}$$

where $U(t)$ is the matrix of $u_{js}(t), j,s = 2,3,\cdots,N+2$. The weak distributed differentiation matrices in x and y directions are $\mathscr{D}^x$ and $\mathscr{D}^y$, respectively, and have similar structures, given in (4.42). The diagonal matrices $\mathcal{M}^x$ and $\mathcal{M}^y$ are the interpolation matrices in x and y directions, defined as $\int_{-1}^{1} h_j(x)\, h_i(x)\, dx$ and $\int_{-1}^{1} h_s(y)\, h_r(y)\, dy$, respectively. $\mathcal{F}(t) = \int_{-1}^{1}\int_{-1}^{1} f(t,x,y)\, h_i(x)\, h_r(y)\, dx$ is

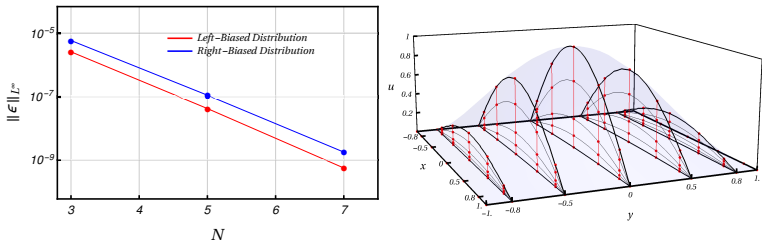

Figure 4.7: (1 + 2)-D two-sided space distributed-order diffusion reaction equation, pseudo-spectral in space and 2^{nd}-order Adams Bashforth in time. (left): L^∞-norm error v.s. N. (right): Time evolution of the solution.

the force therm. Matrix $\mathcal{N}(t)$, associated with the weak form of cubic nonlinearity can be efficiently computed using the property of Lagrange interpolants as discussed in previous sections. Thus, $\mathcal{N}_{ir}(t) = w_i\, w_r\, u_{ir}(t)^3$, where w_i and w_r are the Jacobi quadrature weights.

To investigate the performance of developed scheme in higher dimensional problems, we solve (4.50), subject to homogeneous Dirichlet boundary condition $u(t,x,y) = 0\big|_{\partial\Omega}$ and initial condition $u(0,x,y) = u^{ext}(0,x,y)$, for left- and right- biased $\phi(\alpha)$ (shown in Fig. 4.6 (left)), where in each case we consider similar distributions in both directions x and y, i.e. $\phi_x(\alpha) = \phi_y(\alpha) = \phi(\alpha)$. Moreover, we consider isotropic diffusivity with $\kappa_{l_x} = \kappa_{r_x} = \kappa_{l_y} = \kappa_{r_y} = 10^{-4}$, and a smooth exact solution of the form $u^{ext}(t,x,y) = e^{-0.2t}\, sin(\frac{\pi}{2}(x-1))\, sin(\frac{\pi}{2}(y-1))$. To obtain the force term $f(t,x,y)$, we substitute u^{ext} into (4.50) and take the integral in α-domain using the same quadrature rule as in the weak distributed differentiation matrices, where we need to take the right- and left- sided derivatives of the exact solution for each quadrature point in α-domain. To obtain these fractional derivatives, we first accurately project the exact solution in each direction x and y on the Legendre polynomials $P_{l+1}(x) - P_{l-1}(x)$ and $P_{l+1}(y) - P_{l-1}(y)$, respectively, considering sufficient number of polynomials, and then, by using (3.1) with $\mu = 0$, we obtain the derivatives. We also use a 2^{nd}-order Adams Bashforth method with time step $\Delta t = 10^{-4}$ to march in time. In Fig. 4.7, we show the convergence of numerical solution in L^∞-norm (left), in which we observe that the choice of right-biased distribution function results in slightly larger error. Moreover, in Fig. 4.7 (right) we show the time evolution and diffusion of the solution, where the force term is adjusted such that the exponential decay in time is of order -0.2.

4.5 Detailed Derivations

4.5.1 Polynomials Expansions In Terms Of Jacobi Polynomials

In order to obtain the coefficient ${}^{(1)}\beta_n^j$ in (4.28), we multiply the both side of equation by $p_{k-1}^{-\mu,\mu}$ and the proper weights $(1-\xi)^{-\mu}$ and $(1+\xi)^{\mu}$. Then, we integrate over the whole domain to obtain

$$\int_{-1}^{1}(1-\xi)^{-\mu}(1+\xi)^{\mu}\,\mathcal{G}_j(\xi)\,p_{k-1}^{-\mu,\mu}\;d\xi=\sum_{n=1}^{N+1}{}^{(1)}\beta_n^j\;\int_{-1}^{1}(1-\xi)^{-\mu}(1+\xi)^{\mu}\,p_{k-1}^{-\mu,\mu}\,p_{n-1}^{-\mu,\mu}\;d\xi, \tag{4.53}$$

$$=\sum_{n=1}^{N+1}{}^{(1)}\beta_n^j\;\frac{2}{2n-1}\,\frac{\Gamma(n-\mu)\,\Gamma(n+\mu)}{\Gamma(n)\,(n-1)!}\delta_{nk}\quad\text{by orthogonality of Jacobi polynomials.}$$

Therefore, ${}^{(1)}\beta_k^j=\frac{1}{\gamma_k}\int_{-1}^{1}(1-\xi)^{-\mu}(1+\xi)^{\mu}\,\mathcal{G}_j(\xi)\,p_{k-1}^{-\mu,\mu}\;d\xi,\;j=2,3,\cdots,N+1$, in which $\gamma_k=\frac{2}{2k-1}\,\frac{\Gamma(k-\mu)\,\Gamma(k+\mu)}{\Gamma(k)\,(k-1)!}$.

Similarly, to obtain the coefficient ${}^{(2)}\beta_m^i$ in (4.29), we multiply both side of the equation by $p_{k-1}^{\mu,-\mu}$ and the proper weights $(1-\xi)^{\mu}$ and $(1+\xi)^{-\mu}$, and then integrate over the whole domain. Thus,

$$\int_{-1}^{1}(1-\xi)^{\mu}(1+\xi)^{-\mu}\,\tilde{\mathcal{G}}_j(\xi)\,p_{k-1}^{\mu,-\mu}\;d\xi=\sum_{m=1}^{N+1}{}^{(2)}\beta_m^i\;\int_{-1}^{1}(1-\xi)^{\mu}(1+\xi)^{-\mu}\,p_{k-1}^{\mu,-\mu}\,p_{m-1}^{\mu,-\mu}\;d\xi, \tag{4.54}$$

$$=\sum_{m=1}^{N+1}{}^{(2)}\beta_m^i\;\frac{2}{2m-1}\,\frac{\Gamma(m+\mu)\,\Gamma(m-\mu)}{\Gamma(m)\,(m-1)!}\delta_{mk}\quad\text{by orthogonality of Jacobi polynomials.}$$

Therefore, ${}^{(2)}\beta_k^i=\frac{1}{\gamma_k}\int_{-1}^{1}(1-\xi)^{\mu}(1+\xi)^{-\mu}\,\tilde{\mathcal{G}}_j(\xi)\,p_{k-1}^{\mu,-\mu}\;d\xi,\;i=1,2,\cdots,N$, in which γ_k has the same definition as above.

4.5.2 Efficient Computation of Non-linear Terms

The vector $\mathbf{N}(t)$ is associated with the non-linear reaction term and is computed following Remark 4.4.1 as:

$$
\begin{aligned}
\mathbf{N}(t) &= \left(u_N^3, {}^{(2)}h_i^{\mu}(x)\right)_{\Omega_x} \qquad i = 2, 3, \cdots, N+1, \\
&= \sum_{j=2}^{N+1}\sum_{r=2}^{N+1}\sum_{s=2}^{N+1} u_j\, u_r\, u_s \int_{-1}^{1} {}^{(1)}h_j^{\mu}(x)\ {}^{(1)}h_r^{\mu}(x)\ {}^{(1)}h_s^{\mu}(x)\ {}^{(2)}h_i^{\mu}(x)\ dx, \\
&= \sum_{j=2}^{N+1}\sum_{r=2}^{N+1}\sum_{s=2}^{N+1} (u_j\, u_r\, u_s)(a_j\, a_r\, a_s\, \tilde{a}_i) \int_{-1}^{1} (1-x)^{\mu}(1+x)^{3\mu}\, \mathcal{G}_j(x)\, \mathcal{G}_r(x)\, \mathcal{G}_s(x)\, \tilde{\mathcal{G}}_i(x)\ dx, \\
&= \sum_{q=2}^{N+1} W_q \sum_{j=2}^{N+1}\sum_{r=2}^{N+1}\sum_{s=2}^{N+1} (u_j\, u_r\, u_s)(a_j\, a_r\, a_s\, \tilde{a}_i)\, \mathcal{G}_j(x_q)\, \mathcal{G}_r(x_q)\, \mathcal{G}_s(x_q)\, \tilde{\mathcal{G}}_i(x_q), \\
&= \sum_{q=2}^{N+1} W_q \sum_{j=2}^{N+1}\sum_{r=2}^{N+1}\sum_{s=2}^{N+1} (u_j\, u_r\, u_s)(a_j\, a_r\, a_s\, \tilde{a}_i)\, \delta_{jq}\, \delta_{rq}\, \delta_{sq}\, \tilde{\mathcal{G}}_i(x_q), \\
&= \sum_{q=2}^{N+1} W_q\, (a_q\, u_q)^3 \tilde{a}_i\, \tilde{\mathcal{G}}_i(x_q) \qquad i = 2, 3, \cdots, N+1,
\end{aligned}
\tag{4.55}
$$

where $\{x_q, W_q\}|_{q=2}^{N+1}$ are the Gauss-Lobatto-Jacobi points and weights associated to weight functions $(1-x)^{\mu}$ and $(1+x)^{3\mu}$. We note that since $u_1 = u_{N+2} = 0$, we do not consider $q = 1, N+2$ in the above quadrature rule.

Moreover, following the same Remark 4.4.1 and using (4.35), we compute the vector $\mathbf{D}(t)$ as:

$$
\begin{aligned}
\mathbf{D}(t) &= \Big(u(x,t)\,{}_{-1}\mathcal{D}_x^{\sigma} u(x,t), {}^{(2)}h_i^{\mu}(x)\Big)_{\Omega_x} \qquad i = 2,3,\cdots,N+1, \\
&= \sum_{j=2}^{N+1}\sum_{r=2}^{N+1} u_j\, u_r \int_{-1}^{1} {}^{(1)}h_j^{\mu}(x)\, \Big({}_{-1}\mathcal{D}_x^{\sigma}\, {}^{(1)}h_r^{\mu}(x)\Big)\, {}^{(2)}h_i^{\mu}(x)\, dx, \\
&= \sum_{j=2}^{N+1}\sum_{r=2}^{N+1} u_j\, u_r\, a_j\, \tilde{a}_i \int_{-1}^{1} (1-x)^{\mu}(1+x)^{2\mu-\sigma}\, \mathcal{G}_j(x)\; {}_L\mathbb{D}_{x,r}^{\sigma,\mu}(x)\; \tilde{\mathcal{G}}_i(x)\, dx, \\
&= \sum_{q=2}^{N+1} W_q \sum_{j=2}^{N+1}\sum_{r=2}^{N+1} u_j\, u_r\, a_j\, \tilde{a}_i\; \mathcal{G}_j(x_q)\; {}_L\mathbb{D}_{x,r}^{\sigma,\mu}(x_q)\, \tilde{\mathcal{G}}_i(x_q), \\
&= \sum_{q=2}^{N+1} W_q \sum_{j=2}^{N+1}\sum_{r=2}^{N+1} u_j\, u_r\, a_j\, \tilde{a}_i\; \delta_{jq}\; {}_L\mathbb{D}_{x,r}^{\sigma,\mu}(x_q)\, \tilde{\mathcal{G}}_i(x_q), \\
&= \sum_{q=2}^{N+1} W_q\, u_q\, \tilde{a}_i \left(\sum_{r=2}^{N+1} u_r\, a_r\;\; {}_L\mathbb{D}_{x,r}^{\sigma,\mu}(x_q)\right) \tilde{\mathcal{G}}_i(x_q), \qquad i = 2,3,\cdots,N+1,
\end{aligned}
\tag{4.56}
$$

where $\{x_q, W_q\}|_{q=2}^{N+1}$ are the Gauss-Lobatto-Jacobi points and weights associated to weight functions $(1-x)^{\mu}$ and $(1+x)^{2\mu-\sigma}$. We note that since $u_1 = u_{N+2} = 0$, we do not consider $q = 1, N+2$ in the above quadrature rule.

CHAPTER 5

TEMPORALLY-DISTRIBUTED FRACTIONAL PDES: PETROV-GALERKIN SPECTRAL METHOD

5.1 Background

We construct Petrov-Galerkin spectral methods with a unified fast solver for a class of temporally-distributed FPDEs with constant coefficients subject to Dirichlet boundary/initial conditions. We develop the fast linear solver based on the eigensolutions of the corresponding temporal/spatial mass and stiffness matrices. We carry out the discrete stability and error analysis of the PG method for the two-dimensional case. Eventually, we illustrate the spectral convergence and the efficiency of the method by performing several numerical simulations.

This chapter is organized as follows: in section 5.2, we introduce the preliminaries on fractional calculus, define the distributed fractional Sobolev spaces, the problem, and the corresponding variational form. In section 5.3, we construct the PG methods, formulate the fast solver, and carry out the discrete stability and error analysis. In section 5.4, we provide some numerical tests.

5.2 Definitions

Following [118], we denote the left- and right-sided Reimann-Liouville fractional derivatives by ${}^{RL}_{a}\mathcal{D}^{\nu}_{x} f(x)$ and ${}^{RL}_{x}\mathcal{D}^{\nu}_{b} g(x)$, respectively, in which $g(x) \in C^n[a,b]$. We recall from [5] that ${}^{RL}_{a}\mathcal{D}^{\nu}_{x} g(x) = {}^{C}_{a}\mathcal{D}^{\nu}_{x} g(x) = {}_{a}\mathcal{D}^{\nu}_{x} g(x)$, $\nu \in (0,1)$, when homogeneous Dirichlet initial and boundary conditions are enforced. Following [87], we analytically obtain the fractional derivatives of the Jacobi poly-fractonomials [194], which are later used in developing the numerical scheme, as

$$ {}^{RL}_{-1}\mathcal{D}^{\sigma}_{\xi}\left\{(1+\xi)^{\mu} P^{-\mu,\mu}_{n-1}(\xi)\right\} = \frac{\Gamma(n+\mu)}{\Gamma(n+\mu-\sigma)}(1+\xi)^{\mu-\sigma} P^{-\mu+\sigma,\mu-\sigma}_{n-1}(\xi) \tag{5.1} $$

$$ {}^{RL}_{\xi}\mathcal{D}^{\sigma}_{1}\left\{(1-\xi)^{\mu} P^{\mu,-\mu}_{n-1}(\xi)\right\} = \frac{\Gamma(n+\mu)}{\Gamma(n+\mu-\sigma)}(1-\xi)^{\mu-\sigma} P^{\mu-\sigma,-\mu+\sigma}_{n-1}(\xi) \tag{5.2} $$

in which $\mu, \sigma > 0$ and $P_{n-1}^{\mu,-\mu}(\xi)$ is the standard Jacobi polynomial of order $n-1$. Similarly, the μ-th order fractional derivatives of the Legendre polynomials are given as

$$ {}_{-1}\mathcal{D}_x^{\mu} P_n(x) = \frac{\Gamma(n+1)}{\Gamma(n-\mu+1)} P_n^{\mu,-\mu}(x)\,(1+x)^{-\mu}, \quad {}_{x}\mathcal{D}_1^{\mu} P_n(x) = \frac{\Gamma(n+1)}{\Gamma(n-\mu+1)} P_n^{-\mu,\mu}(x)\,(1-x)^{-\mu}, $$

in which $P_n(x)$ represents the Legendre polynomial of order n.

5.2.1 Distributed Fractional Sobolev Spaces

According to [101], the usual Sobolev space associated with the real index ν_1 on bounded interval $\Lambda_1 = (a_1, b_1)$, is denoted by $H^{\nu_1}(\Lambda_1)$. Due to Lemma 2.6 in [101], $\|\cdot\|_{H^{\nu_1}(\Lambda_1)} \equiv \|\cdot\|_{cH^{\nu_1}(\Lambda_1)}$, where $\|\cdot\|_{cH^{\nu_1}(\Lambda_1)} = \left(\| {}_{x_1}\mathcal{D}_{b_1}^{\nu_1}(\cdot)\|_{L^2(\Lambda_1)}^2 + \| {}_{a_1}\mathcal{D}_{x_1}^{\nu_1}(\cdot)\|_{L^2(\Lambda_1)}^2 + \|\cdot\|_{L^2(\Lambda_1)}^2 \right)^{\frac{1}{2}}$. Let $\Lambda_i = (a_i, b_i) \times \Lambda_{i-1}$ for $i = 2, \cdots, d$, and $\mathcal{X}_1 = H_0^{\nu_1}(\Lambda_1)$, which is associated with the norm $\|\cdot\|_{cH^{\nu_1}(\Lambda_1)}$. Therefore, $\mathcal{X}_d$ is constructed such that $\mathcal{X}_d = H_0^{\nu_d}\Big((a_d, b_d); L^2(\Lambda_{d-1})\Big) \cap L^2(I; \mathcal{X}_{d-1})$, associated with norm $\|\cdot\|_{\mathcal{X}_d} = \left\{ \|\cdot\|_{L^2(\Lambda_d)}^2 + \sum_{i=1}^{d} \left(\| {}_{x_i}\mathcal{D}_{b_i}^{\nu_i}(\cdot)\|_{L^2(\Lambda_d)}^2 + \| {}_{a_i}\mathcal{D}_{x_i}^{\nu_i}(\cdot)\|_{L^2(\Lambda_d)}^2 \right) \right\}^{\frac{1}{2}}$, where

$$ \begin{aligned} \mathcal{X}_{d-1} &= H_0^{\nu_{d-1}}\Big((a_{d-1}, b_{d-1}); L^2(\Lambda_{d-2})\Big) \cap L^2(I; \mathcal{X}_{d-2}), \\ &\vdots \\ \mathcal{X}_2 &= H_0^{\nu_2}\Big((a_2, b_2); L^2(\Lambda_1)\Big) \cap L^2(I; \mathcal{X}_1). \end{aligned} \tag{5.3} $$

Following [87], we denote by $H^{\varphi}(\mathbb{R})$ the *distributed* fractional Sobolev space on $\mathbb{R}$, which is endowed with the following norm $\|\cdot\|_{H^{\varphi}(\mathbb{R})} = \left(\int_{\alpha_1}^{\alpha_2} \varphi(\alpha) \, \| (1+|\omega|^2)^{\frac{\alpha}{2}} \mathcal{F}(\cdot)(\omega)\|_{L^2(\mathbb{R})}^2 \, d\alpha \right)^{\frac{1}{2}}$, where $\varphi \in L^1([\alpha_1, \alpha_2])$, $0 \le \alpha_1 < \alpha_2$. Subsequently, we denote by $H^{\varphi}(I)$ the *distributed* fractional Sobolev space on the finite closed interval $I = (0, T)$, which is defined as $H^{\varphi}(I) = \{v \in L^2(I) | \ \exists \tilde{v} \in H^{\varphi}(\mathbb{R}) \ \ s.t. \ \ \tilde{v}|_I = v\}$, with the the equivalent norms $\|\cdot\|_{lH^{\varphi}(I)}$ and $\|\cdot\|_{rH^{\varphi}(I)}$ in [87], where

$$ \begin{aligned} \|\cdot\|_{lH^{\varphi}(I)} &= \left(\|\cdot\|_{L^2(I)}^2 + \int_{\alpha_1}^{\alpha_2} \varphi(\alpha) \, \| \, {}^{RL}_{0}\mathcal{D}_t^{\alpha}(\cdot)\|_{L^2(I)}^2 \, d\alpha \right)^{\frac{1}{2}}, \\ \|\cdot\|_{rH^{\varphi}(I)} &= \left(\|\cdot\|_{L^2(I)}^2 + \int_{\alpha_1}^{\alpha_2} \varphi(\alpha) \, \| \, {}^{RL}_{t}\mathcal{D}_T^{\alpha}(\cdot)\|_{L^2(I)}^2 \, d\alpha \right)^{\frac{1}{2}}. \end{aligned} \tag{5.4} $$

Let $\Omega = I \times \Lambda_d$. We define

$$ {}_0^l H^{\varphi}\Big(I; L^2(\Lambda_d)\Big) := \Big\{ u \mid \|u(t,\cdot)\|_{L^2(\Lambda_d)} \in H^{\varphi}(I), u|_{t=0} = u|_{x=a_i} = u|_{x=b_i} = 0,\, i = 1, \cdots, d \Big\}, $$

which is equipped with the norm

$$ \|u\|_{l H^{\tau}(I;L^2(\Lambda_d))} = \Big\| \|u(t,\cdot)\|_{L^2(\Lambda_d)} \Big\|_{l H^{\varphi}(I)} = \left(\|u\|^2_{L^2(\Omega)} + \int_{\alpha_1}^{\alpha_2} \varphi(\alpha) \parallel {}^{RL}_{0}\mathcal{D}^{\alpha}_{t}(u) \|^2_{L^2(\Omega)} \, d\alpha \right)^{\frac{1}{2}}. $$

Similarly,

$$ {}_0^r H^{\varphi}\Big(I; L^2(\Lambda_d)\Big) := \Big\{ v \mid \|v(t,\cdot)\|_{L^2(\Lambda_d)} \in H^{\varphi}(I), v|_{t=T} = v|_{x=a_i} = v|_{x=b_i} = 0,\, i = 1, \cdots, d \Big\}, $$

which is equipped with the norm

$$ \|v\|_{r H^{\varphi}(I;L^2(\Lambda_d))} = \Big\| \|v(t,\cdot)\|_{L^2(\Lambda_d)} \Big\|_{r H^{\varphi}(I)} = \left(\|v\|^2_{L^2(\Omega)} + \int_{\alpha_1}^{\alpha_2} \varphi(\alpha) \parallel {}^{RL}_{t}\mathcal{D}^{\alpha}_{T}(v) \|^2_{L^2(\Omega)} \, d\alpha \right)^{\frac{1}{2}}. $$

We define the solution space $\mathcal{B}^{\varphi,\nu_1,\cdots,\nu_d}(\Omega) := {}_0^l H^{\tau}\Big(I; L^2(\Lambda_d)\Big) \cap L^2(I; \mathcal{X}_d)$, endowed with the norm $\|u\|_{\mathcal{B}^{\varphi,\nu_1,\cdots,\nu_d}} = \Big\{ \|u\|^2_{l H^{\varphi}(I;L^2(\Lambda_d))} + \|u\|^2_{L^2(I;\mathcal{X}_d)} \Big\}^{\frac{1}{2}}$. Therefore,

$$ \|u\|_{\mathcal{B}^{\varphi,\nu_1,\cdots,\nu_d}} = \left\{ \|u\|^2_{L^2(\Omega)} + \int_{\alpha_1}^{\alpha_2} \varphi(\alpha) \parallel {}^{RL}_{0}\mathcal{D}^{\alpha}_{t}(u) \|^2_{L^2(\Omega)} \, d\alpha + \sum_{i=1}^{d} \Big(\| {}_{x_i}\mathcal{D}^{\nu_i}_{b_i}(u) \|^2_{L^2(\Omega)} + \| {}_{a_i}\mathcal{D}^{\nu_i}_{x_i}(u) \|^2_{L^2(\Omega)} \Big) \right\}^{\frac{1}{2}}. \tag{5.5} $$

Likewise, we define the test space $\mathfrak{B}^{\varphi,\nu_1,\cdots,\nu_d}(\Omega) := {}^r H^{\varphi}\Big(I; L^2(\Lambda_d)\Big) \cap L^2(I; \mathcal{X}_d)$, endowed with the norm $\|v\|_{\mathfrak{B}^{\tau,\nu_1,\cdots,\nu_d}} = \Big\{ \|v\|^2_{r H^{\tau}(I;L^2(\Lambda_d))} + \|v\|^2_{L^2(I;\mathcal{X}_d)} \Big\}^{\frac{1}{2}}$. Therefore,

$$ \|v\|_{\mathfrak{B}^{\varphi,\nu_1,\cdots,\nu_d}} = \left\{ \|v\|^2_{L^2(\Omega)} + \int_{\alpha_1}^{\alpha_2} \varphi(\alpha) \parallel {}^{RL}_{t}\mathcal{D}^{\alpha}_{T}(v) \|^2_{L^2(\Omega)} \, d\alpha + \sum_{i=1}^{d} \Big(\| {}_{x_i}\mathcal{D}^{\nu_i}_{b_i}(v) \|^2_{L^2(\Omega)} + \| {}_{a_i}\mathcal{D}^{\nu_i}_{x_i}(v) \|^2_{L^2(\Omega)} \Big) \right\}^{\frac{1}{2}}. \tag{5.6} $$

We note that in general, φ can be defined in any possible subset of the interval $[\alpha_1, \alpha_2]$ and thus arbitrarily confines the domain of integration, where the theoretical framework of the problem remains invariant while requiring the solution to have less regularity. The following lemma is useful in construction of the proposed numerical scheme.

Lemma 5.2.1. *[99]: For all $0 < \alpha \leq 1$, if $u \in H^1([a,b])$ such that $u(a) = 0$, and $w \in H^{\alpha/2}([a,b])$, then $({}_a\mathcal{D}_s^{\alpha} u, w)_\Omega = ({}_a\mathcal{D}_s^{\alpha/2} u, {}_s\mathcal{D}_b^{\alpha/2} w)_\Omega$, where $(\cdot,\cdot)_\Omega$ represents the standard inner product in $\Omega = [a,b]$.*

5.2.2 Problem Definition

Let $\alpha \mapsto \varphi(\alpha)$ be a continuous mapping in $[\alpha_1, \alpha_2]$. Then, we define the distributed order fractional derivative as

$$ {}^{D}\mathcal{D}_{\varphi} u(t,x) = \int_{\alpha_1}^{\alpha_2} \varphi(\alpha)\, {}_a^*\mathcal{D}_t^{\alpha} u(t,x)\, d\alpha, \quad t > a, \tag{5.7} $$

where ${}_a^*\mathcal{D}_t^{\alpha}$ denotes the Riemann-Liouville fractional derivative of order α. Next, Let $u \in \mathcal{B}^{\varphi,\nu_1,\cdots,\nu_d}(\Omega)$ for some positive integer d and $\Omega = [0,T] \times [a_1,b_1] \times [a_2,b_2] \times \cdots \times [a_d,b_d]$, where

$$ {}^{D}\mathcal{D}_{\varphi} u + \sum_{j=1}^{d} \left[c_{l_j}\, {}_{a_j}\mathcal{D}_{x_j}^{2\mu_j} u + c_{r_j}\, {}_{x_j}\mathcal{D}_{b_j}^{2\mu_j} u \right] - \sum_{j=1}^{d} \left[\kappa_{l_j}\, {}_{a_j}\mathcal{D}_{x_j}^{2\nu_j} u + \kappa_{r_j}\, {}_{x_j}\mathcal{D}_{b_j}^{2\nu_j} u \right] + \gamma\, u = f, \tag{5.8} $$

in which all the coefficients $\gamma, c_{l_j}, c_{r_j}, \kappa_{l_j}$, and κ_{r_j} are constant, $2\mu_j \in (0,1)$, $2\nu_j \in (1,2)$ for $j = 1,2,\cdots,d$, and $0 < \alpha_1 < \alpha_2 \leq 1$. Problem (5.8) is subject to the Dirichlet initial and boundary conditions, i.e. $u|_{t=0} = 0$ and $u|_{x_j=a_j} = u|_{x_j=b_j} = 0$ for $j = 1,2,\cdots,d$. According to (5.5), the norm associated with $\mathcal{B}^{\varphi,\nu_1,\cdots,\nu_d}(\Omega)$ can be reduced to

$$ \|u\|_{\mathcal{B}^{\varphi,\nu_1,\cdots,\nu_d}(\Omega)} = \left\{ \int_{\alpha_1}^{\alpha_2} \varphi(\alpha) \underbrace{\| {}_0\mathcal{D}_t^{\alpha}(u)\|_{L^2(\Omega)}^2}_{U_I^{\varphi}} d\alpha + \sum_{j=1}^{d} \left[\underbrace{\| {}_{a_j}\mathcal{D}_{x_j}^{\nu_j}(u)\|_{L^2(\Omega)}^2}_{U_{II}^{j}} + \underbrace{\| {}_{x_j}\mathcal{D}_{b_j}^{\nu_j}(u)\|_{L^2(\Omega)}^2}_{U_{III}^{j}} \right] \right\}^{1/2}, $$

and similarly, the norm, associated with $\mathfrak{B}^{\varphi,\nu_1,\cdots,\nu_d}(\Omega)$, in (5.6) is equivalent to

$$ \|v\|_{\mathfrak{B}^{\varphi,\nu_1,\cdots,\nu_d}(\Omega)} = \left\{ \int_{\alpha_1}^{\alpha_2} \varphi(\alpha) \underbrace{\| {}_t\mathcal{D}_T^{\alpha}(v)\|_{L^2(\Omega)}^2}_{V_I^{\varphi}} d\alpha + \sum_{j=1}^{d} \left[\underbrace{\| {}_{x_j}\mathcal{D}_{b_j}^{\nu_j}(v)\|_{L^2(\Omega)}^2}_{V_{II}^{j}} + \underbrace{\| {}_{a_j}\mathcal{D}_{x_j}^{\nu_j}(v)\|_{L^2(\Omega)}^2}_{V_{III}^{j}} \right] \right\}^{1/2}. $$

In order to obtain the variational form of problem, we multiply (5.8) by a proper test function v and integrate over the computational domain. The corresponding continuous bilinear form

$a : \mathcal{B}^{\varphi,\nu_1,\cdots,\nu_d}(\Omega) \times \mathfrak{B}^{\varphi,\nu_1,\cdots,\nu_d}(\Omega) \to \mathbb{R}$ takes the form

$$\begin{aligned} a_\varphi(u,v) = &\int_{\alpha_1}^{\alpha_2} \varphi(\alpha)\, ({}_0\mathcal{D}_t^{\alpha/2}\, u, {}_t\mathcal{D}_T^{\alpha/2}\, v)_\Omega \, d\alpha \\ &+ \sum_{j=1}^{d} \left[c_{l_j} ({}_{a_j}\mathcal{D}_{x_j}^{\mu_j}\, u, {}_{x_j}\mathcal{D}_{b_j}^{\mu_j}\, v)_\Omega + c_{r_j} ({}_{x_j}\mathcal{D}_{a_j}^{\mu_j}\, u, {}_{a_j}\mathcal{D}_{x_j}^{\mu_j}\, v)_\Omega \right] \\ &- \sum_{j=1}^{d} \left[\kappa_{l_j} ({}_{a_j}\mathcal{D}_{x_j}^{\nu_j}\, u, {}_{x_j}\mathcal{D}_{b_j}^{\nu_j}\, v)_\Omega + \kappa_{r_j} ({}_{x_j}\mathcal{D}_{b_j}^{\nu_j}\, u, {}_{a_j}\mathcal{D}_{x_j}^{\nu_j}\, v)_\Omega \right] + \gamma(u,v)_\Omega, \end{aligned} \tag{5.9}$$

where $(\cdot,\cdot)_\Omega$ represents the usual L^2-product. Thus, the problem reads as: find $u \in \mathcal{B}^{\varphi,\nu_1,\cdots,\nu_d}(\Omega)$ such that

$$a_\varphi(u,v) = (f,v)_\Omega, \quad \forall v \in \mathfrak{B}^{\varphi,\nu_1,\cdots,\nu_d}(\Omega). \tag{5.10}$$

Next, we choose proper finite-dimensional subspaces of $U_N \subset \mathcal{B}^{\varphi,\nu_1,\cdots,\nu_d}(\Omega)$ and $V_N \subset \mathfrak{B}^{\varphi,\nu_1,\cdots,\nu_d}(\Omega)$; thus, the discrete problem reads as: find $u_N \in U_N$ such that

$$a_\varphi(u_N,v_N) = (f,v_N)_\Omega, \quad \forall v_N \in V_N. \tag{5.11}$$

5.3 Petrov Galerkin Mathematical Formulation

We construct a Petrov-Galerkin spectral method for the discrete problem $u_N \in U_N$, satisfying the weak form (5.11). We first define the proper finite-dimensional basis/test spaces and then implement the numerical scheme.

5.3.1 Space of Basis (U_N) and Test (V_N) Functions

We employ the Legendre polynomials as the spatial basis, given in the standard domain $\xi \in [-1,1]$ as $\phi_m(\xi) = \sigma_m\big(P_{m+1}(\xi) - P_{m-1}(\xi)\big)$, $m = 1,2,\cdots$. We also employ the poly-fractonomial of first kind [183, 194] as the temporal basis function, given in the standard domain $\eta \in [-1,1]$ as $\psi_n^\tau(\eta) = \sigma_n(1+\eta)^\tau P_{n-1}^{-\tau,\tau}(\eta)$, $n = 1,2,\cdots$. The coefficients σ_m are defined as $\sigma_m = 2 + (-1)^m$. Therefore, we construct the trial space as

$$U_N = span\Big\{\Big(\psi_n^\tau \circ \eta\Big)(t) \prod_{j=1}^{d} \Big(\phi_{m_j} \circ \xi_j\Big)(x_j) : n = 1,2,\cdots,\mathcal{N},\, m_j = 1,2,\cdots,\mathcal{M}_j\Big\},$$

where $\eta(t) = 2t/T - 1$ and $\xi_j(s) = 2\frac{s-a_j}{b_j-a_j} - 1$. The temporal and spatial basis functions naturally satisfy the initial and boundary conditions, respectively. Moreover, we define the temporal and spatial test functions in the standard domain as $\Psi_r^\tau(\eta) = \widetilde{\sigma}_r(1-\eta)^\tau P_{r-1}^{\tau,-\tau}(\eta)$, $r = 1, 2, \cdots$ (poly-fractonomial of second kind) and $\Phi_k^\mu(\xi) = \widetilde{\sigma}_k\left(P_{k+1}(\xi) - P_{k-1}(\xi)\right)$, $k = 1, 2, \cdots$, respectively. The coefficients $\widetilde{\sigma}_k$ are defined as $\widetilde{\sigma}_k = 2\,(-1)^k + 1$. Hence, we construct the corresponding test space as

$$V_N = span\Big\{\Big(\Psi_r^\tau \circ \eta\Big)(t)\prod_{j=1}^{d}\Big(\Phi_{k_j} \circ \xi_j\Big)(x_j) : r = 1, 2, \cdots, \mathcal{N},\ k_j = 1, 2, \cdots, \mathcal{M}_j\Big\}.$$

5.3.2 Implementation of PG Spectral Method

We represent the solution of (5.11) as a linear combination of elements of the solution space U_N. Therefore,

$$u_N(x,t) = \sum_{n=1}^{\mathcal{N}}\sum_{m_1=1}^{\mathcal{M}_1}\cdots\sum_{m_d=1}^{\mathcal{M}_d}\hat{u}_{n,m_1,\cdots,m_d}\Big[\psi_n^\tau(t)\prod_{j=1}^{d}\phi_{m_j}(x_j)\Big] \tag{5.12}$$

in Ω. By substituting the expansion (7.38) into (5.11) and choosing $v_N = \Psi_r^\tau(t)\prod_{j=1}^{d}\Phi_{k_j}(x_j)$, $r = 1, 2, \ldots, \mathcal{N}$, $k_j = 1, 2, \ldots, \mathcal{M}_j$, we obtain the following Lyapunov system

$$\begin{aligned}\Big(S_\tau^\varphi \otimes M_1 \otimes M_2 \cdots \otimes M_d + \sum_{j=1}^{d}[M_\tau \otimes M_1 \otimes \cdots \otimes M_{j-1} \otimes S_j^{Tot} \otimes M_{j+1} \cdots \otimes M_d] \\ + \gamma M_\tau \otimes M_1 \otimes M_2 \cdots \otimes M_d\Big)\mathcal{U} = F,\end{aligned} \tag{5.13}$$

in which $\otimes$ represents the Kronecker product, F denotes the multi-dimensional load matrix whose entries are given as

$$F_{r,k_1,\cdots,k_d} = \int_\Omega f(t, x_1, \cdots, x_d)\Big(\Psi_r^\tau \circ \eta\Big)(t)\prod_{j=1}^{d}\Big(\Phi_{k_j} \circ \xi_j\Big)(x_j)\,d\Omega, \tag{5.14}$$

and $S_j^{Tot} = c_{l_j} \times S_{\mu_j,l} + c_{r_j} \times S_{\mu_j,r} - \kappa_{l_j} \times S_{\nu_j} - \kappa_{r_j} \times S_{\nu_j,r}$. The matrices S_τ^φ and M_τ denote the temporal stiffness and mass matrices, respectively; S_{ν_j}, S_{μ_j} and M_j denote the spatial stiffness and mass matrices, respectively. The entries of spatial mass matrix M_j are computed analytically,

while we employ proper quadrature rules to accurately compute the entries of spatial stiffness S_{ν_j}, S_{μ_j} and temporal mass matrices M_τ. We note that due to the choices of basis/test functions, the obtained mass and stiffness matrices are symmetric. Moreover, we accurately compute the entries of temporal stiffness matrix, S_τ^φ, using theorem (3.1) in [87].

5.3.3 Unified Fast FPDE Solver

We develop a unified fast solver in terms of the generalized eigensolutions in order to formulate a closed-form solution to the Lyapunov system (7.39).

Theorem 5.3.1. *Let $\{\vec{e}^{\,j}_{m_j}, \lambda^j_{m_j}\}_{m_j=1}^{\mathcal{M}_j}$ be the set of general eigen-solutions of the spatial stiffness matrix S_j^{Tot} with respect to the mass matrix M_j. Moreover, let $\{\vec{e}_n^{\,\tau}, \lambda_n^\tau\}_{n=1}^{\mathcal{N}}$ be the set of general eigen-solutions of the temporal mass matrix M_τ with respect to the stiffness matrix S_τ^φ. Then the matrix of unknown coefficients $\mathcal{U}$ is explicitly obtained as*

$$\mathcal{U} = \sum_{n=1}^{\mathcal{N}} \sum_{m_1=1}^{\mathcal{M}_1} \cdots \sum_{m_d=1}^{\mathcal{M}_d} \kappa_{n,m_1,\cdots,m_d}\ \vec{e}_n^{\,\tau} \otimes \vec{e}^{\,1}_{m_1} \otimes \cdots \otimes \vec{e}^{\,d}_{m_d}, \tag{5.15}$$

where $\kappa_{n,m_1,\cdots,m_d}$ is given by

$$\kappa_{n,m_1,\cdots,m_d} = \frac{(\vec{e}_n^{\,\tau}\ \vec{e}^{\,1}_{m_1} \cdots \vec{e}^{\,d}_{m_d})F}{\Big[(\vec{e}_n^{\,\tau T} S_\tau^\varphi \vec{e}_n^{\,\tau}) \prod_{j=1}^d (\vec{e}^{\,jT}_{m_j} M_j \vec{e}^{\,j}_{m_j})\Big] \Lambda_{n,m_1,\cdots,m_d}}, \tag{5.16}$$

in which the numerator represents the standard multi-dimensional inner product, and $\Lambda_{n,m_1,\cdots,m_d}$ is obtained in terms of the eigenvalues of all mass matrices as $\Lambda_{n,m_1,\cdots,m_d} = \Big[(1+\gamma\ \lambda_n^\tau) + \lambda_n^\tau \sum_{j=1}^d (\lambda^j_{m_j})\Big]$.

Proof. Consider the following generalised eigenvalue problems as

$$S_j^{Tot}\ \vec{e}^{\,j}_{m_j} = \lambda^j_{m_j}\ M_j\ \vec{e}^{\,j}_{m_j}, \quad m_j = 1,2,\cdots,\mathcal{M}_j, \quad j = 1,2,\cdots,d, \tag{5.17}$$

$$M_\tau\ \vec{e}_n^{\,\tau} = \lambda_n^\tau\ S_\tau^\varphi\ \vec{e}_n^{\,\tau}, \quad n = 1,2,\cdots,\mathcal{N}. \tag{5.18}$$

Having the spatial and temporal eigenvectors determined in equations (5.18) and (5.17), we can represent the unknown coefficient matrix $\mathcal{U}$ in (7.38) in terms of the aforementioned eigenvectors

as $\mathcal{U} = \sum_{n=1}^{\mathcal{N}} \sum_{m_1=1}^{\mathcal{M}_1} \cdots \sum_{m_d=1}^{\mathcal{M}_d} \kappa_{n,m_1,\cdots,m_d}\ \vec{e}_n^{\,\tau} \otimes \vec{e}_{m_1}^{\,1} \otimes \cdots \otimes \vec{e}_{m_d}^{\,d}$, where $\kappa_{n,m_1,\cdots,m_d}$ is obtained as follows. Following [145], we substitute $\mathcal{U}$ in the corresponding Lyapunov equation and then, take the inner product of both sides of equation by $\vec{e}_q^{\,\tau}\ \vec{e}_{p_1}^{\,1} \cdots \vec{e}_{p_d}^{\,d}$. Therefore, by rearranging the terms, we obtain

$$\kappa_{n,m_1,\cdots,m_d} = \frac{(\vec{e}_n^{\,\tau}\ \vec{e}_{m_1}^{\,1} \cdots \vec{e}_{m_d}^{\,d})F}{\left[(\vec{e}_n^{\,\tau T} S_\tau^\varphi \vec{e}_n^{\,\tau}) \prod_{j=1}^{d} (\vec{e}_{m_j}^{\,jT} M_j \vec{e}_{m_j}^{\,j})\right] \times \left[(1+\gamma\ \lambda_n^\tau) + \lambda_n^\tau \sum_{j=1}^{d} (\lambda_{m_j}^j)\right]}.$$

Since the spatial Mass M_j and temporal stiffness matrices S_τ^φ are diagonal, we have $(\vec{e}_q^{\,\tau T} S_\tau^\varphi \vec{e}_n^{\,\tau}) = 0$ if $q \neq n$, and also $(\vec{e}_{p_j}^{\,jT} M_j \vec{e}_{m_j}^{\,j}) = 0$ if $p_j \neq m_j$, which completes the proof.

□

5.3.4 Stability Analysis

The following theorem provides the discrete stability analysis of the scheme for (1+1)-dimensional temporally-distributed fractional diffusion problem. Such a stability analysis can be extended to the problem of (1+d)-dimensional with both-sided derivatives, which we will be carried out in our future work.

Theorem 5.3.2. *The Petrov-Gelerkin spectral method for (1+1)-D temporally-distributed and space-fractional diffusion problem $a_\varphi(u,v) = l(v)$ is stable, i.e., the discrete* inf-sup *condition*

$$\inf_{\substack{u_N \in U_N \\ u_N \neq 0}} \sup_{\substack{v_N \in V_N \\ v_N \neq 0}} \frac{|a(u_N, v_N)|}{\|v_N\|_{\mathfrak{B}^{\varphi,\nu_1,\cdots,\nu_{d(\Omega)}}} \|u_N\|_{\mathcal{B}^{\varphi,\nu_1,\cdots,\nu_{d(\Omega)}}}} \geq \beta > 0, \tag{5.19}$$

holds with $\beta > 0$ and independent of N.

Proof. See section (5.5.1). □

5.3.5 Error Analysis

Kharazmi et al. [87] performed the error analysis of the distributed order differential equations, where they employed Jacobi polyfractonomials of first kind as the basis function. Following

similar steps, we can show that the projection error in time and space takes the same form. Let $\mathcal{D}^{(r)}u = \frac{\partial^r u}{\partial t^{r_0}\,\partial x_1{}^{r_1}\cdots\partial x_d{}^{r_d}}$, where $r = \sum_{i=0}^{d} r_i$. Thus, if $\mathcal{D}^{(r)}u \in U$ for some integer $r \geq 1$, that is, $\int_{\alpha_1}^{\alpha_2} \varphi(\alpha) \|\, {}_0\mathcal{D}_t^{\frac{\alpha}{2}}(\mathcal{D}^{(r)}u)\|_{L^2} d\alpha < \infty$, and u_N denotes the projection of the exact solution u, then

$$\begin{aligned}\|u - u_N\|_U \;\leq\; \beta\, M^{-r}\Big\{ \|\mathcal{D}^{(r)}u\|^2_{L^2(\Omega)} + \int_{\alpha_1}^{\alpha_2} \varphi(\alpha)\, \|\, {}^{RL}_{0}\mathcal{D}_t^{\alpha}(\mathcal{D}^{(r)}u)\|^2_{L^2(\Omega)}\, d\alpha \\ + \sum_{i=1}^{d} \big(\|\, {}_{x_i}\mathcal{D}_{b_i}^{\nu_i}(\mathcal{D}^{(r)}u)\|^2_{L^2(\Omega)} + \|\, {}_{a_i}\mathcal{D}_{x_i}^{\nu_i}(\mathcal{D}^{(r)}u)\|^2_{L^2(\Omega)} \big) \Big\}^{\frac{1}{2}} \end{aligned} \tag{5.20}$$

Since the *inf-sup* condition holds in theorem 5.3.2, by the Banach-Nečas-Babuška theorem in [51], the error in the numerical scheme is less than or equal to a constant times the projection error.

5.4 Numerical Simulations

We provide numerical examples of the spectral scheme we have proposed. We consider the exact solution of the form $u^{ext} = u_t \prod_{j=1}^{d} u_{\xi_j}$ with finite regularity, where $u_t = t^{p_1+\tau}$, $t \in [0,T]$, and $u_{\xi_j} = (1+\xi_j)^{p_2+\beta}(1-\xi_j)^{p_3+\beta}$, $\xi_j \in [-1,1]$. We obtain the force function by substituting u^{ext} into (5.8), where the advection and diffusion coefficients are considered to be unity in all dimensions.

Figure 5.1 shows the convergence of error via spatial and temporal p-refinement for (1+2)-D problem. In the left sub-figure, $u^{ext} = t^{3+1/2}\prod_{j=1}^{2}(1+\xi_j)^{4+1/2}(1-\xi_j)^{4+1/2}$, for which we choose $N = 4$ to control the error in time and perform p-refinement in space for different values of fractional orders $\{2\mu, 2\nu\} = \{0.5, 1.1\}$ and $\{2\mu, 2\nu\} = \{0.5, 1.9\}$. The results show the expected spectral convergence. In the right sub-figure, we perform p-refinement in time for $u^{ext} = t^{3+\tau}\prod_{j=1}^{2}(1+\xi_j)^4(1-\xi_j)^4$, where $\tau = 0.1, 0.9$ and we choose $\mathcal{M}_1 = \mathcal{M}_2 = 8$ to control the error in space. The choice of ploy-fractonomials as the temporal basis enable the scheme to accurately capture the singularity in time. The obtained results show the convergence of error to machine precision with $N = 4$. Moreover, in Table 5.1, we show the CPU time (which includes the construction of the linear system and load vector) as well as the computed L^2-norm error for the problems of (1+1)- to (1+3)-dimensions, where $p_1 = 3$, $\tau = 0.5$, $p_2 = p_3 = 4$, $\beta = 0.5$, $2\mu = 0.5$, $2\nu = 1.5$.

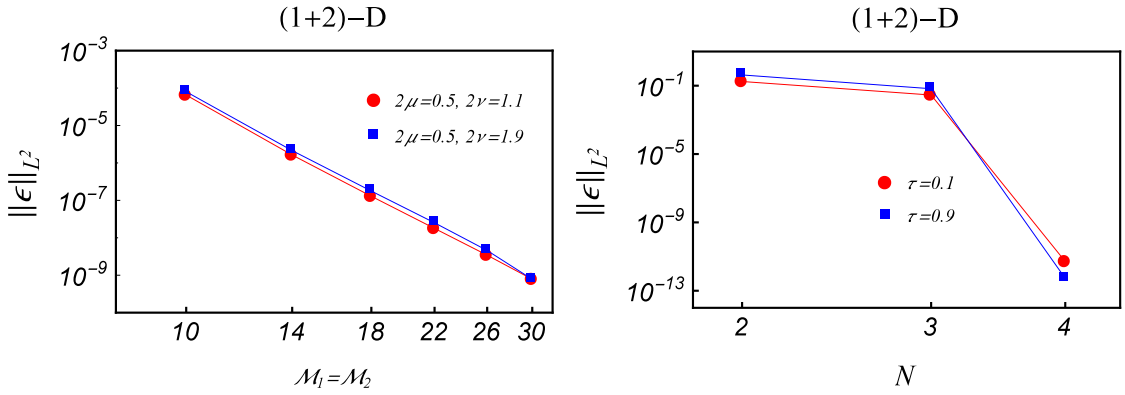

Figure 5.1: PG spectral method, temporal and spatial p-refinement for (1+2)-D problem

Table 5.1: PG spectral method, CPU time (in min) and L^2-norm error for multi-dimensional problems.

	(1+1)-D		(1+2)-D		(1+3)-D	
$N = \mathcal{M}_1 = \mathcal{M}_2 = \mathcal{M}_3$	L^2-norm Error	CPU Time	L^2-norm Error	CPU Time	L^2-norm Error	CPU Time
2	6.2067×10^{-1}	0.6	5.9428×10^{-1}	1	5.1307×10^{-1}	1.7
6	2.7852×10^{-2}	1	2.9233×10^{-2}	1.5	2.6720×10^{-2}	4
10	6.7506×10^{-5}	3.13	7.089×10^{-5}	4.5	6.4714×10^{-5}	27.9
14	1.7541×10^{-6}	20.3	1.8463×10^{-6}	27.5	1.6876×10^{-6}	149

5.5 Proof of Lemmas and Theorems

5.5.1 Proof of Theorem (5.3.2)

Proof. Let $\psi_n^\tau(\eta) = (1+\eta)^\tau P_n^{-\tau,\tau}(\eta)$, $\Psi_n^\tau(\eta) = (1-\eta)^\tau P_n^{\tau,-\tau}(\eta)$, and $u_N = \sum_{n=1}^{N}\sum_{m=0}^{M+1} \bar{u}_{n,m}$ $\psi_n^\tau(t)P_m(x)$, where $u_N \in U_N$. Hence,

$$
\begin{aligned}
U_I^\varphi &= \int_{-1}^{+1}\int_0^T \sum_{n=1}^{N}\sum_{m=0}^{M+1}\sum_{k=1}^{N}\sum_{r=0}^{M+1} \bar{u}_{k,r}\bar{u}_{n,m}\, {}_0\mathcal{D}_t^{\alpha/2}\psi_n^\tau(t)\, {}_0\mathcal{D}_t^{\alpha/2}\psi_k^\tau(t)P_m(x)P_r(x)dtdx \\
&= \sum_{n=1}^{N}\sum_{m=0}^{M+1}\sum_{k=1}^{N}\sum_{r=0}^{M+1} \bar{u}_{k,r}\bar{u}_{n,m} \underbrace{\int_{-1}^{+1} P_m(x)P_r(x)dx}_{C_m^{0,0}\delta_{m,r}} (\frac{T}{2})^{1-2\tau_1}\Gamma_{n-1}^{\tau_1,-\tau_1}\Gamma_{k-1}^{\tau_1,-\tau_1}\times \\
&\int_{-1}^{+1}(1+\eta)^{\tau_1}P_{n-1}^{-\tau_1,\tau_1}(\eta)(1+\eta)^{\tau_1}P_{k-1}^{-\tau_1,\tau_1}(\eta)d\eta, \qquad (5.21)
\end{aligned}
$$

where $\Gamma_{n-1}^{\tau_1,-\tau_1} = \Gamma_{n-1}^{-\tau_1,\tau_1} = \frac{\Gamma(n+\tau_1)}{\Gamma(n)}$ and $\tau_1 = \tau - \frac{\alpha}{2}$. Take $P_n^{-\tau_1,\tau_1}(\eta) = \sum_{q=0}^{n} a_q^{\tau_1,n} P_q^{0,2\tau_1}(\eta)$ then,

$$U_I^{\varphi} = \sum_{n=1}^{N}\sum_{k=1}^{N}\sum_{m=0}^{M+1}\sum_{q_3=1}^{n}\sum_{q_4=1}^{r} \bar{u}_{k,m}\bar{u}_{n,m}\, C_m^{0,0}\,(\frac{T}{2})^{1-2\tau_1}\Gamma_{n-1}^{\tau_1,-\tau_1}\Gamma_{k-1}^{\tau_1,-\tau_1}\, a_{q_3}^{\tau_1,n} a_{q_4}^{\tau_1,r}$$
$$\underbrace{\int_{-1}^{+1}(1+\eta)^{2\tau_1} P_{q_3}^{0,2\tau_1}(\eta) P_{q_4}^{0,2\tau_1}(\eta)d\eta}_{C_{q_3}^{0,2\tau_1}\delta_{q_3,q_4}}$$
$$= \sum_{m=0}^{M+1}\sum_{q_3=1}^{N} {}^{(1)}\breve{u}_{q_3,m}^2 C_{q_3}^{0,2\tau_1} C_m^{0,0}(\frac{T}{2})^{1-2\tau_1} = \sum_{m=0}^{M+1}\sum_{n=1}^{N} {}^{(1)}\breve{u}_{n,m}^2(\frac{T}{2})^{1-2\tau_1}\, C_n^{0,2\tau_1} C_m^{0,0},$$

in which ${}^{(1)}\breve{u}_{n,m} = \sum_{q=0}^{M+1-q} \bar{u}_{q,m}\, a_n^{\tau_1,q}\, \Gamma_{q-1}^{\tau_1,-\tau_1}$. Besides,

$$U_{II}^1 = \int_{-1}^{+1}\int_0^T \sum_{n=1}^{N}\sum_{m=0}^{M+1}\sum_{k=1}^{N}\sum_{r=0}^{M+1} \bar{u}_{k,r}\bar{u}_{n,m}\psi_n^{\tau}(t)\psi_k^{\tau}(t)\, {}_{-1}\mathcal{D}_x^{\nu} P_m(x)\, {}_{-1}\mathcal{D}_x^{\nu} P_r(x)dtdx$$
$$= \sum_{n=1}^{N}\sum_{m=0}^{M+1}\sum_{k=1}^{N}\sum_{r=0}^{M+1} \bar{u}_{k,r}\bar{u}_{n,m}(\frac{T}{2})\int_{-1}^{+1}(1+\eta)^{2\tau} P_{n-1}^{-\tau,\tau}(\eta) P_{k-1}^{-\tau,\tau}(\eta)d\eta\times$$
$$\int_{-1}^{+1}(1+x)^{-2\nu}\Gamma_m^{\nu}\Gamma_r^{\nu} P_m^{\nu,-\nu}(x) P_r^{\nu,-\nu}(x)dx, \tag{5.22}$$

where $\Gamma_m^{\nu} = \frac{m+1}{m-\nu+1}$. By substituting $P_i^{\nu,-\nu}(x) = \sum_{q=0}^{i} b_q^{2\nu,i} P_q^{-2\nu,0}(x)$ and $P_n^{-\tau,\tau}(\eta) = \sum_{q=0}^{n} a_q^{\tau,n} P_q^{0,2\tau}(\eta)$ into (5.22) and reorganizing, we obtain

$$U_{II}^1 = \sum_{n=1}^{N}\sum_{k=1}^{N}\sum_{m=0}^{M+1}\sum_{q_3=1}^{n}\sum_{q_4=1}^{k} {}^{(2)}\breve{u}_{n,m}\, {}^{(2)}\breve{u}_{k,m} C_m^{-2\nu,0}(\frac{T}{2}) a_{q_3}^{\tau,n} a_{q_4}^{\tau,k} \underbrace{\int_{-1}^{+1}(1+\eta)^{2\tau} P_{q_3}^{0,2\tau}(\eta) P_{q_4}^{0,2\tau}(\eta)d\eta}_{C_{q_3}^{0,2\tau}\delta_{q_3,q_4}}$$
$$= \sum_{m=0}^{M+1}\sum_{q_3=1}^{N} {}^{(L)}\breve{u}_{q_3,m}^2 C_{q_3}^{0,2\tau} C_m^{-2\nu,0}(\frac{T}{2}) = \sum_{m=0}^{M+1}\sum_{n=1}^{N} {}^{(L)}\breve{u}_{n,m}^2(\frac{T}{2}) C_n^{0,2\tau} C_m^{-2\nu,0}, \tag{5.23}$$

where ${}^{(2)}\breve{u}_{n,m} = \sum_{q=0}^{M+1-q} \bar{u}_q\, b_m^{2\nu,q}\, \Gamma_q^{\nu}$ and ${}^{(L)}\breve{u}_{n,m} = \sum_{q=1}^{N-n} {}^{(2)}\breve{u}_{q,m} a_n^{\tau,q}$. Let

$$v_N = \sum_{k=1}^{N}\sum_{n=0}^{M+1} \bar{u}_{k,r}(-1)^{k+r}\Psi_k^{\tau}(t) P_r(x).$$

Following the same steps as in U_I^{φ}, for the norm of the test function we have

$$V_I^{\varphi} = \int_{-1}^{+1}\int_0^T \sum_{n=1}^{N}\sum_{m=0}^{M+1}\sum_{k=1}^{N}\sum_{r=0}^{M+1} \bar{u}_{k,r}\bar{u}_{n,m}\,(-1)^{n+k}\,{}_t\mathcal{D}_T^{\alpha/2}\Psi_n^{\tau}(t)\;{}_t\mathcal{D}_T^{\alpha/2}\Psi_k^{\tau}(t)P_m(x)\,P_r(x)(-1)^{r+m}\,dt\,dx$$
$$= \sum_{m=0}^{M+1}\sum_{n=1}^{N} {}^{(1)}\check{v}_{n,m}^2 (\frac{T}{2})^{1-2\tau_1} C_n^{0,2\tau_1} C_m^{0,0}, \tag{5.24}$$

in which we employ $P_n^{\tau_1,-\tau_1}(\eta) = \sum_{q=0}^{n} a_q^{-\tau_1,n} P_q^{2\tau_1,0}(\eta)$ and ${}^{(1)}\check{v}_{n,m} = \sum_{q=0}^{M+1-q} \bar{u}_{n,q}\, a_n^{-\tau_1,q}\, \Gamma_q^{\tau_1,-\tau_1}$.

Besides,

$$V_{II}^1 = \int_{-1}^{+1}\int_0^T \sum_{n=1}^{N}\sum_{m=0}^{M+1}\sum_{k=1}^{N}\sum_{r=0}^{M+1} \bar{u}_{k,r}\bar{u}_{n,m}\,(-1)^{n+k}\Psi_n^{\tau}(t)\,\Psi_k^{\tau}(t)\,(-1)^{r+m}\;{}_{-1}\mathcal{D}_x^{\nu}P_m(x)\;{}_{-1}\mathcal{D}_x^{\nu}P_r(x)\,dt\,dx$$
$$= \sum_{n=1}^{N}\sum_{m=0}^{M+1}\sum_{k=1}^{N}\sum_{r=0}^{M+1} \bar{u}_{k,r}\bar{u}_{n,m}\,(\frac{T}{2})(-1)^{n+k}\int_{-1}^{+1}(1-\eta)^{2\tau}P_{n-1}^{\tau,-\tau}(\eta)P_{k-1}^{\tau,-\tau}(\eta)d\eta\times$$
$$(-1)^{m+r}\int_{-1}^{+1}(1+x)^{-2\nu}\,\Gamma_m^{\nu}\Gamma_r^{\nu}\,P_m^{\nu,-\nu}(x)\,P_r^{\nu,-\nu}(x)dx,$$
$$= \sum_{n=1}^{N}\sum_{k=1}^{N}\sum_{m=0}^{M+1}\sum_{q_3=1}^{n}\sum_{q_4=1}^{r} {}^{(2)}\check{v}_{n,m}\,{}^{(2)}\check{v}_{k,m} C_m^{-2\nu,0}(\frac{T}{2}) a_{q_3}^{-\tau,n} a_{q_4}^{-\tau,r}(-1)^{n+k}\times$$
$$\underbrace{\int_{-1}^{+1}(1-\eta)^{2\tau}P_{q_3}^{2\tau,0}(\eta)P_{q_4}^{2\tau,0}(\eta)d\eta}_{C_{q_3}^{2\tau,0}\delta_{q_3,q_4}=C_{q_3}^{0,2\tau}\delta_{q_3,q_4}}$$
$$= \sum_{m=0}^{M+1}\sum_{q_3=1}^{N} {}^{(L)}\check{v}_{q_3,m}^2 C_{q_3}^{0,2\tau} C_m^{-2\nu,0}(\frac{T}{2}) = \sum_{n=1}^{N}\sum_{m=0}^{M+1} {}^{(L)}\check{v}_{n,m}^2(\frac{T}{2}) C_n^{0,2\tau} C_m^{-2\nu,0}, \tag{5.25}$$

where ${}^{(2)}\check{v}_{n,m} = \sum_{q=0}^{M+1-m}(-1)^q\,\bar{u}_{n,q}\,b_m^{2\nu,q}\,\Gamma_q^{\nu}$, ${}^{(L)}\check{v}_{n,m} = \sum_{i=1}^{N-n}{}^{(2)}\check{v}_{i,m} a_n^{-\tau,i}(-1)^i$, and $P_n^{\tau,-\tau}(\eta) = \sum_{q=0}^{n} a_q^{-\tau,n} P_q^{2\tau,0}(\eta)$. Let $A_I^{\varphi} = ({}_0\mathcal{D}_t^{\alpha/2}\,u_N,\, {}_t\mathcal{D}_T^{\alpha/2}\,v_N)_{\Omega}$ and $A_{II} = \kappa_l({}_{-1}\mathcal{D}_x^{\nu}\,u_N,\, {}_x\mathcal{D}_1^{\nu}\,u_N)_{\Omega}$. By employing $P_{n-1}^{\tau_1,-\tau_1}(x) = \sum_{q=0}^{n-1} a_q^{2\tau_1,n} P_q^{\tau_1,\tau_1}(x)$ and $P_{k-1}^{-\tau_1,\tau_1}(x) = \sum_{q=0}^{k-1}(-1)^{q+k} a_q^{2\tau_1,k} P_q^{\tau_1,\tau_1}(x)$, we

obtain

$$
\begin{aligned}
A_I^{\varphi} &= \int_0^T \int_{-1}^{+1} \sum_{n=1}^{N}\sum_{k=1}^{N}\sum_{m=0}^{M+1}\sum_{r=0}^{M+1} \bar{u}_{n,m}\,\bar{u}_{k,r}\,(-1)^k\,{}_0\mathcal{D}_t^{\alpha/2}\psi_n^{\tau}(t)\,{}_t\mathcal{D}_T^{\alpha/2}\Psi_k^{\tau}(t)(-1)^r P_m(x)\,P_r(x)\,dxdt \\
&= \sum_{n=1}^{N}\sum_{k=1}^{N}\sum_{m=0}^{M+1}\sum_{r=0}^{M+1} \bar{u}_{n,m}\,\bar{u}_{k,r}\,(-1)^r \underbrace{\int_{-1}^{+1} P_m(x)\,P_r(x)dx}_{C_m^{0,0}\delta_{m,r}}(-1)^k(\frac{T}{2})^{1-2\tau_1}\Gamma_{n-1}^{\tau_1,-\tau_1}\Gamma_{k-1}^{\tau_1,-\tau_1}\times \\
&\int_{-1}^{1}(1-\eta^2)^{\tau_1}P_{n-1}^{-\tau_1,\tau_1}(\eta)P_{k-1}^{\tau_1,-\tau_1}(\eta)d\eta = \sum_{n=1}^{N}\sum_{m=0}^{M+1}{}^{(3)}\breve{u}_{n,m}^2\,(-1)^{m+k}(\frac{T}{2})^{1-2\tau_1}\,C_m^{0,0}\,C_n^{\tau_1,\tau_1},
\end{aligned}
\tag{5.26}
$$

where ${}^{(3)}\breve{u}_{n,m} = \sum_{q=1}^{N} a_n^{2\tau_1,q}\Gamma_{q-1}^{\tau_1,-\tau_1}\bar{u}_{q,m}$. Moreover, based on $P_{n-1}^{\tau,-\tau}(\eta) = \sum_{q=0}^{n-1} a_q^{2\tau,n}P_q^{\tau,\tau}(\eta)$, $P_{k-1}^{-\tau,\tau}(\eta) = \sum_{q=0}^{k-1}(-1)^{q+k}a_q^{2\tau,k}P_q^{\tau,\tau}(\eta)$, $P_i^{\nu,-\nu}(x) = \sum_{q=0}^{i} b_q^{2\nu,i}P_q^{-2\nu,0}(x)$, and $P_i^{-\nu,\nu}(x) = \sum_{q=0}^{i}(-1)^{i+q}b_q^{2\nu,i}P_q^{-2\nu,0}(x)$, we get

$$
\begin{aligned}
A_{II} &= \int_0^T \int_{-1}^{+1} \sum_{n=1}^{N}\sum_{k=1}^{N}\sum_{m=0}^{M+1}\sum_{r=0}^{M+1} \bar{u}_{n,m}\,\bar{u}_{k,r}\,\psi_n^{\tau}(t)\Psi_k^{\tau}(t)(-1)^{r+k}\,{}_{-1}\mathcal{D}_x^{\nu}P_m(x)\,{}_x\mathcal{D}_1^{\nu}P_r(x)\,dxdt \\
&= \sum_{n=1}^{N}\sum_{k=1}^{N}\sum_{m=0}^{M+1}\sum_{q_3=1}^{n}\sum_{q_4=1}^{r} {}^{(1)}\tilde{u}_{n,m}\,{}^{(1)}\tilde{u}_{k,m}(-1)^m C_m^{-2\nu,0}(\frac{T}{2})a_{q_3}^{2\tau,n}a_{q_4}^{2\tau,k}(-1)^{q_4}\times \\
&\qquad \underbrace{\int_{-1}^{+1}(1+\eta)^{2\tau}P_{q_3}^{0,2\tau}(\eta)P_{q_4}^{0,2\tau}(\eta)d\eta,}_{C_{q_3}^{0,2\tau}\delta_{q_3,q_4}}
\end{aligned}
$$

which can be simplified to $A_{II} = \sum_{m=0}^{M+1}\sum_{n=1}^{N}{}^{(L)}\tilde{u}_{n,m}^2(-1)^{n+m}(\frac{T}{2})C_n^{0,2\tau}C_m^{-2\nu,0}$, where ${}^{(L)}\tilde{u}_{n,m} = \sum_{q3=1}^{N-n}{}^{(1)}\tilde{u}_{q_3,m}a_n^{\tau,q_3}$ and ${}^{(1)}\tilde{u}_{n,m} = \sum_{i=0}^{M+1}\bar{u}_{n,i}b^{2\nu,q}$. On the other hand, we have $|a(u_N,v_N)| \geq \bar{c}\big[\int_{\alpha_1}^{\alpha_2}\varphi(\alpha)|A_I^{\varphi}| + \kappa_l|A_{II}|\big]$. To compare $|a(u_N,v_N)|$ with $\|u_N\|_{\mathcal{B}^{\varphi,\nu_1,\cdots,\nu_{d(\Omega)}}}\|v_N\|_{\mathfrak{B}^{\varphi,\nu_1,\cdots,\nu_{d(\Omega)}}}$,

$$
|A_I^{\varphi}| = |\sum_{n=1}^{N}\sum_{m=0}^{M+1}(-1)^{m+k}\underbrace{\frac{{}^{(3)}\breve{u}_{n,m}^2\,(\Gamma_{n-1}^{\tau_1,-\tau_1})^2\,C_m^{0,0}\,C_n^{\tau_1,\tau_1}}{{}^{(1)}\breve{u}_{n,m}^2 C_n^{0,2\tau_1}C_m^{0,0}}}_{{}^{(1)}\tilde{\beta}_{n,m}}(\frac{T}{2})^{1-2\tau_1}\,{}^{(1)}\breve{u}_{n,m}^2 C_n^{0,2\tau_1}C_m^{0,0}| \geq \alpha_1\,{}^{(1)}\tilde{\beta}\,U_I^{\varphi}
$$

and

$$|A_{II}| = |\sum_{m=0}^{M+1}\sum_{n=1}^{N}(-1)^{n+m}\underbrace{\frac{{}^{(L)}\tilde{u}^2_{n,m}(\frac{T}{2})C_n^{\tau,\tau}C_m^{-\nu,-\nu}}{{}^{(L)}\check{u}^2_{n,m}(\frac{T}{2})C_n^{0,2\tau}C_m^{-2\nu,0}}}_{{}^{(2)}\tilde{\beta}_{n,m}}{}^{(L)}\check{u}^2_{n,m}(\frac{T}{2})C_n^{0,2\tau}C_m^{-2\nu,0}| \geq \alpha_2\ {}^{(2)}\tilde{\beta}\, U_{II},$$

where ${}^{(2)}\tilde{\beta} = \min\{{}^{(2)}\tilde{\beta}_{n,m}\}$. Besides, we can have

$${}^{(\alpha)}V_I = \sum_{m=0}^{M+1}\frac{{}^{(1)}\check{v}^2_m}{{}^{(1)}\check{u}^2_m}\,{}^{(1)}\check{u}^2_m\, C_m^{-2\nu,0}(\frac{T}{2})C_n^{0,2\tau_1} = \sum_{m=0}^{M+1}{}^{(1)}\check{\beta}_m\ {}^{(1)}\check{u}^2_m\, C_m^{-2\nu,0}(\frac{T}{2})C_n^{0,2\tau_1} \leq {}^{(1)}\check{\beta}\, U_I^{\varphi},$$

$$V_{II} = \sum_{m=0}^{M+1}\frac{{}^{(R)}\check{v}^2_{n,m}}{{}^{(R)}\check{u}^2_{n,m}}\ {}^{(R)}\check{u}^2_{n,m}(\frac{T}{2})C_n^{0,2\tau}C_m^{-2\nu,0} = \sum_{m=0}^{M+1}{}^{(2)}\check{\beta}_{n,m}\ {}^{(R)}\check{u}^2_{n,m}\, C_m^{-2\nu,0}(\frac{T}{2})C_n^{0,2\tau} \leq {}^{(2)}\check{\beta}\, U_{II},$$

where ${}^{(1)}\check{\beta} = max\{{}^{(1)}\check{\beta}_m\}$ and ${}^{(2)}\check{\beta} = max\{{}^{(2)}\check{\beta}_{n,m}\}$. This results in

$$\|v_N\|^2_{\mathfrak{B}^{\varphi,\nu_1,\cdots,\nu_{d(\Omega)}}} \leq \underbrace{max\{{}^{(2)}\check{\beta},{}^{(1)}\check{\beta}\}}_{\tilde{\beta}^2}\|u_N\|^2_{\mathcal{B}^{\varphi,\nu_1,\cdots,\nu_{d(\Omega)}}}.$$

$u \in U$, A_I^{φ}, and A_{II} has finite values, therefore

$$\begin{aligned}|a(u_N,v_N)| &\geq \alpha\left[|A_I^{\varphi}| + \kappa_l|A_{II}||\right] \geq \alpha\left[\alpha_1\ {}^{(1)}\tilde{\beta}\, U_I^{\varphi} + \alpha_2\ {}^{(2)}\tilde{\beta}\kappa_l\, U_{II}\right] \\ &\geq \underbrace{\alpha\, min\{\alpha_1\ {}^{(1)}\tilde{\beta},\ \alpha_2\ {}^{(2)}\tilde{\beta}\kappa_l\}}_{\tilde{\alpha}}\ \|u_N\|^2_{\mathcal{B}^{\varphi,\nu_1,\cdots,\nu_{d(\Omega)}}} \\ &\geq \tilde{\alpha}\,\tilde{\beta}\|u_N\|_{\mathcal{B}^{\varphi,\nu_1,\cdots,\nu_{d(\Omega)}}}\|v_N\|_{\mathfrak{B}^{\varphi,\nu_1,\cdots,\nu_{d(\Omega)}}},\end{aligned} \tag{5.27}$$

which shows that discrete *inf-sup* condition holds for the time-dependent fractional diffusion problem.

□

CHAPTER 6

FRACTIONAL SENSITIVITY EQUATION METHOD: APPLICATIONS TO FRACTIONAL MODEL CONSTRUCTION

6.1 Background

The excellence of fractional operator in accurate prediction of non-locality and memory effects is the inherent non-local nature of singular power-law kernel, whose order is defined as fractional derivative order, i.e. fractional index. However, the key challenges of such models are the excessive computational cost in numerically integrating the convolution operation, and more importantly, introducing fractional derivative orders as extra model parameters, whose values are essentially obtained from experimental data. The sensitivity assessment of fractional models with respect to fractional indecis can build a bridge between experiments and mathematical models to gear observable data via proper optimization techniques, and thus, systematically improve the existing models in both analysis and design approaches. We formulate a mathematical framework by developing a *fractional sensitivity equation method*, where we investigate the response sensitivity of fractional differential equations with respect to model parameters including derivative orders, and further construct an iterative algorithm in order to exploit the obtained sensitivity field in parameter estimation.

Fractional Sensitivity Analysis. Sensitivity assessment approaches are commonly categorized as, finite difference, continuum and discrete derivatives, and computational or automatic differentiation, where the sensitivity coefficients are generally defined as partial derivative of corresponding functions (model output) with respect to design/analysis parameters of interest. Finite difference schemes use a first order Taylor series expansion to approximate the sensitivity coefficients, where accuracy depends strongly on step increment [117, 152]. Continuum and discrete derivative techniques however, differentiate the system response with respect to parameters, where the former, which is also known as sensitivity equation method (SEM, see [107, 193] and references

therein), directly computes the derivatives and obtain a set of (coupled) adjoint continuum sensitivity equations; while the latter performs differentiation after discretization of original equation [155]. Automatic differentiation method also refers to a differentiation of the computer code [29–31]. Fig.2 in [166] provides a descriptive schematic of these different approaches. We extend the continuum derivative technique to develop a *fractional sensitivity equation method* (FSEM) in the context of fractional partial differential equations (FPDEs). To formulate the sensitivity analysis framework, we let q be a set of model parameters including fractional indices and obtain the adjoint *fractional sensitivity equations* (FSEs) by taking the partial derivative of FPDE with respect to q. These adjoint equations introduce a new fractional operator, associated with the *logarithmic-power law* kernel, which to best of our knowledge has been presented for the first time here in the context of fractional sensitivity analysis. The key property of derived FSEs is that they preserve the structure of original FPDE. Thus, similar discretization scheme and forward solver can be readily applied with a minimal required changes.

Model Construction: Estimation of Fractional Indices. Several numerical methods have been developed to solve inverse problem of model construction from available experimental observations or synthetic data. They typically convert the problem of model parameter estimation into an optimization problem, and then, formulate a suitable estimator by minimizing an objective function. These methods are stretched over but no limited to perturbation methods [173], weighted least squares approach [37, 40, 82], nonlinear regression [102], and Levenberg-Marquardt method [38, 64, 180, 181]. We develop a bi-level FSEM-based parameter estimation method in order to construct fractional models, in a sense that the method obtains model coefficients in one level, and then searches for estimate of fractional indices in the next level. We formulate the optimization problem by defining objective functions as two types of model error that measures the difference in computed output/input of fractional model with true output/input in an L^2-norm sense. We further formulate a gradient-based minimizer, employing developed FSEM, and propose a two-stage search algorithm, namely, coarse grid searching and nearby solution. The first stage construct a crude manifold of model error over a coarse discretization of parameter space to locate a local

neighborhood of minimum, and the second stage uses the gradient decent method in order to converge to the minimum point.

Discretization Scheme. The iterative nature of parameter estimators instruct simulation of fractional model at each iteration step of model parameters. Therefore, one of the major tasks in computational model construction is to develop numerical methods that can efficiently discretize the physical domain and accurately solve the fractional model. The sensitivity framework additionally raise the complication by rendering coupled systems of FPDE and adjoint FSEs, and thus, demanding more versatile schemes. In addition to numerous finite difference methods [33, 65, 103, 159, 167, 172, 192, 196], recent works have elaborated efficient spectral schemes, for discretizing FPDEs in physical domain, see e.g., [28, 39, 83, 84, 99, 100, 103, 136, 170]. More recently, Zayernouri et al. [183, 186] developed two new spectral theories on fractional and tempered fractional Sturm-Liouville problems, and introduced explicit corresponding eigenfunctions, namely Jacobi poly-fractonomials of first and second kind. These eignefunctions are comprised of smooth and fractional parts, where the latter can be tunned to capture singularities of true solution. They are successfully employed in constructing discrete solution/test function spaces and developing a series of high-order and efficient Petrov-Galerkin spectral methods, see [86–88, 106, 143–145, 160]. We formulate a numerical scheme in solving coupled system of FPDE and adjoint FSEs by extending the mathematical framework in [145] and accommodating extra required regularity in the underlying function spaces. We employ Jacobi poly-fractonomials and Legendre polynomials as temporal and spatial basis/test functions, respectively, to develop a Petrov-Galerkin (PG) spectral method. The smart choice of coefficients in spatial basis/test functions yields symmetric property in the resulting mass/stiffness matrices, which is then exploited to formulate a fast solver. Following similar procedure as in [145], we also show that the coupled system is mathematically well-posed, and the proposed numerical scheme is stable.

The rest of chapter is organized as follows. In section 6.2, we recall some preliminary definitions in fractional calculus, define the problem using fractional models, introduce proper solution/test spaces, provide some useful lemmas, and then obtain the weak form of the problem. We construct

a Petrov-Galerkin spectral numerical scheme in section 6.3 and carry out discrete stability analysis. We develop FSEM in section 6.4 for FIVP/FPDE and define the underlying mathematical frame work for the coupled system of FPDE and FSEs. Moreover, we develop the FSEM based model construction algorithm in section 6.5 and finally, provide the numerical results in section 6.6.

6.2 Definitions

Definition 6.2.1. We define the following left- and right-sided integro-differential operator with logarithmic-power law kernel, namely *Log-Pow integro-differential operator*, given as,

$$ {}^{RL-LP}_{a}\mathcal{D}^{\sigma}_{x} u(x) = \frac{1}{\Gamma(n-\sigma)} \frac{d^n}{dx^n} \int_a^x \frac{\log(x-s)\, u(s)}{(x-s)^{\sigma-n+1}} ds, \tag{6.1} $$

$$ {}^{RL-LP}_{x}\mathcal{D}^{\sigma}_{b} u(x) = \frac{1}{\Gamma(n-\sigma)} \frac{(-d)^n}{dx^n} \int_x^b \frac{\log(s-x)\, u(s)}{(s-x)^{\sigma-n+1}} ds, \tag{6.2} $$

$$ {}^{C-LP}_{a}\mathcal{D}^{\sigma}_{x} u(x) = \frac{1}{\Gamma(n-\sigma)} \int_a^x \frac{\log(x-s)\, u^{(n)}(s)}{(x-s)^{\sigma-n+1}} ds, \tag{6.3} $$

$$ {}^{C-LP}_{x}\mathcal{D}^{\sigma}_{b} u(x) = \frac{1}{\Gamma(n-\sigma)} \int_x^b \frac{\log(s-x)\, u^{(n)}(s)}{(s-x)^{\sigma-n+1}} ds, \tag{6.4} $$

where $RL-LP$ and $C-LP$ stand for Log-Pow integro-differential operator, which partially resemble the fractional derivative in Riemann-Liouville and Caputo sense, respectively. The following lemma shows a useful relation between the two aforementioned operators.

Lemma 6.2.2. *Let $x \in [a,b]$. Then, the following relation holds.*

Part A: $\sigma \in (0,1)$

$$ {}^{RL-LP}_{a}\mathcal{D}^{\sigma}_{x} u(x) = \frac{u(a)}{\Gamma(1-\sigma)} \frac{\log(x-a)}{(x-a)^{\sigma}} + {}^{C-LP}_{a}\mathcal{D}^{\sigma}_{x} u(x). \tag{6.5} $$

Part B: $\sigma \in (1,2)$

$$ {}^{RL-LP}_{a}\mathcal{D}^{\sigma}_{x} u(x) = \frac{u(a)}{\Gamma(2-\sigma)} \frac{1+(1-\sigma)\log(x-a)}{(x-a)^{\sigma}} + \frac{u'(a)}{\Gamma(2-\sigma)} \frac{\log(x-a)}{(x-a)^{\sigma-1}} + {}^{C-LP}_{a}\mathcal{D}^{\sigma}_{x} u(x). \tag{6.6} $$

Proof. See section 6.7.1 for proof. □

6.2.1 Problem Definition

Let $\Omega = (0,T] \times (a_1, b_1) \times (a_2, b_2) \times \cdots \times (a_d, b_d)$ be the computational domain for some positive integer d. We define $u(t, \mathbf{x}; \mathbf{q}) : \Omega \times Q \to \mathbb{R}$, where

$$\mathbf{q} = \{\alpha, \beta_1, \beta_2, \cdots, \beta_d, k_1, k_2, \cdots, k_d\}$$

is the vector of model parameters containing the fractional indices and model coefficients, and $Q = [0,1] \times [1,2]^d \times \mathbb{R}_+^d$ is the space of parameters. Thus, for any $\mathbf{q} \in Q$, the transport field $u(t, \mathbf{x}; \mathbf{q}) : \Omega \to \mathbb{R}$. We consider the FPDE of strong form $\mathcal{L}^q(u) = f$, subject to Dirichlet initial and boundary conditions, where $\mathcal{L}$ is a linear two-sided fractional operator, given as follows

$$ {}_0\mathcal{D}_t^{\alpha} u(t, \mathbf{x}; \mathbf{q}) - \sum_{j=1}^{d} k_j \left[{}_{a_j}\mathcal{D}_{x_j}^{\beta_j} + {}_{x_j}\mathcal{D}_{b_j}^{\beta_j} \right] u(t, \mathbf{x}; \mathbf{q}) = f(t, \mathbf{x}; \mathbf{q}), \tag{6.7}$$

$$ u|_{t=0} = 0, \tag{6.8}$$

$$ u|_{x=a_j} = u|_{x=b_j} = 0, \tag{6.9}$$

in which $\alpha \in (0,1)$, $\beta_j \in (1,2)$, k_j are real positive constant coefficients, and the fractional derivatives are taken in the Riemann-Liouville sense. In the rest of this chapter, we drop the pre-superscript RL for the sake of simplicity and abbreviation; we state the type of derivative if need be.

6.2.2 Mathematical Framework: Fractional Sobolev Spaces

We define some functional spaces and their associated norms [87, 99]. By $H^{\sigma}(\mathbb{R}) = \left\{ u(t) | u \in L^2(\mathbb{R}); (1 + |\omega|^2)^{\frac{\sigma}{2}} \mathcal{F}(u)(\omega) \in L^2(\mathbb{R}) \right\}$, $\sigma \geq 0$, we denote the fractional Sobolev space on $\mathbb{R}$, endowed with norm $\|u\|_{H_{\mathbb{R}}^{\sigma}} = \|(1 + |\omega|^2)^{\frac{\sigma}{2}} \mathcal{F}(u)(\omega)\|_{L^2(\mathbb{R})}$, where $\mathcal{F}(u)$ represents the Fourier transform of u. Subsequently, we denote by $H^{\sigma}(\Lambda) = \left\{ u \in L^2(\Lambda) \,|\, \exists \tilde{u} \in H^{\sigma}(\mathbb{R}) \; s.t. \; \tilde{u}|_{\Lambda} = u \right\}$, $\sigma \geq 0$, the fractional Sobolev space on any finite closed interval, e.g. $\Lambda = (a, b)$, with norm

$\|u\|_{H^\sigma(\Lambda)} = \inf_{\tilde{u}\in H^\sigma_{\mathbb{R}}, \tilde{u}|_\Lambda = u} \|\tilde{u}\|_{H^\sigma(\mathbb{R})}$. We define the following useful norms as:

$$\|\cdot\|_{l H^\sigma(\Lambda)} = \left(\|\, {}_a\mathcal{D}_x^\sigma(\cdot)\|^2_{L^2(\Lambda)} + \|\cdot\|^2_{L^2(\Lambda)}\right)^{\frac{1}{2}},$$
$$\|\cdot\|_{r H^\sigma(\Lambda)} = \left(\|\, {}_x\mathcal{D}_b^\sigma(\cdot)\|^2_{L^2(\Lambda)} + \|\cdot\|^2_{L^2(\Lambda)}\right)^{\frac{1}{2}},$$
$$\|\cdot\|_{c H^\sigma(\Lambda)} = \left(\|\, {}_x\mathcal{D}_b^\sigma(\cdot)\|^2_{L^2(\Lambda)} + \|\, {}_a\mathcal{D}_x^\sigma(\cdot)\|^2_{L^2(\Lambda)} + \|\cdot\|^2_{L^2(\Lambda)}\right)^{\frac{1}{2}},$$

where the equivalence of $\|\cdot\|_{l H^\sigma(\Lambda)}$ and $\|\cdot\|_{r H^\sigma(\Lambda)}$ are shown in [53, 99, 100]. We show the equivalence of these two norms with $\|\cdot\|_{c H^\sigma(\Lambda)}$ in the following lemma.

Lemma 6.2.3. *Let $\sigma \geq 0$ and $\sigma \neq n - \frac{1}{2}$. Then, the norms $\|\cdot\|_{l H^\sigma(\Lambda)}$ and $\|\cdot\|_{r H^\sigma(\Lambda)}$ are equivalent to $\|\cdot\|_{c H^\sigma(\Lambda)}$.*

Proof. See section 6.7.2 for proof. □

We also define $C_0^\infty(\Lambda)$ as the space of smooth functions with compact support in (a, b). We denote by ${}^l H_0^\sigma(\Lambda)$, ${}^r H_0^\sigma(\Lambda)$, and ${}^c H_0^\sigma(\Lambda)$ as the closure of $C_0^\infty(\Lambda)$ with respect to the norms $\|\cdot\|_{l H^\sigma(\Lambda)}$, $\|\cdot\|_{r H^\sigma(\Lambda)}$, and $\|\cdot\|_{c H^\sigma(\Lambda)}$.

Lemma 6.2.4 ([53, 100])**.** *The Sobolev spaces ${}^l H_0^\sigma(\Lambda)$, ${}^r H_0^\sigma(\Lambda)$, and ${}^c H_0^\sigma(\Lambda)$ are equal and their seminorms are equivalent to $|\cdot|^*_{H^\sigma(\Lambda)} = \left|\left({}_a\mathcal{D}_x^\sigma(\cdot), {}_x\mathcal{D}_b^\sigma(\cdot)\right)\right|^{\frac{1}{2}}_\Lambda$*

Based on Lemma 6.2.4, and assuming that $\left|({}_a\mathcal{D}_x^\sigma u, {}_x\mathcal{D}_b^\sigma v)_\Lambda\right| > 0$ and $\left|({}_x\mathcal{D}_b^\sigma u, {}_a\mathcal{D}_x^\sigma v)_\Lambda\right| > 0$, we can prove that $\left|({}_a\mathcal{D}_x^\sigma u, {}_x\mathcal{D}_b^\sigma v)_\Lambda\right| \geq \beta_1 |u|_{l H^\sigma(\Lambda)} |v|_{r H^\sigma(\Lambda)}$ and $\left|({}_x\mathcal{D}_b^\sigma u, {}_a\mathcal{D}_x^\sigma v)_\Lambda\right| \geq \beta_2 |u|_{r H^\sigma(\Lambda)} |v|_{l H^\sigma(\Lambda)}$, where β_1 and β_2 are positive constants. Following [145], we define the corresponding solution and test spaces of our problem. Thus, by letting $\Lambda_1 = (a_1, b_1)$, $\Lambda_j = (a_j, b_j) \times \Lambda_{j-1}$ for $j = 2, \cdots, d$, we define $\mathcal{X}_1 = H_0^{\frac{\beta_1}{2}}(\Lambda_1)$, which is associated with the norm

$\|\cdot\|_{{}_cH^{\frac{\beta_1}{2}}(\Lambda_1)}$, and accordingly, $\mathcal{X}_j$, $j = 2, \cdots, d$ as

$$\mathcal{X}_2 = H_0^{\frac{\beta_2}{2}}\Big((a_2, b_2); L^2(\Lambda_1)\Big) \cap L^2((a_2, b_2); \mathcal{X}_1), \tag{6.10}$$

$$\vdots$$

$$\mathcal{X}_d = H_0^{\frac{\beta_d}{2}}\Big((a_d, b_d); L^2(\Lambda_{d-1})\Big) \cap L^2((a_d, b_d); \mathcal{X}_{d-1}), \tag{6.11}$$

associated with norms $\|\cdot\|_{\mathcal{X}_j} = \left\{\|\cdot\|^2_{H_0^{\frac{\beta_j}{2}}\left((a_j,b_j);L^2(\Lambda_{j-1})\right)} + \|\cdot\|^2_{L^2\left((a_j,b_j);\mathcal{X}_{j-1}\right)}\right\}^{\frac{1}{2}}$, $j = 2, 3, \cdots, d$.

Lemma 6.2.5. *Let $\beta_j \geq 0$ and $\beta_j \neq n - \frac{1}{2}$ for $j = 1, 2, \cdots, d$. Then,*

$$\|\cdot\|^2_{\mathcal{X}_j} \equiv \sum_{i=1}^{j}\left(\|{}_{x_i}\mathcal{D}^{\beta_i/2}_{b_i}(\cdot)\|^2_{L^2(\Lambda_j)} + \|{}_{a_i}\mathcal{D}^{\beta_i/2}_{x_i}(\cdot)\|^2_{L^2(\Lambda_j)}\right) + \|\cdot\|^2_{L^2(\Lambda_j)}.$$

Proof. See section 6.7.3 for proof. □

Moreover, by letting ${}_0C^\infty(I)$ and $C_0^\infty(I)$ be the space of smooth functions with compact support in $(0, T]$ and $[0, T)$, respectively, we define ${}^lH^s(I)$ and ${}^rH^s(I)$ as the closure of ${}_0C^\infty(I)$ and $C_0^\infty(I)$ with respect to the norms $\|\cdot\|_{{}^lH^s(I)}$ and $\|\cdot\|_{{}^rH^s(I)}$. We also define

$${}^l_0H^{\frac{\alpha}{2}}\Big(I; L^2(\Lambda_d)\Big) = \Big\{u \,\Big|\, \|u(t,\cdot)\|_{L^2(\Lambda_d)} \in H^{\frac{\alpha}{2}}(I), u|_{t=0} = u|_{x=a_j} = u|_{x=b_j} = 0,\ j = 1, 2, \cdots, d\Big\},$$
$${}^r_0H^{\frac{\alpha}{2}}\Big(I; L^2(\Lambda_d)\Big) = \Big\{v \,\Big|\, \|v(t,\cdot)\|_{L^2(\Lambda_d)} \in H^{\frac{\alpha}{2}}(I), v|_{t=T} = v|_{x=a_j} = v|_{x=b_j} = 0,\ j = 1, 2, \cdots, d\Big\},$$

equipped with norms $\|u\|_{{}^lH^{\frac{\alpha}{2}}(I;L^2(\Lambda_d))}$ and $\|u\|_{{}^rH^{\frac{\alpha}{2}}(I;L^2(\Lambda_d))}$, respectively, which take the following forms

$$\|u\|_{{}^lH^{\frac{\alpha}{2}}(I;L^2(\Lambda_d))} = \Big\|\|u(t,\cdot)\|_{L^2(\Lambda_d)}\Big\|_{{}^lH^{\frac{\alpha}{2}}(I)} = \Big(\|{}_0\mathcal{D}_t^{\frac{\alpha}{2}}(u)\|^2_{L^2(\Omega)} + \|u\|^2_{L^2(\Omega)}\Big)^{\frac{1}{2}}, \tag{6.12}$$

$$\|u\|_{{}^rH^{\frac{\alpha}{2}}(I;L^2(\Lambda_d))} = \Big\|\|u(t,\cdot)\|_{L^2(\Lambda_d)}\Big\|_{{}^rH^{\frac{\alpha}{2}}(I)} = \Big(\|{}_t\mathcal{D}_T^{\frac{\alpha}{2}}(u)\|^2_{L^2(\Omega)} + \|u\|^2_{L^2(\Omega)}\Big)^{\frac{1}{2}}. \tag{6.13}$$

Solution and Test Spaces. We define the solution space U and test space V, respectively, as

$$U = {}^l_0H^{\frac{\alpha}{2}}\Big(I; L^2(\Lambda_d)\Big) \cap L^2(I; \mathcal{X}_d), \quad V = {}^r_0H^{\frac{\alpha}{2}}\Big(I; L^2(\Lambda_d)\Big) \cap L^2(I; \mathcal{X}_d), \tag{6.14}$$

endowed with norms

$$\|u\|_U = \left\{ \|u\|^2_{{}_l H^{\frac{\alpha}{2}}(I;L^2(\Lambda_d))} + \|u\|^2_{L^2(I;\mathcal{X}_d)} \right\}^{\frac{1}{2}}, \quad \|v\|_V = \left\{ \|v\|^2_{{}_r H^{\frac{\alpha}{2}}(I;L^2(\Lambda_d))} + \|v\|^2_{L^2(I;\mathcal{X}_d)} \right\}^{\frac{1}{2}}, \tag{6.15}$$

Using Lemma 7.3.2, we can show that

$$\|u\|_{L^2(I;\mathcal{X}_d)} = \left\| \|u(t,.)\|_{\mathcal{X}_d} \right\|_{L^2(I)} = \left\{ \|u\|^2_{L^2(\Omega)} + \sum_{j=1}^{d} \left(\| {}_{x_j}\mathcal{D}_{b_j}^{\frac{\beta_j}{2}} u \|^2_{L^2(\Omega)} + \| {}_{a_j}\mathcal{D}_{x_j}^{\frac{\beta_j}{2}} u \|^2_{L^2(\Omega)} \right) \right\}^{\frac{1}{2}}. \tag{6.16}$$

Therefore, by (7.24) we write (7.23) as

$$\|u\|_U = \left\{ \|u\|^2_{L^2(\Omega)} + \| {}_0\mathcal{D}_t^{\frac{\alpha}{2}} u \|^2_{L^2(\Omega)} + \sum_{j=1}^{d} \left(\| {}_{x_j}\mathcal{D}_{b_j}^{\frac{\beta_j}{2}} u \|^2_{L^2(\Omega)} + \| {}_{a_j}\mathcal{D}_{x_j}^{\frac{\beta_j}{2}} u \|^2_{L^2(\Omega)} \right) \right\}^{\frac{1}{2}}, \tag{6.17}$$

$$\|v\|_V = \left\{ \|v\|^2_{L^2(\Omega)} + \| {}_t\mathcal{D}_T^{\frac{\alpha}{2}} v \|^2_{L^2(\Omega)} + \sum_{j=1}^{d} \left(\| {}_{x_j}\mathcal{D}_{b_j}^{\frac{\beta_j}{2}} v \|^2_{L^2(\Omega)} + \| {}_{a_j}\mathcal{D}_{x_j}^{\frac{\beta_j}{2}} v \|^2_{L^2(\Omega)} \right) \right\}^{\frac{1}{2}}. \tag{6.18}$$

The following lemmas help us obtain the weak formulation of our problem, construct the numerical scheme and further prove the stability of our method.

Lemma 6.2.6 ([99])**.** *For all $\alpha \in (0,1)$, if $u \in H^1([0,T])$ such that $u(0) = 0$, and $v \in H^{\alpha/2}([0,T])$, then $({}_0\mathcal{D}_t^{\alpha} u, v)_\Omega = ({}_0\mathcal{D}_t^{\alpha/2} u, {}_t\mathcal{D}_T^{\alpha/2} v)_\Omega$, where $(\cdot,\cdot)_\Omega$ represents the standard inner product in $\Omega = [0,T]$.*

Lemma 6.2.7 ([87])**.** *Let $1 < \beta < 2$, a and b be arbitrary finite or infinite real numbers. Assume $u \in H^\beta(a,b)$ such that $u(a) = 0$, also ${}_x\mathcal{D}_b^{\beta/2} v$ is integrable in $\Omega = (a,b)$ such that $v(b) = 0$. Then, $({}_a\mathcal{D}_x^{\beta} u, v)_\Omega = ({}_a\mathcal{D}_x^{\beta/2} u, {}_x\mathcal{D}_b^{\beta/2} v)_\Omega$.*

We generalize Lemma 7.3.4 to the two-sided $(1+d)$-dimensional case (see section 6.7.4 for proof).

Lemma 6.2.8. *Let $1 < \beta_j < 2$ for $j = 1, 2, \cdots, d$, and $u, v \in \mathcal{X}_d$. Then,*

$$\left({}_{a_j}\mathcal{D}_{x_j}^{\beta_j} u, v \right)_{\Lambda_d} = \left({}_{a_j}\mathcal{D}_{x_j}^{\frac{\beta_j}{2}} u, {}_{x_j}\mathcal{D}_{b_j}^{\frac{\beta_j}{2}} v \right)_{\Lambda_d}, \qquad \left({}_{x_j}\mathcal{D}_{b_j}^{\beta_j} u, v \right)_{\Lambda_d} = \left({}_{x_j}\mathcal{D}_{b_j}^{\frac{\beta_j}{2}} u, {}_{a_j}\mathcal{D}_{x_j}^{\frac{\beta_j}{2}} v \right)_{\Lambda_d}.$$

6.2.3 Weak Formulation

For any set of model parameter $\mathbf{q}$, we obtain the weak system, i.e. the variational form of the problem (6.7) subject to the given initial/boundary conditions, by multiplying the equation with proper test functions and integrate over the whole computational domain Ω. Therefore, using Lemmas 7.3.3-7.3.5, the bilinear form can be written as

$$a(u,v) = ({}_0\mathcal{D}_t^{\frac{\alpha}{2}}\, u, {}_t\mathcal{D}_T^{\frac{\alpha}{2}}\, v)_\Omega - \sum_{j=1}^{d} k_j \Big[({}_{a_j}\mathcal{D}_{x_j}^{\frac{\beta_j}{2}}\, u, {}_{x_j}\mathcal{D}_{b_j}^{\frac{\beta_j}{2}}\, v)_\Omega + ({}_{x_j}\mathcal{D}_{b_j}^{\frac{\beta_j}{2}}\, u, {}_{a_j}\mathcal{D}_{x_j}^{\frac{\beta_j}{2}}\, v)_\Omega \Big], \quad (6.19)$$

and thus, by letting $\tilde{U}$ and $\tilde{V}$ be the proper solution/test spaces, the problem reads as: find $u \in \tilde{U}$ such that

$$a(u,v) = (f,v)_\Omega, \quad \forall v \in \tilde{V}. \quad (6.20)$$

6.3 Petrov-Galerkin Spectral Method

We define the following finite dimensional solution and test spaces. We employ Legendre polynomials $\phi_{m_j}(\xi)$, $j = 1, 2, \cdots, d$, and Jacobi poly-fractonomial of first kind $\psi_n^\tau(\eta)$ [183, 186], as the spatial and temporal bases, respectively, given in their corresponding standard domain as

$$\phi_{m_j}(\xi) = \sigma_{m_j}\big(P_{m_j+1}(\xi) - P_{m_j-1}(\xi)\big), \quad \xi \in [-1,1] \qquad m_j = 1, 2, \cdots, \quad (6.21)$$

$$\psi_n^\tau(\eta) = \sigma_n\, {}^{(1)}\mathcal{P}_n^\tau(\eta) = \sigma_n (1+\eta)^\tau P_{n-1}^{-\tau,\tau}(\eta), \quad \eta \in [-1,1] \quad n = 1, 2, \cdots, \quad (6.22)$$

in which $\sigma_{m_j} = 2 + (-1)^{m_j}$. Therefore, by performing affine mappings $\eta = 2\frac{t}{T} - 1$ and $\xi = 2\frac{x-a_j}{b_j-a_j} - 1$ from the computational domain to the standard domain, we construct the solution space U_N as

$$U_N = span\Big\{ \Big(\psi_n^\tau \circ \eta\Big)(t) \prod_{j=1}^{d} \Big(\phi_{m_j} \circ \xi\Big)(x_j) \ : n = 1, 2, \cdots, \mathcal{N},\ m_j = 1, 2, \cdots, \mathcal{M}_j \Big\}. \quad (6.23)$$

We note that the choice of temporal and spatial basis functions naturally satisfy the initial and boundary conditions, respectively. The parameter τ in the temporal basis functions plays a role of fine tunning parameter, which can be chosen properly to capture the singularity of exact solution.

Moreover, we employ Legendre polynomials $\Phi_{r_j}(\xi)$, $j = 1, 2, \cdots, d$, and Jacobi poly-fractonomial of second kind $\Psi_k^\tau(\eta)$, as the spatial and temporal test functions, respectively, given in their corresponding standard domain as

$$\Phi_{r_j}(\xi) = \widetilde{\sigma}_{r_j}\big(P_{r_j+1}(\xi) - P_{r_j-1}(\xi)\big), \quad \xi \in [-1, 1] \qquad r_j = 1, 2, \cdots, \tag{6.24}$$

$$\Psi_k^\tau(\eta) = \widetilde{\sigma}_k\, {}^{(2)}\mathcal{P}_k^{\,\tau}(\eta) = \widetilde{\sigma}_k (1-\eta)^\tau\, P_{k-1}^{\tau,-\tau}(\eta), \quad \eta \in [-1, 1] \quad k = 1, 2, \cdots, \tag{6.25}$$

where $\widetilde{\sigma}_{r_j} = 2\,(-1)^{r_j} + 1$. Therefore, by similar affine mapping we construct the test space V_N as

$$V_N = span\left\{ \Big(\Psi_k^\tau \circ \eta\Big)(t) \prod_{j=1}^{d} \Big(\Phi_{r_j} \circ \xi_j\Big)(x_j) \;\; : k = 1, 2, \cdots, \mathcal{N},\; r_j = 1, 2, \cdots, \mathcal{M}_j \right\}. \tag{6.26}$$

We can show that our choice of basis/test functions satisfy the extra regularity imposed by the Log-Pow integro-differential operator. Thus, since $U_N \subset \tilde{U} \subset U$ and $V_N \subset \tilde{V} \subset V$, the problems (6.59) and (6.60) read as: find $u_N \in U_N$ such that

$$a_h(u_N, v_N) = l(v_N), \quad \forall v_N \in V_N, \tag{6.27}$$

where $l(v_N) = (f, v_N)$; and find $Su_N \in U_N$ such that

$$a_h(Su_N, w_N) = l(w_N), \quad \forall w_N \in V_N, \tag{6.28}$$

where $l(w_N) = (\mathrm{f}_{q_i}, w_N)$. Also, the discrete bilinear form $a_h(u_N, v_N)$ can be written as

$$\begin{aligned} a_h(u_N, v_N) = {} & ({}_0\mathcal{D}_t^{\frac{\alpha}{2}}\, u_N, {}_t\mathcal{D}_T^{\frac{\alpha}{2}}\, v_N)_\Omega \\ & - \sum_{j=1}^{d} k_j \Big[({}_{a_j}\mathcal{D}_{x_j}^{\frac{\beta_j}{2}}\, u_N, {}_{x_j}\mathcal{D}_{b_j}^{\frac{\beta_j}{2}}\, v_N)_\Omega + ({}_{x_j}\mathcal{D}_{b_j}^{\frac{\beta_j}{2}}\, u_N, {}_{a_j}\mathcal{D}_{x_j}^{\frac{\beta_j}{2}}\, v_N)_\Omega \Big]. \end{aligned} \tag{6.29}$$

We expand the approximate solution $u_N \in U_N$, satisfying the discrete bilinear form (7.37), in the following form

$$u_N(t, \mathbf{x}) = \sum_{n=1}^{\mathcal{N}} \sum_{m_1=1}^{\mathcal{M}_1} \cdots \sum_{m_d=1}^{\mathcal{M}_d} \hat{u}_{n,m_1,\cdots,m_d} \left[\psi_n^\tau(t) \prod_{j=1}^{d} \phi_{m_j}(x_j) \right], \tag{6.30}$$

and obtain the corresponding Lyapunov system by substituting (7.38) into (7.37) by choosing $v_N(t,\mathbf{x}) = \Psi_k^\tau(t)\prod_{j=1}^d \Phi_{r_j}(x_j)$, $k = 1,2,\ldots,\mathcal{N}$, $r_j = 1,2,\ldots,\mathcal{M}_j$. Therefore,

$$\Big[S_T \otimes M_1 \otimes M_2 \cdots \otimes M_d + \sum_{j=1}^{d} M_T \otimes M_1 \otimes \cdots \otimes M_{j-1} \otimes S_j \otimes M_{j+1} \cdots \otimes M_d\Big]\,\mathcal{U} = F, \quad (6.31)$$

in which $\otimes$ represents the Kronecker product, F denotes the multi-dimensional load matrix whose entries are given as

$$F_{k,r_1,\cdots,r_d} = \int_\Omega f(t,\mathbf{x})\Big(\Psi_k^\tau \circ \eta\Big)(t)\prod_{j=1}^{d}\Big(\Phi_{r_j} \circ \xi_j\Big)(x_j)\,d\Omega, \quad (6.32)$$

and $\mathcal{U}$ is the matrix of unknown coefficients. The matrices S_T and M_T denote the temporal stiffness and mass matrices, respectively; and the matrices S_j and M_j denote the spatial stiffness and mass matrices, respectively. We obtain the entries of spatial mass matrix M_j analytically and employ proper quadrature rules to accurately compute the entries of other matrices S_T, M_T and S_j.

We note that the choices of basis/test functions, employed in developing the PG scheme leads to symmetric mass and stiffness matrices, providing useful properties to further develop a fast solver. The following Theorem 7.3.6 provides a unified fast solver, developed in terms of the generalized eigensolutions in order to obtain a closed-form solution to the Lyapunov system (7.39).

Theorem 6.3.1 (Unified Fast FPDE Solver [143, 145])**.** *Let $\{\vec{e}_{m_j}, \lambda_{m_j}\}_{m_j=1}^{\mathcal{M}_j}$ be the set of general eigen-solutions of the spatial stiffness matrix S_j with respect to the mass matrix M_j. Moreover, let $\{\vec{e}_n^{\,\tau}, \lambda_n^\tau\}_{n=1}^{\mathcal{N}}$ be the set of general eigen-solutions of the temporal mass matrix M_T with respect to the stiffness matrix S_T. Then, the matrix of unknown coefficients $\mathcal{U}$ is explicitly obtained as*

$$\mathcal{U} = \sum_{n=1}^{\mathcal{N}}\sum_{m_1=1}^{\mathcal{M}_1}\cdots\sum_{m_d=1}^{\mathcal{M}_d}\kappa_{n,m_1,\cdots,m_d}\;\vec{e}_n^{\,\tau}\otimes\vec{e}_{m_1}\otimes\cdots\otimes\vec{e}_{m_d}, \quad (6.33)$$

where $\kappa_{n,m_1,\cdots,m_d}$ is given by

$$\kappa_{n,m_1,\cdots,m_d} = \frac{(\vec{e}_n^{\,\tau}\,\vec{e}_{m_1}\cdots\vec{e}_{m_d})F}{\Big[(\vec{e}_n^{\,\tau T}\,S_T\,\vec{e}_n^{\,\tau})\,\prod_{j=1}^{d}(\vec{e}_{m_j}^{\,T}\,M_j\,\vec{e}_{m_j})\Big]\Lambda_{n,m_1,\cdots,m_d}}, \quad (6.34)$$

in which the numerator represents the standard multi-dimensional inner product, and $\Lambda_{n,m_1,\cdots,m_d}$ *is obtained in terms of the eigenvalues of all mass matrices as*

$$\Lambda_{n,m_1,\cdots,m_d} = \Big[(1+\gamma\ \lambda_n^\tau) + \lambda_n^\tau \sum_{j=1}^{d}(\lambda_{m_j})\Big].$$

6.3.1 Stability Analysis

We show the well-posedness of defined problem and prove the stability of proposed numerical scheme.

Lemma 6.3.2. *Let* $\alpha \in (0,1)$, $\Omega = I \times \Lambda_d$, *and* $u \in {}_0^l H^{\alpha/2}(I; L^2(\Lambda_d))$. *Then,*

$$\Big|\Big({}_0\mathcal{D}_t^{\alpha/2}u, {}_t\mathcal{D}_T^{\alpha/2}v\Big)_\Omega\Big| \equiv \|u\|_{l H^{\alpha/2}(I;L^2(\Lambda_d))}\, \|v\|_{r H^{\alpha/2}(I;L^2(\Lambda_d))}, \quad \forall v \in {}_0^r H^{\alpha/2}(I; L^2(\Lambda_d)).$$

Proof. See section 6.7.5 for proof. □

By equivalence of function spaces ${}^l H_0^\sigma(\Lambda)$, ${}^r H_0^\sigma(\Lambda)$, and ${}^c H_0^\sigma(\Lambda)$ and also their associated norms $\|\cdot\|_{l H^\sigma(\Lambda)}$, $\|\cdot\|_{r H^\sigma(\Lambda)}$, and $\|\cdot\|_{c H^\sigma(\Lambda)}$; and also by following similar steps as in Lemma 7.3.7, we can also prove that

$$\big|\big({}_{a_d}\mathcal{D}_{x_d}^{\beta_d/2}u, {}_{x_d}\mathcal{D}_{b_d}^{\beta_d/2}v\big)_{\Lambda_d}\big| \equiv |u|_{{}_c H^{\beta_d/2}\left((a_d,b_d);L^2(\Lambda_{d-1})\right)}\, |v|_{{}_c H^{\beta_d/2}\left((a_d,b_d);L^2(\Lambda_{d-1})\right)}, \tag{6.35}$$

$$\big|\big({}_{x_d}\mathcal{D}_{b_d}^{\beta_d/2}u, {}_{a_d}\mathcal{D}_{x_d}^{\beta_d/2}v\big)_{\Lambda_d}\big| \equiv |u|_{{}_c H^{\beta_d/2}\left((a_d,b_d);L^2(\Lambda_{d-1})\right)}\, |v|_{{}_c H^{\beta_d/2}\left((a_d,b_d);L^2(\Lambda_{d-1})\right)}. \tag{6.36}$$

Lemma 6.3.3 (Continuity)**.** *The bilinear form* (7.28) *is continuous, i.e.,*

$$\forall u \in U,\ \exists \beta > 0, \quad s.t. \quad |a(u,v)| \le \beta\ \|u\|_U\ \|v\|_V, \quad \forall v \in V. \tag{6.37}$$

Proof. The proof directly concludes from (7.43), (7.44) and Lemma 7.3.7. □

Theorem 6.3.4 (Stability)**.** *The following inf-sup condition holds for the bilinear form* (7.28)*, i.e.,*

$$\inf_{0\neq u\in U}\ \sup_{0\neq v\in V}\ \frac{|a(u,v)|}{\|v\|_V\ \|u\|_U} \ge \beta > 0, \tag{6.38}$$

where $\Omega = I \times \Lambda_d$ *and* $\sup_{u\in U} |a(u,v)| > 0$.

Proof. See section 6.7.6 for proof. □

Theorem 6.3.5 (well-posedness)**.** *For all* $0 < \alpha < 1$*,* $\alpha \neq 1$*, and* $1 < \beta_j < 2$*, and* $j = 1, \cdots, d$*, there exists a unique solution to* (7.29)*, continuously dependent on* f*, which belongs to the dual space of* U*.*

Proof. Lemmas 7.3.8 (continuity) and 7.3.9 (stability) yield the well-posedness of weak form (7.29) in (1+d)-dimension due to the generalized Babuška-Lax-Milgram theorem. □

Since the defined basis and test spaces are Hilbert spaces, and $U_N \subset U$ and $V_N \subset V$, we can prove that the developed Petrov-Gelerkin spectral method is stable and the following condition holds

$$\inf_{0 \neq u_N \in U_N} \sup_{0 \neq v \in V_N} \frac{|a(u_N, v_N)|}{\|v_N\|_V \ \|u_N\|_U} \geq \beta > 0, \tag{6.39}$$

with $\beta > 0$ and independent of N, where $\sup_{u_N \in U_N} |a(u_N, v_N)| > 0, \ \forall v_N \in V_N$.

We recall again here that the adjoint FSEs have similar bilinear form; and since $\tilde{U} \subset U$ and $\tilde{V} \subset V$, the obtained results are also applicable to them.

6.4 Fractional Sensitivity Equation Method (FSEM)

We define the sensitivity coefficients as the partial derivative of transport field u with respect to the model parameters q_i, i.e.

$$S_{u,q_i} = \frac{\partial u}{\partial q_i}, \quad i = 1, 2, \cdots, 2d + 1, \tag{6.40}$$

assuming that the partial derivative is well-defined. To obtain the governing equation of evolution of sensitivity fields, i.e. FSEs, we first take the partial derivative of left- and right-sided fractional derivative (1.16) and (1.17) with respect to their orders. Therefore, by letting $\sigma \in (n-1, n]$, $x \in [a, b]$, $\mathcal{A}_n(\sigma) = \Gamma(n-\sigma)\frac{\partial}{\partial \sigma}\frac{1}{\Gamma(n-\sigma)}$, we have

$$\frac{\partial}{\partial \sigma}({}_a\mathcal{D}_x^\sigma u) = {}_a\mathcal{D}_x^\sigma S_{u,\sigma} + \mathcal{A}_n(\sigma)\, {}_a\mathcal{D}_x^\sigma u - {}^{LP}_a\mathcal{D}_x^\sigma u, \tag{6.41}$$

$$\frac{\partial}{\partial \sigma}({}_x\mathcal{D}_b^\sigma u) = {}_x\mathcal{D}_b^\sigma S_{u,\sigma} + \mathcal{A}_n(\sigma)\, {}_x\mathcal{D}_b^\sigma u - {}^{LP}_x\mathcal{D}_b^\sigma u. \tag{6.42}$$

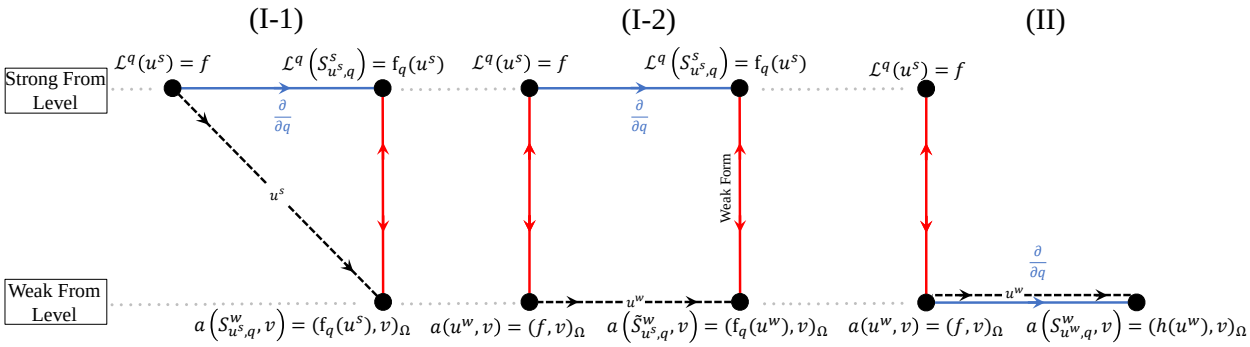

Figure 6.1: Schematic of strategies in deriving the weak form of FSEs. (I-1): first take $\frac{\partial}{\partial q}$ and then obtain the weak formulation, fed by strong solution u^s. (I-2): first take $\frac{\partial}{\partial q}$ and then obtain the weak formulation, fed by weak solution u^w. (II): first obtain the weak formulation and then take $\frac{\partial}{\partial q}$, fed by weak solution u^w.

The pre-super script LP stands for the *Log-Pow integro-differential operator*, given in (6.1)-(6.4), which we introduce here, for the first time in the context of FSEs.

Remark 6.4.1. *In the sequel, we only use the RL − LP operator and thus, for the sake of simplicity, we drop the pre-super script RL and C and only use them when it is necessary to distinguish between the two senses of derivatives.*

We derive the adjoint FSEs by pursuing two different strategies I and II, shown schematically in Fig. 6.1. We adopt the notation of u^s and u^w to distinguish the solution to strong and weak form of the problem for ease of describing the two following strategies. In the first strategy, we first take the partial derivative of FPDE with respect to the model parameters q, and then, obtain the weak form of problem. If u^s is known, then we follow I-1 (left figure), otherwise we formulate and solve the weak form of FPDE to obtain weak solution u^w and follow I-2 (middle figure).

$$\text{I-1:}\quad \mathcal{L}^q(u^s) = f \xrightarrow{\frac{\partial}{\partial q}} \mathcal{L}^q(S^s_{u^s,q}) = \mathrm{f}_q(u^s) \xrightarrow{\text{weak form}} a(S^w_{u^s,q}, v) = (\mathrm{f}_q(u^s), v)_\Omega \tag{6.43}$$

$$\text{I-2:}\quad \mathcal{L}^q(u^s) = f \xrightarrow{\frac{\partial}{\partial q}} \mathcal{L}^q(S^s_{u^s,q}) = \mathrm{f}_q(u^s) \xrightarrow{\text{weak form}} a(\tilde{S}^w_{u^s,q}, v) = (\mathrm{f}_q(u^w), v)_\Omega \tag{6.44}$$

Via proper construction of the corresponding subspaces, we discretize and solve $a(S^w_{u^s,q}, v) = (\mathrm{f}_q(u^s), v)_\Omega$ and $a(\tilde{S}^w_{u^s,q}, v) = (\mathrm{f}_q(u^w), v)_\Omega$ in I-1 and I-2, respectively. We can show that $\|\tilde{S}^w_{u^s,q}$ −

$S^w_{u^s,q}\|_{L^2} \to 0$ as $u^w \to u^s$ by stability/error analysis of employed numerical scheme, where the solution space has the extra regularity required by the Log-Pow integro-differential operator in f_q.

Remark 6.4.2. *The solution to strong form of FPDE, i.e. u^s can be analytically/numerically computed (by Laplace transform and finite difference method for example), or may be available as prior experimental data, and thus, can be fed directly to construct f_q in FSEs (see left sub-figure in Fig. 6.1). This is used in parameter estimation for model construction, section 6.5.*

In the second strategy, we first obtain the weak form of FPDE, and then take the partial derivative with respect to the model parameters q. In this case, we procure $(h(u^w), v)$ as the right hand side of weak formulation, which is fed by the weak solution u^w. In this case, the function h requires less regularity for the solution space due to the Log-Pow integro-differential operator, since the order of kernel is less compare to the first strategy.

$$\text{II:} \quad \mathcal{L}^q(u^s) = f \xrightarrow{\text{weak form}} a(u^w, v) = (f, v)_\Omega \xrightarrow{\frac{\partial}{\partial q}} a(S^w_{u^w,q}, v) = (h(u^w), v)_\Omega \tag{6.45}$$

In the next subsection, we adopt the two strategies to derive adjoint FSE to a fractional initial value problem, where we show the corresponding right-hand-side and the imposed extra regularity in each case. We then, extend the derivation to the case FPDE, in which we adopt strategy I-2.

6.4.1 FSEM (FIVP)

Let $\Omega = (0, T]$ be the computational time domain and define $u(t;\alpha) : \Omega \times (0,1) \to \mathbb{R}$. We consider the case of fractional initial value problem (FIVP) by letting the coefficients k_j's to be zero in (6.7), and thus obtain the following FIVP, subject to Dirichlet initial condition, as ${}_0\mathcal{D}^\alpha_t u(t;\alpha) = f(t;\alpha)$, $u(0) = 0$. By taking the partial derivative with respect to α, we obtain the adjoint FSE in the strong form as ${}_0\mathcal{D}^\alpha_t S_{u,\alpha} = \mathrm{f}_\alpha$, $S_{u,q}|_{(t=0)} = 0$, where $\mathrm{f}_\alpha = S_{f,\alpha} - \mathcal{A}_1(\alpha)\ {}_0\mathcal{D}^\alpha_t u + {}^{LP}_0\mathcal{D}^\alpha_t u$. Following strategy I, we obtain

$$a(S_{u,\alpha}, v)_\Omega = (\mathrm{f}_\alpha, v)_\Omega, \tag{6.46}$$

$$(\mathrm{f}_\alpha, v)_\Omega = (S_{f,\alpha}, v)_\Omega - \mathcal{A}_1(\alpha)\ ({}_0\mathcal{D}^{\frac{\alpha}{2}}_t u, {}_t\mathcal{D}^{\frac{\alpha}{2}}_T v)_\Omega + ({}^{LP}_0\mathcal{D}^\alpha_t u, v)_\Omega. \tag{6.47}$$

In this case, constructing the right-hand-side imposes extra strong regularity of $\| {}^{LP}_{0}\mathcal{D}^{\alpha}_{t} u\|_{L^2} < \infty$ to the solution of FIVP. However, by following startegy II, we obtain

$$a(S_{u,\alpha}, v)_\Omega = h(v), \tag{6.48}$$

$$h(v) = (S_{f,\alpha}, v)_\Omega + (f, S_{v,\alpha})_\Omega - \mathcal{A}_1(\frac{\alpha}{2})\ ({}_0\mathcal{D}^{\frac{\alpha}{2}}_{t} u, {}_t\mathcal{D}^{\frac{\alpha}{2}}_{T} v)_\Omega - ({}_0\mathcal{D}^{\frac{\alpha}{2}}_{t} u, {}_t\mathcal{D}^{\frac{\alpha}{2}}_{T} S_{v,\alpha})_\Omega \tag{6.49}$$
$$+ \frac{1}{2}({}^{LP}_{0}\mathcal{D}^{\frac{\alpha}{2}}_{t} u, {}_t\mathcal{D}^{\frac{\alpha}{2}}_{T} v)_\Omega + \frac{1}{2}({}_0\mathcal{D}^{\frac{\alpha}{2}}_{t} u, {}^{LP}_{t}\mathcal{D}^{\frac{\alpha}{2}}_{T} v)_\Omega,$$

where, the function h imposes extra weak regularity of $\| {}^{LP}_{0}\mathcal{D}^{\frac{\alpha}{2}}_{t} u\|_{L^2} < \infty$ and $\| {}^{LP}_{t}\mathcal{D}^{\frac{\alpha}{2}}_{T} v\|_{L^2} < \infty$ to the solution. We computationally study and make sure that the solution to (6.46) converges to (6.48).

6.4.2 FSEM (FPDE)

We consider the problem (6.7)-(7.3). We adopt strategy I-2 and derive the adjoint FSEs and their corresponding weak form, where to construct the right-hand-side, we also obtain the weak form of FPDE. Thus, we solve a coupled system of FPDE and FSEs. By taking the partial derivatives of (6.7) with respect to model parameters q_i, $i = 1, 2, \cdots, 2d+1$, we obtain the corresponding adjoint FSEs as

$$\boxed{\mathcal{L}^q\ S_{u,\alpha} = \mathrm{f}_\alpha\ ,\quad \mathcal{L}^q\ S_{u,\beta_j} = \mathrm{f}_{\beta_j}\ ,\quad \mathcal{L}^q\ S_{u,k_j} = \mathrm{f}_{k_j}\ ,\quad j = 1, 2, \cdots, d\ ,} \tag{6.50}$$

in which

$$\mathcal{L}^q(\cdot) = {}_0\mathcal{D}^{\alpha}_{t}(\cdot) - \sum_{j=1}^{d} k_j \left[-a_j \mathcal{D}^{\beta_j}_{x_j} + {}_{x_j}\mathcal{D}^{\beta_j}_{b_j}\right](\cdot) \tag{6.51}$$

$$\mathrm{f}_\alpha = S_{f,\alpha} - \mathcal{A}_1(\alpha)\, {}_0\mathcal{D}^{\alpha}_{t} u + {}^{LP}_{0}\mathcal{D}^{\alpha}_{t} u \tag{6.52}$$

$$\mathrm{f}_{\beta_j} = S_{f,\beta_j} + k_j\, \mathcal{A}_2(\beta_j) \left[{}_{a_k}\mathcal{D}^{\beta_j}_{x_j} + {}_{x_j}\mathcal{D}^{\beta_j}_{b_k}\right] u - k_j \left[{}^{LP}_{a_k}\mathcal{D}^{\beta_j}_{x_j} + {}^{LP}_{x_j}\mathcal{D}^{\beta_j}_{b_k}\right] u, \tag{6.53}$$

$$\mathrm{f}_{k_j} = S_{f,k_j} + \left[-a_j \mathcal{D}^{\beta_j}_{x_j} + {}_{x_j}\mathcal{D}^{\beta_j}_{b_j}\right] u. \tag{6.54}$$

Moreover, by taking the partial derivative of initial and boundary conditions (7.2) and (7.3), respectively, with respect to model parameters, we obtain the following conditions for $i = 1, 2, \cdots, 2d+1$,

as

$$S_{u,q_i}\big|_{t=0} = \frac{\partial S_{u,q_i}}{\partial t}\big|_{t=0} = 0, \quad S_{u,q_i}\big|_{x=a_j} = S_{u,q_i}\big|_{x=b_j} = 0, \ j = 1, 2, \cdots, d. \tag{6.55}$$

6.4.3 Mathematical Framework: Coupled System of The FPDE and Derived FSEs

We extend the solution/test spaces, defined in (7.22) by imposing the "extra regularities" due to the right-hand-side of adjoint FSEs (6.50), and define the proper underlying spaces for solving the coupled system of adjoint FSEs and FPDE.

Solution/Test Spaces. Let

$$\mathcal{H}_0^{\frac{\beta_j}{2}}(\Lambda_j) = \Big\{ u \in H_0^{\frac{\beta_j}{2}}(\Lambda_j) \Big| \sqrt{\| {}_{a_j}^{LP}\mathcal{D}_{x_j}^{\beta_j} u\|^2_{L^2(\Lambda_j)} + \| {}_{x_j}^{LP}\mathcal{D}_{b_j}^{\beta_j} u\|^2_{L^2(\Lambda_j)}} < \infty \Big\}, \ j = 1, 2, \cdots, d,$$

associated with the norm $\| \cdot \|_{{}^{c}H^{\frac{\beta_j}{2}}(\Lambda_j)}$. We define $\mathcal{X}_1 = \mathcal{H}_0^{\frac{\beta_1}{2}}(\Lambda_1)$, and accordingly, $\mathcal{X}_j$, $j = 2, \cdots, d$ as

$$\mathcal{X}_2 = \mathcal{H}_0^{\frac{\beta_2}{2}}((a_2, b_2); L^2(\Lambda_1)) \cap L^2((a_2, b_2); \mathcal{X}_1), \tag{6.56}$$

$$\vdots$$

$$\mathcal{X}_d = \mathcal{H}_0^{\frac{\beta_d}{2}}((a_d, b_d); L^2(\Lambda_{d-1})) \cap L^2((a_d, b_d); \mathcal{X}_{d-1}), \tag{6.57}$$

associated with the similar norm $\| \cdot \|_{\mathcal{X}_d}$. Thus, we define the corresponding "solution space" $\tilde{U}$ and "test space" $\tilde{V}$, respectively, as

$$\tilde{U} = {}_0^l\mathcal{H}^{\frac{\alpha}{2}}\Big(I; L^2(\Lambda_d)\Big) \cap L^2(I; \mathcal{X}_d), \quad \tilde{V} = {}_0^r\mathcal{H}^{\frac{\alpha}{2}}\Big(I; L^2(\Lambda_d)\Big) \cap L^2(I; \mathcal{X}_d), \tag{6.58}$$

endowed with similar norms (7.26) and (7.27), where

$${}_0^l\mathcal{H}^{\frac{\alpha}{2}}\Big(I; L^2(\Lambda_d)\Big) =$$

$$\Big\{ u \Big| \|u(t,\cdot)\|_{L^2(\Lambda_d)} \in H^{\frac{\alpha}{2}}(I), \| {}_0^{LP}\mathcal{D}_t^{\alpha} u\|_{L^2(I)} < \infty, u|_{t=0} = u|_{x=a_j} = u|_{x=b_j} = 0, \ j = 1, 2, \cdots, d \Big\},$$

$${}_0^r\mathcal{H}^{\frac{\alpha}{2}}\Big(I; L^2(\Lambda_d)\Big) =$$

$$\Big\{ v \Big| \|v(t,\cdot)\|_{L^2(\Lambda_d)} \in H^{\frac{\alpha}{2}}(I), \| {}_t^{LP}\mathcal{D}_T^{\alpha} u\|_{L^2(I)} < \infty, v|_{t=T} = v|_{x=a_j} = v|_{x=b_j} = 0, \ j = 1, 2, \cdots, d \Big\},$$

equipped with norms $\|u\|_{{}_l H^{\frac{\alpha}{2}}(I;L^2(\Lambda_d))}$ and $\|u\|_{{}_r H^{\frac{\alpha}{2}}(I;L^2(\Lambda_d))}$, respectively.

Weak Formulation. Since derived FSEs (6.50) preserve the structure of FPDE (6.7), the bilinear form of corresponding weak formulation takes the same form as (7.28). Therefore, By letting $\tilde{U}$ and $\tilde{V}$ be the solution/test spaces, defined in (6.58), the problem reads as: find $u \in \tilde{U}$ such that

$$a(u, v) = (f, v)_\Omega, \quad \forall v \in \tilde{V}, \tag{6.59}$$

and find $S_{u,q_i} \in U$, $1 = 1, 2, \cdots, 2d + 1$ such that

$$a(S_{u,q_i}, w) = (\mathrm{f}_{q_i}, w)_\Omega \quad \forall w \in V, \tag{6.60}$$

where U and V are defined in (7.22).

6.5 Fractional Model Construction

We employ the developed FSEM in order to construct an iterative algorithm to estimate model parameters from known solution (or available sets of data). We formulate the iterative algorithm by minimizing an objective model error function. We recall again here that in our fractional model, the set of model parameters is $q = \{\alpha, \beta_1, \beta_2, \cdots, \beta_d, k_1, k_2, \cdots, k_d\}$, and here, we mainly focus on estimation of fractional indices. Thus, assuming the model coefficients $\{k_1, k_2, \cdots, k_d\}$ to be given/known, we reduce the model parameter set to $q = \{\alpha, \beta_1, \beta_2, \cdots, \beta_d\} \in Q \subset \mathbb{R}^{1+d}$.

6.5.1 Model Error

The fractional model can be simply visualized as Fig. 6.2, where $\mathcal{L}^q u = f$. We denote by the superscript $(^*)$ as the exact values of quantities. Therefore, $\mathcal{L}^{q^*} u^* = f^*$, where u^*, f^* are the exact solution and force functions, respectively, and q^* is the set of exact model parameters. Obviously, by choosing different values of model parameters (fractional indices), the fractional model observes the input differently, and thus, results in a different output. This leads to two types of *model error*, namely, type-I and type-II, described as follows. We note that the introduced model errors are zero at the exact values q^*, by definition.

Figure 6.2: Schematic of fractional model

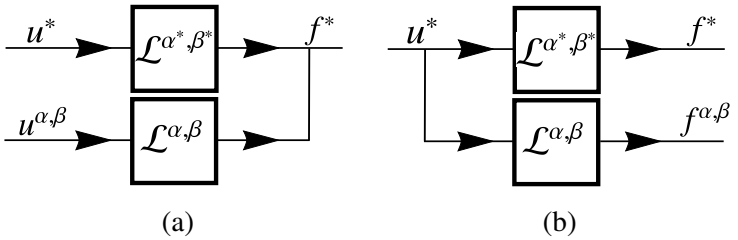

Figure 6.3: Schematic of variation of fractional model based on (a) model error type-I and (b) model error type-II.

6.5.1.1 Model Error: Type-I

In model error type-I, we consider the output of model to be fixed, i.e, $f = f^*$, however, changing parameters makes the fractional model to observe the variated input u^q as opposed to u^*. Therefore, we define the model error as the difference between variated and exact inputs, i.e. $E(q) = ||u^q - u^*||_{L^2}$. The schematic of variation of model from the exact model is shown in Fig. 6.3 (a). For each variated model, we accurately compute the numerical approximation, u_N^q, by solving (6.7), where by increasing the number of terms in the approximate solution, we make sure that the function $E(q) = ||u_N^q - u^*||_{L^2}$ solely describes the model error with minimum discretization error. The proposed iterative algorithm, as will be discussed later, involves the gradient of model error with respect to the model parameters. Thus, we take the partial derivative of E with respect to q, as

$$S_{E,q} = \frac{\partial E}{\partial q} = \frac{\int_\Omega S_{uq,q}\,(u_N^q - u^*)\; d\Omega}{E} \tag{6.61}$$

where $S_{uq,q}$ denotes the sensitivity fields, which is numerically obtained by solving FSEs (6.50). We note that in this case, since f is fixed and therefore, not sensitive to any parameter, we exclude the first term in the definition of force functions f_α and f_β.

6.5.1.2 Model Error: type-II

In model error type-II, we consider the input of model to be fixed, i.e, $u = u^*$, however, changing parameters makes the fractional model to result in the variated output f^q as opposed to f^*. Therefore, we define the model error as the difference between variated and exact outputs, i.e. $E(q) = ||f^q - f^*||_{L^2}$. The schematic of variation of model from the exact model is shown in Fig. 6.3 (b). In this case, unlike model error type-I, the model error and its gradient can be expressed analytically. Therefore, they do not contain any discretization error.

6.5.2 Model Error Minimization: Iterative Algorithm

We minimize the model error by formulating a two-stages algorithm. Since we do not have prior information about the variated solution/force function, it is difficult to analytically predict the behavior of introduced model error. However, in every example, we numerically study the behavior of a low resolution model error manifold on a coarse grid, and then, perform the local minimization. The minimization problem is written as:

$$\min_{q \in Q} \Big(E(q) \Big), \tag{6.62}$$

in which $E(q) : Q \to \mathbb{R}$, and we assume that the problem is solvable, i.e. there exist a minimum point $q^* \in Q$. Proper choice of initial guess in local minimization is of great importance, where a wrong initial guess, not falling within small enough adjacency of minimum, may never converge. Therefore, the iterative convergence in a hypercube space of parameters is highly connected to an optimal initial guess for each parameter. In the sequel, we delineate the two stages of our algorithm, namely, stage I: *coarse grid* searching, and stage II: *nearby solution*.

In stage I, we progressively divide the hypercube parameter space into subspaces to narrow down the objective search region into a smaller region. This division process is not necessarily unique and can be done in different ways, among which we discuss the easy-to-implement one here, where in each progression step, we choose the subspace with minimum error at its corner. We carry out the coarse grid searching till we reach a small enough region, in which the nearby solution (stage

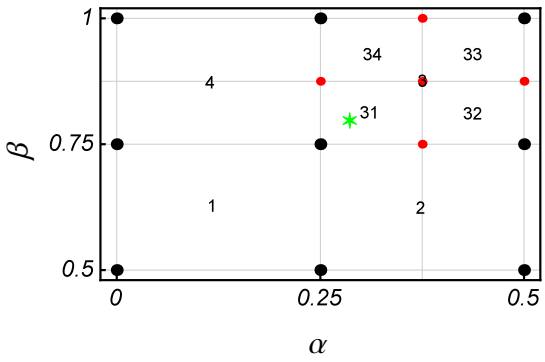

Figure 6.4: Iterative algorithm: coarse grid searching for $(1+1)$-D parameter space, where $\alpha^* = 0.3$ and $\beta^* = 0.8$.

II) is valid. As an example, we consider a $(1+1)$-D fractional model with $q^* = \{\alpha^*, \beta^*\} = \{0.3, 0.8\}$ as the exact fractional indices in the parameter surface, shown in Fig. 6.4. We divide the parameter space into four equal subspaces and by computing the error at corner points of each subsurface (black dots), we shrink the search region (to the labeled subsurface 3). We progress further once again in a similar fashion, divide the subsurface, and compute the error at corner points (red dots). We finally, narrow down the search region into labeled subsurface 31. We see that in this case, with computing the error only at 14 points, we can efficiently narrow down the parameter space into a small enough search region, in which we can perform stage II of the algorithm.

In stage II of the algorithm, we employ a gradient decent method, in which by starting from an initial guess $q^0 = \{\alpha^0, \beta_1^0, \beta_2^0, \cdots, \beta_d^0\}$ in the obtained search region from stage I, we produce a minimizing sequence q^i, $i = 1, 2, \cdots$, where

$$q^{i+1} = q^i + \Delta q^i, \tag{6.63}$$

and the increment $\Delta q^i = s^i p^i$ contains both the step size s^i and normalized step direction p^i. The superscript i indicates the iteration index. We obtain the normalized direction p^i by computing the gradient of model error with respect to the parameters. The step size is usually computed by performing a line search such that $E(q^i + s\, p^i)$ is minimized over $\forall s \in \mathbb{R}$. However, in our case the method does not produce well-scaled search directions, and we need to approximate the current

step size, using the previous one. Thus,

$$p^i = -\frac{\nabla E(q^i)}{\|\nabla E(q^i)\|}, \qquad s^i = s^{i-1}\frac{\nabla E(q^{i-1})^T\, p^{i-1}}{\nabla E(q^i)^T\, p^i}, \tag{6.64}$$

where the first iteration size is obtained, using the Taylor expansion of model error about q^0.

6.5.3 Fractional Model Construction: FSEM-based Iterative Algorithm

Let $\Omega = [0,T] \times [-1,1]$ be the computational domain. We consider the (1 + 1)-D case of FPDE (6.7), subject to the initial and boundary conditions (7.2) and (7.3), respectively, where the adjoint FSEs are given in (6.50). Assuming that the exact transport field $u^*(t,x)$ and force function $f^*(t,x)$ are given, then,

$$ {}_0\mathcal{D}_t^{\alpha^*} u^* - k\left({}_{-1}\mathcal{D}_x^{\beta^*} + {}_x\mathcal{D}_1^{\beta^*} \right) u^* = f^* \tag{6.65}$$

in which $\{\alpha^*, \beta^*\}$ are the exact fractional indices and the coefficient k is known.

By considering the two types of model error, we use the developed iterative formulation and follow the steps below to obtain the optimal model parameters. In each iteration, the increments are obtained, using (6.64).

For each model error we follow different steps, given below. Based on the model error I, we follow

1. Initial guess $q^0 = \{\alpha^0, \beta^0\}$
2. **Do** $i = 0, 1, \cdots$
3. Solve for $u_N^{q^i}$: FPDE
4. Compute the model error $E = ||u_N^{q^i} - u^*||_{L^2}$
5. **If** $E <$ tolerance, **Then** Break, **Otherwise** Continue
6. Solve for sensitivity fields: FSEs
7. Compute the model error gradient using sensitivity field
8. Compute the iteration increment Δq^i
9. March in parameter space $q^{i+1} = q^i + \Delta q^i$
10. **End**

and based on the model error II, we follow

1. Initial guess $q^0 = \{\alpha^0, \beta^0\}$
2. **Do** $i = 0, 1, \cdots$
3. Compute the model error $E = ||\mathcal{L}^{q^i} u^* - \mathcal{L}^{q^*} u^*||_{L^2}$
4. **If** $E <$ tolerance, **Then** Break, **Otherwise** Continue
5. Compute the model error gradient using sensitivity field (analytically available)
6. Compute the iteration increment Δq^i
7. March in parameter space $q^{i+1} = q^i + \Delta q^i$
8. **End**

Remark 6.5.1. *In the first iteration, we compute the step size, using the Taylor expansion of the model error about the initial guess* $\{\alpha^0, \beta^0\}$*, which we separate into two directions as*

$$E\Big|_{\{\alpha^*,\beta^*\}} \approx E\Big|_{\{\alpha^0,\beta^0\}} + S_{E,\alpha}\Big|_{\{\alpha^0,\beta^0\}} (\alpha^* - \alpha^0), \qquad E\Big|_{\{\alpha^*,\beta^*\}} \approx E\Big|_{\{\alpha^0,\beta^0\}} + S_{E,\beta}\Big|_{\{\alpha^0,\beta^0\}} (\beta^* - \beta^0). \tag{6.66}$$

Knowing that $E\Big|_{\{\alpha^*,\beta^*\}} = 0$*, we obtain the parameters at next iterations as* $\alpha^1 = \alpha^0 + \Delta\alpha^0$ *and* $\beta^1 = \beta^0 + \Delta\beta^0$*, in which*

$$\Delta\alpha^0 \approx -\frac{E\Big|_{\{\alpha^0,\beta^0\}}}{S_{E,\alpha}\Big|_{\{\alpha^0,\beta^0\}}}, \qquad \Delta\beta^0 \approx -\frac{E\Big|_{\{\alpha^0,\beta^0\}}}{S_{E,\beta}\Big|_{\{\alpha^0,\beta^0\}}}. \tag{6.67}$$

6.6 Numerical Results

In the first part of numerical results, we investigate the performance of developed PG scheme in solving FPDE and the adjoint FSEs. We consider the coupled (1 + 1)-d FPDE and FSEs with one-sided fractional derivative and $k = 1$, as

$$ {}_0\mathcal{D}_t^\alpha u - {}_{-1}\mathcal{D}_x^\beta u = f, \tag{6.68}$$

$$ {}_0\mathcal{D}_t^\alpha S_{u,\alpha} - {}_{-1}\mathcal{D}_x^\beta S_{u,\alpha} = S_{f,\alpha} - \mathcal{A}_1(\alpha)\, {}_0\mathcal{D}_t^\alpha u + {}^{LP}_{0}\mathcal{D}_t^\alpha u, \tag{6.69}$$

$$ {}_0\mathcal{D}_t^\alpha S_{u,\beta} - {}_{-1}\mathcal{D}_x^\beta S_{u,\beta} = S_{f,\beta} + \mathcal{A}_2(\beta)\, {}_{-1}\mathcal{D}_x^\beta u - {}^{LP}_{-1}\mathcal{D}_x^\beta u. \tag{6.70}$$

We consider two cases of exact solution as

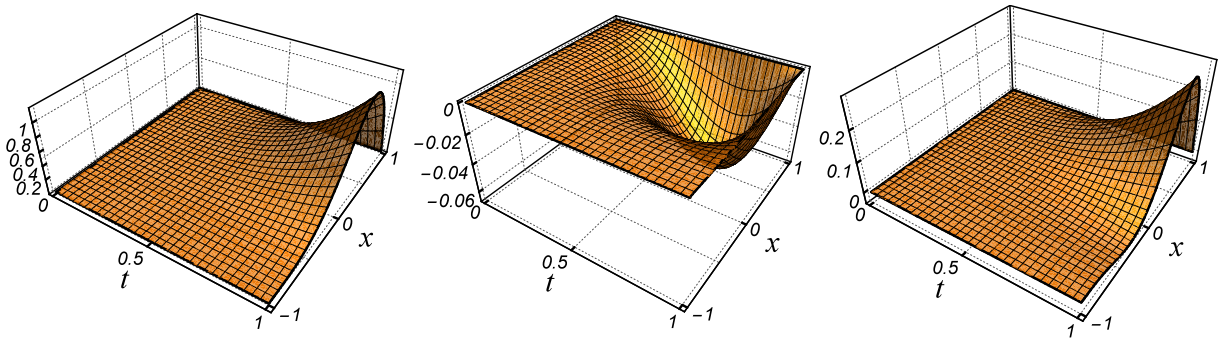

Figure 6.5: Plot of exact functions for case I with $\alpha/2 = 0.25$ and $\beta/2 = 0.75$: exact solution u^{ext} (left), exact sensitivity field $S_{u^{ext},\alpha} = \frac{\partial u^{ext}}{\partial \alpha}$ (middle), exact sensitivity field $S_{u^{ext},\beta} = \frac{\partial u^{ext}}{\partial \beta}$ (right).

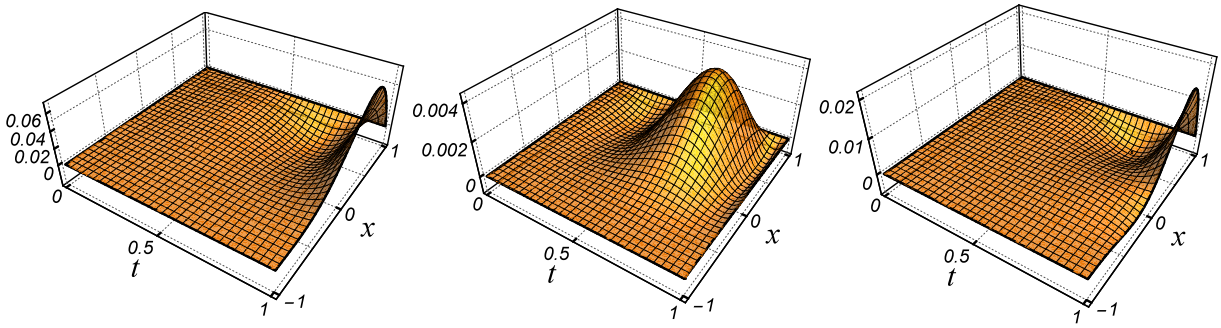

Figure 6.6: Plot of exact functions for case II with $\alpha/2 = 0.25$ and $\beta/2 = 0.75$: exact solution u^{ext} (left), exact sensitivity field $S_{u^{ext},\alpha}$ (middle), exact sensitivity field $S_{u^{ext},\beta}$ (right).

- Case I: $u^{ext}(t,x) = t^{3+\alpha/2}\left((1+x)^{3+\beta/2} - \frac{1}{2}(1+x)^{4+\beta/2}\right)$,
- Case II: $u^{ext}(t,x) = t^{3+\alpha/2}(t-0.4)(t-0.9)\left((1+x)^{3+\beta/2} - \frac{1}{2}(1+x)^{4+\beta/2}\right)$.

where $\alpha/2 = 0.25$, and $\beta/2 = 0.75$. The exact solution and sensitivity fields, obtained by taking $\frac{\partial}{\partial \alpha}$ and $\frac{\partial}{\partial \beta}$ of the exact solutions, are shown in Fig. 6.5 and 6.6 for the two cases I and II, respectively. We employ the developed PG method to solve FPDE (6.68) and obtain u_N, which we use to construct the right hand side of adjoint FSEs. Then, we again employ the developed PG method to solve FSEs (6.69) and (6.70) and obtain the numerical sensitivity fields, $S_{N_{u,\alpha}}$, $S_{N_{u,\beta}}$. We study the L^2-norm convergence of our proposed method by increasing the number of basis functions, as shown in Fig. 6.7.

- **Fractional Model Construction.** The second part of numerical results is dedicated to study the efficiency of developed iterative algorithm in obtaining the set of model parameters q

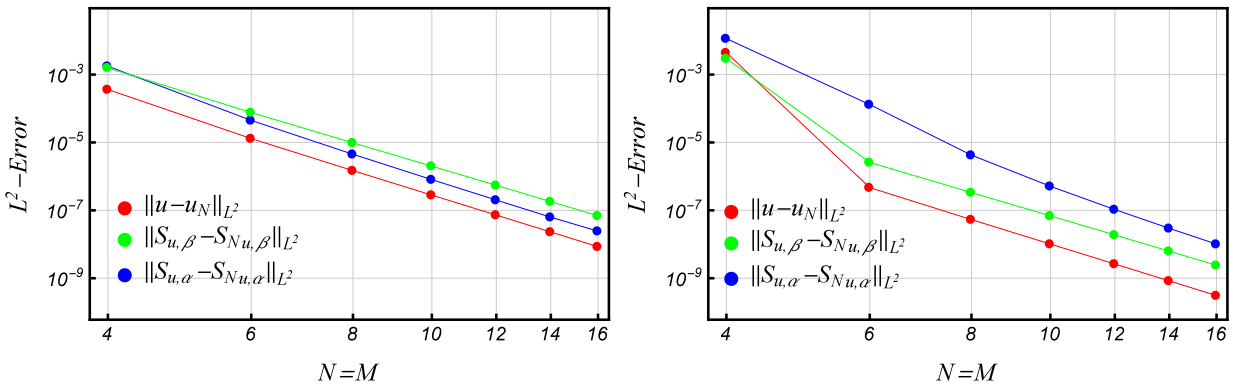

Figure 6.7: PG spectral method, L^2-norm convergence study: (1 + 1)-d FPDE adjoint to corresponding FSEs with one-sided fractional derivative, $k = 1$, $\alpha/2 = 0.25$, and $\beta/2 = 0.75$, for Case I (left) and Case II (right), where $N = M$.

(fractional indices) and thus, construct the fractional model. We test our developed scheme by method of fabricated solution, assuming a given set of input (exact solution) and output (force term) for our fractional model.

We begin with a fractional IVP of the form ${}_0\mathcal{D}_t^{\alpha} u(t) = f(t)$, $\alpha \in (0,1)$, and assume that the exact solution and force function are given as,

$$u^*(t) = sin(5\pi\,\alpha^*/2)\, t^{3+\alpha^*/2},$$
$$f^*(t) = sin(5\pi\,\alpha^*/2)\, \frac{\Gamma(4+\alpha^*/2)}{\Gamma(4-\alpha^*/2)}\, t^{3-\alpha^*/2},$$

and the fractional order α is the unknown model parameter. We start from an initial guess α^0 and use the developed iterative algorithm to converge to the true value of fractional index α. We also consider a fractional BVP of the form ${}_{-1}\mathcal{D}_x^{\beta} u(x) = f(x)$, $\beta \in (1,2)$, and assume that the exact solution and force function are given as,

$$u^*(x) = (1+x)^{3+\beta^*/2} - \frac{1}{2}(1+x)^{4+\beta^*/2}$$
$$f^*(x) = \frac{\Gamma(4+\beta^*/2)}{\Gamma(4-\beta^*/2)}(1+x)^{3+\beta^*/2} - \frac{1}{2}\frac{\Gamma(5+\beta^*/2)}{\Gamma(5-\beta^*/2)}(1+x)^{4+\beta^*/2}$$

and the fractional order β is the unknown model parameter. We again use the developed iterative algorithm to capture the true value of fractional index β, starting from an initial guess β^0.

Table 6.1: Fractional model construction for the two cases of fractional IVP.

Iteration Index	${}_0\mathcal{D}_t^{\alpha} u(t) = f(t)$	
i	α^i	α^i
initial guess	0.300000	0.900000
1	0.971980	0.320520
2	0.900418	0.300068
3	0.900000	0.300000
True Value	0.9	0.3

Table 6.2: Fractional model construction for the two cases of fractional BVP.

Iteration Index	${}_{-1}\mathcal{D}_x^{\beta} u(x) = f(x)$	
i	β^i	β^i
initial guess	1.100000	1.9000000
1	1.882020	1.228040
2	1.708120	1.106096
3	1.700020	1.100016
4	1.700000	1.100000
True Value	1.7	1.1

Tables 6.1 and 6.2 show two examples for each case of fractional IVP and BVP, where the true values of fractional orders are $\alpha^* = 0.3$, $\alpha^* = 0.9$, $\beta^* = 1.1$, and $\beta^* = 1.7$. We observe that the proposed iterative formulation converges accurately to the exact values with in few numbers of iterations. We note that in the case of fractional IVP and BVP, the search region is already small enough so that the nearby solution is valid, and therefore, we only need to perform the second stage of iterative algorithm.

Moreover, we consider FPDE of the form ${}_0\mathcal{D}_t^{\alpha} u - k\, {}_{-1}\mathcal{D}_x^{\beta} u = f$. We assume the exact solution $u^* = t^{1+\alpha^*/2}\left((1+x)^{3+\beta^*/2} - \frac{1}{2}(1+x)^{4+\beta^*/2}\right)$ and plug it into the FPDE with given $\{\alpha^*, \beta^*\}$ to obtain the exact force function f^*. We study the example, in which, $\{\alpha^*, \beta^*\} = \{0.1, 1.64\}$. We perform the two stages of iterative algorithm, where in the first stage, we shrink down the search region 16 time smaller than the original size, by computing the model error at 8 points (See Fig. 6.8, right). Then, in the next stage, we start from the initial guess $\{\alpha^0, \beta^0\} = \{0.125, 1.75\}$, and observe that the developed iterative method converges to a close neighborhood of true values $\{0.1, 1.64\}$ within 10^{-3} tolerance.

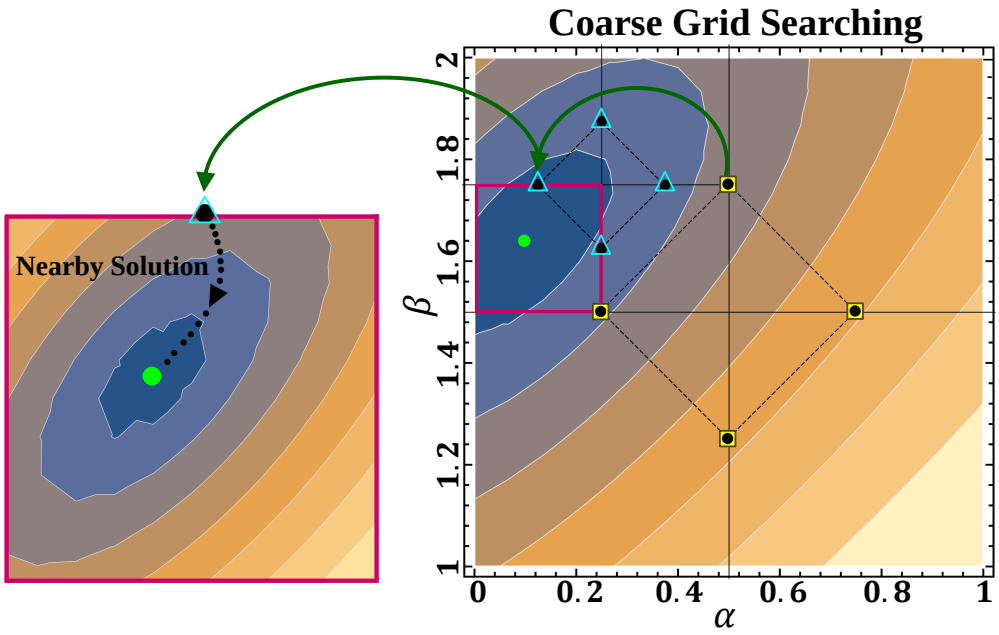

Figure 6.8: Fractional model construction for the case FPDE, using FSEM based iterative algorithm. The true values of fractional indices are $\{\alpha^*, \beta^*\} = \{0.1, 1.64\}$.

The developed model construction method can also be applied in formulating fractional models to study complex time-varying nonlinear fluid-solid interaction phenomena [2, 3, 9] and also the effect of damping in structural vibrations [182].

6.7 Proof of Lemmas and Theorems

6.7.1 Proof of Lemma 6.2.2

Part A: $\sigma \in (0,1)$. We start from the $RL-PL$ definition, given in (6.1).

$$
\begin{aligned}
{}^{RL-LP}_{a}\mathcal{D}^{\sigma}_{x} u &= \frac{1}{\Gamma(1-\sigma)} \frac{d}{dx} \int_a^x (x-s)^{-\sigma} \, \log(x-s)\, u(s)\, ds, \ \text{(integrate by parts)} \qquad (6.71)\\
&= \frac{1}{\Gamma(1-\sigma)} \frac{d}{dx} \Big\{ \frac{u(s)\,(x-s)^{1-\sigma}}{(-\sigma+1)^2} (1-(-\sigma+1)\,\log(x-s)) \Big|_{s=a}^{s=x} \\
&\quad - \int_a^x \frac{(x-s)^{-\sigma+1}}{(-\sigma+1)^2} \,(1-(-\sigma+1)\,\log(x-s))\, u'(s)\, ds \Big\}, \\
&= \frac{1}{\Gamma(1-\sigma)} \frac{d}{dx} \Big\{ \frac{u(a)\,(x-a)^{1-\sigma}}{(-\sigma+1)^2} (1-(-\sigma+1)\,\log(x-a)) \\
&\quad - \int_a^x \frac{(x-s)^{-\sigma+1}}{(-\sigma+1)^2} \,(1-(-\sigma+1)\,\log(x-s))\, u'(s)\, ds \Big\}, \\
&= \frac{u(a)}{\Gamma(1-\sigma)} \frac{\log(x-a)}{(x-a)^{\sigma}} + \frac{1}{\Gamma(1-\sigma)} \int_a^x \frac{\log(x-s)}{(x-s)^{-\sigma}} \, u'(s)\, ds, \ \text{(by Leibnitz rule)} \\
&= \frac{u(a)}{\Gamma(1-\sigma)} \frac{\log(x-a)}{(x-a)^{\sigma}} + {}^{C-LP}_{a}\mathcal{D}^{\sigma}_{x} u
\end{aligned}
$$

Part B: $\sigma \in (1,2)$. Similarly, we start from the $RL-PL$ definition, given in (6.1).

$$
\begin{aligned}
{}^{RL-LP}_{a}\mathcal{D}^{\sigma}_{x} u &= \frac{1}{\Gamma(2-\sigma)} \frac{d^2}{dx^2} \int_a^x (x-s)^{-\sigma+1} \log(x-s)\, u(s)\, ds, \quad \text{(integrate by parts twice)} \\
&= \frac{1}{\Gamma(2-\sigma)} \frac{d^2}{dx^2} \Big\{ \frac{u(s)\,(x-s)^{-\sigma+2}}{(-\sigma+2)^2} (1-(-\sigma+2)\log(x-s)) \Big|_{s=a}^{s=x} \\
&\quad - \frac{u'(s)\,(x-s)^{-\sigma+3}}{(-\sigma+2)^2(-\sigma+3)^2} (1-2(-\sigma+3)+(-\sigma+3)(-\sigma+2)\log(x-s)) \Big|_{s=a}^{s=x} \\
&\quad + \int_a^x \frac{(x-s)^{-\sigma+3}}{(-\sigma+2)^2(-\sigma+3)^2} (1-2(-\sigma+3)+(-\sigma+3)(-\sigma+2)\log(x-s))\, u''(s)\, ds \Big\}, \\
&= \frac{1}{\Gamma(2-\sigma)} \frac{d^2}{dx^2} \Big\{ \frac{u(a)\,(x-a)^{-\sigma+2}}{(-\sigma+2)^2} (1-(-\sigma+2)\log(x-a)) \\
&\quad - \frac{u'(a)\,(x-a)^{-\sigma+3}}{(-\sigma+2)^2(-\sigma+3)^2} (1-2(-\sigma+3)+(-\sigma+3)(-\sigma+2)\log(x-a)) \\
&\quad + \int_a^x \frac{(x-s)^{-\sigma+3}}{(-\sigma+2)^2(-\sigma+3)^2} (1-2(-\sigma+3)+(-\sigma+3)(-\sigma+2)\log(x-s))\, u''(s)\, ds \Big\}, \\
&= \frac{u(a)}{\Gamma(2-\sigma)} \frac{1+(-\sigma+1)\log(x-a)}{(x-a)^{\sigma}} + \frac{u'(a)}{\Gamma(2-\sigma)} \frac{\log(x-a)}{(x-a)^{\sigma-1}} \\
&\quad + \frac{1}{\Gamma(2-\sigma)} \int_a^x (x-s)^{-\sigma+1} \log(x-s)\, u''(s)\, ds, \quad \text{(by Leibnitz rule)} \\
&= \frac{u(a)}{\Gamma(1-\sigma)} \frac{1+(-\sigma+1)\log(x-a)}{(x-a)^{\sigma}} + \frac{u'(a)}{\Gamma(1-\sigma)} \frac{\log(x-a)}{(x-a)^{\sigma-1}} + {}^{C-PL}_{a}\mathcal{D}^{\sigma}_{x} u.
\end{aligned}
\tag{6.72}
$$

6.7.2 Proof of Lemma 7.3.1

In Lemma 2.1 in [100] and also in [53], it is shown that $\|\cdot\|_{l_{H^\sigma(\Lambda)}}$ and $\|\cdot\|_{r_{H^\sigma(\Lambda)}}$ are equivalent. Therefore, for $u \in H^\sigma(\Lambda)$, there exist positive constants C_1 and C_2 such that

$$
\|u\|_{H^\sigma(\Lambda)} \le C_1 \|u\|_{l_{H^\sigma(\Lambda)}}, \quad \|u\|_{H^\sigma(\Lambda)} \le C_2 \|u\|_{r_{H^\sigma(\Lambda)}}, \tag{6.73}
$$

which leads to

$$\begin{aligned}\|u\|^2_{H^\sigma(\Lambda)} &\leq C_1^2\|u\|^2_{l\,H^\sigma(\Lambda)} + C_2^2\|u\|^2_{r\,H^\sigma(\Lambda)},\\ &= C_1^2\,\|\,{}_a\mathcal{D}_x^\sigma\,(u)\|^2_{L^2(\Lambda)} + C_2^2\,\|\,{}_x\mathcal{D}_b^\sigma\,(u)\|^2_{L^2(\Lambda)} + (C_1^2+C_2^2)\,\|u\|^2_{L^2(\Lambda)},\\ &\leq \tilde{C}_1\,\|u\|^2_{c\,H^\sigma(\Lambda)}, \end{aligned} \tag{6.74}$$

where $\tilde{C}_1$ is a positive constant. Similarly, we can show that $\|u\|^2_{c\,H^\sigma(\Lambda)} \leq \tilde{C}_2\,\|u\|_{H^\sigma(\Lambda)}$, where $\tilde{C}_2$ is a positive constant.

6.7.3 Proof of Lemma 7.3.2

$\mathcal{X}_1$ is endowed with the norm $\|\cdot\|_{\mathcal{X}_1}$, where $\|\cdot\|_{\mathcal{X}_1} \equiv \|\cdot\|_{c\,H^{\beta_1/2}(\Lambda_1)}$ by Lemma 7.3.1. Moreover, $\mathcal{X}_2$ is associated with the norm

$$\|\cdot\|_{\mathcal{X}_2} \equiv \left\{\|\cdot\|^2_{c\,H_0^{\beta_2/2}\left((a_2,b_2);L^2(\Lambda_1)\right)} + \|\cdot\|^2_{L^2\left((a_2,b_2);\mathcal{X}_1\right)}\right\}^{\frac{1}{2}}, \tag{6.75}$$

where

$$\begin{aligned}&\|u\|^2_{c\,H_0^{\beta_2/2}\left((a_2,b_2);L^2(\Lambda_1)\right)} \qquad (6.76)\\ &= \int_{a_1}^{b_1}\left(\int_{a_2}^{b_2} |\,{}_{a_2}\mathcal{D}_{x_2}^{\beta_2/2}u|^2\,dx_2 + \int_{a_2}^{b_2} |\,{}_{x_2}\mathcal{D}_{b_2}^{\beta_2/2}u|^2\,dx_2 + \int_{a_2}^{b_2}|u|^2\,dx_2\right)dx_1\\ &= \int_{a_1}^{b_1}\int_{a_2}^{b_2} |\,{}_{a_2}\mathcal{D}_{x_2}^{\beta_2/2}u|^2\,dx_2dx_1 + \int_{a_1}^{b_1}\int_{a_2}^{b_2} |\,{}_{x_2}\mathcal{D}_{b_2}^{\beta_2/2}u|^2\,dx_2dx_1 + \int_{a_1}^{b_1}\int_{a_2}^{b_2}|u|^2\,dx_2dx_1\\ &= \|\,{}_{x_2}\mathcal{D}_{b_2}^{\beta_2/2}\,(u)\|^2_{L^2(\Lambda_d)} + \|\,{}_{a_2}\mathcal{D}_{x_2}^{\beta_2/2}\,(u)\|^2_{L^2(\Lambda_d)} + \|u\|^2_{L^2(\Lambda_d)}, \qquad (6.77)\end{aligned}$$

and

$$\begin{aligned}&\|u\|^2_{L^2\left((a_2,b_2);\mathcal{X}_1\right)}\\ &= \int_{a_2}^{b_2}\left(\int_{a_1}^{b_1} |\,{}_{a_1}\mathcal{D}_{x_1}^{\beta_1/2}u|^2\,dx_1 + \int_{a_1}^{b_1} |\,{}_{x_1}\mathcal{D}_{b_1}^{\beta_1/2}u|^2\,dx_1 + \int_{a_1}^{b_1}|u|^2\,dx_1\right)dx_2\\ &= \int_{a_2}^{b_2}\int_{a_1}^{b_1} |\,{}_{a_1}\mathcal{D}_{x_1}^{\beta_1/2}u|^2dx_1dx_2 + \int_{a_2}^{b_2}\int_{a_1}^{b_1} |\,{}_{x_1}\mathcal{D}_{b_1}^{\beta_1/2}u|^2dx_1dx_2 + \int_{a_2}^{b_2}\int_{a_1}^{b_1}|u|^2dx_1dx_2\\ &= \|\,{}_{x_1}\mathcal{D}_{b_1}^{\beta_1/2}\,u\|^2_{L^2(\Lambda_2)} + \|\,{}_{a_1}\mathcal{D}_{x_1}^{\beta_1/2}\,u\|^2_{L^2(\Lambda_2)} + \|u\|^2_{L^2(\Lambda_2)}. \qquad (6.78)\end{aligned}$$

We use the mathematical induction to carry out the proof. Therefore, we assume the following equality holds

$$\|\cdot\|_{\mathcal{X}_{k-1}} \equiv \left\{ \sum_{i=1}^{k-1} \left(\| {}_{x_i}\mathcal{D}_{b_i}^{\beta_i/2}(\cdot)\|^2_{L^2(\Lambda_{k-1})} + \| {}_{a_i}\mathcal{D}_{x_i}^{\beta_i/2}(\cdot)\|^2_{L^2(\Lambda_{k-1})} \right) + \|\cdot\|^2_{L^2(\Lambda_{k-1})} \right\}^{\frac{1}{2}}. \quad (6.79)$$

Since,

$$\begin{aligned}
&\|u\|^2_{{}_cH_0^{\beta_k/2}\left((a_k,b_k);L^2(\Lambda_{k-1})\right)} \\
&= \int_{\Lambda_{k-1}} \left(\int_{a_k}^{b_k} |\, {}_{a_k}\mathcal{D}_{x_k}^{\beta_k/2}u|^2\, dx_k + \int_{a_k}^{b_k} |\, {}_{x_k}\mathcal{D}_{b_k}^{\beta_k/2}u|^2\, dx_k + \int_{a_k}^{b_k} |u|^2\, dx_k \right) d\Lambda_{k-1} \\
&= \int_{\Lambda_{k-1}} \int_{a_k}^{b_k} |\, {}_{a_k}\mathcal{D}_{x_k}^{\beta_k/2}u|^2\, dx_k d\Lambda_{k-1} + \int_{\Lambda_{k-1}} \int_{a_k}^{b_k} |\, {}_{x_k}\mathcal{D}_{b_k}^{\beta_k/2}u|^2\, dx_k d\Lambda_{k-1} \\
&\quad + \int_{\Lambda_{k-1}} \int_{a_k}^{b_k} |u|^2\, dx_k d\Lambda_{k-1} \\
&= \| {}_{x_k}\mathcal{D}_{b_k}^{\beta_k/2}(u)\|^2_{L^2(\Lambda_k)} + \| {}_{a_k}\mathcal{D}_{x_k}^{\beta_k/2}(u)\|^2_{L^2(\Lambda_k)} + \|u\|^2_{L^2(\Lambda_k)},
\end{aligned}$$

and

$$\begin{aligned}
&\|u\|^2_{L^2\left((a_k,b_k);\mathcal{X}_{k-1}\right)} \\
&= \int_{a_k}^{b_k} \left(\sum_{i=1}^{k-1} \left(\int_{\Lambda_{k-1}} |\, {}_{a_i}\mathcal{D}_{x_i}^{\beta_i/2}u|^2 d\Lambda_{k-1} + \int_{\Lambda_{k-1}} |\, {}_{x_i}\mathcal{D}_{b_i}^{\beta_i/2}u|^2 d\Lambda_{k-1} \right) + \int_{\Lambda_{k-1}} |u|^2 d\Lambda_{k-1} \right) dx_k \\
&= \sum_{i=1}^{k-1} \left(\int_{\Lambda_k} |\, {}_{a_i}\mathcal{D}_{x_i}^{\beta_i/2}u|^2 d\Lambda_k + \int_{\Lambda_k} |\, {}_{x_i}\mathcal{D}_{b_i}^{\beta_i/2}u|^2 d\Lambda_k \right) + \int_{\Lambda_k} |u|^2 d\Lambda_k \\
&= \sum_{i=1}^{k-1} \left(\| {}_{x_i}\mathcal{D}_{b_i}^{\beta_i/2}u\|^2_{L^2(\Lambda_k)} + \| {}_{a_i}\mathcal{D}_{x_i}^{\beta_i/2}u\|^2_{L^2(\Lambda_k)} \right) + \|u\|^2_{L^2(\Lambda_k)},
\end{aligned}$$

we can show that

$$\|\cdot\|_{\mathcal{X}_k} \equiv \left\{ \sum_{i=1}^{k} \left(\| {}_{x_i}\mathcal{D}_{b_i}^{\beta_i/2}(\cdot)\|^2_{L^2(\Lambda_k)} + \| {}_{a_i}\mathcal{D}_{x_i}^{\beta_i/2}(\cdot)\|^2_{L^2(\Lambda_k)} \right) + \|\cdot\|^2_{L^2(\Lambda_k)} \right\}^{\frac{1}{2}}. \quad (6.80)$$

6.7.4 Proof of Lemma 7.3.5

According to [87], we have ${}_{a_i}\mathcal{D}_{x_i}^{\beta_i} u = {}_{a_i}\mathcal{D}_{x_i}^{\beta_i/2}({}_{a_i}\mathcal{D}_{x_i}^{\beta_i/2} u)$ and ${}_{x_i}\mathcal{D}_{b_i}^{\beta_i/2} u = {}_{x_i}\mathcal{D}_{b_i}^{\beta_i/2}({}_{x_i}\mathcal{D}_{b_i}^{\beta_i/2} u)$. Let $\bar{u} = {}_{a_i}\mathcal{D}_{x_i}^{\beta_i/2} u$. Then,

$$
\begin{aligned}
({}_{a_i}\mathcal{D}_{x_i}^{\beta_i} u, v)_{\Lambda_d} &= ({}_{a_i}\mathcal{D}_{x_i}^{\beta_i/2}\bar{u}, v)_{\Lambda_d} = \int_{\Lambda_d} \frac{1}{\Gamma(1-\beta_i/2)}\Big[\frac{d}{dx_i}\int_{a_i}^{x_i} \frac{\bar{u}(s)\,ds}{(x_i-s)_i^{\beta}/2}\Big] v\, d\Lambda_d \\
&= \Big\{\frac{v}{\Gamma(1-\beta_i/2)\int_{a_i}^{x_i}\frac{\bar{u}ds}{(x_i-s)^{\beta_i/2}}}\Big\}_{x_i=a_i}^{b_i} - \int_{\Lambda_d} \frac{1}{\Gamma(1-\beta_i/2)}\int_{a_i}^{x_i} \frac{\bar{u}(s)\,ds}{(x_i-s)^{\beta_i/2}}\frac{dv}{dx_i}\, d\Lambda_d. \qquad (6.81)
\end{aligned}
$$

Based on the homogeneous boundary conditions, $\Big\{\frac{v}{\Gamma(1-\beta_i/2)\int_{a_i}^{x_i}\frac{\bar{u}ds}{(x_i-s)^{\beta_i/2}}}\Big\}_{x_i=a_i}^{b_i} = 0$. Therefore,

$$
({}_{a_i}\mathcal{D}_{x_i}^{\beta_i} u, v)_{\Lambda_d} = -\int_{\Lambda_i} \frac{1}{\Gamma(1-\beta_i/2)}\int_{a_i}^{x_i} \frac{\bar{u}(s)\,ds}{(x_i-s)^{\beta_i/2}}\frac{dv}{dx_i}\, d\Lambda_i. \qquad (6.82)
$$

Moreover, we find that

$$
\begin{aligned}
&\frac{d}{ds}\int_{a_i}^{b_i} \frac{u}{(x_i-s)^{\beta_i/2}} dx_i = \frac{d}{ds}\Big\{\{\frac{v\,(x_i-s)^{1-\beta_i/2}}{1-\beta_i/2}\}_{x_i=s_i}^{b_i} - \frac{1}{1-\beta_i/2}\int_s^{b_i}\frac{dv}{dx_i}(x_i-s)^{1-\beta_i/2} dx_i\Big\} \\
&= -\frac{1}{1-\beta_i/2}\int_s^{b_i}\frac{dv}{dx_i}(x_i-s)^{1-\beta_i/2}\, dx_i = \int_s^{b_i}\frac{\frac{dv}{dx_i}}{(x_i-s)^{\beta_i/2}}\, dx_i. \qquad (6.83)
\end{aligned}
$$

Therefore, we get

$$
({}_{a_i}\mathcal{D}_{x_i}^{\beta_i/2}\bar{u}, v)_{\Lambda_d} = -\int_{\Lambda_d}\frac{1}{\Gamma(1-\nu)_i}\bar{u}(s)\big(-\frac{d}{ds}\int_s^{b_i}\frac{v}{(x_i-s)^{\beta_i/2}}dx_i\big)\, ds = (\bar{u}, {}_{x_i}\mathcal{D}_{b_i}^{\beta_i/2} v)_{\Lambda_d}.
$$

6.7.5 Proof of Lemma 7.3.7

We know that

$$
\Big|\Big({}_0\mathcal{D}_t^{\alpha/2} u, {}_t\mathcal{D}_T^{\alpha/2} v\Big)_\Omega\Big| = \Big(\int_{\Lambda_d}\int_0^T |\,{}_0\mathcal{D}_t^{\alpha/2} u\;{}_t\mathcal{D}_T^{\alpha/2} v|^2\, dt d\Lambda_d\Big)^{\frac{1}{2}}.
$$

Therefore, by Hölder inequality

$$
\begin{aligned}
&\left|\left({}_0\mathcal{D}_t^{\alpha/2}u, {}_t\mathcal{D}_T^{\alpha/2}v\right)_\Omega\right| \\
&\le \Big(\int_{\Lambda_d}\int_0^T |\,{}_0\mathcal{D}_t^{\alpha/2}u|^2\,dtd\Lambda_d\Big)^{\frac{1}{2}}\Big(\int_{\Lambda_d}\int_0^T |\,{}_t\mathcal{D}_T^{\alpha/2}v|^2\,dtd\Lambda_d\Big)^{\frac{1}{2}} \\
&\le \Big(\int_{\Lambda_d}\int_0^T |\,{}_0\mathcal{D}_t^{\alpha/2}u|^2\,dtd\Lambda_d + \int_{\Lambda_d}\int_0^T |u|^2\,dtd\Lambda_d\Big)^{\frac{1}{2}}\times \\
&\quad\Big(\int_{\Lambda_d}\int_0^T |\,{}_t\mathcal{D}_T^{\alpha/2}v|^2\,dtd\Lambda_d + \int_{\Lambda_d}\int_0^T |v|^2\,dtd\Lambda_d\Big)^{\frac{1}{2}} \\
&= \|\,{}_0\mathcal{D}_t^{\alpha/2}u\|_{L^2(\Omega)}\,\|\,{}_t\mathcal{D}_T^{\alpha/2}v\|_{L^2(\Omega)} = \|u\|_{l_{H^{\alpha/2}(I;L^2(\Lambda_d))}}\|v\|_{r_{H^{\alpha/2}(I;L^2(\Lambda_d))}}.
\end{aligned}
$$

Moreover, by equivalence of $|\cdot|_{H^s(I)} \equiv |\cdot|^*_{H^s(I)} = |\cdot|^{1/2}_{l_{H^s(I)}}|\cdot|^{1/2}_{r_{H^s(I)}}$ we have

$$
\begin{aligned}
|({}_0\mathcal{D}_t^{\alpha/2}u, {}_t\mathcal{D}_T^{\alpha/2}v)_I| &= \int_0^T |\,{}_0\mathcal{D}_t^{\alpha/2}u\;{}_t\mathcal{D}_T^{\alpha/2}v|^2\,dt \\
&\ge \int_0^T |\,{}_0\mathcal{D}_t^{\alpha/2}u|^2dt\int_0^T |\,{}_t\mathcal{D}_T^{\alpha/2}v|^2\,dt \qquad (6.84)\\
&\ge \tilde{\beta}_1\|u\|_{l_{H^s(I)}}\|v\|_{r_{H^s(I)}},
\end{aligned}
$$

where $0 < \tilde{\beta}_1 \le 1$. Therefore,

$$
\begin{aligned}
|({}_0\mathcal{D}_t^{\alpha/2}u, {}_t\mathcal{D}_T^{\alpha/2}v)_\Omega|^2 &= \int_{\Lambda_d}\int_0^T |\,{}_0\mathcal{D}_t^{\alpha/2}u\;{}_t\mathcal{D}_T^{\alpha/2}v|^2\,dt\,d\Lambda_d \\
&\ge \int_{\Lambda_d}\Big(\int_0^T |\,{}_0\mathcal{D}_t^{\alpha/2}u|^2dt\int_0^T |\,{}_t\mathcal{D}_T^{\alpha/2}v|^2\,dt\Big)\,d\Lambda_d \\
&\ge \bar{\beta}\int_{\Lambda_d}\int_0^T |\,{}_0\mathcal{D}_t^{\alpha/2}u|^2dtd\Lambda_d\int_{\Lambda_d}\int_0^T |\,{}_t\mathcal{D}_T^{\alpha/2}v|^2\,dt\,\Lambda_d \\
&\ge \bar{\beta}\tilde{\beta}_2\|u\|_{l_{H^s(I)}}\|v\|_{r_{H^s(I)}}, \qquad (6.85)
\end{aligned}
$$

where $0 < \tilde{\beta}_2 \le 1$ and $0 < \bar{\beta}$.

6.7.6 Proof of The Stability Theorem 7.3.9

Part A: $d = 1$. It is evident that u and v are in Hilbert spaces (see [53, 100]). For $0 < \tilde{\beta} \leq 1$, we have

$$
\begin{aligned}
&|a(u,v)| \\
&= |({}_0\mathcal{D}_t^{\alpha/2}(u), {}_t\mathcal{D}_T^{\alpha/2}(v))_\Omega + ({}_{a_1}\mathcal{D}_{x_1}^{\beta_1/2}(u), {}_{x_1}\mathcal{D}_{b_1}^{\beta_1/2}(v))_\Omega \qquad (6.86)\\
&\quad + ({}_{a_1}\mathcal{D}_{x_1}^{\beta_1/2}(u), {}_{x_1}\mathcal{D}_{b_1}^{\beta_1/2}(v))_\Omega + (u,v)_\Omega| \\
&\geq \tilde{\beta}\Big(|({}_0\mathcal{D}_t^{\alpha/2}(u), {}_t\mathcal{D}_T^{\alpha/2}(v))_\Omega| + |({}_{a_1}\mathcal{D}_{x_1}^{\beta_1/2}(u), {}_{x_1}\mathcal{D}_{b_1}^{\beta_1/2}(v))_\Omega| \qquad (6.87)\\
&\quad + |({}_{a_1}\mathcal{D}_{x_1}^{\beta_1/2}(u), {}_{x_1}\mathcal{D}_{b_1}^{\beta_1/2}(v))_\Omega| + |(u,v)_\Omega|\Big),
\end{aligned}
$$

since $\sup_{u\in U}|a(u,v)| > 0$. Next, by equivalence of spaces and their associated norms, (7.43), and (7.44), we obtain

$$
\begin{aligned}
|({}_0\mathcal{D}_t^{\alpha/2}(u), {}_t\mathcal{D}_T^{\alpha/2}(v))_\Omega| &\geq C_1 \| {}_0\mathcal{D}_t^{\alpha/2} u\|_{L^2(\Omega)} \| {}_t\mathcal{D}_T^{\alpha/2} v\|_{L^2(\Omega)},\\
|({}_{a_1}\mathcal{D}_{x_1}^{\beta_1/2}(u), {}_{x_1}\mathcal{D}_{b_1}^{\beta_1/2}(v))_\Omega| &\geq C_2 \| {}_{a_1}\mathcal{D}_{x_1}^{\beta_1/2} u\|_{L^2(\Omega)} \| {}_{x_1}\mathcal{D}_{b_1}^{\beta_1/2} v\|_{L^2(\Omega)},
\end{aligned}
$$

and

$$
|({}_{x_1}\mathcal{D}_{b_1}^{\beta_1/2}(u), {}_{a_1}\mathcal{D}_{x_1}^{\beta_1/2}(v))_\Omega| \geq C_3 \| {}_{x_1}\mathcal{D}_{b_1}^{\beta_1/2} u\|_{L^2(\Omega)} \| {}_{a_1}\mathcal{D}_{x_1}^{\beta_1/2} v\|_{L^2(\Omega)}, \qquad (6.88)
$$

where C_1, C_2, and C_3 are positive constants. Therefore,

$$
\begin{aligned}
|a(u,v)| \geq\ & \tilde{C}\tilde{\beta}\Big\{\| {}_0\mathcal{D}_t^{\alpha/2} u\|_{L^2(\Omega)} \| {}_t\mathcal{D}_T^{\alpha/2} v\|_{L^2(\Omega)} + \| {}_{a_1}\mathcal{D}_{x_1}^{\beta_1/2} u\|_{L^2(\Omega)} \| {}_{x_1}\mathcal{D}_{b_1}^{\beta_1/2} v\|_{L^2(\Omega)} \\
&+ \| {}_{a_1}\mathcal{D}_{x_1}^{\beta_1/2} u\|_{L^2(\Omega)} \| {}_{x_1}\mathcal{D}_{b_1}^{\beta_1/2} v\|_{L^2(\Omega)}\Big\}, \qquad (6.89)
\end{aligned}
$$

where $\tilde{C}$ is $min\{C_1, C_2, C_3\}$. Also, the norm $\|u\|_U \|v\|_V$ is equivalent to the right hand side of inequality (6.89). Therefore, $|a(u,v)| \geq C \|u\|_U \|v\|_V$.

Part B: $d > 1$. Similarly, we have

$$
\begin{aligned}
&|a(u,v)| \geq \qquad (6.90)\\
&\beta\Big(|({}_0\mathcal{D}_t^{\alpha/2}(u), {}_t\mathcal{D}_T^{\alpha/2}(v))_\Omega| + \sum_{i=1}^{d}\Big(|({}_{a_i}\mathcal{D}_{x_i}^{\beta_i/2}(u), {}_{x_i}\mathcal{D}_{b_i}^{\beta_i/2}(v))_\Omega| + |({}_{a_i}\mathcal{D}_{x_i}^{\beta_i/2}(u), {}_{x_i}\mathcal{D}_{b_i}^{\beta_i/2}(v))_\Omega|\Big)\Big),
\end{aligned}
$$

where $0 < \beta \leq 1$. Recalling that as the direct consequences of (7.43), we obtain

$$|({}_{a_i}\mathcal{D}_{x_i}^{\beta_i/2}(u), {}_{x_i}\mathcal{D}_{b_i}^{\beta_i/2}(v))_\Omega| \equiv \|{}_{a_i}\mathcal{D}_{x_i}^{\beta_i/2}(u)\|_{L^2(\Omega)} \|{}_{x_i}\mathcal{D}_{b_i}^{\beta_i/2}(v)\|_{L^2(\Omega)},$$
$$|({}_{x_i}\mathcal{D}_{b_i}^{\beta_i/2}(u), {}_{a_i}\mathcal{D}_{x_i}^{\beta_i/2}(v))_\Omega| \equiv \|{}_{x_i}\mathcal{D}_{b_i}^{\beta_i/2}(u)\|_{L^2(\Omega)} \|{}_{a_i}\mathcal{D}_{x_i}^{\beta_i/2}(v)\|_{L^2(\Omega)}.$$

Thus,

$$\sum_{i=1}^{d}\Big(|({}_{a_i}\mathcal{D}_{x_i}^{\beta_i/2}(u), {}_{x_i}\mathcal{D}_{b_i}^{\beta_i/2}(v))_\Omega| + |({}_{x_i}\mathcal{D}_{b_i}^{\beta_i/2}(u), {}_{a_i}\mathcal{D}_{x_i}^{\beta_i/2}(v))_\Omega|\Big), \tag{6.91}$$
$$\geq \tilde{C}\sum_{i=1}^{d}\Big(\|{}_{a_i}\mathcal{D}_{x_i}^{\beta_i/2}(u)\|_{L^2(\Omega)} \|{}_{x_i}\mathcal{D}_{b_i}^{\beta_i/2}(v)\|_{L^2(\Omega)} + \|{}_{x_i}\mathcal{D}_{b_i}^{\beta_i/2}(u)\|_{L^2(\Omega)} \|{}_{a_i}\mathcal{D}_{x_i}^{\beta_i/2}(v)\|_{L^2(\Omega)}\Big),$$
$$\geq \tilde{C}_1\tilde{\beta}\sum_{i=1}^{d}\Big(\|{}_{a_i}\mathcal{D}_{x_i}^{\beta_i/2}(u)\|_{L^2(\Omega)} + \|{}_{x_i}\mathcal{D}_{b_i}^{\beta_i/2}(u)\|_{L^2(\Omega)}\Big)\times$$
$$\sum_{j=1}^{d}\Big(\|{}_{x_j}\mathcal{D}_{b_j}^{\nu_j}(v)\|_{L^2(\Omega)}, + \|{}_{a_j}\mathcal{D}_{x_j}^{\nu_j}(v)\|_{L^2(\Omega)}\Big),$$

for $u, v \in L^2(I; \mathcal{X}_d)$, where $0 < \tilde{C}$ and $0 < \tilde{\beta} \leq 1$. Furthermore, Lemma 7.3.7 yields

$$|({}_0\mathcal{D}_t^{\alpha/2}(u), {}_t\mathcal{D}_T^{\alpha/2}(v))_\Omega| \equiv \|u\|_{{}_rH^{\alpha/2}(I;L^2(\Lambda_d))} \|v\|_{{}_lH^{\alpha/2}(I;L^2(\Lambda_d))}. \tag{6.92}$$

Therefore, from (6.91) and (6.92) we have

$$|a(u,v)| \geq \beta\Big(\|u\|_{{}_rH^{\alpha/2}(I;L^2(\Lambda_d))} \|v\|_{{}_lH^{\alpha/2}(I;L^2(\Lambda_d))} + \|u\|_{L^2(I;\mathcal{X}_d)} \|v\|_{L^2(I;\mathcal{X}_d)}\Big), \tag{6.93}$$

where

$$\|u\|_{{}_rH^{\alpha/2}(I;L^2(\Lambda_d))} \|v\|_{{}_lH^{\alpha/2}(I;L^2(\Lambda_d))} + \|u\|_{L^2(I;\mathcal{X}_d)} \|v\|_{L^2(I;\mathcal{X}_d)}$$
$$\geq \tilde{C}_2\Big(\|u\|_{{}_rH^{\alpha/2}(I;L^2(\Lambda_d))} + \|u\|_{L^2(I;\mathcal{X}_d)}\Big)\Big(\|v\|_{{}_lH^{\alpha/2}(I;L^2(\Lambda_d))} + \|v\|_{L^2(I;\mathcal{X}_d)}\Big) \tag{6.94}$$

for $u \in U$, $v \in U$ and $0 < \tilde{C}_2 \leq 1$. By considering (6.93) and (6.94), we get

$$|a(u,v)| \geq C\,\|u\|_U\|v\|_V. \tag{6.95}$$

CHAPTER 7

OPERATOR-BASED UNCERTAINTY QUANTIFICATION FOR STOCHASTIC FRACTIONAL PDES

7.1 Background

Significant approximations as inherent part of assumptions upon which the model is built, lack of information about true values of parameters (incomplete data), and random nature of quantities being modeled pervade uncertainty in the corresponding mathematical formulations [41, 142]. In this work, we develop an uncertainty quantification (UQ) framework in the context of stochastic fractional partial differential equations (SFPDEs), in which we characterize different sources of uncertainties and further propagate the associated randomness to the system response quantity of interest (QoI). The intention of this work is not to introduce new mathematical theories or methods for UQ, but rather to bring forward practical solutions using existing theories in an attempt to overcome the computational challenges of UQ in fractional models.

Types and Sources of Uncertainty. The model uncertainties are in general being classified as aleatory and epistemic according to their fundamental essence. It is important to retain the separation between these two sources in order to assess the predictive efficiency of model [45, 125]. Aleatory uncertainty impacts output of interest due to natural variation of inputs and parameters; it is irreducible and commonly treated with probability theory. Epistemic uncertainty, however, results from lack of knowledge about the system of interest and can be reduced by obtaining additional information. The epistemic uncertainties are broadly characterized as *i)* model uncertainties, occurring in model inputs, numerical approximation errors, and model form uncertainty; and *ii)* data uncertainties due to measurement inaccuracy and sparse or imprecise data. The model uncertainty encompasses all model parameters coming from geometry, constitutive laws, and fields equation, while also pertaining surrounding interactions, such as boundary conditions and random forcing sources (noise). Numerical approximations, which are an essence of differential equations since

they generally do not lend themselves to analytical solutions, introduce uncertainty by imposing different sources of discretization error, iterative convergence error, and round off error. In this work, we only consider the epistemic uncertainty in our fractional model and thus, introduce the fractional derivative orders as new set of model parameters in addition to model coefficients. We note that the values of these new parameters are strongly tied to the distribution of underlying stochastic process and their statistics are estimated from experimental observations in practice, see e.g. [18, 26].

Uncertainty Framework. Conventional approaches in parametric UQ of differential equations is based around Monte Carlo sampling (MCS) [54], which performs ensemble of forward calculations to map the uncertain input space to the uncertain output space. This method enjoys from being embarrassingly parallelizable and can be implement quite readily on high dimensional random spaces. However, the key issue is the slow rate of convergence $\sim 1/\sqrt{N}$ with N number of realization, which consequently imposes exhaustively so many operations of forward solver, makes it not practical for expensive simulations. Other methods such as sequential MCS [43] and multilevel sequential MSC [27] are also developed and recently used in [77] to improve the parametric uncertainty assessment in elliptic nonlocal equations. An alternative to expensive MCS is to build surrogate models. An extensive comparison of two widely used ones, namely polynomial chaos and Gaussian process, are provided in a recent work [133]. Polynomial chaos, in which the output of stochastic model is represented as a series expansion of input parameters, was initially applied in [63], and later extended and used in [92, 127, 165, 176, 177]. It is also generalized and used in constructing stochastic Galerkin methods [16, 17, 94, 95] for problems with higher-dimensional random spaces. Other non-sampling numerical methods, including but not limited to perturbation method [13, 149, 163, 174] and moment equation method [108, 109] are also developed, however their applications are restricted to stochastic systems with relatively low-dimensional random space. These so-called "*intrusive*" approaches typically do not treat the forward solver as a black-box, rather require some knowledge and reformulation of the governing equations and thus, may not be practical in many problems with complex codes.

A wide range of "*non-intrusive*" techniques mostly stretch over sampling, quadrature, and regression, see [133] and references therein. More recently, high-order probabilistic collocation methods (PCM), employing the idea of interpolation/collocation in the random spaces, are developed in [14, 129, 175]. These methods limit the sample points to an efficient subset of random space, while adequately sampling the necessary range. The excellence in use of PCM is twofold; it has the benefit of easily sampling at nodal points that naturally leads to independent realizations of the problem as in MCS, and the advantage of fast convergence rate. The challenging post processing of solution statistics, which can essentially be described as a high-dimensional integration problem, can also be resolved by adopting sparse grid generators, such as Smolyak algorithm [129, 151]. The use of sparse grids, as opposed to full tensor product construction from one-dimensional quadrature rules, will effectively reduce the number of sampling, while preserving a fast convergence rate to high level of accuracy.

Forward Solver. A core task in computational forward UQ is to form an efficient numerical method, which for each realizations of random variables can accurately solves and simulates the deterministic counterpart of stochastic model in the physical domain. Such numerical method is usually called "*forward solver*" or "*simulator*". In the case of FPDEs, the excessive cost of numerical approximations due to the inherent nonlocal nature of fractional differential equations additionally become more challenging when generally most of uncertainty propagation techniques instruct operations of forward solver many times. This requires implementation of more efficient numerical schemes, which can manage increasing computational costs while maintaining sufficiently low error level in mitigating the corresponding uncertainties. In addition to numerous finite difference methods for solving FPDEs [33, 65, 103, 159, 167, 172, 192, 196], recent works have elaborated efficient spectral schemes, for discretizing FPDEs in physical domain, see e.g., [28, 39, 83, 84, 99, 100, 103, 136, 170]. More recently, Zayernouri et al. [183, 186] developed two new spectral theories on fractional and tempered fractional Sturm-Liouville problems, and introduced explicit corresponding eigenfunctions, namely *Jacobi poly-fractonomials* of first and second kind. These eignefunctions are comprised of smooth and fractional parts, where the latter can be tunned to

capture singularities of true solution. They are successfully employed in constructing discrete solution/test function spaces and developing a series of high-order and efficient Petrov-Galerkin spectral methods, see [86–88, 106, 143–145, 160].

The main focus of this work is to develop an operator-based computational forward UQ framework in the context of stochastic fractional partial differential equation. Assuming that the mathematical model under consideration is well-posed and accounts in principle for all features of underlying phenomena, we identify three main sources of uncertainty, *i*) parametric uncertainty, including fractional indices as new set of random parameters appeared in the operator, *ii*) additive noises, which incorporates all intrinsic/extrinsic unknown forcing sources as lumped random inputs, and *iii*) numerical approximations. Computational challenges arise when the admissible space of random inputs is infinite-dimensional, e.g. problems subject to additive noise [137], and thus, the framework involves uncertainty parametrization via a finite number of random space basis. Unlike the classical approach in modeling random inputs, which considers idealized uncorrelated processes (white noises), we model the random inputs as more/fully correlated random processes (colored noises), and parametrize them via Karhunen-Loève (KL) expansion by assuming finite-dimensional noise assumption. This yields the problem in finite dimensional random space. We then, propagate the parametric uncertainties into the system response by applying PCM. We obtain the corresponding deterministic FPDE for each realization of random variables, using the Smolyak sparse grid generators for low to moderately high dimensions. In order to formulate the forward solver, we follow [145] and develop a high-order Petrov-Galerkin (PG) spectral method to solve for each realization of SFPDE in the physical domain, employing Jacobi poly-fractonomials in addition to Legendre polynomials as temporal and spatial basis/test functions, respectively. The smart choice of coefficients in construction of spatial basis/test functions yields symmetric properties in the resulting mass/stiffness matrix, which is then exploited to formulate an efficient fast solver. We also show that for each realization of random variables, the deterministic problem is mathematically well-posed and the proposed forward solver is stable. By adopting sufficient number of basis in the physical domain, we eliminate the epistemic uncertainty associated with numerical approximation

and isolate the impact of parametric uncertainty on system response QoI.

The organization of this chapter is as follows. We formulate the stochastic system in section 7.2, and parametrize the random inputs. We also develop the stochastic sampling, namely PCM and MCS for our stochastic problem. We further construct the deterministic solver in section 7.3, and provide the numerical results in section 7.4.

7.2 Forward Uncertainty Framework

7.2.1 Formulation of Stochastic FPDE

Let $\mathbb{D} = [0,T] \times [a_1, b_1] \times [a_2, b_2] \times \cdots \times [a_d, b_d]$ be the physical computational domain for some positive integer d and stochastic function $u(t, \mathbf{x}; \omega) : \mathbb{D} \times \Omega \to \mathbb{R}$, where $\omega \in \Omega$ denotes the random inputs of the system in a properly defined complete probability space $(\Omega, \mathcal{F}, \mathbb{P})$. We consider the following SFPDE, subject to certain homogeneous Dirichlet initial/boundary conditions and stochastic process as additional force function, given as

$$\mathcal{L}^{q(\omega)} u(t, \mathbf{x}; \omega) = F(t, \mathbf{x}; \omega) \tag{7.1}$$

$$u\,\big|_{t=0} = 0, \tag{7.2}$$

$$u\,\big|_{x=a_j} = u\,\big|_{x=b_j} = 0, \tag{7.3}$$

such that for $\mathbb{P}$-almost everywhere $\omega \in \Omega$ the equation holds. The stochastic fractional operator and force term, are given respectively as:

$$\mathcal{L}^{q(\omega)} = {}_0\mathcal{D}_t^{\alpha(\omega)} - \sum_{j=1}^{d} k_j \left[{}_{a_j}\mathcal{D}_{x_j}^{\beta_j(\omega)} + {}_{x_j}\mathcal{D}_{b_j}^{\beta_j(\omega)} \right] \tag{7.4}$$

$$F(t, \mathbf{x}; \omega) = h(t, \mathbf{x}) + f(t; \omega), \tag{7.5}$$

where the fractional indices $\alpha(\omega) \in (0,1)$ and $\beta_j(\omega) \in (1,2)$, $j = 1, 2, \cdots d$ are mutually independent random variables, k_j are real positive constant coefficients, and the fractional derivatives are taken in the Riemann-Liouville sense. We assume that the driving terms h and f are properly posed, such that Eqns. (7.1)-(7.3) is well-posed $\mathbb{P}$-a.e. $\omega \in \Omega$, and also the solution in physical

domain $\mathbb{D}$ is smooth enough such that we can construct a numerical scheme to solve each realization of SFPDE. As an extension to future works, the stochastic operator Eqn. (7.4) can be extended to $\alpha(\omega) \in (1,2)$ for the case of wave equations, and thus applied in formulating fractional models to study complex time-varying nonlinear fluid-solid interaction phenomena [2, 3, 9] and also the effect of damping in structural vibrations [182].

7.2.2 Representation of the Noise: Dimension Reduction

We approximate the additional random forcing term by representing $f(t;\omega)$ into its finite dimensional version and thus, reduce the infinite-dimensional probability space to a finite-dimensional space. This is achieved via truncating Karhunen-Loève (KL) expansion with the desired accuracy[110].

Let $(\Omega, \mathcal{F}, \mathbb{P})$ be a complete probability space, where Ω is the space of events, $\mathcal{F} \subset 2^{\Omega}$ denotes the σ-algebra of sets in Ω, and $\mathbb{P}$ is the probability measure. The random field $f(t;\omega)$ has the ensemble mean $\mathbb{E}\{f(t;\omega)\} = \bar{f}(t)$, finite variance $\mathbb{E}\{[f(t;\omega) - \bar{f}(t)]^2\}$ and covariance $C_f(t_1,t_2) = \mathbb{E}\{[f(t_1;\omega) - \bar{f}(t_1)][f(t_2;\omega) - \bar{f}(t_2)]\}$. The KL expansion of $f(t;\omega)$ takes the form

$$f(t;\omega) = \bar{f}(t) + \sum_{k=1}^{\infty} \sqrt{\lambda_k}\, \psi_k(t)\, Q_k(\omega), \tag{7.6}$$

where $\boldsymbol{Q}(\omega) = \{Q_k(\omega)\}\big|_{k=1}^{k=\infty}$ is a set of mutually uncorrelated random variables with zero mean and unit variance, while $\psi_k(t)$ and λ_k are the eigenfunction and eigenvalues of the covariance kernel $C_f(t_1,t_2)$. We obtain the covariance kernel C_f and its eigenvalues and eigenfunctions, following [156] and by solving a stochastic Helmholtz equation

$$\triangle f(t;\omega) - m^2 f(t;\omega) = g(t;\omega), \tag{7.7}$$

where the random forcing $g(t;\omega)$ is a white-noise process with zero mean and unit variance. The eigenvalues and eigenvectors of Eqn. (7.7) form a Fourier series, so that the KL expansion Eqn. (7.6) is replaced with its sine Fourier series version

$$f(t;\omega) = \bar{f}(t;\omega) + \sum_{k=1}^{\infty} a_k\, \sin\left(\frac{2k\pi\, t}{T}\right) Q_k(\omega), \tag{7.8}$$

in which the random variables $Q_k(\omega)$ are chosen to be *uniformly* distributed with probability density function $\rho_k(q_k)$. T is the length of the process along the t-axis, and the coefficients

$$a_k = \frac{2}{\sqrt{T}\ell^2}\left[1 + \left(\frac{2\pi k}{T\ell}\right)^2\right]^{-1}, \tag{7.9}$$

where $\ell = T/A$ and A is the correlation length of $f(t;\omega)$. To ensure that the random variables $Q_k(\omega)$ have zero mean and unit variance, we define them on $Q_k(\omega) \in [-\sqrt{3}, \sqrt{3}]$. We note that this process is consistent to the zero-Dirichlet initial condition given in Eqn. (7.2). Next, in order to render Eqn. (7.8) computable, we truncate the infinite series with a prescribed ($\approx 90\%$) fraction of the energy of the process, following the finite-dimensional noise assumption in stochastic computations. To this end, we set $T = 1$, the correlation length $A = T/2$, and consider only the first four terms in the KL expansion. Let $f_M(t;\omega) = \frac{1}{\mu}\sum_{k=1}^{M} a_k \sin\left(\frac{2k\pi t}{T}\right) Q_k(\omega)$ denote the normalized truncated expansion, assuming $\bar{f}_M(t;\omega) = 0$, where $\mu = \max_t\left\{\sigma_{f_M}\right\}$ and σ_{f_M} is the standard deviation of $f_M(t;\omega)$. Thus, we represent the random process to be employed in Eqn. (7.1) as

$$f(t;\omega) = \epsilon f_M(t;\omega) \tag{7.10}$$

where ϵ is the amplitude of process.

Therefore, the formulation of SFPDE Eqn. (7.1) can be posed as follows: Find $u(t,\mathbf{x};\omega)$: $\mathbb{D}\times\Omega \to \mathbb{R}$ such that $\forall t, \mathbf{x} \in \mathbb{D}$

$$\begin{aligned} &{}_0\mathcal{D}_t^{\alpha(\omega)} u(t,\mathbf{x};\omega) - \sum_{j=1}^{d} k_j \left[{}_{a_j}\mathcal{D}_{x_j}^{\beta_j(\omega)} + {}_{x_j}\mathcal{D}_{b_j}^{\beta_j(\omega)}\right] u(t,\mathbf{x};\omega) \\ &= h(t,\mathbf{x}) + f(t; Q_1(\omega), Q_2(\omega), \cdots, Q_M(\omega)) \end{aligned} \tag{7.11}$$

holds $\mathbb{P}$-a.s. for $\omega \in \Omega$, subject to the homogeneous initial and boundary conditions.

7.2.3 Input Parametrization

Let $Z : \Omega \rightarrow \mathbb{R}^{\mathcal{N}}$ be the set of $\mathcal{N} = 1 + d + M$ independent random parameters, given as

$$\begin{aligned} Z &= \left\{ Z_i \right\}_{i=1}^{\mathcal{N}} \\ &= \left\{ \alpha(\omega), \beta_1(\omega), \beta_2(\omega), \cdots, \beta_d(\omega), Q_1(\omega), Q_2(\omega), \cdots, Q_M(\omega) \right\} \end{aligned}$$

with probability density functions $\rho_i : \Gamma_i \rightarrow \mathbb{R}$, $i = 1, 2, \cdots, \mathcal{N}$, where their images $\Gamma_i \equiv Z_i(\Omega)$ are bounded intervals in $\mathbb{R}$. The joint probability density function (PDF)

$$\rho(\boldsymbol{\xi}) = \prod_{i=1}^{\mathcal{N}} \rho_i(Z_i), \quad \forall \boldsymbol{\xi} \in \Gamma \tag{7.12}$$

with the support $\Gamma = \prod_{i=1}^{\mathcal{N}} \Gamma_i \subset \mathbb{R}^{\mathcal{N}}$ constitutes a mapping of the sample space Ω onto the target space Γ. Therefore, a random vector $\boldsymbol{\xi} = (\xi_1, \xi_2, \ldots, \xi_{\mathcal{N}}) \in \Gamma$ denote an arbitrary point in the parametric space.

According to the Doob-Dynkin lemma [132], the solution $u(t, \mathbf{x}; \omega)$ can be expressed as $u(t, \mathbf{x}; \boldsymbol{\xi})$, which provides a very useful tool to work in the target space rather than the abstract sample space. Thus, the formulation of SFPDE Eqn. (7.1) can be posed as: Find $u(t, \mathbf{x}; \boldsymbol{\xi}) : \mathbb{D} \times \Gamma \rightarrow \mathbb{R}$ such that $\forall t, \mathbf{x} \in \mathbb{D}$

$$\begin{aligned} &{}_0\mathcal{D}_t^{\alpha(\boldsymbol{\xi})} u(t, \mathbf{x}; \boldsymbol{\xi}) - \sum_{j=1}^{d} k_j \left[{}_{a_j}\mathcal{D}_{x_j}^{\beta_j(\boldsymbol{\xi})} + {}_{x_j}\mathcal{D}_{b_j}^{\beta_j(\boldsymbol{\xi})} \right] u(t, \mathbf{x}; \boldsymbol{\xi}) \\ &= h(t, \mathbf{x}) + f(t; \boldsymbol{\xi}) \end{aligned} \tag{7.13}$$

holds ρ-a.s. for $\boldsymbol{\xi}(\omega) \in \Gamma$ and $\forall t, \mathbf{x} \in \mathbb{D}$, subject to proper initial and boundary conditions.

7.2.4 Stochastic Sampling

We expound the two sampling methods, MCS and PCM to sample from random space and, then propagate the associated uncertainties by computing the statistics of stochastic solutions via post processing.

Monte Carlo Sampling: MCS. The general procedure in statistical Monte Carlo sampling is the three following steps.

1. Generating a set of random variables $\boldsymbol{\xi}_i, i = 1, 2, \cdots, K$ for a prescribed number of realizations K.

2. Solving the deterministic problem Eqn. (7.13) and obtaining the solution $u_i = u(t, \mathbf{x}; \boldsymbol{\xi}_i)$ for each $i = 1, 2, \cdots, K$.

3. Computing the solution statistics, e.g. $\mathbb{E}[u] = \frac{1}{M} \sum_{i=1}^{M} u_i$.

We note that step 1 and 3 are pre- and post- processing steps, respectively. Step 2 requires repetitive simulation of deterministic counterpart of the problem, which we obtain by developing a Petrov-Galerkin spectral method in the physical domain. Although MCS is relatively easy to implement once a deterministic forward solver is developed, it requires too many samplings for the solution statistics to converge, and yet the extra numerical cost due to non-locality and memory effect in fractional operators are still remained. In addition, the number of required sampling also grows rapidly as the dimension of problem increases, resulting in an exhaustively long run time for the statistics to converge.

Probability Collocation Method: PCM. We employ a high-order stochastic discretization in the random space following [56, 175] in order to construct a probabilistic collocation method (PCM), which yields a high convergence rate with much fewer number of sampling. The idea of PCM is based on polynomial interpolation, however in the random space. Let $\Theta_{\mathcal{N}} = \left\{ \xi_i \right\}_{i=1}^{\mathcal{J}}$ be a set of prescribed sampling points. By employing the Lagrange interpolation polynomials L_i, the polynomial approximation $\mathcal{I}$ of the stochastic solution u in the random space can be expressed as:

$$\hat{u}(t, \mathbf{x}; \boldsymbol{\xi}) = \mathcal{I} u(t, \mathbf{x}; \boldsymbol{\xi}) = \sum_{i=1}^{\mathcal{J}} u(t, \mathbf{x}; \xi_i) L_i(\boldsymbol{\xi}). \tag{7.14}$$

Therefore, the collocation procedure of solving Eqn. (7.13) to obtain the stochastic solution u is:

$$R\left(\hat{u}(t, \mathbf{x}; \boldsymbol{\xi})\right)\Big|_{\xi_i} = \left(\mathcal{L}^{q(\boldsymbol{\xi})}\, \hat{u}(t, \mathbf{x}; \boldsymbol{\xi})) - F(t, \mathbf{x}; \boldsymbol{\xi}) \right)\Big|_{\xi_i} = 0, \tag{7.15}$$

for $i = 1, 2, \cdots, \mathcal{J}$, where $\mathcal{L}^q$ is given in Eqn. (7.4). By using the property of Lagrange interpolants that satisfy the Kronecker delta at the interpolation points, we obtain:

$$\mathcal{L}^{q(\xi_i)}\, u(t, \mathbf{x}; \xi_i)) = F(t, \mathbf{x}; \xi_i), \quad i = 1, 2, \cdots, \mathcal{J}, \tag{7.16}$$

subject to proper initial/boundary conditions. Thus, the probabilistic collocation procedure is equivalent to solving $\mathcal{J}$ deterministic problems Eqn. (7.16) with conditions Eqn. (7.2) and Eqn. (7.3). Once the deterministic solutions are obtained at each sampling point, the numerical stochastic solution is interpolated, using Eqn. (7.14) to construct a global approximate $\hat{u}(t, \mathbf{x}; \boldsymbol{\xi})$. We then obtain the solution statistics as

$$\mathbb{E}[\hat{u}] = \int_{\Gamma} \hat{u}(t, \mathbf{x}; \boldsymbol{\xi})\, \rho(\boldsymbol{\xi})\, \mathrm{d}\boldsymbol{\xi}, \;\; \sigma[u] = \sqrt{\mathbb{E}[\hat{u}^2] - \mathbb{E}[\hat{u}]^2}. \tag{7.17}$$

The above integrals can be computed efficiently by letting the interpolation/collocation points to be the same as a set of cubature rules $\Theta_{\mathcal{N}} = \left\{ \xi_i \right\}_{i=1}^{\mathcal{J}}$ on the parametric space with integration weights $\{\mathbf{w}_i\}_{i=1}^{\mathcal{J}}$, which are employed in computing the integral. By property of Kronecker delta of Lagrange interpolant and use of any quadrature rule over the above integral yields

$$\mathbb{E}[\hat{u}(t, \mathbf{x} : \boldsymbol{\xi})] \approx \sum_{i=1}^{\mathcal{J}} w_i\, u(t, \mathbf{x}; \xi_i). \tag{7.18}$$

Choice of Collocation/Interpolation Points. A natural choice of the sampling points is the tensor-product of one-dimensional sets, which is efficients for low-dimensional random spaces. However, in high-dimensional multivariate case, where $\mathcal{N} > 6$, the tensor-product interpolation operators are computationally expensive due to the increasing nested summation loops. In addition, the total number of sampling points grows rapidly by increase of dimension by $\mathcal{J}^{\mathcal{N}}$, where $\mathcal{J}$ is the number of points in each direction.

Another choice that provides an alternative to the more costly full tensor product rule is the isotropic Smolyak sparse grid operator $A(w, \mathcal{N})$ [129, 151] with two input parameters dimension size $\mathcal{N}$ and the level of grid w. The Smolyak algorithm significantly reduces the total number of sampling points; see Fig. 7.1 for comparison of $A(2,2)$, $A(4,2)$, and $A(6,2)$ with full tensor product rule for a two-dimensional random spaces. The total number of sampling points for each case is

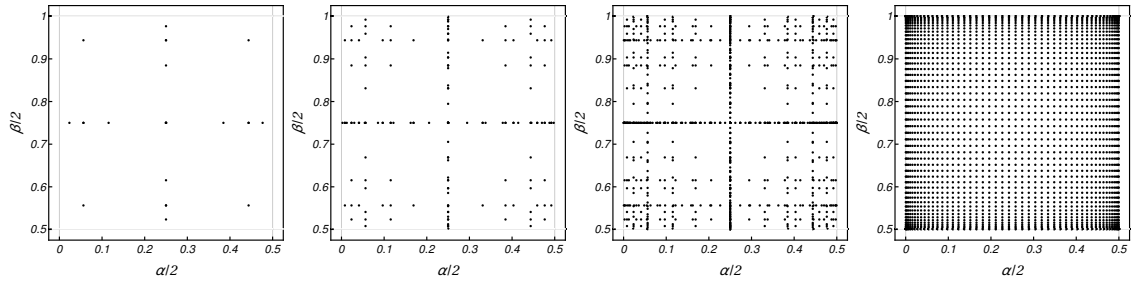

(a) (b) (c) (d)

Figure 7.1: Illustration of sampling nodal points in two-dimensional random space, using Smolyak sparse grid generator (a) $A(2,2)$, (b) $A(4,2)$,(c) $A(6,2)$; and (d) full tensor product rule with 50 points in each direction. The total number of points in each case is, 25, 161, 837, and 2500, respectively.

Space dimensionality	Full tensor product	Smolyak sparse grid generator $A(w,\mathcal{N})$				
$\mathcal{N}$		$w=2$	$w=4$	$w=6$	$w=8$	$w=10$
2	10^2	25	161	837	4105	19469
5	10^5	131	3376	45458	440953	3542465
15	10^{15}	1066	197176	15480304		
25	10^{25}	2901	1445975			
55	10^{55}	87780				

Table 7.1: The total number of nodal points in random space sampling, using Smolyak sparse grid generator and full tensor product with 10 points in each direction.

also listed in Tab.7.1. More research has also been devoted to the analysis and construction of Smolyak sparse grids [24, 130, 131, 175].

7.3 Forward Deterministic Solver

For each realization of random variables in the employed sampling methods, the stochastic model yields a deterministic FPDE, left to be solved in the physical domain. We recall that for every $\boldsymbol{\xi}_i$, $i = 1, 2, \cdots$ in SFPDE Eqn. (7.13), the deterministic problem is recast as:

$$ {}_0\mathcal{D}_t^{\alpha} u(t,\mathbf{x}) - \sum_{j=1}^{d} k_j \left[{}_{a_j}\mathcal{D}_{x_j}^{\beta_j} + {}_{x_j}\mathcal{D}_{b_j}^{\beta_j} \right] u(t,\mathbf{x}) = h(t,\mathbf{x}) + f(t), \tag{7.19} $$

subject to the same initial/boundary conditions as Eqn. (7.2) and Eqn. (7.3). In the sequel, we develop a Petrov-Galerkin spectral method to numerically solve the deterministic problem in the physical domain. We also show the wellposedness of deterministic problem in a weak sense and

further investigate the stability of proposed numerical scheme.

7.3.1 Mathematical Framework

We define the useful functional spaces and their associated norms [87, 99]. By $H^\sigma(\mathbb{R}) = \left\{u(t)|u \in L^2(\mathbb{R});\ (1+|\omega|^2)^{\frac{\sigma}{2}}\mathcal{F}(u)(\omega) \in L^2(\mathbb{R})\right\}$, $\sigma \geq 0$, we denote the fractional Sobolev space on $\mathbb{R}$, endowed with norm $\|u\|_{H^\sigma_{\mathbb{R}}} = \|(1+|\omega|^2)^{\frac{\sigma}{2}}\mathcal{F}(u)(\omega)\|_{L^2(\mathbb{R})}$, where $\mathcal{F}(u)$ represents the Fourier transform of u. Subsequently, we denote by $H^\sigma(\Lambda) = \left\{u \in L^2(\Lambda)\,|\,\exists\,\tilde{u} \in H^\sigma(\mathbb{R})\ s.t.\ \tilde{u}|_\Lambda = u\right\}$, $\sigma \geq 0$, the fractional Sobolev space on any finite closed interval, e.g. $\Lambda = (a,b)$, with norm $\|u\|_{H^\sigma(\Lambda)} = \inf_{\tilde{u}\in H^\sigma_{\mathbb{R}}, \tilde{u}|_\Lambda = u} \|\tilde{u}\|_{H^\sigma(\mathbb{R})}$. We define the following useful norms as:

$$
\begin{aligned}
\|\cdot\|_{{}^lH^\sigma(\Lambda)} &= \left(\|\,{}_a\mathcal{D}_x^\sigma(\cdot)\|^2_{L^2(\Lambda)} + \|\cdot\|^2_{L^2(\Lambda)}\right)^{\frac{1}{2}},\\
\|\cdot\|_{{}^rH^\sigma(\Lambda)} &= \left(\|\,{}_x\mathcal{D}_b^\sigma(\cdot)\|^2_{L^2(\Lambda)} + \|\cdot\|^2_{L^2(\Lambda)}\right)^{\frac{1}{2}},\\
\|\cdot\|_{{}^cH^\sigma(\Lambda)} &= \left(\|\,{}_x\mathcal{D}_b^\sigma(\cdot)\|^2_{L^2(\Lambda)} + \|\,{}_a\mathcal{D}_x^\sigma(\cdot)\|^2_{L^2(\Lambda)} + \|\cdot\|^2_{L^2(\Lambda)}\right)^{\frac{1}{2}},
\end{aligned}
$$

where the equivalence of $\|\cdot\|_{{}^lH^\sigma(\Lambda)}$ and $\|\cdot\|_{{}^rH^\sigma(\Lambda)}$ are shown in [53, 99, 100].

Lemma 7.3.1. *Let $\sigma \geq 0$ and $\sigma \neq n-\frac{1}{2}$. Then, the norms $\|\cdot\|_{{}^lH^\sigma(\Lambda)}$ and $\|\cdot\|_{{}^rH^\sigma(\Lambda)}$ are equivalent to $\|\cdot\|_{{}^cH^\sigma(\Lambda)}$.*

We also define $C_0^\infty(\Lambda)$ as the space of smooth functions with compact support in (a,b). We denote by ${}^lH_0^\sigma(\Lambda)$, ${}^rH_0^\sigma(\Lambda)$, and ${}^cH_0^\sigma(\Lambda)$ as the closure of $C_0^\infty(\Lambda)$ with respect to the norms $\|\cdot\|_{{}^lH^\sigma(\Lambda)}$, $\|\cdot\|_{{}^rH^\sigma(\Lambda)}$, and $\|\cdot\|_{{}^cH^\sigma(\Lambda)}$. It is shown in [53, 100] that these Sobolev spaces are equal and their seminorms are also equivalent to $|\cdot|^*_{H^\sigma(\Lambda)} = \left|\left({}_a\mathcal{D}_x^\sigma(\cdot), {}_x\mathcal{D}_b^\sigma(\cdot)\right)\right|^{\frac{1}{2}}_\Lambda$. Therefore, we can prove that $\left|({}_a\mathcal{D}_x^\sigma u, {}_x\mathcal{D}_b^\sigma v)_\Lambda\right| \geq \beta\,|u|_{{}^lH^\sigma(\Lambda)}\,|v|_{{}^rH^\sigma(\Lambda)}$ and $\left|({}_x\mathcal{D}_b^\sigma u, {}_a\mathcal{D}_x^\sigma v)_\Lambda\right| \geq \beta\,|u|_{{}^rH^\sigma(\Lambda)}\,|v|_{{}^lH^\sigma(\Lambda)}$, in which β is a positive constant.

Moreover, by letting ${}_0C^\infty(I)$ and $C_0^\infty(I)$ be the space of smooth functions with compact support in $(0,T]$ and $[0,T)$, respectively, we define ${}^lH^s(I)$ and ${}^rH^s(I)$ as the closure of ${}_0C^\infty(I)$ and $C_0^\infty(I)$ with respect to the norms $\|\cdot\|_{{}^lH^s(I)}$ and $\|\cdot\|_{{}^rH^s(I)}$. Other equivalent useful semi-norms associated

with $H^s(I)$ are also introduced in [53, 99], as $|\cdot|_{lH^s(I)} = \|{}_0\mathcal{D}_t^s(\cdot)\|_{L^2(I)}$, $|\cdot|_{rH^s(I)} = \|{}_t\mathcal{D}_T^s(\cdot)\|_{L^2(I)}$, $|\cdot|^*_{H^s(I)} = \left|\left({}_0\mathcal{D}_t^s(\cdot), {}_t\mathcal{D}_T^s(\cdot)\right)_I\right|^{\frac{1}{2}}$, where $|\cdot|^*_{H^s(I)} \equiv |\cdot|^{\frac{1}{2}}_{lH^s(I)} |\cdot|^{\frac{1}{2}}_{rH^s(I)}$.

Borrowing definitions from [145], we define the following spaces, which we use later in construction of corresponding solution and test spaces of our problem. Thus, by letting $\Lambda_1 = (a_1, b_1)$, $\Lambda_j = (a_j, b_j) \times \Lambda_{j-1}$ for $j = 2, \cdots, d$, we define $\mathcal{X}_1 = H_0^{\frac{\beta_1}{2}}(\Lambda_1)$, which is associated with the norm $\|\cdot\|_{{}^cH^{\frac{\beta_1}{2}}(\Lambda_1)}$, and accordingly, $\mathcal{X}_j$, $j = 2, \cdots, d$ as

$$\begin{aligned} \mathcal{X}_2 &= H_0^{\frac{\beta_2}{2}}\Big((a_2, b_2); L^2(\Lambda_1)\Big) \cap L^2((a_2, b_2); \mathcal{X}_1), \qquad (7.20)\\ &\vdots \\ \mathcal{X}_d &= H_0^{\frac{\beta_d}{2}}\Big((a_d, b_d); L^2(\Lambda_{d-1})\Big) \cap L^2((a_d, b_d); \mathcal{X}_{d-1}), \qquad (7.21) \end{aligned}$$

associated with norms

$$\|\cdot\|_{\mathcal{X}_j} = \left\{ \|\cdot\|^2_{H_0^{\frac{\beta_j}{2}}\left((a_j,b_j);L^2(\Lambda_{j-1})\right)} + \|\cdot\|^2_{L^2\left((a_j,b_j);\mathcal{X}_{j-1}\right)} \right\}^{\frac{1}{2}},$$

for $j = 2, 3, \cdots, d$.

Lemma 7.3.2. *Let $\beta_j \geq 0$ and $\beta_j \neq n - \frac{1}{2}$. Then, for $j = 1, 2, \cdots, d$*

$$\begin{aligned} &\|\cdot\|_{\mathcal{X}_j} \equiv \\ &\left\{ \sum_{i=1}^{j} \left(\|{}_{x_i}\mathcal{D}_{b_i}^{\beta_i/2}(\cdot)\|^2_{L^2(\Lambda_j)} + \|{}_{a_i}\mathcal{D}_{x_i}^{\beta_i/2}(\cdot)\|^2_{L^2(\Lambda_j)} \right) + \|\cdot\|^2_{L^2(\Lambda_j)} \right\}^{\frac{1}{2}}. \end{aligned}$$

Solution and Test Spaces

We define the "solution space" U and "test space" V, respectively, as

$$\begin{aligned} U &= {}_0^lH^{\frac{\alpha}{2}}\Big(I; L^2(\Lambda_d)\Big) \cap L^2(I; \mathcal{X}_d), \\ V &= {}_0^rH^{\frac{\alpha}{2}}\Big(I; L^2(\Lambda_d)\Big) \cap L^2(I; \mathcal{X}_d), \qquad (7.22) \end{aligned}$$

endowed with norms

$$\|u\|_U = \left\{ \|u\|^2_{{}_l H^{\frac{\alpha}{2}}(I;L^2(\Lambda_d))} + \|u\|^2_{L^2(I;\mathcal{X}_d)} \right\}^{\frac{1}{2}},$$
$$\|v\|_V = \left\{ \|v\|^2_{{}_r H^{\frac{\alpha}{2}}(I;L^2(\Lambda_d))} + \|v\|^2_{L^2(I;\mathcal{X}_d)} \right\}^{\frac{1}{2}}, \tag{7.23}$$

where $I = [0,T]$, and

$${}^l_0H^{\frac{\alpha}{2}}\Big(I;L^2(\Lambda_d)\Big) =$$
$$\Big\{u \,\Big|\, \|u(t,\cdot)\|_{L^2(\Lambda_d)} \in H^{\frac{\alpha}{2}}(I), u|_{t=0} = u|_{x=a_j} = u|_{x=b_j} = 0\Big\},$$
$${}^r_0H^{\frac{\alpha}{2}}\Big(I;L^2(\Lambda_d)\Big) =$$
$$\Big\{v \,\Big|\, \|v(t,\cdot)\|_{L^2(\Lambda_d)} \in H^{\frac{\alpha}{2}}(I), v|_{t=T} = v|_{x=a_j} = v|_{x=b_j} = 0\Big\},$$

equipped with norms $\|u\|_{{}_l H^{\frac{\alpha}{2}}(I;L^2(\Lambda_d))}$ and $\|u\|_{{}_r H^{\frac{\alpha}{2}}(I;L^2(\Lambda_d))}$, respectively. We can show that these norms take the following forms

$$\begin{aligned}
\|u\|_{{}_l H^{\frac{\alpha}{2}}(I;L^2(\Lambda_d))} &= \Big\| \|u(t,\cdot)\|_{L^2(\Lambda_d)} \Big\|_{{}_l H^{\frac{\alpha}{2}}(I)} \\
&= \Big(\| {}_0\mathcal{D}_t^{\frac{\alpha}{2}}(u)\|^2_{L^2(\Omega)} + \|u\|^2_{L^2(\Omega)} \Big)^{\frac{1}{2}}, \\
\|u\|_{{}_r H^{\frac{\alpha}{2}}(I;L^2(\Lambda_d))} &= \Big\| \|u(t,\cdot)\|_{L^2(\Lambda_d)} \Big\|_{{}_r H^{\frac{\alpha}{2}}(I)} \\
&= \Big(\| {}_t\mathcal{D}_T^{\frac{\alpha}{2}}(u)\|^2_{L^2(\Omega)} + \|u\|^2_{L^2(\Omega)} \Big)^{\frac{1}{2}}.
\end{aligned} \tag{7.24}$$

Also, using Lemma 7.3.2, we can show that

$$\begin{aligned}
\|u\|_{L^2(I;\mathcal{X}_d)} &= \Big\| \|u(t,.)\|_{\mathcal{X}_d} \Big\|_{L^2(I)} \\
&= \left\{ \|u\|^2_{L^2(\Omega)} + \sum_{j=1}^{d} \left(\| {}_{x_j}\mathcal{D}_{b_j}^{\frac{\beta_j}{2}}(u)\|^2_{L^2(\Omega)} + \| {}_{a_j}\mathcal{D}_{x_j}^{\frac{\beta_j}{2}}(u)\|^2_{L^2(\Omega)} \right) \right\}^{\frac{1}{2}}.
\end{aligned} \tag{7.25}$$

Therefore, Eqn. (7.23) can be written as

$$\|u\|_U = \Big\{\|u\|^2_{L^2(\Omega)} + \|\,{}_0\mathcal{D}_t^{\frac{\alpha}{2}}(u)\|^2_{L^2(\Omega)} + \sum_{j=1}^{d}\big(\|\,{}_{x_j}\mathcal{D}_{b_j}^{\frac{\beta_j}{2}}(u)\|^2_{L^2(\Omega)} + \|\,{}_{a_j}\mathcal{D}_{x_j}^{\frac{\beta_j}{2}}(u)\|^2_{L^2(\Omega)}\big)\Big\}^{\frac{1}{2}}, \tag{7.26}$$

$$\|v\|_V = \Big\{\|v\|^2_{L^2(\Omega)} + \|\,{}_t\mathcal{D}_T^{\frac{\alpha}{2}}(v)\|^2_{L^2(\Omega)} + \sum_{j=1}^{d}\big(\|\,{}_{x_j}\mathcal{D}_{b_j}^{\frac{\beta_j}{2}}(v)\|^2_{L^2(\Omega)} + \|\,{}_{a_j}\mathcal{D}_{x_j}^{\frac{\beta_j}{2}}(v)\|^2_{L^2(\Omega)}\big)\Big\}^{\frac{1}{2}}. \tag{7.27}$$

7.3.2 Weak Formulation

The following lemmas help us obtain the weak formulation of deterministic problem in the physical domain and construct the numerical scheme.

Lemma 7.3.3. *[99]: For all $\alpha \in (0,1)$, if $u \in H^1([0,T])$ such that $u(0) = 0$, and $v \in H^{\alpha/2}([0,T])$, then $({}_0\mathcal{D}_t^{\alpha}u, v)_\Omega = ({}_0\mathcal{D}_t^{\alpha/2}u\,,\,{}_t\mathcal{D}_T^{\alpha/2}v)_\Omega$, where $(\cdot,\cdot)_\Omega$ represents the standard inner product in $\Omega = [0,T]$.*

Lemma 7.3.4. *[87]: Let $1 < \beta < 2$, a and b be arbitrary finite or infinite real numbers. Assume $u \in H^\beta(a,b)$ such that $u(a) = 0$, also ${}_x\mathcal{D}_b^{\beta/2}v$ is integrable in (a,b) such that $v(b) = 0$. Then, $({}_a\mathcal{D}_x^{\beta}u\,,\,v) = ({}_a\mathcal{D}_x^{\beta/2}u\,,\,{}_x\mathcal{D}_b^{\beta/2}v)$.*

Lemma 7.3.5. *Let $1 < \beta_j < 2$ for $j = 1,2,\cdots,d$, and $u, v \in \mathcal{X}_d$. Then,*

$$\big({}_{a_j}\mathcal{D}_{x_j}^{\beta_j}u, v\big)_{\Lambda_d} = \big({}_{a_j}\mathcal{D}_{x_j}^{\frac{\beta_j}{2}}u, {}_{x_j}\mathcal{D}_{b_j}^{\frac{\beta_j}{2}}v\big)_{\Lambda_d},$$
$$\big({}_{x_j}\mathcal{D}_{b_j}^{\beta_j}u, v\big)_{\Lambda_d} = \big({}_{x_j}\mathcal{D}_{b_j}^{\frac{\beta_j}{2}}u, {}_{a_j}\mathcal{D}_{x_j}^{\frac{\beta_j}{2}}v\big)_{\Lambda_d}.$$

For any realization of Eqn. (7.13), we obtain the weak system, i.e. the variational form of the deterministic counterpart of the problem, subject to the given initial/boundary conditions, by multiplying the equation with proper test functions and integrate over the whole computational

domain $\mathbb{D}$. Using Lemmas 7.3.3-7.3.5, the bilinear form can be written as

$$\begin{aligned} a(u,v) =& ({}_0\mathcal{D}_t^{\frac{\alpha}{2}}\, u, {}_t\mathcal{D}_T^{\frac{\alpha}{2}}\, v)_{\mathbb{D}} \\ &- \sum_{j=1}^{d} k_j \Big[({}_{a_j}\mathcal{D}_{x_j}^{\frac{\beta_j}{2}}\, u, {}_{x_j}\mathcal{D}_{b_j}^{\frac{\beta_j}{2}}\, v)_{\mathbb{D}} + ({}_{x_j}\mathcal{D}_{b_j}^{\frac{\beta_j}{2}}\, u, {}_{a_j}\mathcal{D}_{x_j}^{\frac{\beta_j}{2}}\, v)_{\mathbb{D}} \Big], \end{aligned} \tag{7.28}$$

and thus, by letting U and V be the proper solution/test spaces, the problem reads as: find $u \in U$ such that

$$a(u,v) = (\mathrm{f}, v)_{\mathbb{D}}, \quad \forall v \in V, \tag{7.29}$$

where $\mathrm{f} = h(t,\mathbf{x}) + f(t)$.

7.3.3 Petrov-Galerkin Spectral Method

We define the following finite dimensional solution and test spaces. We employ Legendre polynomials $\phi_{m_j}(\xi)$, $j = 1, 2, \cdots, d$, and Jacobi poly-fractonomial of first kind $\psi_n^{\tau}(\eta)$ [183, 186], as the spatial and temporal bases, respectively, given in their corresponding standard domain as

$$\phi_{m_j}(\xi) = \sigma_{m_j}\big(P_{m_j+1}(\xi) - P_{m_j-1}(\xi)\big), \tag{7.30}$$

$$\psi_n^{\tau}(\eta) = \sigma_n\, {}^{(1)}\mathcal{P}_n^{\tau}(\eta) = \sigma_n (1+\eta)^{\tau} P_{n-1}^{-\tau,\tau}(\eta), \tag{7.31}$$

in which $\xi \in [-1,1]$, $m_j = 1, 2, \cdots$, $\sigma_{m_j} = 2 + (-1)^{m_j}$, $\eta \in [-1,1]$, $n = 1, 2, \cdots$, and $\sigma_n = 2 + (-1)^n$. Therefore, by performing affine mappings $\eta = 2\frac{t}{T} - 1$ and $\xi = 2\frac{x - a_j}{b_j - a_j} - 1$ from the computational domain to the standard domain, we construct the solution space U_N as

$$\begin{aligned} U_N = span \Big\{ & \Big(\psi_n^{\tau} \circ \eta\Big)(t) \prod_{j=1}^{d} \Big(\phi_{m_j} \circ \xi\Big)(x_j) \\ & : n = 1, 2, \cdots, \mathcal{N},\ m_j = 1, 2, \cdots, \mathcal{M}_j \Big\}. \end{aligned} \tag{7.32}$$

We note that the choice of temporal and spatial basis functions naturally satisfy the initial and boundary conditions, respectively. The parameter τ in the temporal basis functions plays a role of fine tunning parameter, which can be chosen properly to capture the singularity of exact solution.

Moreover, we employ Legendre polynomials $\Phi_{r_j}(\xi)$, $j = 1, 2, \cdots, d$, and Jacobi poly-fractonomial of second kind $\Psi_k^{\tau}(\eta)$, as the spatial and temporal test functions, respectively, given in their corresponding standard domain as

$$\Phi_{r_j}(\xi) = \widetilde{\sigma}_{r_j}\big(P_{r_j+1}(\xi) - P_{r_j-1}(\xi)\big), \tag{7.33}$$

$$\Psi_k^{\tau}(\eta) = \widetilde{\sigma}_k\, {}^{(2)}\mathcal{P}_k^{\tau}(\eta) = \widetilde{\sigma}_k(1-\eta)^{\tau}\, P_{k-1}^{\tau,-\tau}(\eta), \tag{7.34}$$

where $\xi \in [-1, 1]$, $r_j = 1, 2, \cdots$, $\widetilde{\sigma}_{r_j} = 2\,(-1)^{r_j} + 1$, $\eta \in [-1, 1]$, $k = 1, 2, \cdots$, and $\widetilde{\sigma}_k = 2\,(-1)^k + 1$. Therefore, by similar affine mapping we construct the test space V_N as

$$V_N = span\Big\{ \Big(\Psi_k^{\tau} \circ \eta\Big)(t) \prod_{j=1}^{d} \Big(\Phi_{r_j} \circ \xi_j\Big)(x_j) \\ : k = 1, 2, \cdots, \mathcal{N},\ r_j = 1, 2, \cdots, \mathcal{M}_j \Big\}. \tag{7.35}$$

Thus, since $U_N \subset U$ and $V_N \subset V$, the problems Eqn. (7.29) read as: find $u_N \in U_N$ such that

$$a_h(u_N, v_N) = l(v_N), \quad \forall v_N \in V_N, \tag{7.36}$$

where $l(v_N) = (\mathrm{f}, v_N)$. The discrete bilinear form $a_h(u_N, v_N)$ can be written as

$$a_h(u_N, v_N) = ({}_0\mathcal{D}_t^{\frac{\alpha}{2}}\, u_N, {}_t\mathcal{D}_T^{\frac{\alpha}{2}}\, v_N)_{\mathbb{D}} \\ - \sum_{j=1}^{d} k_j \Big[({}_{a_j}\mathcal{D}_{x_j}^{\frac{\beta_j}{2}}\, u_N, {}_{x_j}\mathcal{D}_{b_j}^{\frac{\beta_j}{2}}\, v_N)_{\mathbb{D}} + ({}_{x_j}\mathcal{D}_{b_j}^{\frac{\beta_j}{2}}\, u_N, {}_{a_j}\mathcal{D}_{x_j}^{\frac{\beta_j}{2}}\, v_N)_{\mathbb{D}} \Big]. \tag{7.37}$$

We expand the approximate solution $u_N \in U_N$, satisfying the discrete bilinear form Eqn. (7.37), in the following form

$$u_N(t, \mathbf{x}) = \\ \sum_{n=1}^{\mathcal{N}} \sum_{m_1=1}^{\mathcal{M}_1} \cdots \sum_{m_d=1}^{\mathcal{M}_d} \hat{u}_{n,m_1,\cdots,m_d} \Big[\Big(\psi_n^{\tau} \circ \eta\Big)(t) \prod_{j=1}^{d} \Big(\phi_{m_j} \circ \xi\Big)(x_j) \Big], \tag{7.38}$$

and obtain the corresponding Lyapunov system by substituting Eqn. (7.38) into Eqn. (7.37) by choosing

$$v_N(t,\mathbf{x}) = \left(\Psi_k^\tau \circ \eta\right)(t) \prod_{j=1}^{d} \left(\Phi_{r_j} \circ \xi_j\right)(x_j),\ k = 1,2,\ldots,\mathcal{N},\ r_j = 1,2,\ldots,\mathcal{M}_j.$$

Therefore,

$$\begin{aligned} &\Big[S_T \otimes M_1 \otimes M_2 \cdots \otimes M_d \\ &+ \sum_{j=1}^{d} M_T \otimes M_1 \otimes \cdots \otimes M_{j-1} \otimes S_j \otimes M_{j+1} \cdots \otimes M_d\Big]\,\mathcal{U} = F, \end{aligned} \tag{7.39}$$

in which $\otimes$ represents the Kronecker product, F denotes the multi-dimensional load matrix whose entries are given as

$$F_{k,r_1,\cdots,r_d} = \int_{\mathbb{D}} \mathrm{f}(t,\mathbf{x}) \left(\Psi_k^\tau \circ \eta\right)(t) \prod_{j=1}^{d} \left(\Phi_{r_j} \circ \xi_j\right)(x_j)\, d\mathbb{D}, \tag{7.40}$$

and $\mathcal{U}$ is the matrix of unknown coefficients. The matrices S_T and M_T denote the temporal stiffness and mass matrices, respectively; and the matrices S_j and M_j denote the spatial stiffness and mass matrices, respectively. We obtain the entries of spatial mass matrix M_j analytically and employ proper quadrature rules to accurately compute the entries of other matrices S_T, M_T and S_j.

We note that the choices of basis/test functions, employed in developing the PG scheme leads to symmetric mass and stiffness matrices, providing useful properties to further develop a fast solver. The following Theorem 7.3.6 provides a unified fast solver, developed in terms of the generalized eigensolutions in order to obtain a closed-form solution to the Lyapunov system Eqn. (7.39).

Theorem 7.3.6 (Unified Fast FPDE Solver [145])**.** *Let $\{\vec{e}_{m_j}, \lambda_{m_j}\}_{m_j=1}^{\mathcal{M}_j}$ be the set of general eigen-solutions of the spatial stiffness matrix S_j with respect to the mass matrix M_j. Moreover, let $\{\vec{e}_n^{\,\tau}, \lambda_n^\tau\}_{n=1}^{\mathcal{N}}$ be the set of general eigen-solutions of the temporal mass matrix M_T with respect to the stiffness matrix S_T. Then, the matrix of unknown coefficients $\mathcal{U}$ is explicitly obtained as*

$$\mathcal{U} = \sum_{n=1}^{\mathcal{N}} \sum_{m_1=1}^{\mathcal{M}_1} \cdots \sum_{m_d=1}^{\mathcal{M}_d} \kappa_{n,m_1,\cdots,m_d}\ \vec{e}_n^{\,\tau} \otimes \vec{e}_{m_1} \otimes \cdots \otimes \vec{e}_{m_d}, \tag{7.41}$$

where $\kappa_{n,m_1,\cdots,m_d}$ *is given by*

$$\kappa_{n,m_1,\cdots,m_d} = \frac{(\vec{e}_n^{\,\tau}\ \vec{e}_{m_1} \cdots \vec{e}_{m_d})F}{\Big[(\vec{e}_n^{\,\tau^T}\ S_T\ \vec{e}_n^{\,\tau})\ \prod_{j=1}^{d}(\vec{e}_{m_j}^{T}\ M_j\ \vec{e}_{m_j})\Big]\Lambda_{n,m_1,\cdots,m_d}}, \tag{7.42}$$

in which the numerator represents the standard multi-dimensional inner product, and $\Lambda_{n,m_1,\cdots,m_d}$ *is obtained in terms of the eigenvalues of all mass matrices as*

$$\Lambda_{n,m_1,\cdots,m_d} = \Big[1 + \lambda_n^{\tau} \sum_{j=1}^{d}(\lambda_{m_j})\Big].$$

7.3.4 Stability Analysis

We show the well-posedness of deterministic problem and prove the stability of proposed PG scheme.

Lemma 7.3.7. *Let* $\alpha \in (0,1)$, $\Omega = I \times \Lambda_d$, *and* $u \in {}_0^l H^{\alpha/2}(I; L^2(\Lambda_d))$. *Then,*

$$\begin{aligned}
&\Big|\Big({}_0\mathcal{D}_t^{\alpha/2}u, {}_t\mathcal{D}_T^{\alpha/2}v\Big)_\Omega\Big| \\
&\equiv \|u\|_{{}^l H^{\alpha/2}(I;L^2(\Lambda_d))}\,\|v\|_{{}^r H^{\alpha/2}(I;L^2(\Lambda_d))}, \quad \forall v \in {}_0^r H^{\alpha/2}(I; L^2(\Lambda_d)).
\end{aligned}$$

Moreover,

$$\begin{aligned}
&|\big({}_{a_d}\mathcal{D}_{x_d}^{\beta_d/2}u, {}_{x_d}\mathcal{D}_{b_d}^{\beta_d/2}v\big)_{\Lambda_d}| \\
&\equiv |u|_{{}^c H^{\beta_d/2}\left((a_d,b_d);L^2(\Lambda_{d-1})\right)}\ |v|_{{}^c H^{\beta_d/2}\left((a_d,b_d);L^2(\Lambda_{d-1})\right)},
\end{aligned} \tag{7.43}$$

and

$$\begin{aligned}
&|\big({}_{x_d}\mathcal{D}_{b_d}^{\beta_d/2}u, {}_{a_d}\mathcal{D}_{x_d}^{\beta_d/2}v\big)_{\Lambda_d}| \\
&\equiv |u|_{{}^c H^{\beta_d/2}\left((a_d,b_d);L^2(\Lambda_{d-1})\right)}\ |v|_{{}^c H^{\beta_d/2}\left((a_d,b_d);L^2(\Lambda_{d-1})\right)}.
\end{aligned} \tag{7.44}$$

Lemma 7.3.8 (Continuity)**.** *The bilinear form Eqn.* (7.28) *is continuous, i.e.,*

$$\forall u \in U,\ \exists\, \beta > 0, \quad s.t. \quad |a(u,v)| \le \beta\ \|u\|_U\ \|v\|_V, \quad \forall v \in V. \tag{7.45}$$

Proof. The proof directly concludes from Eqn. (7.43) and Lemma 7.3.7. □

Theorem 7.3.9 (Stability)**.** *The following inf-sup condition holds for the bilinear form Eqn.* (7.28)*, i.e.,*

$$\inf_{u\neq 0\in U}\sup_{v\neq 0\in V}\frac{|a(u,v)|}{\|v\|_V\ \|u\|_U}\geq\beta>0, \tag{7.46}$$

where $\Omega = I\times\Lambda_d$ *and* $\sup_{u\in U}|a(u,v)|>0$.

Theorem 7.3.10 (well-posedness)**.** *For all* $0<\alpha<1$, $\alpha\neq 1$, *and* $1<\beta_j<2$, *and* $j=1,\cdots,d$, *there exists a unique solution to Eqn.* (7.29)*, continuously dependent on* f*, where* f *belongs to the dual space of* U.

Proof. Lemmas 7.3.8 (continuity) and 7.3.9 (stability) yield the well-posedness of weak form Eqn. (7.29) in (1+d)-dimension due to the generalized Babuška-Lax-Milgram theorem. □

Since the defined basis and test spaces are Hilbert spaces, and $U_N\subset U$ and $V_N\subset V$, we can prove that the developed Petrov-Gelerkin spectral method is stable and the following condition holds

$$\inf_{u_N\neq 0\in U_N}\sup_{v\neq 0\in V_N}\frac{|a(u_N,v_N)|}{\|v_N\|_V\ \|u_N\|_U}\geq\beta>0, \tag{7.47}$$

with $\beta>0$ and independent of N, where $\sup_{u_N\in U_N}|a(u_N,v_N)|>0$.

7.4 Numerical Results

We investigate the performance of developed numerical methods by considering couple of numerical simulations. We compare MCS and PCM in random space discretization while using PG method in physical domain. We note that by several numerical examples, we make sure that the developed PG method is stable and accurate in solving each deterministic problem; the results are not provided here.

7.4.1 Low-Dimensional Random Inputs

As the first case, we consider a stochastic fractional initial value problem (IVP) with random fractional index by letting the diffusion coefficient to be zero, and also ignoring the additional

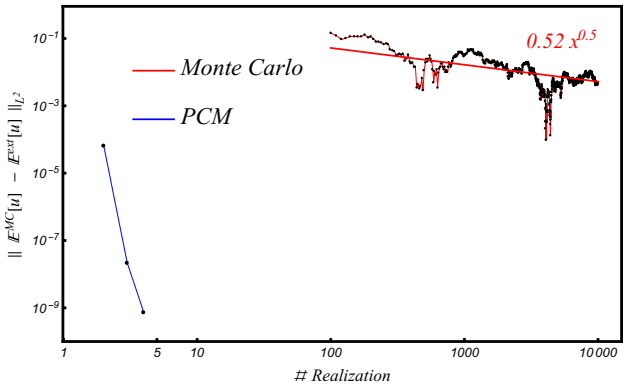

Figure 7.2: L^2-norm convergence rate of MCM and PCM for stochastic fractional IVP Eqn. (7.48).

random input and only taking $h(t)$ as the external forcing term. Therefore, we obtain

$$ {}_0\mathcal{D}_t^{\alpha(\xi)} u(t;\xi) = h(t), \tag{7.48} $$

subject to zero initial condition, where $u(t,\xi) : (0,T] \times \Lambda \rightarrow \mathbb{R}$. We let $u^{ext}(t) = \frac{\alpha}{2}\, t^{3+\frac{\alpha}{2}}$, $h(t) = {}_0\mathcal{D}_t^{\alpha(\xi)} u^{ext}(t)$ for each realization of α. In this case, by choosing the tunning parameter τ in the temporal basis function to be $\frac{\alpha}{2}$, we can efficiently employ PG numerical scheme and also obtain the exact expectation by rendering the exact solution to be random with similar distribution as the random fractional index. Fig. 7.2 shows the L^2-norm convergence rate of MCS and PCM in comparison of solution expectation with $\mathbb{E}^{ext}[u] = \mathbb{E}[u^{ext}]$. The results confirms converges rate of 0.5 for MCS, while in PCM, the statistics of solution converges accurately very fast, using only few numbers of realizations. In this example, by ignoring the additional random input to the system, we take the advantage of having the exact random solution to be available.

As another example, we also consider Eqn. (7.48) with additional random input, expanded by KL expansion with $M = 4$, as:

$$ {}_0\mathcal{D}_t^{\alpha(\xi)} u(t;\boldsymbol{\xi}) = h(t) + \sum_{k=1}^{M} a_k \, \sin\left(\frac{2k\pi\, t}{T}\right) \xi_k, \tag{7.49} $$

with two cases $h(t) = t^2$ and $h(t) = sin(\pi t)$. Fig. 7.3 shows the mean value and variance of solution for 10^4 sampling of MCS compared to 625 realizations in PCM.

Moreover, we consider (1+1)-D one-sided SFPDE given in Eqn. (7.13), where $d = 1$ and the diffusion coefficient is k_l. We ignore the additional random input and consider $h(t,x)$ as the only

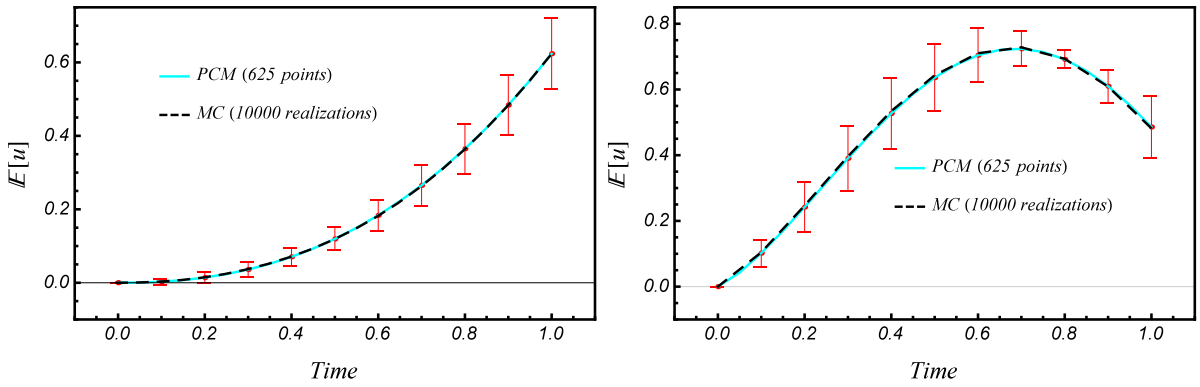

Figure 7.3: Expectation of solution to Eqn. (7.49) with uncertainty (standard deviation) bounds, employing MCS and PCM for (left) $h(t) = t^2$ and (right) $h(t) = sin(\pi t)$.

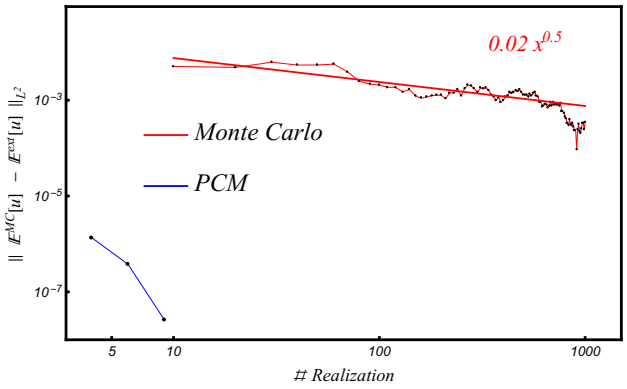

Figure 7.4: L^2-norm convergence rate of MCM and PCM for SFPDE Eqn. (7.50).

external forcing term. Therefore, we obtain

$$ {}_0\mathcal{D}_t^{\alpha(\xi_1)} u(t,x;\boldsymbol{\xi}) - k_l \, {}_{-1}\mathcal{D}_x^{\beta(\xi_2)} u(t,x;\boldsymbol{\xi}) = h(t,x), \tag{7.50} $$

subject to zero initial/boundary conditions, where $u(t,x;\boldsymbol{\xi}) : (0,T]\times(-1,1)\times\Lambda \rightarrow \mathbb{R}$, and the only random variables are the fractional indices α and β. We let $u^{ext}(t,x) = t^{3+\tau}\left((1+x)^{3+\mu} - \frac{1}{2}(1+x)^{4+\mu}\right)$, and choose $\tau = \alpha/2$ and $\mu = \beta/2$. For each realization of α and β, we obtain the force function $h(t,x)$ by substituting the corresponding u^{ext} to Eqn. (7.50). Defining $\mathbb{E}^{ext}[u] = \mathbb{E}[u^{ext}]$, Fig. 7.4 shows the L^2-norm convergence of solution expectation as compared to the exact expectation. We observe that PCM converges accurately with only few number of realizations.

Considering additional random input, expanded by KL expansion with $M = 4$, the problem can

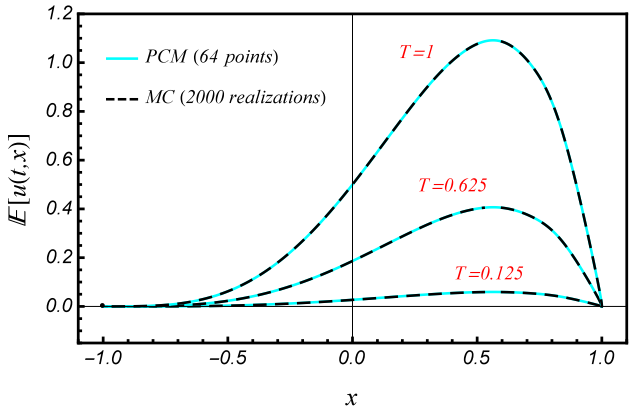

Figure 7.5: Expectation of solution to Eqn. (7.51), employing MCS and PCM at $t = 0.125, 0.625, 1$.

be recast as

$$
\begin{aligned}
{}_0\mathcal{D}_t^{\alpha(\boldsymbol{\xi})} u(t,x;\boldsymbol{\xi}) - k_l \, {}_{-1}\mathcal{D}_x^{\beta(\boldsymbol{\xi})} u(t,x;\boldsymbol{\xi}) \\
= h(t,x) + \sum_{k=1}^{M} a_k \, \sin\left(\frac{2k\pi\, t}{T}\right) \xi_k
\end{aligned}
\tag{7.51}
$$

subject to zero initial/boundary conditions. Fig. 7.5 shows the mean value and variance of solution for MCS and PCM at different times.

Remark 7.4.1. *We note that generally use of the sparse grid operators in obtaining solution statistics is more effective when dimension of the random space is higher than 6. Thus, in the numerical examples for low-dimensional random inputs, we employ the easy-to-implement tensor product nodal sets.*

7.4.2 Moderate- to High-Dimensional Random Inputs

We render the problem with higher number of terms in KL expansion of random inputs in Eqn. (7.51) by choosing $M = 10$ and $M = 20$. This yields the dimension of random space $\mathcal{N} = 12$ and $\mathcal{N} = 22$, respectively. As mentioned in Remark 7.4.1, in the case of high-dimensional random space constructing grid based on tensor product rule results in very expensive computation of solution statistics due to exhaustive increase of forward solver instruction. Table 7.1 shows the comparison between different level of Smolyak algorithm and tensor product rule. Therefore, to obtain the

solution statistics, we employ the Smolyak sparse grid generator in the developed PCM. For each cases of KL expansion, we generate the sparse grid on two levels $w = 1$ and $w = 2$, i.e. $A(1, 12)$, $A(2, 12)$, $A(1, 22)$, and $A(2, 22)$, where we let the higher resolution case be a benchmark value to the solution statistics, based on which we compute and normalize the error. We observe that for both cases $\mathcal{N} = 12$ and $\mathcal{N} = 22$, the normalized error in computing the expectation and standard deviation of solution are of orders $\mathcal{O}(10^{-7})$ and $\mathcal{O}(10^{-3})$, respectively.

CHAPTER 8

NONLINEAR VIBRATION OF FRACTIONAL VISCOELASTIC CANTILEVER BEAM: APPLICATION TO STRUCTURAL HEALTH MONITORING

8.1 Background

We investigate the nonlinear vibration of a viscoelastic cantilever beam with fractional constitutive relation, subject to base excitation. We consider the general form of distributed-order fractional differential equation and use extended Hamilton's principle to derive the governing equations of motion for fractional Kelvin-Voigt viscoelastic model, which is then solved via a spectral decomposition in space. By direct numerical integration of resulting temporal fractional ODE, we observe an anomalous power-law decay rate of amplitude in the linearized model. The nonlinear equation is solved by perturbation analysis, where we replace the expensive numerical time integration with a cubic algebraic equation to solve for frequency response of the system. We report the super sensitivity of response amplitude to the fractional element parameters at free vibration, and bifurcation in steady-state amplitude at primary resonance. We further use the observed vibration-based features of system response for different values of fractional derivative order to develop a parameter estimation framework, which can be used to assess the heath of considered beam by assuming a threshold in the model parameters.

8.2 Mathematical Formulation

We formulate the mathematical model of the considered physical system. We discuss the main assumptions and theorems, used to derive the equation of motion. We employ spectral decomposition to discretize the problem and further use the perturbation method to solve the resulting nonlinear equations.

8.2.1 Nonlinear In-Plane Vibration of a Visco-Elastic Cantilever Beam

We consider the nonlinear response of a slender isotropic visco-elastic cantilever beam with lumped mass M at the tip, subject to harmonic transverse base excitation, V_b. We use the nonlinear Euler-Bernoulli beam theory to obtain the governing equations, where the geometric nonlinearities in a cantilever beam with symmetric cross section is included in the equations of motion. We assume that the beam is idealized as an inextensional one, i.e., stretching of the neutral axis is insignificant, and the effects of warping and shear deformation are ignored. We also assume that the considered slender beam with symmetrical cross section undergoes purely planar flexural vibration. Therefore, we consider the in-plane transverse vibration of the beam and reduce the problem to 1-dimension. Fig. 8.1 shows the lateral deformation of the cantilever beam with cross section area A and mass per unit length m, where the axial displacement along length of beam and the lateral displacement are denoted by $u(s,t)$ and $v(s,t)$, respectively. As the beam deforms, we let the inertial coordinate system (x, y, z) rotates about the z axis by the rotation angle $\psi(s,t)$ to the coordinate system (ξ, η, ζ), where

$$\begin{bmatrix} \mathbf{e}_\xi \\ \mathbf{e}_\eta \\ \mathbf{e}_\zeta \end{bmatrix} = \begin{pmatrix} cos(\psi) & sin(\psi) & 0 \\ -sin(\psi) & cos(\psi) & 0 \\ 0 & 0 & 1 \end{pmatrix} \begin{bmatrix} \mathbf{e}_x \\ \mathbf{e}_y \\ \mathbf{e}_z \end{bmatrix},$$

and $\mathbf{e}_i$ is the unit vector of i coordinate. Thus, angular velocity and curvature of the beam at any point along the length of the beam s and any time t can be written as

$$\boldsymbol{\omega}(s,t) = \dot{\psi} e_z, \quad \boldsymbol{\rho}(s,t) = \psi' e_z, \tag{8.1}$$

where over dot and prime denote the derivative with respect to time and space, respectively.

The total displacement and velocity of an arbitrary point along the y axis takes the form:

$$\mathbf{r} = (u - \eta \ \sin(\psi))\, \mathbf{e}_x + (v + V_b + \eta \ \cos(\psi))\, \mathbf{e}_y, \tag{8.2}$$

$$\dot{\mathbf{r}} = (\dot{u} - \eta\, \dot{\psi} \ \cos(\psi))\, \mathbf{e}_x + (\dot{v} + \dot{V}_b - \eta\, \dot{\psi} \ \sin(\psi))\, \mathbf{e}_y. \tag{8.3}$$

We also let an arbitrary element CD of the beam's neutral axis, which is of length ds and located at a distance s from the origin O, move to the element C^*D^*, see Fig. 8.3. The displacement

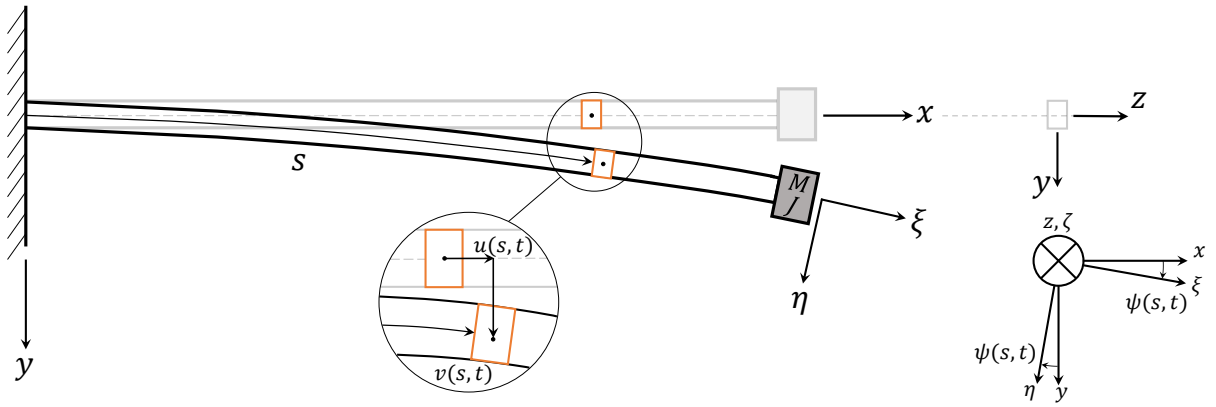

Figure 8.1: In-plane lateral deformation of a slender isotropic cantilever beam. $u(s,t)$ and $v(s,t)$ are the axial and lateral displacements, and $\psi(s,t)$ is the rotation angle about z axis.

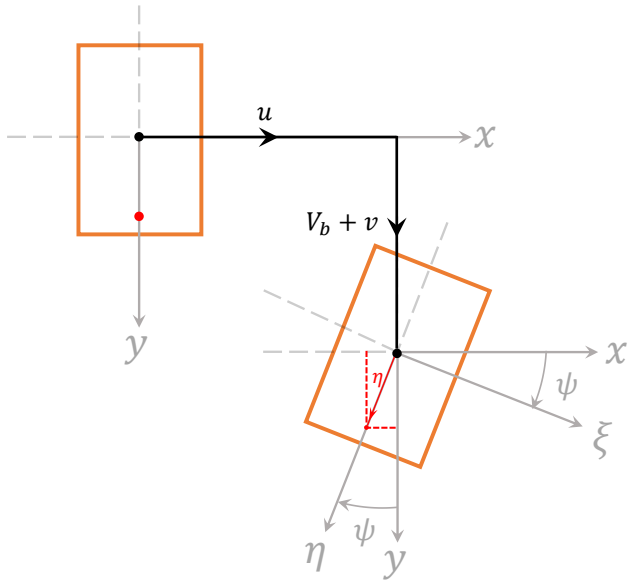

Figure 8.2: Detailed in-plane lateral deformation of a slender isotropic cantilever beam. The figure shows total deformation of an arbitrary point (the red point) as the beam undergoes deformation. This deformation is comprised of the axial displacement of the beam u, the lateral displacement of beam in addition to the base motion $v + V_b$, and the displacement due to rotation ψ.

components of points C and D are denoted by (u, v) and $(u + du, v + dv)$, respectively. The strain $e(s,t)$ at the arbitrary point C is then given by

$$e = \frac{ds^* - ds}{ds} = \frac{\sqrt{(ds + du)^2 + dv^2} - ds}{ds} = \sqrt{(1 + u')^2 + v'^2} - 1. \tag{8.4}$$

The inextensionality constraint, i.e. $e = 0$, becomes

$$1 + u' = (1 - v'^2)^{1/2}. \tag{8.5}$$

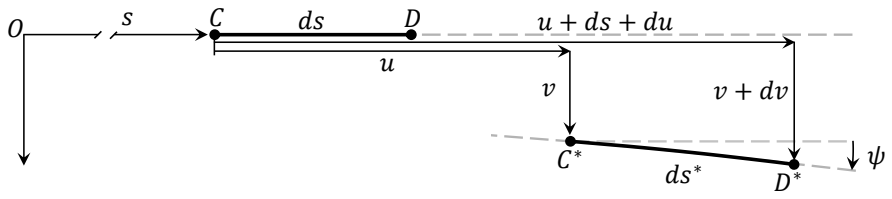

Figure 8.3: Deformation of an arbitrary element of the beam. CD extends, traverses, and rotates to C^*D^*.

Moreover, based on the assumption of no transverse shear deformation and using (8.5), we have

$$\psi = \tan^{-1}\frac{v'}{1+u'} = \tan^{-1}\frac{v'}{(1-v'^2)^{1/2}}. \tag{8.6}$$

Using the expansion $\tan^{-1}(x) = x - \frac{1}{3}x^3 + \cdots$, the curvature can be approximated up to cubic term as

$$\begin{aligned}\psi &= v'(1-v'^2)^{-1/2} - \frac{1}{3}v'^3(1-v'^2)^{-3/2} + \cdots \\ &\simeq v'(1+\frac{1}{2}v'^2) - \frac{1}{3}v'^3 \simeq v' + \frac{1}{6}v'^3\end{aligned} \tag{8.7}$$

Therefore, the angular velocity and curvature of the beam, i.e. $\dot{\psi}$ and ψ', respectively, can be approximated as:

$$\dot{\psi} \simeq \dot{v}' + \frac{1}{2}\dot{v}'v'^2 \simeq \dot{v}'(1+\frac{1}{2}v'^2), \tag{8.8}$$

$$\psi' \simeq v'' + \frac{1}{2}v''v'^2 \simeq v''(1+\frac{1}{2}v'^2). \tag{8.9}$$

By the Euler-Bernoulli beam assumptions a slender, no-transverse-shear with no strains in the plane of cross sectional plane, the strain-curvature relation takes the form

$$\varepsilon(s,t) = -\eta\,\psi'(s,t) \tag{8.10}$$

8.2.2 Viscoelasticity: Boltzmann Superposition Principle

Many experimental observations in the literature show viscoelastic behavior of material in different environmental/boundary conditions, meaning that they do not behave purely elastic and there exists

some internal dissipation mechanism. In such cases, the resulting stress has a memory depending on the velocity of all earlier deformations, which can be described by the Boltzmann superposition principle. When the specimen is under loading, the material instantaneously reacts elastically and then, immediately starts to relax, where dissipation takes place. Thus, as a step increase in elongation (from the stretch $\lambda = 1$ to some λ) is imposed, the developed stress in the material will be a function of time and the stretch:

$$K(\lambda, t) = G(t)\,\sigma^{(e)}(\lambda), \tag{8.11}$$

where $G(t)$ is the reduced relaxation function and $\sigma^{(e)}$ is the elastic response (in absence of any viscosity). $\sigma^{(e)}$ can also be interpreted as tensile stress response in a sufficiently high rate loading experiment. The Boltzmann superposition principle states that the stresses from different small deformations are additive, meaning that the total tensile stress of the specimen at time t is obtained from the superposition of infinitesimal changes in stretch at some prior time τ_j, given as $G(t-\tau_j)\frac{\partial\sigma^{(e)}[\lambda(\tau_j)]}{\partial\lambda}\delta\lambda(\tau_j)$. Therefore,

$$\sigma(t) = \sum_{\tau_j<t} G(t-\tau_j)\frac{\partial\sigma^{(e)}[\lambda(\tau_j)]}{\partial\lambda}\frac{\delta\lambda(\tau_j)}{\delta\tau_j}\delta\tau_j, \tag{8.12}$$

where in the limiting case $\delta\tau_j \to 0$ gives the integral form of the equation as

$$\sigma(t) = \int_{-\infty}^{t} G(t-\tau)\,\frac{\partial\sigma^{(e)}[\lambda(\tau)]}{\partial\lambda}\,\frac{\partial\lambda}{\partial\tau}\,d\tau = \int_{-\infty}^{t} G(t-\tau)\,\dot{\sigma}^{(e)}\,d\tau. \tag{8.13}$$

Exponential Relaxation, Classical Models: The relaxation function $G(t)$ is traditionally analyzed into the summation of exponential functions with different exponents and constants as

$$G(t) = \frac{\sum C_i e^{-t/\tau_i}}{\sum C_i}. \tag{8.14}$$

For the simple case of a single exponential term (Maxwell model), we have $G(t) = e^{-t/\tau}$. Thus, in the case of zero initial strain we have

$$\sigma(t) = \int_0^t e^{-(t-\tilde{t})/\tau}\,E\dot{\varepsilon}\,d\tilde{t}, \tag{8.15}$$

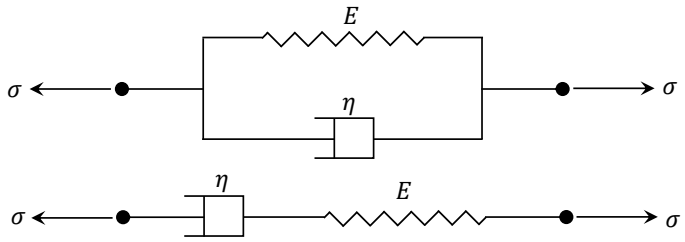

Figure 8.4: Classical visco-elastic models as a combination of spring (purely elastic) and dash-pot (purely viscous) elements. Kelvin-Voigt (top) and Maxwell (bottom) rheological models.

which solves the integer-order differential equation $\dot{\varepsilon} = \frac{1}{E}\dot{\sigma} + \frac{1}{\eta}\sigma$, where the relaxation time constant $\tau = \eta/E$, is obtained from experimental observations. The Maxwell model is in fact a combination of purely elastic and viscous elements in series, see Fig. 8.4. Other different combinations of purely elastic and viscous elements in series and parallel give rise to various rheological models with distinctive properties, each of which can be used to model different types of material. The key issue is that they require complicated combinations of elastic and viscous elements in order to model the complex hereditary behavior of material, yet they cannot fully capture it as the building blocks do not reflect any memory dependence in the material response. Moreover, they introduce a relatively large number of model parameters, which adverse the condition of ill-posed inverse problem of model fitting.

Power-Law Relaxation, Fractional Models: The mechanical stress appeared at the deformation of viscoelastic materials decreases as power-law functions in time, suggesting that relaxation of stress obeys a power law behavior and the relaxation time can not be described with single time scale anymore [116]. Therefore, by letting the kernel in (8.13) have a power-law form, the tensile stress takes the form of

$$\sigma(t) = \int_{-\infty}^{t} \frac{g(\alpha)}{(t-\tau)^{\alpha}} E\dot{\varepsilon}\, d\tau = E\, g(\alpha) \int_{-\infty}^{t} \frac{\dot{\varepsilon}}{(t-\tau)^{\alpha}}\, d\tau, \tag{8.16}$$

where the elastic response $\sigma^{(e)} = E\varepsilon$. If we choose $g(\alpha) = \frac{1}{\Gamma(1-\alpha)}$, then the integro-differential operator (8.16) gives the Liouville-Weyl fractional derivative. Under the hypothesis of causal histories, stating that the viscoelastic body is quiescent for all time prior to some starting point

$t = 0$, the equation (8.16) can be written as

$$\begin{aligned}\sigma(t) &= \varepsilon(0^+)\,\frac{E\,g(\alpha)}{t^\alpha} + E\,g(\alpha)\int_0^t \frac{\dot{\varepsilon}}{(t-\tau)^\alpha}\,d\tau, \\ &= \varepsilon(0^+)\,\frac{E\,g(\alpha)}{t^\alpha} + E\;{}_0^C\mathcal{D}_t^\alpha\,\varepsilon, \\ &= {}_0^{RL}\mathcal{D}_t^\alpha\,\varepsilon,\end{aligned} \tag{8.17}$$

where ${}_0^C\mathcal{D}_t^\alpha$ and ${}_0^{RL}\mathcal{D}_t^\alpha$ are the Caputo and Riemann-Liouville fractional derivatives. The constitutive equation (8.17) introduces the Scott Blair element [115, 116, 138, 160], which can be though of as an interpolation between a pure elastic (spring) and a pure viscous (dash pot) elements.

In a more general sense, where the material contain a spectrum of power-law relaxation, the single order fractional constitutive model can be extended to the distributed-order one. Thus, we let the relaxation function $G(t)$ in (8.13) not be only a single order power-law as in (8.16), but rather be distributed over a range. This leads to a distributed form of constitutive equations expressed as

$$\int_{\beta_{min}}^{\beta_{max}} \Phi(\beta)\;{}_0\mathcal{D}_t^\beta\sigma(t)\,d\beta = \int_{\alpha_{min}}^{\alpha_{max}} \Psi(\alpha)\;{}_0\mathcal{D}_t^\alpha\varepsilon(t)\,d\alpha, \tag{8.18}$$

where $\Phi(\beta)$ and $\Psi(\alpha)$ are distribution functions that can confine the theoretical terminals β_{min}, β_{max}, α_{min}, and α_{max} according to the physical realization of problem. By choosing different distribution functions $\Phi(\beta)$ and $\Psi(\alpha)$, one can design distinctive rheological models to get different types of behavior. We note that if we let the distribution functions be delta functions, the distributed order model becomes the following multi-term model:

$$\left(1 + \sum_{k=1}^{p\sigma} a_k\;{}_0\mathcal{D}_t^{\beta_k}\right)\sigma(t) = \left(c + \sum_{k=1}^{p\varepsilon} b_k\;{}_0\mathcal{D}_t^{\alpha_k}\right)\varepsilon(t). \tag{8.19}$$

Here, we let $\Phi(\beta) = \delta(\beta)$ and $\Psi(\alpha) = E_\infty\delta(\alpha) + E_\alpha\delta(\alpha - \alpha_0)$, and thus, recover the fractional Kelvin-Voigt model as

$$\sigma(t) = E_\infty\,\varepsilon(t) + E_\alpha\;{}_0^{RL}\mathcal{D}_t^\alpha\,\varepsilon(t), \tag{8.20}$$

where $\alpha \in (0, 1)$. Since we only have one single derivative order α, we drop the subscript zero for the sake of simplification.

8.2.3 Extended Hamilton's Principle

We derive the equations of motion by employing the extended Hamilton's principle

$$\int_{t_1}^{t_2} (\delta T - \delta W)\, dt = 0,$$

where δT and δW are the variations of kinetic energy and total work [119]. The only source of external input to the our system of interest is the base excitation, which superposes base velocity to the beam velocity, and thus contributes to the kinetic energy. Hence, the total work only includes the internal work done by the induced stresses and its variation can be expressed in the general form as [32]

$$\delta W = \int_{\mathbb{V}} \sigma\, \delta\varepsilon\, dv, \tag{8.21}$$

where the integral is taken over the whole system volume $\mathbb{V}$. The volumetric stress σ includes both the conservative part, σ_c, due to elastic and the non-conservative part, σ_{nc}, due to viscous deformation, where the former constitutes the potential energy of the system. There has been some attempts in the literature to separate the conservative and non-conservative parts of fractional constitutive equations to define the free energy of the system [105]. We note that as this separation is not trivial for sophisticated fractional constitutive equations, and as we do not deal with free energy of our system, we would rather leave the total work not separated and thus do not compute the potential energy and work done by non-conservative forces separately. In the considered cantilever beam with symmetric constant cross sections, we recast the integral (8.21) as $\delta W = \int_0^L \int_A \sigma\, \delta\varepsilon\, dA\ ds$. We obtain the variation of strain as $\delta\varepsilon = -\eta\, \delta\psi'$, using (8.10). Therefore, by assuming the constitutive equation (8.20), the variation of total work is expressed as

$$\begin{aligned}
\delta w &= \int_0^L \int_A \left(-\eta\, E_\infty\, \psi' - \eta\, E_\alpha\ {}^{RL}_{0}\mathcal{D}^{\alpha}_{t}\, \psi'\right) (-\eta\, \delta\psi')\, dA\ ds \\
&= \int_0^L \left(E_\infty \left(\int_A \eta^2 dA\right) \psi' + E_\alpha \left(\int_A \eta^2 dA\right) {}^{RL}_{0}\mathcal{D}^{\alpha}_{t}\, \psi'\right) \delta\psi'\ ds \\
&= \int_0^L \left(E_\infty\, I\, \psi' + E_\alpha\, I\ {}^{RL}_{0}\mathcal{D}^{\alpha}_{t}\, \psi'\right) \delta\psi'\ ds
\end{aligned} \tag{8.22}$$

where $I = \int_A \eta^2 \, dA$. By approximation (8.9), we write the variation of curvature as

$$\delta\psi' = (1 + \frac{1}{2}v'^2)\,\delta v'' + v''\,v'\,\delta v'. \tag{8.23}$$

Therefore, the variation of total energy becomes

$$\begin{aligned}\delta w = &\int_0^L \left(E_\infty I\, v''(1 + \frac{1}{2}v'^2) + E_\alpha I\ {}^{RL}_{0}\mathcal{D}_t^\alpha\, v''(1 + \frac{1}{2}v'^2)\right)(1 + \frac{1}{2}v'^2)\,\delta v''\ ds \\ &+ \int_0^L \left(E_\infty I\, v''(1 + \frac{1}{2}v'^2) + E_\alpha I\ {}^{RL}_{0}\mathcal{D}_t^\alpha\, v''(1 + \frac{1}{2}v'^2)\right) v''\,v'\,\delta v'\ ds\end{aligned} \tag{8.24}$$

By expanding the terms and integrating by parts, we have

$$\begin{aligned}\delta w = &\int_0^L \left(\left(E_\infty I\, v''(1 + \frac{1}{2}v'^2) + E_\alpha I\ {}^{RL}_{0}\mathcal{D}_t^\alpha\, v''(1 + \frac{1}{2}v'^2)\right)(1 + \frac{1}{2}v'^2)\right)''\ \delta v\ ds \\ &- \int_0^L \left(\left(E_\infty I\, v''(1 + \frac{1}{2}v'^2) + E_\alpha I\ {}^{RL}_{0}\mathcal{D}_t^\alpha\, v''(1 + \frac{1}{2}v'^2)\right) v''\,v'\right)'\ \delta v\ ds \\ &+ \left(E_\infty I\, v''(1 + \frac{1}{2}v'^2) + E_\alpha I\ {}^{RL}_{0}\mathcal{D}_t^\alpha\, v''(1 + \frac{1}{2}v'^2)\right)(1 + \frac{1}{2}v'^2)\,\delta v'\Big|_0^L \\ &- \left(\left(E_\infty I\, v''(1 + \frac{1}{2}v'^2) + E_\alpha I\ {}^{RL}_{0}\mathcal{D}_t^\alpha\, v''(1 + \frac{1}{2}v'^2)\right)(1 + \frac{1}{2}v'^2)\right)'\ \delta v\Big|_0^L \\ &+ \left(E_\infty I\, v''(1 + \frac{1}{2}v'^2) + E_\alpha I\ {}^{RL}_{0}\mathcal{D}_t^\alpha\, v''(1 + \frac{1}{2}v'^2)\right) v''\,v'\,\delta v\Big|_0^L\end{aligned} \tag{8.25}$$

The prescribed geometry boundary conditions at the base of the beam, $s = 0$, allow the variation of deflection and its first derivative to be zero at $s = 0$, i.e. $\delta v(0,t) = \delta v'(0,t) = 0$. Therefore,

$$\begin{aligned}\delta w = &\int_0^L \left(\left(E_\infty I\, v''(1 + \frac{1}{2}v'^2) + E_\alpha I\ {}^{RL}_{0}\mathcal{D}_t^\alpha\, v''(1 + \frac{1}{2}v'^2)\right)(1 + \frac{1}{2}v'^2)\right)''\ \delta v\ ds \\ &- \int_0^L \left(\left(E_\infty I\, v''(1 + \frac{1}{2}v'^2) + E_\alpha I\ {}^{RL}_{0}\mathcal{D}_t^\alpha\, v''(1 + \frac{1}{2}v'^2)\right) v''\,v'\right)'\ \delta v\ ds \\ &+ \left(E_\infty I\, v''(1 + \frac{1}{2}v'^2) + E_\alpha I\ {}^{RL}_{0}\mathcal{D}_t^\alpha\, v''(1 + \frac{1}{2}v'^2)\right)(1 + \frac{1}{2}v'^2)\Big|_{s=L}\ \delta v'(L,t) \\ &- \left(\left(E_\infty I\, v''(1 + \frac{1}{2}v'^2) + E_\alpha I\ {}^{RL}_{0}\mathcal{D}_t^\alpha\, v''(1 + \frac{1}{2}v'^2)\right)(1 + \frac{1}{2}v'^2)\right)'\Big|_{s=L}\ \delta v(L,t) \\ &+ \left(E_\infty I\, v''(1 + \frac{1}{2}v'^2) + E_\alpha I\ {}^{RL}_{0}\mathcal{D}_t^\alpha\, v''(1 + \frac{1}{2}v'^2)\right) v''\,v'\Big|_{s=L}\ \delta v(L,t)\end{aligned} \tag{8.26}$$

Let ϱ be mass per unit volume of the beam, M and J be the mass and rotatory inertia of the lumped mass at the tip of beam. By considering the displacement and velocity of the beam given in (8.2) and (8.3), respectively, the kinetic energy is obtained as

$$
\begin{aligned}
T &= \frac{1}{2}\int_0^L \int_A \varrho\, \dot{\mathbf{r}}^2\, dA\, ds + \frac{1}{2}M\left(\dot{u}^2 + (\dot{v}+\dot{V}_b)^2\right)\Big|_{s=L} + \frac{1}{2}J\dot{\psi}^2\Big|_{s=L}, \qquad (8.27)\\
&= \frac{1}{2}\int_0^L \int_A \varrho\left\{(\dot{u}-\eta\,\dot{\psi}\,\cos(\psi))^2 + (\dot{v}+\dot{V}_b-\eta\,\dot{\psi}\,\sin(\psi))^2\right\} dA\, ds\\
&\quad + \frac{1}{2}M\left(\dot{u}^2 + (\dot{v}+\dot{V}_b)^2\right)\Big|_{s=L} + \frac{1}{2}J\dot{\psi}^2\Big|_{s=L},\\
&= \frac{1}{2}\int_0^L \int_A \varrho\left\{\dot{u}^2 - 2\eta\,\dot{u}\,\dot{\psi}\,\cos(\psi) + \eta^2\,\dot{\psi}^2\,\cos^2(\psi) + \dot{v}^2 + \dot{V}_b^2 + 2\dot{v}\,\dot{V}_b\right.\\
&\quad \left. - 2\eta\,(\dot{v}^2+\dot{V}_b)\dot{\psi}\,\sin(\psi) + \eta^2\dot{\psi}^2\,\sin^2(\psi)\right\} dA\, ds\\
&\quad + \frac{1}{2}M\left(\dot{u}^2 + (\dot{v}+\dot{V}_b)^2\right)\Big|_{s=L} + \frac{1}{2}J\dot{\psi}^2\Big|_{s=L},\\
&= \frac{1}{2}\int_0^L \int_A \varrho\left\{\dot{u}^2 + \dot{v}^2 + \dot{V}_b^2 + 2\dot{v}\,\dot{V}_b - 2\eta\,\dot{u}\,\dot{\psi}\,\cos(\psi) + \eta^2\,\dot{\psi}^2\right.\\
&\quad \left. - 2\eta\,(\dot{v}^2+\dot{V}_b)\dot{\psi}\,\sin(\psi)\right\} dA\, ds + \frac{1}{2}M\left(\dot{u}^2 + (\dot{v}+\dot{V}_b)^2\right)\Big|_{s=L} + \frac{1}{2}J\dot{\psi}^2\Big|_{s=L}.
\end{aligned}
$$

Let

$$
\rho = \int_A \varrho\, dA, \quad \mathcal{J}_1 = \int_A \varrho\,\eta\, dA, \quad \mathcal{J}_2 = \int_A \varrho\,\eta^2 dA.
$$

ρ is the mass per unit length of the beam, $\mathcal{J}_1$ is the first moment of inertia and is zero because the reference point of coordinate system attached to the cross section coincides with the mass centroid, and $\mathcal{J}_2$ is the second moment of inertia, which is very small for slender beam and can be ignored [66]. Assuming that the velocity along the length of the beam, $\dot{u}$, is relatively small compared to the lateral velocity $\dot{v}+\dot{V}_b$, the kinetic energy of the beam can be reduced to

$$
T = \frac{1}{2}\rho\int_0^L (\dot{v}+\dot{V}_b)^2\, ds + \frac{1}{2}M(\dot{v}+\dot{V}_b)^2\Big|_{s=L} + \frac{1}{2}J\dot{\psi}^2\Big|_{s=L}, \qquad (8.28)
$$

where its variation can be taken as

$$
\delta T = \rho\int_0^L (\dot{v}+\dot{V}_b)\,\delta\dot{v}\, ds + M(\dot{v}+\dot{V}_b)\,\delta\dot{v}\Big|_{s=L} + J\dot{\psi}\,\delta\dot{\psi}\Big|_{s=L}, \qquad (8.29)
$$

in which $\dot{\psi}$ is given in (8.8) and $\delta\dot{\psi}$ can be obtained as $\delta\dot{\psi} \simeq (1 + \frac{1}{2}v'^2)\delta\dot{v}' + v'\dot{v}'\delta v'$. Therefore,

$$\delta T = \rho \int_0^L (\dot{v} + \dot{V}_b)\,\delta\dot{v}\,ds + M(\dot{v} + \dot{V}_b)\,\delta\dot{v}\Big|_{s=L} + J\left(\dot{v}'(1 + v'^2)\delta\dot{v}' + v'\dot{v}'^2\delta v'\right)\Big|_{s=L}. \tag{8.30}$$

The time integration of δT takes the following form through integration by parts

$$\begin{aligned}
&\int_{t_1}^{t_2} \delta T\,dt \qquad (8.31)\\
=&\int_{t_1}^{t_2} \left\{ \rho \int_0^L (\dot{v} + \dot{V}_b)\,\delta\dot{v}\,ds + M(\dot{v} + \dot{V}_b)\,\delta\dot{v}\Big|_{s=L} \right.\\
&\left. + J\left(\dot{v}'(1 + v'^2)\delta\dot{v}' + v'\dot{v}'^2\delta v'\right)\Big|_{s=L} \right\} dt\\
=&\int_{t_1}^{t_2} \rho \int_0^L (\dot{v} + \dot{V}_b)\,\delta\dot{v}\,ds\,dt + M\int_{t_1}^{t_2} (\dot{v} + \dot{V}_b)\,\delta\dot{v}\Big|_{s=L} dt\\
&+ J\int_{t_1}^{t_2} \left(\dot{v}'(1 + v'^2)\delta\dot{v}' + v'\dot{v}'^2\delta v'\right)\Big|_{s=L} dt\\
=&\rho \int_0^L \int_{t_1}^{t_2} (\dot{v} + \dot{V}_b)\,\delta\dot{v}\,dt\,ds + M\int_{t_1}^{t_2} (\dot{v} + \dot{V}_b)\,\delta\dot{v}\,dt\,\Big|_{s=L}\\
&+ J\int_{t_1}^{t_2} \left(\dot{v}'(1 + v'^2)\delta\dot{v}' + v'\dot{v}'^2\delta v'\right)\,dt\,\Big|_{s=L}\\
=&\rho \int_0^L \left[(\dot{v} + \dot{V}_b)\,\delta v\Big|_{t_1}^{t_2} - \int_{t_1}^{t_2} (\ddot{v} + \ddot{V}_b)\,\delta v\,dt \right] ds\\
&+ M(\dot{v} + \dot{V}_b)\,\delta v\Big|_{s=L}\Big|_{t_1}^{t_2} - M\int_{t_1}^{t_2} (\ddot{v} + \ddot{V}_b)\,\delta v\,dt\,\Big|_{s=L}\\
&+ J\dot{v}'(1 + v'^2)\delta v'\,\Big|_{s=L}\Big|_{t_1}^{t_2} - J\int_{t_1}^{t_2} \left(\ddot{v}'(1 + v'^2) + v'\dot{v}'^2\right)\delta v'\,dt\,\Big|_{s=L}\\
=&-\int_{t_1}^{t_2} \left\{ \rho \int_0^L (\ddot{v} + \ddot{V}_b)\,\delta v\,ds + M(\ddot{v} + \ddot{V}_b)\,\delta v\,\Big|_{s=L} \right.\\
&\left. + J\left(\ddot{v}'(1 + v'^2) + v'\dot{v}'^2\right)\delta v'\,\Big|_{s=L} \right\} dt,
\end{aligned}$$

where we consider that $\delta v = \delta v' = 0$ at $t = t_1$ and $t = t_2$. Therefore, the extended Hamilton's principle takes the form

$$\begin{aligned}
&\int_{t_1}^{t_2} \Bigg\{ \\
&\int_0^L \Bigg[-\rho(\ddot{v} + \ddot{V}_b) - \left(\left(E_\infty I\, v''(1 + \frac{1}{2}v'^2) + E_\alpha I\, {}^{RL}_{0}\mathcal{D}^\alpha_t\, v''(1 + \frac{1}{2}v'^2) \right)(1 + \frac{1}{2}v'^2) \right)'' \\
&\qquad + \left(\left(E_\infty I\, v''(1 + \frac{1}{2}v'^2) + E_\alpha I\, {}^{RL}_{0}\mathcal{D}^\alpha_t\, v''(1 + \frac{1}{2}v'^2) \right) v''\, v' \right)' \Bigg] \delta v\, ds \\
&- M(\ddot{v} + \ddot{V}_b)\Big|_{s=L} \delta v(L,t) - J\left(\ddot{v}'(1 + v'^2) + v'\dot{v}'^2 \right)\Big|_{s=L} \delta v'(L,t) \\
&- \left(E_\infty I\, v''(1 + \frac{1}{2}v'^2) + E_\alpha I\, {}^{RL}_{0}\mathcal{D}^\alpha_t\, v''(1 + \frac{1}{2}v'^2) \right)(1 + \frac{1}{2}v'^2)\Big|_{s=L} \delta v'(L,t) \\
&+ \left(\left(E_\infty I\, v''(1 + \frac{1}{2}v'^2) + E_\alpha I\, {}^{RL}_{0}\mathcal{D}^\alpha_t\, v''(1 + \frac{1}{2}v'^2) \right)(1 + \frac{1}{2}v'^2) \right)'\Big|_{s=L} \delta v(L,t) \\
&- \left(E_\infty I\, v''(1 + \frac{1}{2}v'^2) + E_\alpha I\, {}^{RL}_{0}\mathcal{D}^\alpha_t\, v''(1 + \frac{1}{2}v'^2) \right) v''\, v'\Big|_{s=L} \delta v(L,t) \Bigg\}\, dt = 0.
\end{aligned} \tag{8.32}$$

Invoking the arbitrariness of virtual displacement δv, we obtain the strong form of the equation of motion as:

$$\begin{aligned}
&\rho\, \ddot{v} + E_\infty I \left(v''(1 + \frac{1}{2}v'^2)^2 \right)'' + E_\alpha I \left((1 + \frac{1}{2}v'^2)\, {}^{RL}_{0}\mathcal{D}^\alpha_t\, v''(1 + \frac{1}{2}v'^2) \right)'' \\
&- E_\infty I \left(v'\, v''^2 (1 + \frac{1}{2}v'^2) \right)' - E_\alpha I \left(v'\, v''\, {}^{RL}_{0}\mathcal{D}^\alpha_t\, v''(1 + \frac{1}{2}v'^2) \right)' = -\rho\, \ddot{V}_b,
\end{aligned} \tag{8.33}$$

which is subject to the following natural boundary conditions:

$$\begin{aligned}
&J\left(\ddot{v}'(1 + v'^2) + v'\dot{v}'^2 \right) + E_\infty I\, v''(1 + \frac{1}{2}v'^2)^2 \\
&+ E_\alpha I\, (1 + \frac{1}{2}v'^2)\, {}^{RL}_{0}\mathcal{D}^\alpha_t\, v''(1 + \frac{1}{2}v'^2) \Big|_{s=L} = 0, \\
&M(\ddot{v} + \ddot{V}_b) - \left(E_\infty I\, v''(1 + \frac{1}{2}v'^2)^2 + E_\alpha I\, (1 + \frac{1}{2}v'^2)\, {}^{RL}_{0}\mathcal{D}^\alpha_t\, v''(1 + \frac{1}{2}v'^2) \right)' \\
&\qquad + \left(E_\infty I\, v'\, v''^2 (1 + \frac{1}{2}v'^2) + E_\alpha I\, v'\, v''\, {}^{RL}_{0}\mathcal{D}^\alpha_t\, v''(1 + \frac{1}{2}v'^2) \right) \Big|_{s=L} = 0.
\end{aligned} \tag{8.34}$$

Following a similar approach as in (8.9) in deriving the beam curvature, we obtain the approximations below, where we only consider up to third order terms and remove the higher order terms

(HOTs).

$$
\begin{aligned}
v''(1+\frac{1}{2}v'^2)^2 &= v'' + v''v'^2 + \text{HOTs} \\
(1+\frac{1}{2}v'^2)\ {}^{RL}_{0}\mathcal{D}^{\alpha}_{t}\ v''(1+\frac{1}{2}v'^2) &= {}^{RL}_{0}\mathcal{D}^{\alpha}_{t}\ v''(1+\frac{1}{2}v'^2) + \frac{1}{2}v'^2\ {}^{RL}_{0}\mathcal{D}^{\alpha}_{t}\ v'' + \text{HOTs} \\
v'\,v''^2(1+\frac{1}{2}v'^2) &= v'\,v''^2 + \text{HOTs} \\
v'\,v''\ {}^{RL}_{0}\mathcal{D}^{\alpha}_{t}\ v''(1+\frac{1}{2}v'^2) &= v'\,v''\ {}^{RL}_{0}\mathcal{D}^{\alpha}_{t}\ v'' + \text{HOTs}
\end{aligned}
$$

Therefore, the strong form can be approximated up to the third order and the problem then reads as: find $v \in V$ such that

$$
\begin{aligned}
& m\,\ddot{v} + \left(v'' + v''v'^2\right)'' - \left(v'\,v''^2\right)' + E_r\ \left({}^{RL}_{0}\mathcal{D}^{\alpha}_{t}\ v''(1+\frac{1}{2}v'^2) + \frac{1}{2}v'^2\ {}^{RL}_{0}\mathcal{D}^{\alpha}_{t}\ v''\right)'' \\
& - E_r\ \left(v'\,v''\ {}^{RL}_{0}\mathcal{D}^{\alpha}_{t}\ v''\right)' = -m\,\ddot{V}_b,
\end{aligned}
\tag{8.35}
$$

$$
\begin{aligned}
& m\,\ddot{v} + \left(v'' + v''v'^2 + E_r\ {}^{RL}_{0}\mathcal{D}^{\alpha}_{t}\ v''(1+\frac{1}{2}v'^2) + \frac{1}{2}E_r v'^2\ {}^{RL}_{0}\mathcal{D}^{\alpha}_{t}\ v''\right)'' \\
& - \left(v'\,v''^2 + E_r v'\,v''\ {}^{RL}_{0}\mathcal{D}^{\alpha}_{t}\ v''\right)' = -m\,\ddot{V}_b,
\end{aligned}
\tag{8.36}
$$

subject to the following boundary conditions:

$$
\begin{aligned}
& v\Big|_{s=0} = v'\Big|_{s=0} = 0, \\
& \frac{Jm}{\rho}\left(\ddot{v}'(1+v'^2) + v'\dot{v}'^2\right) + \left(v'' + v''v'^2 + E_r\ {}^{RL}_{0}\mathcal{D}^{\alpha}_{t}\ v''(1+\frac{1}{2}v'^2) + \frac{1}{2}E_r\,v'^2\ {}^{RL}_{0}\mathcal{D}^{\alpha}_{t}\ v''\right)\ \Big|_{s=L} = 0, \\
& \frac{Mm}{\rho}(\ddot{v} + \ddot{V}_b) - \left(v'' + v''v'^2 + E_r\ {}^{RL}_{0}\mathcal{D}^{\alpha}_{t}\ v''(1+\frac{1}{2}v'^2) + \frac{1}{2}E_r\,v'^2\ {}^{RL}_{0}\mathcal{D}^{\alpha}_{t}\ v''\right)' \\
& + \left(v'\,v''^2 + E_r\,v'\,v''\ {}^{RL}_{0}\mathcal{D}^{\alpha}_{t}\ v''\right)\ \Big|_{s=L} = 0,
\end{aligned}
\tag{8.37}
$$

where $m = \frac{\rho}{E_\infty I}$ and $E_r = \frac{E_\alpha}{E_\infty}$.

8.2.4 Nondimensionalization

Let the dimensionless variables

$$
\begin{aligned}
&s^* = \frac{s}{L}, \quad v^* = \frac{v}{L}, \quad t^* = t\left(\frac{1}{mL^4}\right)^{1/2}, \quad E_r^* = E_r\left(\frac{1}{mL^4}\right)^{\alpha/2}, \\
&J^* = \frac{J}{\rho L^3}, \quad M^* = \frac{M}{\rho L}, \quad V_b^* = \frac{V_b}{L}.
\end{aligned} \tag{8.38}
$$

We obtain the following dimensionless equation by substituting the above dimensionless variables.

$$
\begin{aligned}
&m\frac{L}{mL^4}\frac{\partial^2 v^*}{\partial t^{*2}} \\
&+ \frac{1}{L^2}\frac{\partial^2}{\partial s^{*2}}\left[\frac{L}{L^2}\frac{\partial^2 v^*}{\partial s^{*2}} + \frac{L}{L^2}\frac{\partial^2 v^*}{\partial s^{*2}}(\frac{L}{L}\frac{\partial v^*}{\partial s^*})^2 + \frac{E_r^*(mL^4)^{\alpha/2}}{2}\frac{1}{(mL^4)^{\alpha/2}}\frac{L}{L^2}(\frac{L}{L})^2\,{}^{RL}_{0}\mathcal{D}^{\alpha}_{t^*}\frac{\partial^2 v^*}{\partial s^{*2}}(\frac{\partial v^*}{\partial s^*})^2\right. \\
&\left.+ E_r^*(mL^4)^{\alpha/2}\frac{1}{(mL^4)^{\alpha/2}}\frac{L}{L^2}\,{}^{RL}_{0}\mathcal{D}^{\alpha}_{t^*}\frac{\partial^2 v^*}{\partial s^{*2}} + \frac{1}{2}E_r^*(mL^4)^{\alpha/2}(\frac{L}{L}\frac{\partial v^*}{\partial s^*})^2\frac{1}{(mL^4)^{\alpha/2}}\frac{L}{L^2}\,{}^{RL}_{0}\mathcal{D}^{\alpha}_{t^*}\frac{\partial^2 v^*}{\partial s^{*2}}\right] \\
&- \frac{1}{L}\frac{\partial}{\partial s^*}\left[\frac{L}{L}\frac{\partial v^*}{\partial s^*}(\frac{L}{L^2}\frac{\partial^2 v^*}{\partial s^{*2}})^2 + E_r^*(mL^4)^{\alpha/2}\frac{L}{L}\frac{\partial v^*}{\partial s^*}\frac{L}{L^2}\frac{\partial^2 v^*}{\partial s^{*2}}\frac{1}{(mL^4)^{\alpha/2}}\frac{L}{L^2}\,{}^{RL}_{0}\mathcal{D}^{\alpha}_{t^*}\frac{\partial^2 v^*}{\partial s^{*2}}\right] \\
&= -m\frac{L}{mL^4}\frac{\partial^2 V_b^*}{\partial t^{*2}},
\end{aligned} \tag{8.39}
$$

which can be simplified to

$$
\begin{aligned}
&\frac{\partial^2 v^*}{\partial t^{*2}} + \frac{\partial^2}{\partial s^{*2}}\left[\frac{\partial^2 v^*}{\partial s^{*2}} + \frac{\partial^2 v^*}{\partial s^{*2}}(\frac{\partial v^*}{\partial s^*})^2 + \frac{E_r^*}{2}\,{}^{RL}_{0}\mathcal{D}^{\alpha}_{t^*}\frac{\partial^2 v^*}{\partial s^{*2}}(\frac{\partial v^*}{\partial s^*})^2 + E_r^*\,{}^{RL}_{0}\mathcal{D}^{\alpha}_{t^*}\frac{\partial^2 v^*}{\partial s^{*2}}\right. \\
&\qquad\left.+ \frac{1}{2}E_r^*(\frac{\partial v^*}{\partial s^*})^2\,{}^{RL}_{0}\mathcal{D}^{\alpha}_{t^*}\frac{\partial^2 v^*}{\partial s^{*2}}\right] - \frac{\partial}{\partial s^*}\left[\frac{\partial v^*}{\partial s^*}(\frac{\partial^2 v^*}{\partial s^{*2}})^2 + E_r^*\frac{\partial v^*}{\partial s^*}\frac{\partial^2 v^*}{\partial s^{*2}}\,{}^{RL}_{0}\mathcal{D}^{\alpha}_{t^*}\frac{\partial^2 v^*}{\partial s^{*2}}\right] = -\frac{\partial^2 V_b^*}{\partial t^{*2}},
\end{aligned} \tag{8.40}
$$

The dimensionless boundary conditions are also obtained by substituting dimensionless variables in (8.37). We can show similarly that they preserve their structure as:

$$
\begin{aligned}
& v^* \Big|_{s^*=0} = \frac{\partial v^*}{\partial s^*} \Big|_{s^*=0} = 0, \\
& \frac{J^* \rho L^3 m}{\rho} \frac{1}{mL^4} \left[\frac{\partial^3 v^*}{\partial t^* \partial^2 s^*} \left(1 + \left(\frac{\partial v^*}{\partial s^*} \right)^2 \right) + \frac{\partial v^*}{\partial s^*} \left(\frac{\partial^2 v^*}{\partial t^* \partial s^*} \right)^2 \right] \\
& + \frac{1}{L} \left[\frac{\partial^2 v^*}{\partial s^{*2}} + \frac{\partial^2 v^*}{\partial s^{*2}} (\frac{\partial v^*}{\partial s^*})^2 + \frac{E_r^*}{2} \, {}^{RL}_{0}\mathcal{D}^{\alpha}_{t^*} \frac{\partial^2 v^*}{\partial s^{*2}} (\frac{\partial v^*}{\partial s^*})^2 + E_r^* \, {}^{RL}_{0}\mathcal{D}^{\alpha}_{t^*} \frac{\partial^2 v^*}{\partial s^{*2}} \right. \\
& \left. + \frac{1}{2} E_r^* (\frac{\partial v^*}{\partial s^*})^2 \, {}^{RL}_{0}\mathcal{D}^{\alpha}_{t^*} \frac{\partial^2 v^*}{\partial s^{*2}} \right] \Bigg|_{s^*=1} = 0, \\
& \frac{M^* \rho L m}{\rho} \frac{L}{mL^4} \left(\frac{\partial^2 v^*}{\partial^2 t^*} + \frac{\partial^2 V_b^*}{\partial^2 t^*} \right) \\
& - \frac{1}{L^2} \frac{\partial v^*}{\partial s^*} \left[\frac{\partial^2 v^*}{\partial s^{*2}} + \frac{\partial^2 v^*}{\partial s^{*2}} (\frac{\partial v^*}{\partial s^*})^2 + \frac{E_r^*}{2} \, {}^{RL}_{0}\mathcal{D}^{\alpha}_{t^*} \frac{\partial^2 v^*}{\partial s^{*2}} (\frac{\partial v^*}{\partial s^*})^2 \right. \\
& \left. + E_r^* \, {}^{RL}_{0}\mathcal{D}^{\alpha}_{t^*} \frac{\partial^2 v^*}{\partial s^{*2}} + \frac{1}{2} E_r^* (\frac{\partial v^*}{\partial s^*})^2 \, {}^{RL}_{0}\mathcal{D}^{\alpha}_{t^*} \frac{\partial^2 v^*}{\partial s^{*2}} \right] \\
& + \frac{1}{L^2} \left[\frac{\partial v^*}{\partial s^*} (\frac{\partial^2 v^*}{\partial s^{*2}})^2 + E_r^* \frac{\partial v^*}{\partial s^*} \frac{\partial^2 v^*}{\partial s^{*2}} \, {}^{RL}_{0}\mathcal{D}^{\alpha}_{t^*} \frac{\partial^2 v^*}{\partial s^{*2}} \right] \Bigg|_{s^*=1} = 0,
\end{aligned}
$$

Therefore, the dimensionless equation of motion becomes (after dropping * for the sake of simplicity)

$$
\begin{aligned}
& \ddot{v} + \left(v'' + v'' v'^2 + E_r \, {}^{RL}_{0}\mathcal{D}^{\alpha}_{t} \, v'' (1 + \frac{1}{2} v'^2) + \frac{1}{2} E_r v'^2 \, {}^{RL}_{0}\mathcal{D}^{\alpha}_{t} \, v'' \right)'' \\
& \quad - \left(v' \, v''^2 + E_r v' \, v'' \, {}^{RL}_{0}\mathcal{D}^{\alpha}_{t} \, v'' \right)' = -\ddot{V}_b,
\end{aligned}
\tag{8.41}
$$

which is subject to the following dimensionless boundary conditions

$$
\begin{aligned}
& v \Big|_{s=0} = v' \Big|_{s=0} = 0, \\
& J \left(\ddot{v}' (1 + v'^2) + v' \dot{v}'^2 \right) + \left(v'' + v'' v'^2 + E_r \, {}^{RL}_{0}\mathcal{D}^{\alpha}_{t} \, v'' (1 + \frac{1}{2} v'^2) + \frac{1}{2} E_r \, v'^2 \, {}^{RL}_{0}\mathcal{D}^{\alpha}_{t} \, v'' \right) \Big|_{s=1} = 0, \\
& M(\ddot{v} + \ddot{V}_b) - \left(v'' + v'' v'^2 + E_r \, {}^{RL}_{0}\mathcal{D}^{\alpha}_{t} \, v'' (1 + \frac{1}{2} v'^2) + \frac{1}{2} E_r \, v'^2 \, {}^{RL}_{0}\mathcal{D}^{\alpha}_{t} \, v'' \right)' \\
& + \left(v' \, v''^2 + E_r \, v' \, v'' \, {}^{RL}_{0}\mathcal{D}^{\alpha}_{t} \, v'' \right) \Big|_{s=1} = 0,
\end{aligned}
\tag{8.42}
$$

8.2.5 Weak Formulation

We obtain the weak form of the problem by multiplying the equation with proper test functions $\tilde{v}(s) \in \tilde{V}$ and integrating over the dimensionless spatial computational domain $\Omega_s = [0, 1]$. The test function satisfies the geometric boundary conditions, i.e. $\tilde{v}(0) = \tilde{v}'(0) = 0$. Therefore, by changing the order of integral and temporal derivatives, and through integration by parts, the weak form of problem can be written as

$$\int_0^1 \ddot{v}\,\tilde{v}\,ds + \int_0^1 \left(v'' + v''v'^2 + E_r\,{}^{RL}_{0}\mathcal{D}_t^{\alpha}\,v''(1+\frac{1}{2}v'^2) + \frac{1}{2}E_r v'^2\,{}^{RL}_{0}\mathcal{D}_t^{\alpha}\,v''\right)''\,\tilde{v}\,ds \tag{8.43}$$
$$-\int_0^1 \left(v'\,v''^2 + E_r v'\,v''\,{}^{RL}_{0}\mathcal{D}_t^{\alpha}\,v''\right)'\,\tilde{v}\,ds = -\int_0^1 \ddot{V}_b\,\tilde{v}\,ds,$$

where we transfer the spatial derivative load to the test function through integration by parts as

$$\frac{\partial^2}{\partial t^2}\int_0^1 v\,\tilde{v}\,ds + \int_0^1 \left(v'' + v''v'^2 + E_r\,{}^{RL}_{0}\mathcal{D}_t^{\alpha}\,v''(1+\frac{1}{2}v'^2) + \frac{1}{2}E_r v'^2\,{}^{RL}_{0}\mathcal{D}_t^{\alpha}\,v''\right)\tilde{v}''\,ds \tag{8.44}$$
$$+\int_0^1 \left(v'\,v''^2 + E_r v'\,v''\,{}^{RL}_{0}\mathcal{D}_t^{\alpha}\,v''\right)\tilde{v}'\,ds + M(\ddot{v}+\ddot{V}_b)\tilde{v}\Big|_{s=1}$$
$$+J\left(\ddot{v}'(1+v'^2) + v'\dot{v}'^2\right)\tilde{v}'\Big|_{s=1} = -\ddot{V}_b\int_0^L \tilde{v}\,ds.$$

By rearranging the terms, we get

$$\frac{\partial^2}{\partial t^2}\left(\int_0^1 v\,\tilde{v}\,ds + M\,v\,\tilde{v}\Big|_{s=1} + J\,v'\,\tilde{v}'\Big|_{s=1}\right) + J\left(\ddot{v}'v'^2 + v'\dot{v}'^2\right)\tilde{v}'\Big|_{s=1} \tag{8.45}$$
$$+\int_0^1 v''\,\tilde{v}''\,ds + E_r\int_0^1 {}^{RL}_{0}\mathcal{D}_t^{\alpha}\,v''\,\tilde{v}''\,ds$$
$$+\int_0^1 v''v'^2\,\tilde{v}''\,ds + \int_0^1 v'\,v''^2\,\tilde{v}'\,ds + \frac{E_r}{2}\int_0^1 {}^{RL}_{0}\mathcal{D}_t^{\alpha}\,v''v'^2\,\tilde{v}''\,ds + \frac{E_r}{2}\int_0^1 v'^2\,{}^{RL}_{0}\mathcal{D}_t^{\alpha}\,v''\,\tilde{v}''\,ds$$
$$+E_r\int_0^1 v'\,v''\,{}^{RL}_{0}\mathcal{D}_t^{\alpha}\,v''\,\tilde{v}'\,ds = -\ddot{V}_b\left(\int_0^1 \tilde{v}\,ds + M\,\tilde{v}\Big|_{s=1}\right).$$

8.2.6 Assumed Mode: A Spectral Galerkin Approximation In Space

We employ the following modal discretization to obtain a reduced-order model of the beam. Therefore,

$$v(s,t) \simeq v_N(s,t) = \sum_{n=1}^{N} q_n(t)\,\phi_n(s), \tag{8.46}$$

where the spatial functions $\phi_n(s),\ n = 1,2,\cdots,N$ are assumed *a priori* and the temporal functions $q_n(t),\ n = 1,2,\cdots,N$ are the unknown modal coordinates. The assumed modes $\phi_n(s)$ in discretization (8.46) are obtained in section 8.5 by solving the corresponding eigenvalue problem of linear counterpart of our model. Hence, we construct the proper finite dimensional spaces of basis/test functions as:

$$V_N = \tilde{V}_N = span\left\{\ \phi_n(x) : n = 1,2,\cdots,N\ \right\}. \tag{8.47}$$

Thus, since $V_N = \tilde{V}_N \subset V = \tilde{V}$, problem (8.45) read as: find $v_N \in V_N$ such that

$$\begin{aligned}
&\frac{\partial^2}{\partial t^2}\left(\int_0^1 v_N\,\tilde{v}_N\,ds + M\,v_N\,\tilde{v}_N\Big|_{s=1} + J\,v_N'\,\tilde{v}_N'\Big|_{s=1}\right) \\
&+ J\left(\ddot{v}_N' {v_N'}^2 + v_N'\dot{v}_N'^2\right)\tilde{v}_N'\Big|_{s=1} + \int_0^1 v_N''\,\tilde{v}_N''\,ds \\
&+ E_r\int_0^1 {}^{RL}_{0}\mathcal{D}_t^{\alpha}\,v_N''\,\tilde{v}_N''\,ds + \int_0^1 v_N'' {v_N'}^2\,\tilde{v}_N''\,ds \\
&+ \int_0^1 v_N'\,{v_N''}^2\,\tilde{v}_N'\,ds + \frac{E_r}{2}\int_0^1 {}^{RL}_{0}\mathcal{D}_t^{\alpha}\,v_N'' {v_N'}^2\,\tilde{v}_N''\,ds \\
&+ \frac{E_r}{2}\int_0^1 {v_N'}^2\,{}^{RL}_{0}\mathcal{D}_t^{\alpha}\,v_N''\,\tilde{v}_N''\,ds + E_r\int_0^1 v_N'\,v_N''\,{}^{RL}_{0}\mathcal{D}_t^{\alpha}\,v_N''\,\tilde{v}_N'\,ds \\
&= -\ddot{V}_b\left(\int_0^1 \tilde{v}_N\,ds + M\,\tilde{v}_N\Big|_{s=1}\right),
\end{aligned} \tag{8.48}$$

for all $\tilde{v}_N \in \tilde{V}_N$.

8.2.7 Single Mode Approximation

We assume that the only active mode of vibration is the primary one, which encapsulates most of the fundamental dynamics of our complex system. Therefore, we start with a unimodal discretization

$v_N = q(t)\,\phi(s)$, where we let $N = 1$ in (8.46) and drop subscript 1 for simplicity. Upon substituting, we obtain

$$\begin{aligned} &\mathcal{M}\,\ddot{q} + \mathcal{J}(\ddot{q}\,q^2 + q\,\dot{q}^2) + \mathcal{K}_l\,q + E_r\,C_l\;{}^{RL}_{0}\mathcal{D}^{\alpha}_{t}\,q + 2\mathcal{K}_{nl}\,q^3 \\ &+ \frac{E_r\,C_{nl}}{2}\left({}^{RL}_{0}\mathcal{D}^{\alpha}_{t}\,q^3 + 3\,q^2\;{}^{RL}_{0}\mathcal{D}^{\alpha}_{t}\,q\right) = -\mathcal{M}_b\,\ddot{V}_b, \end{aligned} \tag{8.49}$$

in which

$$\begin{aligned} &\mathcal{M} = \int_0^1 \phi^2\,ds + M\,\phi^2(1) + J\,\phi'^2(1), \quad \mathcal{J} = J\,\phi'^4(1), \\ &\mathcal{K}_l = C_l = \int_0^1 \phi''^2\;ds, \quad \mathcal{K}_{nl} = C_{nl} = \int_0^1 \phi'^2\,\phi''^2\;ds, \\ &\mathcal{M}_b = \int_0^1 \phi\,ds + M\,\phi(1). \end{aligned} \tag{8.50}$$

8.3 Linearized Equation: Direct Numerical Time Integration

We linearize the obtained equation, governing the time evolution of the first vibration mode by removing the nonlinear terms. Therefore, in the absence of base excitation, (8.49) takes the following form

$$\ddot{q} + E_r\,c_l\;{}^{RL}_{0}\mathcal{D}^{\alpha}_{t}\,q + k_l\,q = 0 \tag{8.51}$$

in which the coefficients $c_l = \frac{C_l}{\mathcal{M}}$ and $k_l = \frac{\mathcal{K}_l}{\mathcal{M}}$ are given in (8.50). The linearized equation (8.51) can be thought of as a fractionally damped oscillator, shown schematically in Fig. 8.5 (right). This setting describes the vibration of a lumped fractional Kelvin-Voigt model. By letting $E_r = 1$, the dimensionless parameters $c_l = k_l = 1.24$ with a unit mass at the tip, i.e. $M = 1$. We find the time response of the linearized model (8.51) using a direct finite difference time integration scheme, which employs $L1$ scheme [96, 104] and Newmark method to approximate the fractional derivative and the inertial term, respectively. The Newmark method is of second order accuracy and thus the overall accuracy of the developed scheme is governed by the error level of $L1$ scheme, which is of order $2-\alpha$.

Fig. 8.5 (left) shows the time response of free vibration of a fractionally damped oscillator. The absolute value of $q(t)$ versus time for different values of α is plotted in Log-Log scale. We observe that in the long time, the amplitude of oscillation decays with a power-law, whose rate is governed by the order of fractional derivative α and increases by increasing α (see blue lines in the figure). By replacing the fractional damper with a classical integer-order one, we see that the amplitude decays exponentially and not anymore by a power-law (see the dotted red line in the figure). These results are in perfect agreement with the power-law and exponential relaxation kernel, described in Sec. 8.2.2. We note that since the fractional element is inherently a viscoelastic element that interpolates between the two spring and dash-pot elements (see Sec. 8.2.2 for more discussion and references), it contributes both in the stiffness and damping ratio of the system. As α increases, the fractional element converges to purely viscous element, and thus the system becomes softer (less stiff), resulting in frequency reduction. This frequency shift can be seen from the drift of consecutive amplitude peaks to the right as α is increased. The fractional linear oscillators are also considered in [161] as a case of systems with memory, where their interaction with a fluctuating environment causes the time evolution of the system to be intermittent. The authors in [161] apply the Koopman operator theory to the corresponding integer order system and then make a Lèvy transformation in time to recover long-term memory effects; they observe a power-law behavior in the amplitude decay of the system's response. Such an anomalous decay rate has also been investigated in [150] for an extended theory of decay of classical vibrational models brought into nonlinear resonances. The authors report a "non-exponential" decay in variables describing the dynamics of the system in the presence of dissipation and also a sharp change in the decay rate close to resonance.

Remark 8.3.1. *The change in fractional derivative order, α, is a notion of stiffening/softening of a viscoelastic material modeled via fractional constitutive equations. As shown in Fig. 8.5 (left), the value of α directly affects the decay rate of free vibration. This strong relation can be used to develop a prediction framework, which takes time series of free vibrations as an input, and returns an estimation of the level of material stiffness as a reflection of the health of the system of interest.*

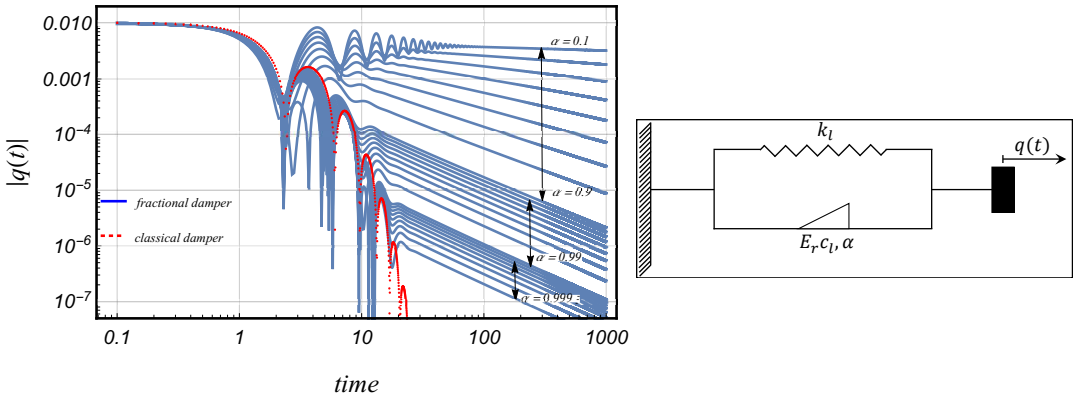

Figure 8.5: Power-Law Decay: Time response of linear fractionally damped oscillator using Newmark and $L1$ scheme. The fractional damper has two constants $E_r\ c_l$ and α as the coefficient and derivative order of fractional operator.

8.4 Perturbation Analysis of Nonlinear Equation

Nonlinear terms in equation (8.49) give rise to expensive time integration schemes. We use perturbation analysis to investigate the behavior of a nonlinear system, where we reduce the nonlinear fractional differential equation to an algebraic equation to solve for the steady state amplitude and phase of vibration.

8.4.1 Method of Multiple Scales

To investigate the dynamics of the system described by (8.49), we use the method of multiple scales [128, 141]. The new independent time scales and the integer-order derivative with respect to them are defined as

$$T_m = \epsilon^m\, t, \qquad D_m = \frac{\partial}{\partial T_m}, \qquad m = 0, 1, 2, \cdots . \tag{8.52}$$

It is also convenient to utilize another representation of the fractional derivative as in equation (5.82) in [147], which according to the Riemann-Liouville fractional derivative, is equivalent to the

fractional power of the operator of conventional time-derivative, i.e. ${}^{RL}_{0}\mathcal{D}^{\alpha}_{t} = (\frac{d}{dt})^{\alpha}$. Therefore,

$$\begin{aligned} \frac{d}{dt} &= D_0 + \epsilon D_1 + \cdots, \\ \frac{d^2}{dt^2} &= D_0^2 + 2\epsilon D_0 D_1 + \cdots, \\ {}^{RL}_{0}\mathcal{D}^{\alpha}_{t} &= (\frac{d}{dt})^{\alpha} = D_0^{\alpha} + \epsilon\alpha D_0^{\alpha-1} D_1 + \cdots, \end{aligned} \tag{8.53}$$

The solution $q(t)$ can then be represented in terms of series

$$q(T_0, T_1, \cdots) = q_0(T_0, T_1, \cdots) + \epsilon q_1(T_0, T_1, \cdots) + \epsilon^2 q_2(T_0, T_1, \cdots) + \cdots \tag{8.54}$$

We assume that the coefficients in the equation of motion has the following scaling

$$\frac{\mathcal{J}}{\mathcal{M}} = \epsilon\, m_{nl}, \quad \frac{\mathcal{K}_l}{\mathcal{M}} = k_l = \omega_0^2, \quad \frac{\mathcal{C}_l}{\mathcal{M}} = \epsilon\, c_l, \quad \frac{\mathcal{K}_{nl}}{\mathcal{M}} = \epsilon\, k_{nl}, \quad \frac{\mathcal{C}_{nl}}{\mathcal{M}} = \epsilon\, c_{nl}, \tag{8.55}$$

and the base excitation $-\frac{\mathcal{M}_b}{\mathcal{M}}\,\ddot{V}_b$ is a harmonic function of form $\epsilon\, F\cos(\Omega\, t)$. Thus, (8.49) can be expanded as

$$\begin{aligned} &(D_0^2 + 2\epsilon D_0 D_1 + \cdots)(q_0 + \epsilon q_1 + \cdots) \\ &+ \epsilon\, m_{nl}(D_0^2 + 2\epsilon D_0 D_1 + \cdots)(q_0 + \epsilon q_1 + \cdots) \times (q_0 + \epsilon q_1 + \cdots)^2 \\ &+ \epsilon\, m_{nl}(q_0 + \epsilon q_1 + \cdots) \times ((D_0 + \epsilon D_1 + \cdots)(q_0 + \epsilon q_1 + \cdots))^2 \\ &+ \omega_0^2\,(q_0 + \epsilon q_1 + \cdots) \\ &+ \epsilon\, E_r\, c_l\,(D_0^{\alpha} + \epsilon\alpha D_0^{\alpha-1} D_1 + \cdots)(q_0 + \epsilon q_1 + \cdots) \\ &+ 2\epsilon\, k_{nl}\,(q_0 + \epsilon q_1 + \cdots)^3 \\ &+ \frac{1}{2}\epsilon\, E_r\, c_{nl}\,(D_0^{\alpha} + \epsilon\alpha D_0^{\alpha-1} D_1 + \cdots)(q_0 + \epsilon q_1 + \cdots)^3 \\ &+ \frac{3}{2}\epsilon\, E_r\, c_{nl}\,(q_0 + \epsilon q_1 + \cdots)^2 \left[(D_0^{\alpha} + \epsilon\alpha D_0^{\alpha-1} D_1 + \cdots)(q_0 + \epsilon q_1 + \cdots)\right] \\ &= \epsilon\, F\cos(\Omega\, T_0). \end{aligned} \tag{8.56}$$

By collecting similar coefficients of zero-th and first orders of ϵ, we obtain the following equations

$$O(\epsilon^0): \quad D_0^2 q_0 + \omega_0^2 q_0 = 0, \tag{8.57}$$

$$\begin{aligned} O(\epsilon^1): \quad D_0^2 q_1 + \omega_0^2 q_1 = & -2D_0 D_1 q_0 - m_{nl} \left(q_0^2 D_0^2 q_0 + q_0 (D_0 q_0)^2 \right) \\ & - E_r\, c_l\, D_0^\alpha q_0 - 2\, k_{nl}\, q_0^3 - \frac{1}{2} E_r\, c_{nl}\, D_0^\alpha q_0^3 \\ & - \frac{3}{2} E_r\, c_{nl}\, q_0^2 D_0^\alpha q_0 + F \cos(\Omega T_0). \end{aligned} \tag{8.58}$$

The solution to (8.57) is of the form

$$q_0(T_0, T_1) = A(T_1)\, e^{i\,\omega_0\, T_0} + c.c \tag{8.59}$$

where “c.c" denotes the complex conjugate. By substituting (8.59) into the right-hand-side of (8.58), we observe that different resonance cases are possible. In each case, we obtain the corresponding solvability conditions by removing the secular terms, i.e. the terms that grow in time unbounded. Then, we write A in the polar form $A = \frac{1}{2} a\, e^{i\,\varphi}$, where the real valued functions a and φ are the amplitude and phase lag of time response, respectively. Thus, the solution $q(t)$ becomes

$$q(t) = a(\epsilon\, t) \cos(\omega_0\, t + \varphi(\epsilon\, t)) + O(\epsilon), \tag{8.60}$$

where the governing equations of a and φ are obtained by separating the real and imaginary parts.

8.4.1.1 Case 1: No Lumped Mass At The Tip

In this case, $M = J = 0$, and thus, given the functions $\varphi_1(x)$ in section 8.5, the coefficients are computed as $\mathcal{M} = 1$, $\mathcal{K}_l = C_l = 12.3624$, $\mathcal{M}_b = 0.782992$, and $\mathcal{K}_{nl} = C_{nl} = 20.2203$. We consider the following cases:

• Free Vibration, $F = 0$: Super Sensitivity to α

In this case, the beam is not externally excited and thus, $F = 0$. By removing the secular terms that are the coefficients of $e^{i\,\omega_0\, T_0}$ in the solvability condition, we find the governing equations of

solution amplitude and phase as

$$\frac{da}{dT_1} = -E_r\,\omega_0^{\alpha-1}\sin(\alpha\frac{\pi}{2})\left(\frac{1}{2}\,c_l\,a + \frac{3}{8}\,c_{nl}\,a^3\right), \tag{8.61}$$

$$\frac{d\varphi}{dT_1} = \frac{1}{2}c_l\,E_r\,\omega_0^{\alpha-1}\,\cos\left(\frac{\pi\alpha}{2}\right) + \frac{3}{4}c_{nl}\,E_r\,\omega_0^{\alpha-1}\,\cos\left(\frac{\pi\alpha}{2}\right)\,a^2 + \frac{3}{4}\,\omega_0^{-1}\,k_{nl}\,a^2. \tag{8.62}$$

We can see from the first equation (8.61) that the amplitude of free vibration decays out, where the decay rate $\tau_d = c_l\,E_r\,\omega_0^{\alpha-1}\sin(\alpha\frac{\pi}{2})$ directly depends on values of the fractional derivative α and the coefficients E_r (see Fig. 8.6). We introduce the sensitivity index $S_{\tau_d,\alpha}$ as the partial derivative

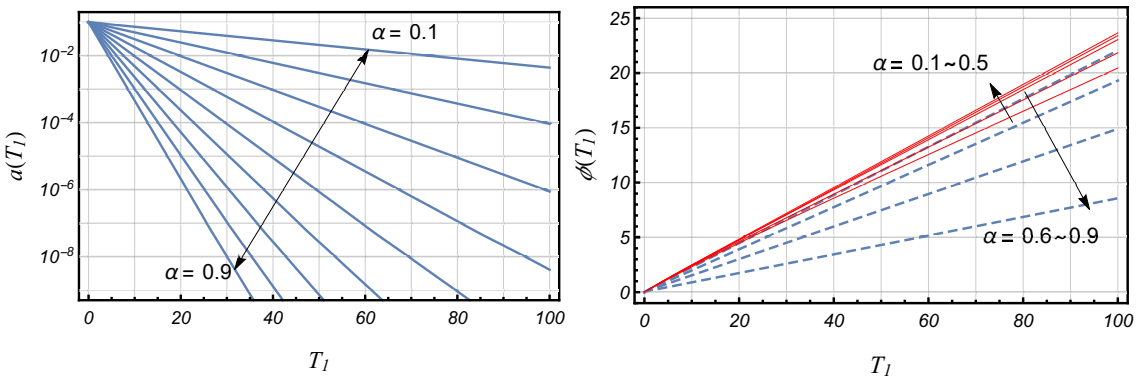

Figure 8.6: Free vibration of the viscoelastic cantilever beam with no lumped mass at the tip. The rate of decay of amplitude strongly depends on the fractional derivative order α and the coefficient E_r. The left figure (log-linear scale) shows the rapid increase in amplitude decaying as α is increased and $E_r = 0.1$. The right figure (linear scale) shows the phase lag $\varphi(\epsilon t)$, where its increase rate decreases as α is increased.

of decay rate with respect to α, i.e.

$$S_{\tau_d,\alpha} = \frac{d\tau_d}{d\alpha} = \frac{\pi}{2}c_l\,E_r\,\omega_0^{\alpha-1}\,\cos(\alpha\frac{\pi}{2}) + c_l\,E_r\,\omega_0^{\alpha-1}\sin(\alpha\frac{\pi}{2})\log(\omega_0). \tag{8.63}$$

The sensitivity index is computed and plotted in Fig. 8.7 for the same set of parameters as in Fig. 8.6. There exists a critical value

$$\alpha_{cr} = -\frac{2}{\pi}\tan^{-1}\left(\frac{\pi}{2\,\log(\omega_0)}\right), \tag{8.64}$$

where $S_{\tau_d,\alpha} = 0$. We observe in Fig. 8.7 that by increasing α when $\alpha < \alpha_{cr}$, i.e. introducing more viscosity to the system, the dissipation rate, and thus decay rate, increases; this can be thought of as a softening (stiffness-decreasing) region. Further increasing α when $\alpha > \alpha_{cr}$, will reversely

results in decrease of decay rate; this can be thought of as a hardening (more stiffening) region. We also note that α_{cr} solely depends on value of ω_0, given in (8.55), and even though the value of E_r affects decay rate, it does not change the value of α_{cr}.

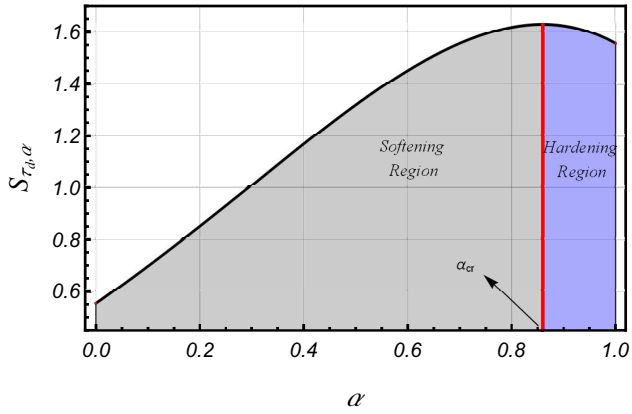

Figure 8.7: Free vibration of the viscoelastic cantilever beam with no lumped mass at the tip. This graph shows sensitivity of the decay rate τ_d with respect to change of α. Increasing α when $\alpha < \alpha_{cr}$ leads to higher dissipation and decay rate. The reverse effect is observed when $\alpha > \alpha_{cr}$. By softening and hardening we reflect to the regions where increasing α (introducing extra viscosity) leads to higher and lower decay rate, respectively.

• Primary Resonance Case, $\Omega \approx \omega_0$

In the case of primary resonance, the excitation frequency is close to the natural frequency of the system. We let $\Omega = \omega_0 + \epsilon\,\Delta$, where Δ is called the detuning parameter and thus, write the force function as $\frac{1}{2}F\,e^{i\,\Delta\,T_1}\,e^{i\,\omega_0\,T_0} + c.c$. In this case, the force function also contributes to the secular terms. Therefore, we find the governing equations of solution amplitude and phase as

$$\frac{da}{dT_1} = -E_r\,\omega_0^{\alpha-1}\,\sin(\alpha\frac{\pi}{2})\left(\frac{1}{2}\,c_l\,a + \frac{3}{8}\,c_{nl}\,a^3\right) + \frac{1}{2}f\,\omega_0^{-1}\,\sin(\Delta T_1 - \varphi), \tag{8.65}$$

$$a\,\frac{d\varphi}{dT_1} = \frac{1}{2}c_l\,E_r\,\omega_0^{\alpha-1}\,\cos(\frac{\pi\alpha}{2})\,a + \frac{3}{4}c_{nl}\,E_r\,\omega_0^{\alpha-1}\,\cos(\frac{\pi\alpha}{2})\,a^3 + \frac{3}{4}\,\omega_0^{-1}\,k_{nl}\,a^3 - \frac{1}{2}f\,\omega_0^{-1}\,\cos(\Delta T_1 - \varphi), \tag{8.66}$$

in which the four parameters $\{\alpha, E_r, f, \Delta\}$ mainly change the frequency response of the system. The equations (8.65) and (8.66) can be transformed into an autonomous system, where the T_1 does not appear explicitly, by letting

$$\gamma = \Delta\,T_1 - \varphi.$$

The steady state solution occur when $\frac{da}{dT_1} = \frac{d\varphi}{dT_1} = 0$, that gives

$$E_r\,\omega_0^{\alpha-1}\sin(\frac{\pi\alpha}{2})\left(\frac{c_l}{2}a + \frac{3c_{nl}}{8}a^3\right) = \frac{f}{2\,\omega_0}\sin(\gamma), \tag{8.67}$$

$$\left(\Delta - \frac{c_l}{2}E_r\,\omega_0^{\alpha-1}\,\cos(\frac{\pi\alpha}{2})\right)a - \frac{3}{4}\left(c_{nl}\,E_r\,\omega_0^{\alpha-1}\,\cos(\frac{\pi\alpha}{2}) + \omega_0^{-1}\,k_{nl}\right)a^3 = \frac{f}{2\,\omega_0}\cos(\gamma), \tag{8.68}$$

and thus, by squaring and adding these two equations, we get

$$\begin{aligned}&\left[\frac{c_l}{2}E_r\,\omega_0^{\alpha-1}\sin(\frac{\pi\alpha}{2})\,a + \frac{3c_{nl}}{8}E_r\,\omega_0^{\alpha-1}\sin(\frac{\pi\alpha}{2})\,a^3\right]^2 \\ &+\left[\left(\Delta - \frac{c_l}{2}E_r\,\omega_0^{\alpha-1}\,\cos(\frac{\pi\alpha}{2})\right)a - \frac{3}{4}\left(c_{nl}\,E_r\,\omega_0^{\alpha-1}\,\cos(\frac{\pi\alpha}{2}) + \omega_0^{-1}\,k_{nl}\right)a^3\right]^2 = \frac{f^2}{4\,\omega_0^2}.\end{aligned} \tag{8.69}$$

This can be written in a simpler way as

$$\left[A_1\,a + A_2\,a^3\right]^2 + \left[B_1\,a + B_2\,a^3\right]^2 = C, \tag{8.70}$$

where

$$\begin{aligned}&A_1 = \frac{c_l}{2}E_r\,\omega_0^{\alpha-1}\sin(\frac{\pi\alpha}{2}), \qquad A_2 = \frac{3c_{nl}}{8}E_r\,\omega_0^{\alpha-1}\sin(\frac{\pi\alpha}{2}), \quad C = \frac{f^2}{4\,\omega_0^2},\\ &B_1 = \Delta - \frac{c_l}{2}E_r\,\omega_0^{\alpha-1}\,\cos(\frac{\pi\alpha}{2}), \quad B_2 = -\frac{3}{4}\left(c_{nl}\,E_r\,\omega_0^{\alpha-1}\,\cos(\frac{\pi\alpha}{2}) + \omega_0^{-1}\,k_{nl}\right).\end{aligned}$$

Hence, the steady state response amplitude is the admissible root of

$$(A_2^2 + B_2^2)a^6 + (2A_1A_2 + 2B_1B_2)a^4 + (A_1^2 + B_1^2)a^2 - C = 0, \tag{8.71}$$

which is a cubic equation in a^2. The discriminant of a cubic equation of the form $ax^3+bx^2+cx+d = 0$ is given as $\vartheta = 18abcd - 4b^3d + b^2c^2 - 4ac^3 - 27a^2d^2$. The cubic equation (8.71) has one real root when $\vartheta < 0$ and three distinct real roots when $\vartheta > 0$. The main four parameters $\{\alpha, E_r, f, \Delta\}$ dictate the value of coefficients $\{A_1, A_2, B_1, B_2, C\}$, the value of discriminant ϑ, and thus the number of admissible steady state amplitudes. We see that for fixed values of $\{\alpha, E_r, f\}$, by sweeping the detuning parameter Δ from lower to higher excitation frequency, the stable steady state amplitude bifurcates into two stable branches and one unstable branch, where they converge back to a stable amplitude by further increasing Δ. Fig. 8.8 (left) shows the bifurcation diagram by sweeping the

detuning parameter Δ and for different values of α when $E_r = 0.3$ and $f = 1$. The solid and dashed black lines are the stable and unstable amplitudes, respectively. The blue lines connect the bifurcation points (red dots) for each value of α. We see that the bifurcation points are strongly related to the value of α, meaning that by introducing extra viscosity to the system, i.e. increasing the value of α, the amplitudes bifurcate and then converge back faster. The right panel of Fig. 8.8 shows the frequency response of the system, i.e. the magnitude of steady state amplitudes versus excitation frequency. As the excitation frequency is swept to the right, the steady state amplitude increases, reaches a peak value, and then jumps down (see e.g. red dashed line for $\alpha = 0.4$). The peak amplitude and the jump magnitude decreases as α is increased.

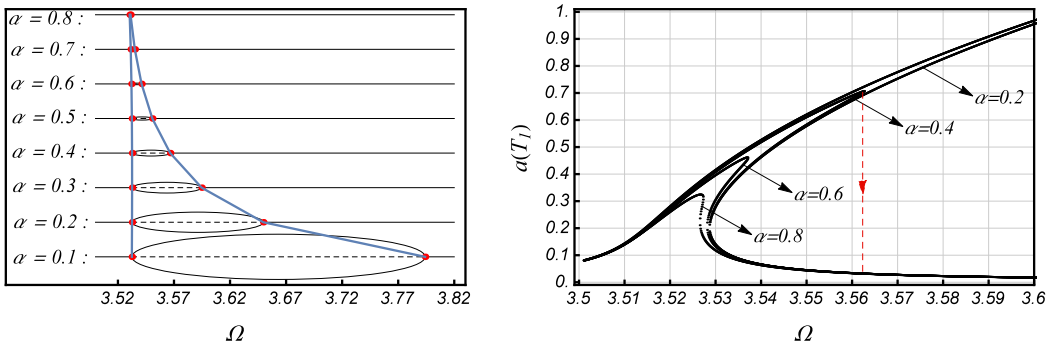

Figure 8.8: Primary resonance of the viscoelastic cantilever beam with no lumped mass at the tip. Steady state amplitude (right) and its bifurcation diagram (left) by changing the detuning parameter Δ for different values of α and $E_r = 0.3, f = 1$.

The coefficient $E_r = \frac{E_\infty}{E_\alpha}$ is the proportional contribution of fractional and pure elastic element. At a certain value while increasing this parameter, we see that the bifurcation disappears and the frequency response of system slightly changes. Fig. 8.9 shows the frequency response of the system for different values of $\{\alpha, E_r\}$ when $f = 0.5$. In each sub-figure, we let α be fixed and then plot the frequency response for $E_r = \{0.1, 0.2, \cdots, 1\}$; the amplitude peak moves down as E_r is increased. For higher values of E_r, we see that as α is increased, the amplitude peaks drift back to the left, showing a softening behavior in the system response.

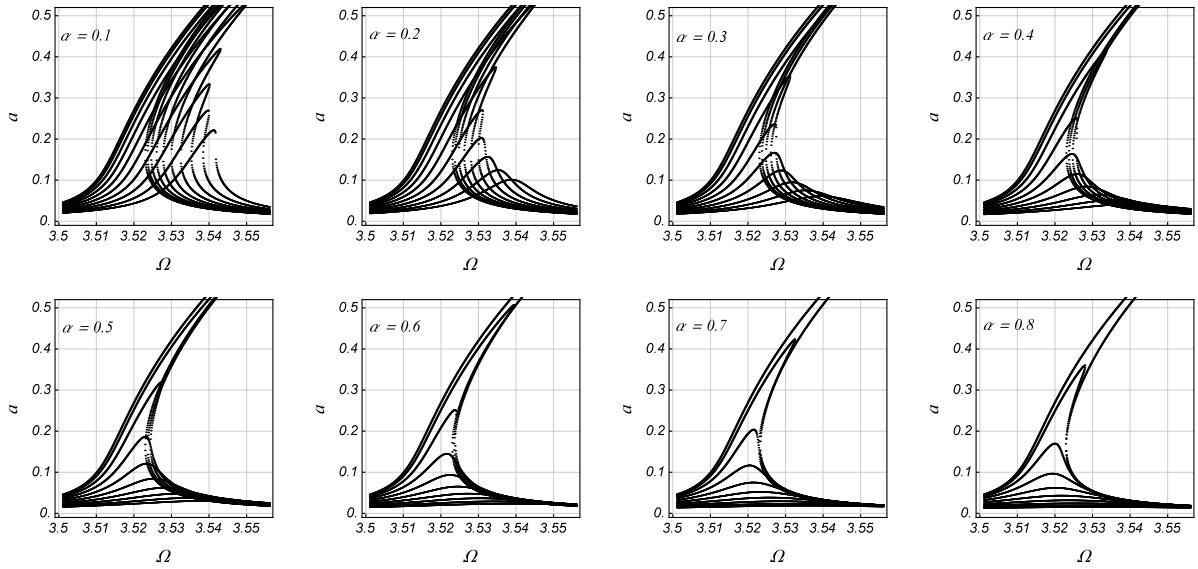

Figure 8.9: Frequency-Response curve for the case of primary resonance in the viscoelastic cantilever beam with no lumped mass at the tip. Each sub-figure corresponds to a fixed value of α and f when $E_r = \{0.1, 0.2, \cdots, 1\}$. As effect of fractional element becomes more pronounced, i.e. α and E_r increase, the curve moves down and drift to left.

8.4.1.2 Case 2: Lumped Mass At The Tip

In this case, $M = J = 1$, and thus, given the functions $\phi_1(x)$ in section 8.5, the coefficients are computed as $\mathcal{M} = 1 + 70.769J + 7.2734M$, $\mathcal{J} = 5008.25$, $\mathcal{K}_l = C_l = 98.1058$, $\mathcal{M}_b = -0.648623 - 2.69692M$, and $\mathcal{K}_{nl} = C_{nl} = 2979.66$. Similar to Case 1, we consider the following cases:

• Free Vibration, $F = 0$

Following the same steps as in Case 1, we see that the equation governing amplitude preserve its structure, but the governing equation of phase contains an extra term accommodating the m_{nl}.

$$\frac{da}{dT_1} = -E_r\,\omega_0^{\alpha-1}\sin(\alpha\frac{\pi}{2})\left(\frac{1}{2}\,c_l\,a + \frac{3}{8}\,c_{nl}\,a^3\right), \tag{8.72}$$

$$\begin{aligned}\frac{d\varphi}{dT_1} = {} & \frac{1}{2}c_l\,E_r\,\omega_0^{\alpha-1}\,\cos\left(\frac{\pi\alpha}{2}\right) + \frac{3}{4}c_{nl}\,E_r\,\omega_0^{\alpha-1}\,\cos\left(\frac{\pi\alpha}{2}\right)\,a^2 \\ & + \frac{3}{4}\,\omega_0^{-1}\,k_{nl}\,a^2 - \frac{1}{4}\,m_{nl}\,\omega_0\,a^2.\end{aligned} \tag{8.73}$$

This extra term does not significantly alter the behavior of phase and the whole system.

• Primary Resonance Case, $\Omega \approx \omega_0$

Similar to the free vibration, we see that the equation governing amplitude preserves its structure while the governing equation of phase contains an extra term accommodating the m_{nl}

$$\frac{da}{dT_1} = -E_r\,\omega_0^{\alpha-1}\,\sin(\alpha\frac{\pi}{2})\left(\frac{1}{2}\,c_l\,a + \frac{3}{8}\,c_{nl}\,a^3\right) + \frac{1}{2}f\,\omega_0^{-1}\,\sin(\Delta T_1 - \varphi), \tag{8.74}$$

$$a\,\frac{d\varphi}{dT_1} = \frac{1}{2}c_l\,E_r\,\omega_0^{\alpha-1}\,\cos(\frac{\pi\alpha}{2})\,a + \frac{3}{4}c_{nl}\,E_r\,\omega_0^{\alpha-1}\,\cos(\frac{\pi\alpha}{2})\,a^3 + \frac{3}{4}\,\omega_0^{-1}\,k_{nl}\,a^3 \tag{8.75}$$
$$- \frac{1}{2}f\,\omega_0^{-1}\,\cos(\Delta T_1 - \varphi) - \frac{1}{4}\,m_{nl}\,\omega_0\,a^3.$$

Transforming the equations into an autonomous system by letting $\gamma = \Delta T_1 - \varphi$, we obtain the governing equation of steady state solution as

$$\left[\frac{c_l}{2}E_r\,\omega_0^{\alpha-1}\,\sin(\frac{\pi\alpha}{2})\,a + \frac{3c_{nl}}{8}E_r\,\omega_0^{\alpha-1}\,\sin(\frac{\pi\alpha}{2})\,a^3\right]^2 \tag{8.76}$$
$$\left[\left(\Delta - \frac{c_l}{2}E_r\,\omega_0^{\alpha-1}\,\cos(\frac{\pi\alpha}{2})\right)a - \frac{3}{4}\left(c_{nl}\,E_r\,\omega_0^{\alpha-1}\,\cos(\frac{\pi\alpha}{2}) + \omega_0^{-1}\,k_{nl} + \frac{1}{3}\,m_{nl}\,\omega_0\right)a^3\right]^2 = \frac{f^2}{4\,\omega_0^2},$$

which, similar to Case 1, can be written as

$$(A_2^2 + B_2^2)a^6 + (2A_1A_2 + 2B_1B_2)a^4 + (A_1^2 + B_1^2)a^2 - C = 0,$$

where all the A_1, A_2, B_1, and C are the same as in Case 1, but

$$B_2 = -\frac{3}{4}\left(c_{nl}\,E_r\,\omega_0^{\alpha-1}\,\cos(\frac{\pi\alpha}{2}) + \omega_0^{-1}\,k_{nl} + \frac{1}{3}\,m_{nl}\,\omega_0\right).$$

The corresponding cubic equation can be solved to obtain the bifurcation diagram and also the frequency response of the system. However, in addition to Case 1, we have an extra parameter m_{nl} which affects the response of the system.

Remark 8.4.1. *The model parameters in fact describe the properties of the system of interest. As the system undergoes cyclic loading, the development of damage due to initial imperfections and defects inside the material changes the system properties, and thus, it's response. This can be used to develop a machine learning tool that takes the observed experimental data as input and then, predicts the system health by inferring model parameters. The developed framework here provides a forward simulation to construct many cases of training sets for the learning tool.*

8.5 Eigenvalue Problem of Linear Model

The assumed modes $\phi_i(s)$ in discretization (8.46) are obtained by solving the corresponding eigenvalue problem of free vibration of undamped linear counterparts to our model. Thus, the dimensionless linearized undamped equation of motion takes the form

$$\frac{\partial^2}{\partial t^2} v(s,t) + \frac{\partial^4}{\partial s^4} v(s,t) = 0. \tag{8.77}$$

subject to linearized boundary conditions:

$$\begin{aligned} v(0,t) &= 0, & v''(1,t) &= -J\,\ddot{v}'(1,t), \\ v'(0,t) &= 0, & v'''(1,t) &= M\,\ddot{v}(1,t), \end{aligned} \tag{8.78}$$

where $\dot{(\,)} = \frac{d}{dt}$ and $(\,)' = \frac{d}{ds}$. We derive the corresponding eigenvalue problem by applying the separation of variables, i.e. $v(x,t) = X(s)T(t)$ to (8.77). Therefore,

$$\begin{aligned} &\ddot{T}(t)X(s) + T(t)X''''(s) = 0, \\ &\frac{\ddot{T}(t)}{T(t)} + \frac{X''''(s)}{X(s)} = 0, \\ &\frac{\ddot{T}(t)}{T(t)} = -\frac{X''''(s)}{X(s)} = \lambda, \end{aligned} \tag{8.79}$$

which gives the following equations

$$\ddot{T}(t) + \omega^2 T(t) = 0, \tag{8.80}$$

$$X''''(s) - \beta^4 X(s) = 0, \tag{8.81}$$

where $\beta^4 = \omega^2$ and the boundary conditions are

$$\begin{aligned} X(0) &= 0, & X''(1) &= J\,\omega^2\,X'(1), \\ X'(0) &= 0, & X'''(1) &= -M\,\omega^2\,X(1). \end{aligned}$$

the solution to (8.81) is of the form $X(s) = A\sin(\beta s) + B\cos(\beta s) + C\sinh(\beta s) + D\cosh(\beta s)$, where $C = -A$ and $D = -B$, using the boundary conditions at $s = 0$. Therefore,

$$X(s) = A\left(\sin(\beta s) - \sinh(\beta s)\right) + B\left(\cos(\beta s) - \cosh(\beta s)\right).$$

Applying the first bondary condition at $s = 1$, i.e. $X''(1) = J\,\omega^2\,X'(1)$ gives

$$B = -\frac{\sin(\beta) + \sinh(\beta) + J\beta^3(\cos(\beta) - \cosh(\beta))}{\cos(\beta) + \cosh(\beta) - J\beta^3(\sin(\beta) - \sinh(\beta))}A,$$

that results in

$$X(s) = A\left[(\sin(\beta s) - \sinh(\beta s)) - \frac{\sin(\beta) + \sinh(\beta) + J\beta^3(\cos(\beta) - \cosh(\beta))}{\cos(\beta) + \cosh(\beta) - J\beta^3(\sin(\beta) - \sinh(\beta))}\,(\cos(\beta s) - \cosh(\beta s))\right].$$

Finally, using the second boundary condition at $s = 1$ gives the following transcendental equation to solve for β's for the case that $M = J = 1$:

$$-\left(1 + \beta^4 + \cos(\beta)\cosh(\beta)\right) + \beta\,(\sin(\beta)\cosh(\beta) - \cos(\beta)\sinh(\beta)) \tag{8.82}$$

$$+\beta^3\,(\sin(\beta)\cosh(\beta) - \sinh(\beta)\cosh(\beta)) + \beta^4\,(\sin(\beta)\sinh(\beta) + \cos(\beta)\cosh(\beta)) = 0. \tag{8.83}$$

The first eigenvalue is computed as $\beta_1^2 = \omega_1 = 1.38569$, which results to the following first normalized eigenfunction, given in Fig. 8.10.

$$X_1(s) = 5.50054\sin(\beta_1 s) - 0.215842\cos(\beta_1 s) - 5.50054\sinh(\beta_1 s) + 0.215842\cosh(\beta_1 s),$$

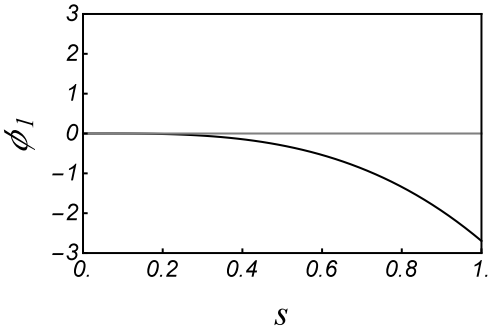

Figure 8.10: The first eigenfunctions, $X_1(s)$, of the undamped linear counterpart of our model. It is used as the spatial functions in the single mode approximation.

We note that (8.82) reduces to $1 + \cos(\beta)\cosh(\beta) = 0$ for the case that there is no lumped mass at the tip of beam; this in fact gives the natural frequencies of a linear cantilever beam. In this case, the first eigenvalue is computed as $\beta_1^2 = \omega_1 = 3.51602$, which results to the following first normalized eigenfunction, given in Fig. 8.11.

$$X_1(s) = 0.734096 \sin(\beta_1 s) - \cos(\beta_1 s) - 0.734096 \sinh(\beta_1 s) + \cosh(\beta_1 s).$$

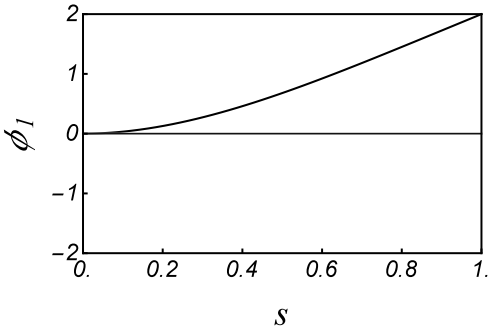

Figure 8.11: The first eigenfunctions, $X_1(s)$, of the undamped linear counterpart of our model with no lumped mass at the tip. It is used as the spatial functions in the single mode approximation.

CHAPTER 9

SUMMARY AND FUTURE WORKS

Fractional PDEs are the proper mathematical models to describe the anomalous behavior in a wide range of physical phenomenon. The order of fractional derivatives in these equations are considered as an additional set of model parameter, whose values are strongly tied to the experimental observations. Estimation of parameters in fractional models is not a trivial procedure since the main parameters, i.e. fractional derivatives appear as the order of derivatives. This imposes an extra challenge in developing proper mathematical frameworks, which are computationally efficient to handle such inverse problems. More importantly, the inherent randomness of experimental observations introduce uncertainty in the order of derivatives and thus model output; such uncertainty demands an out-of-box thinking to be assessed. Theses challenges even become more important to resolve as the inherent bottleneck of non-locality in fractional PDEs leads to expensive computations with excessive computer-memory storage requirements and insufficient computational accuracy. Utilization of local numerical methods, such as finite difference method can take long time on ordinary computers even for one dimensional problems with a single derivative orders. These lead to more serious issue in higher dimensional nonlinear problems with distributed order derivatives, where the problem os defined over a complex geometry.

To overcome these challenges, we first develop a Petrov-Galerkin spectral element method, which can solve fractional boundary value problems in each time step of numerical time integration techniques. In chapter 2, we developed a new C^0-continuous Petrov-Galerkin spectral element method for the one-sided space-fractional Helmholtz equation ${}_0\mathcal{D}_x^{\alpha}u(x) - \lambda u(x) = f(x)$, $\alpha \in (1,2)$, subject to homogeneous boundary conditions. We obtained a weak form, in which the entire fractional derivative load was transferred onto the test functions, allowing us to efficiently employ the standard modal spectral element bases while incorporating Jacobi poly-fractonomials as the test functions. We seamlessly extended the standard procedure of assembling to *non-local assembling* in order to construct the global linear system from local (elemental) mass/stiffness matrices and

non-local history matrices. The key to the efficiency of the developed PG method is twofold: i) our formulation allows the construction of elemental mass and stiffness matrices in the standard domain $[-1, 1]$ once, and ii) we efficiently obtain the non-local (history) stiffness matrices, in which the non-locality is presented *analytically*. We also investigated local basis/test functions in addition to local basis with global test functions. We demonstrated that the former choice leads to a better-conditioned system and approximability in the spectral element formulation when higher polynomial orders are needed. Moreover, we showed the exponential rate of convergence considering smooth solutions as well as singular solutions with interior singularity; also, the spectral (algebraic) rate of convergence in singular solutions with singularities at boundaries. We also presented the retrieval process of history matrices on uniform grids, which results in faster and more efficient construction and solution of the linear system compared to the on-line computation. In addition, we constructed two non-uniform grids over the computational domain (namely, kernel-driven and geometrically progressive grids), and demonstrated the effectiveness of the non-uniform grids in accurately capturing singular solutions, using fewer number of elements and higher order polynomials. We finally performed a systematic numerical study of non-local effects via both full and partial (history) fading in order to better enhance the computational efficiency of the scheme.

In chapter 3, we developed two spectrally-accurate schemes, namely the Petrov-Galerkin spectral method and the fractional spectral collocation method for distributed order fractional differential equations. The two schemes were constructed based on the recently developed spectral theory for fractional Sturm-Liouville problems (FSLPs). In the Petrov-Galerkin method, we employed the Jacobi poly-fractonomials as the bases, which are the eigenfunctions of FSLP-I, and the poly-fractonomial eigenfunctions of FSLP-II as the test functions. We carried out the discrete stability analysis of the proposed scheme employing some equivalent/bilinear-induced norms based on the defined distributed Sobolev spaces and their associated norms. In addition, we performed a convergence study of the proposed scheme. In the collocation method, we employed fractional Lagrange interpolants satisfying the Kronecker delta property at the collocation points, and then we obtained the corresponding distributed differentiation matrices to discretize the strong problem.

The existing schemes in the literature are mostly employing finite difference methods. The main challenge in these methods, in comparison to spectral methods, is the history calculation as well as extensive memory allocation while they deliver fixed algebraic accuracies. The recent spectral theory on fractional Sturm-Liouville problems (FSLPs) in [186] naturally motivates the use of Petrov-Galerkin spectral methods, where the arising bilinear forms are comprised of left- and right-sided fractional derivatives. The eigen-functions of FSLPs can be employed naturally as the bases and test spaces, where their left- and right-sided derivatives are obtained analytically. These functions consist of a polynomial part and a fractional part, where the former leaves the fractional order, μ, as a free parameter to capture solution singularities, hence, to tune up the accuracy of the scheme from being algebraically convergent to exponential convergent. In fact, the Case-III of numerical examples demonstrated how a proper choice of fractional part of the bases provides the exact solution with only one term expansion. Furthermore, we proved that the distributed bilinear form can be approximated with a spectral/exponential accuracy using a proper quadrature rule. The PG spectral method treats the nonlocal effects efficiently through a global spectral method and provides a nice mathematical framework for performing theoretical studies, however, treating nonlinear problems remains a challenge. To this end, we constructed a spectrally accurate fractional spectral collocation method employing fractional Lagrange interpolants, where for linear problems the two developed schemes become equivalent in terms of the rate of convergence.

The distribution function, $\phi(\alpha)$, defined the distribution of the differentiation fractional-order, α, and it could arbitrarily confine the domain over which the fractional differentiation is taken. If ϕ was integrable in a compact support in $[\alpha_{min}, \alpha_{max}]$, then $H^{\alpha_{min}}(\mathbb{R}) \supseteq {}^{\phi}\mathcal{H}(\mathbb{R}) \supseteq H^{\alpha_{max}}(\mathbb{R})$. Hence, ϕ could play a crucial rule in defining the underlying solution space properly. In anomalous physical processes, the distribution function can be obtained from experimental data, where the inherent data uncertainty can be incorporated through the ϕ obtained from the observed data, hence, leading to a robust data-driven simulation framework for multi-physics problems.

In chapter 4, we combined the two modal and nodal expansions, and developed a pseudo-spectral accurate scheme based where we employed two types of fractional Lagrange interpolants as the

nodal basis and test functions in the weak sense of problem and obtained the corresponding weak distributed differentiation matrix. We further investigated the condition number of the resulting linear system for different choices of distribution function and interpolation points. We showed that among the considered choices, the roots of Jacobi polynomials leads to better condition number. Moreover, we introduced a set of distributed pre-conditioners based on the distribution function in the DODEs and Jacobi poly-fractonomials of second kind. We showed that applying the designed pre-conditioners can further improve the condition number of the linear system. The constructed basis functions are comprised of a polynomial part and a fractional part, where the former leaves the fractional order, μ, as a free parameter to capture solution singularities. We showed in the example of initial value problems that by tunning the interpolation parameter, we can achieve the highest rate of convergence with minimal degrees of freedom.

The developed Petrov-Galerkin (PG) spectral method in chapter 3 has also the benefit of spectral accuracy in solving DODEs. However, the remaining challenge was to treat nonlinear problems. We showed through several examples of $(1+1)$-D and $(1+2)$-D time dependent space distributed-order nonlinear problems, that the proposed pseudo-spectral scheme can efficiently treat nonlinearity, while keeping the same rate of convergence. We computed the associated nonlinear vectors with less complexity, using the Kronecker delta property of the basis and test functions. Moreover, in comparison to fractional collocation methods, we showed that the proposed scheme leads to a better conditioning, yet still requires performing additional quadrature integration in spatial domain. The current scheme also benefits from the well-established mathematical framework of Babuška-Lax-Milgram theorem, which can be used along with the defined underlying distributed sobolev space and the sharp estimates, provided by the equivalent/bilinear-induced associated norms, to perform the analysis of scheme. We intent to carry out and report these analysis in our future works.

In chapter 5, we extended the derivation to fractional PDEs and developed a Petrov-Galerkin spectral method for high dimensional temporally-distributed fractional partial differential equations with two-sided derivatives in a space-time hypercube. We employed Jacobi poly-fractonomials and Legendre polynomials as the temporal and spatial basis/test functions, respectively. To solve the

corresponding Lyapunov linear system, we further formulated a fast linear solver and performed the corresponding discrete stability and error analysis. We also carried out several numerical simulations to examine the performance of the method.

In order to formulate a sensitivity frame work, in chapter 6, we developed a fractional sensitivity equation method (FSEM) in order to analyze the sensitivity of fractional models (FIVPs, FBVPs, and FPDEs) with respect to their parameters. We derived the adjoint governing dynamics of sensitivity coefficients, i.e. fractional sensitivity equations (FSEs), by taking the partial derivative of FDE with respect to the model parameters, and showed that they preserve the structure of original FDE. We also introduced a new fractional operator, associated with logarithmic-power law kernel, for the first time in the context of FSEM. We extended the existing proper underlying function spaces to respect the extra regularities imposed by FSEs and proved the well-posedness of problem. Moreover, we developed a Petrov-Galerkin (PG) spectral method by employing Jacobi polyfractonomials and Legendre polynomials as basis/test functions, and proved its stability. We further used the developed FSEM to formulate an optimization problem in order to construct the fractional model by estimating the model parameters. We defined two types of model error as objective functions and proposed a two-stages search algorithm to minimize them. We presented the steps of iterative algorithm in a pseudo code. Finally, we examined the performance of proposed numerical scheme in solving coupled FPDE and FSEs, where we numerically study the convergence rate of error. We also investigated the efficiency of developed iterative algorithm in estimating the derivative order for different cases of fractional models.

In chapter 7, we developed a mathematical framework to numerically quantify the solution uncertainty of a stochastic FPDE, associated with the randomness of model parameters. The stochastic FPDE is reformulated by rendering the problem with random fractional indices, subject to additional random noise. We used the truncated Karhunen-Loéve expansion to parametrize the additive noise. Then, by employing a non-intrusive probabilistic collocation method (PCM), we propagated the associated randomness to the system response, by using Smolyak sparse grid generator to construct the set of sample point in the random space. We also formulated a forward

solver to simulate the deterministic counterpart of the stochastic problem for each realization of random variables. We showed that the deterministic problem is mathematically well-posed in a weak sense. Furthermore, by employing Jacobi poly-fractonomials and Legendre polynomials as the temporal and spatial basis/test functions, respectively, we developed a Petrove-Galerkin spectral method to solve the deterministic problem in the physical domain. We also proved that the inf-sup condition holds for the proposed numerical scheme, and thus, it is stable. By considering several numerical examples with low- to high-dimensional random spaces, we examined the performance of our stochastic discretization. We showed that in each case, PCM converges very fast to a very high level of accuracy with very few number of sampling.

Finally, in chapter 8, we further apply the developed mathematical tools to investigate the nonlinear vibration of a viscoelastic cantilever beam. In the absence of external excitation, the response amplitude of free vibration reveals a super-sensitivity with respect to the fractional order. Primary resonance of the beam subject to base excitation also discloses a softening behavior in the frequency response of the beam. These unique features can be used further to build a vibration-based health monitoring platform.

9.0.1 Future Works

Many open issues remain in this field to be addressed in our future work. Here, we list some of them as follows:

• **PG spectral element method for two sided derivatives:** The one-sided Helmholtz equation in chapter 2 can be extended to its two-sided version. However, in that case due to the presence of the left- and right-sided derivatives, the corresponding integration-by-parts require the test functions to vanish at both boundaries. Therefore, the introduced choices of test functions in this work would not form a proper test space for the two-sided version. This requires further investigation as future work.

• **Fractional operator with logarithmic power-law kernel:** The sensitivity analysis of fractional differential equations introduced new class of integro-differential operators with weaker singular

kernel of logarithmic power-law type. Proper development of calculus for these operators is needed to efficiently deal with computation of sensitivity fields. Following the same derivation as in chapter 6, we can take the derivative of fractional Strum-Liouville eigenvalue problem to obtain a new class of eigenvalue problems for these operators. This is still an open problem to be investigated further.

• **Application to bio-tissue mechanics:** Many application of viscoelastic modeling are in bio-engineering and bio-tissue mechanics. They also include problems, where human body undergoes certain dynamical loading due to environmental/work conditions. The excessive body motion can adversely induce undesired vibration to vital organs such as human brain, leading to irrecoverable damages. Fractional models provide a tool to model and study the viscoelastic behavior of human organs. The developed framework in this thesis can be further employed to find accurate parameters of these model, and thus calculating safe operating regions, within which, the organ would experience less damage. Such application requires the extension of developed parameter estimation and uncertainty framework to the case with limited real data sets as they are not largely available for human bodies.

• **Modal analysis of fractional viscoelasticity:** The eigenfunctions of fractional time derivatives are not exponential functions anymore. For linear fractional oscillator, the Mittag Leffler functions can be used as they incorporate memory dependence. But, in more complex viscoelastic modeling, which lead to nonlinearity in fractional differential equation, it is not very clear ho we can use these functions. The extension of modal analysis for viscoelastic materials as well as interactive systems with viscoelastic behavior (such as elastic solid immersed in viscous fluid) can be further investigated in future works.

• **Variable order fractional model:** The order of fractional models directly relates to the distinctive characteristics of underlying physical phenomena. Over a course of time, these properties changes, and thus the fractional models should be re-calibrated. Instead, a variable order model can be developed, where the evolution of fractional orders are such that they comply with the time evolution of physical properties. This will requires additional dynamics, which models/describe the change of derivative orders in time.

• **Application of real data in the developed fractional model construction framework:** In general, the inverse problem of parameter estimation is an ill-posed problem. Even though we showed computationally that the introduced model errors as the objective function to minimize has solely one minimum, we should extent the analysis to mathematically prove the existence of minimum(s). More importantly, the method should be examined by real data sets, as their incompleteness imposes extra challenge in minimizing the objective function.

BIBLIOGRAPHY

BIBLIOGRAPHY

[1] Acar, Gizem D & Brian F Feeny. 2017. Bend-bend-twist vibrations of a wind turbine blade. *Wind Energy* .

[2] Afzali, Fatemeh, Gizem D Acar & Brian F Feeny. 2017. Analysis of the periodic damping coefficient equation based on floquet theory. In *Asme 2017 international design engineering technical conferences and computers and information in engineering conference*, V008T12A050–V008T12A050. American Society of Mechanical Engineers.

[3] Afzali, Fatemeh, Onur Kapucu & Brian F Feeny. 2016. Vibrational analysis of vertical-axis wind-turbine blades. In *Asme 2016 international design engineering technical conferences and computers and information in engineering conference. american society of mechanical engineers*, .

[4] Ainsworth, M. & J. T. Oden. 2011. *A posteriori error estimation in finite element analysis*, vol. 37.

[5] Askey, R. & J. Fitch. 1969. Integral representations for Jacobi polynomials and some applications. *Journal of Mathematical Analysis and Applications* 26. 411–437.

[6] Atanackovic, T. M., S. Pilipovic & D. Zorica. 2009. Time distributed-order diffusion-wave equation. i. Volterra-type equation. *Proceedings of the Royal Society A: Mathematical, Physical and Engineering Science* 465(2106). 1869–1891.

[7] Atanackovic, Teodor M. 2003. On a distributed derivative model of a viscoelastic body. *Comptes Rendus Mecanique* 331(10). 687–692.

[8] Atanackovic, Teodor M, Stevan Pilipovic, Bogoljub Stankovic & Dusan Zorica. 2014. *Fractional calculus with applications in mechanics: Vibrations and diffusion processes*. John Wiley & Sons.

[9] Atanackovic, Teodor M, Stevan Pilipovic, Bogoljub Stankovic & Dusan Zorica. 2014. *Fractional calculus with applications in mechanics: vibrations and diffusion processes*. John Wiley & Sons.

[10] Atanackovic, TM. 2002. A generalized model for the uniaxial isothermal deformation of a viscoelastic body. *Acta Mechanica* 159(1-4). 77–86.

[11] Atanackovic, T.M., L. Oparnica & S. Pilipović. 2009. Distributional framework for solving fractional differential equations. *Integral Transforms and Special Functions* 20(3-4). 215–222.

[12] Atanackovic, T.M., S. Pilipovic & D. Zorica. 2009. Existence and calculation of the solution to the time distributed order diffusion equation. *Physica Scripta* 2009(T136). 014012.

[13] Babuška, I. & P. Chatzipantelidis. 2002. On solving elliptic stochastic partial differential equations. *Computer Methods in Applied Mechanics and Engineering* 191(37). 4093–4122.

[14] Babuška, I., F. Nobile & R. Tempone. 2007. A stochastic collocation method for elliptic partial differential equations with random input data. *SIAM Journal on Numerical Analysis* 45(3). 1005–1034.

[15] Babuška, I. & M. Suri. 1994. The p and h-p versions of the finite element method, basic principles and properties. *SIAM review* 36(4). 578–632.

[16] Babuska, I., R. Tempone & G. E. Zouraris. 2004. Galerkin finite element approximations of stochastic elliptic partial differential equations. *SIAM Journal on Numerical Analysis* 42(2). 800–825.

[17] Babuška, I., R. Tempone & G. E. Zouraris. 2005. Solving elliptic boundary value problems with uncertain coefficients by the finite element method: the stochastic formulation. *Computer methods in applied mechanics and engineering* 194(12). 1251–1294.

[18] Baeumer, B., D. A. Benson, M. M. Meerschaert & S. W. Wheatcraft. 2001. Subordinated advection-dispersion equation for contaminant transport. *Water Resources Research* 37(6). 1543–1550.

[19] Baeumer, B., D. A. Benson, M.M. Meerschaert & S. W. Wheatcraft. 2001. Subordinated advection-dispersion equation for contaminant transport. *Water Resources Research* 37(6). 1543–1550.

[20] Bagley, RL & PJ Torvik. 2000. On the existence of the order domain and the solution of distributed order equations-part i. *International Journal of Applied Mathematics* 2(7). 865–882.

[21] Bagley, RL & PJ Torvik. 2000. On the existence of the order domain and the solution of distributed order equations-part ii. *International Journal of Applied Mathematics* 2(8). 965–988.

[22] Bagley, Ronald L & Peter J Torvik. 1986. On the fractional calculus model of viscoelastic behavior. *Journal of Rheology* 30(1). 133–155.

[23] BAGLEY, RONALDL. 1989. Power law and fractional calculus model of viscoelasticity. *AIAA journal* 27(10). 1412–1417.

[24] Barthelmann, V., E. Novak & K. Ritter. 2000. High dimensional polynomial interpolation on sparse grids. *Advances in Computational Mathematics* 12(4). 273–288.

[25] Beck, James Vere & Kenneth J Arnold. 1977. *Parameter estimation in engineering and science*. James Beck.

[26] Benson, D. A., S. W. Wheatcraft & M. M. Meerschaert. 2000. Application of a fractional advection-dispersion equation. *Water Resources Research* 36(6). 1403–1412.

[27] Beskos, A., A. Jasra, K. Law, R. Tempone & Y. Zhou. 2017. Multilevel sequential monte carlo samplers. *Stochastic Processes and their Applications* 127(5). 1417–1440.

[28] Bhrawy, A. H., E. H. Doha, D. Baleanu & S. S. Ezz-Eldien. 2015. A spectral tau algorithm based on Jacobi operational matrix for numerical solution of time fractional diffusion-wave equations. *Journal of Computational Physics* 293. 142–156.

[29] Bischof, C., P. Khademi, A. Mauer-Oats & A. Carle. 1996. Adifor 2.0: Automatic differentiation of fortran 77 program. *IEEE Computaitonal Science and Engineering* .

[30] Bischof, C., B. Land & A. Vehreschild. 2003. Automatic differentiation for matlab program, 2:50–53. Proceeding in applied mathematics and mechanics.

[31] Bischof, C., L. Roh & A. Mauer-Oats. 1997. Adic: an extensible automatic differentiation tool for ansi-c. *Software Practice and Experience* .

[32] Bonet, Javier & Richard D Wood. 1997. *Nonlinear continuum mechanics for finite element analysis*. Cambridge university press.

[33] Cao, J. & C. Xu. 2013. A high order schema for the numerical solution of the fractional ordinary differential equations. *Journal of Computational Physics* 238(1). 154–168.

[34] Caputo, Michelle. 2001. Distributed order differential equations modelling dielectric induction and diffusion. *Fractional Calculus and Applied Analysis* 4(4). 421–442.

[35] Carella, Alfredo Raúl. 2012. *Spectral finite element methods for solving fractional differential equations with applications in anomalous transport*: Norwegian University of Science and Technology dissertation.

[36] del Castillo-Negrete, D., B. A. Carreras & V. E. Lynch. 2004. Fractional diffusion in plasma turbulence. *Physics of Plasmas (1994-present)* 11(8). 3854–3864.

[37] Chakraborty, P., M. M. Meerschaert & C. Y. Lim. 2009. Parameter estimation for fractional transport: A particle-tracking approach. *Water resources research* 45(10).

[38] Chen, S., F. Liu, X. Jiang, I. Turner & K. Burrage. 2016. Fast finite difference approximation for identifying parameters in a two-dimensional space-fractional nonlocal model with variable diffusivity coefficients. *SIAM Journal on Numerical Analysis* 54(2). 606–624.

[39] Chen, S., J. Shen & L. Wang. 2014. Generalized Jacobi functions and their applications to fractional differential equations. *arXiv preprint arXiv:1407.8303* .

[40] Cho, Y., I. Kim & D. Sheen. 2015. A fractional-order model for minmod millennium. *Mathematical biosciences* 262. 36–45.

[41] Cullen, A. C. & H. C. Frey. 1999. *Probabilistic techniques in exposure assessment: a handbook for dealing with variability and uncertainty in models and inputs*. Springer Science & Business Media.

[42] Dehghan, M., M. Abbaszadeh & A. Mohebbi. 2016. Legendre spectral element method for solving time fractional modified anomalous sub-diffusion equation. *Applied Mathematical Modelling* 40(5). 3635–3654.

[43] Del Moral, P., A. Doucet & A. Jasra. 2006. Sequential monte carlo samplers. *Journal of the Royal Statistical Society: Series B (Statistical Methodology)* 68(3). 411–436.

[44] Deng, W.H. & J.S. Hesthaven. 2013. Local discontinuous Galerkin methods for fractional diffusion equations. *ESAIM: Mathematical Modelling and Numerical Analysis (Accepted)* .

[45] Der Kiureghian, Armen & Ove Ditlevsen. 2009. Aleatory or epistemic? does it matter? *Structural Safety* 31(2). 105–112.

[46] Diethelm, K. & N. J. Ford. 2001. Numerical solution methods for distributed order differential equations. *Fractional Calculus and Applied Analysis* 4. 531–542.

[47] Diethelm, K. & N. J. Ford. 2009. Numerical analysis for distributed-order differential equations. *Journal of Computational and Applied Mathematics* 225(1). 96–104.

[48] Diethelm, K., N. J. Ford & A. D. Freed. 2004. Detailed error analysis for a fractional Adams method. *Numerical Algorithms* 36(1). 31–52.

[49] Diethelm, Kai & Neville J Ford. 2009. Numerical analysis for distributed-order differential equations. *Journal of Computational and Applied Mathematics* 225(1). 96–104.

[50] Duong, P. L. T., E. Kwok & M. Lee. 2016. Deterministic analysis of distributed order systems using operational matrix. *Applied Mathematical Modelling* 40(3). 1929–1940.

[51] Ern, A. & J. Guermond. 2013. *Theory and practice of finite elements*, vol. 159. Springer Science & Business Media.

[52] Ervin, V. J. & J. P. Roop. 2006. Variational formulation for the stationary fractional advection dispersion equation. *Numer. Methods Partial Differential Equations* 22(3). 558–576.

[53] Ervin, V. J. & J. P. Roop. 2007. Variational solution of fractional advection dispersion equations on bounded domains in R^d. *Numerical Methods for Partial Differential Equations* 23(2). 256.

[54] Fishman, G. S. 1996. Monte carlo: Concepts, algorithms, and applications.

[55] Fix, GJ & JP Roof. 2004. Least squares finite-element solution of a fractional order two-point boundary value problem. *Computers & Mathematics with Applications* 48(7). 1017–1033.

[56] Foo, J., X. Wan & G. E. Karniadakis. 2008. The multi-element probabilistic collocation method (ME-PCM): Error analysis and applications. *J. Comput. Phys.* 227. 9572–9595.

[57] Ford, N. J., M. L. Morgado & M. Rebelo. 2014. A numerical method for the distributed order time-fractional diffusion equation. In *Fractional differentiation and its applications (icfda), 2014 international conference on*, 1–6. IEEE.

[58] Ford, N. J., M. L. Morgado & M. Rebelo. 2015. An implicit finite difference approximation for the solution of the diffusion equation with distributed order in time. *Electronic Transactions on Numerical Analysis* 44. 289–305.

[59] Fung, Yuan-cheng. 2013. *Biomechanics: mechanical properties of living tissues*. Springer Science & Business Media.

[60] Gao, G., H. Sun & Z. Sun. 2015. Some high-order difference schemes for the distributed-order differential equations. *Journal of Computational Physics* 298. 337–359.

[61] Gao, G. & Z. Sun. 2015. Two alternating direction implicit difference schemes with the extrapolation method for the two-dimensional distributed-order differential equations. *Computers & Mathematics with Applications* 69(9). 926–948.

[62] Gao, G. & Z. Sun. 2015. Two unconditionally stable and convergent difference schemes with the extrapolation method for the one-dimensional distributed-order differential equations. *Numerical Methods for Partial Differential Equations* .

[63] Ghanem, R. G. & P. D Spanos. 2003. *Stochastic finite elements: a spectral approach*. Courier Corporation.

[64] Ghazizadeh, H. R., A. Azimi & M. Maerefat. 2012. An inverse problem to estimate relaxation parameter and order of fractionality in fractional single-phase-lag heat equation. *International Journal of Heat and Mass Transfer* 55(7). 2095–2101.

[65] Gorenflo, R., F. Mainardi, D. Moretti & P. Paradisi. 2002. Time fractional diffusion: a discrete random walk approach. *Nonlinear Dynamics* 29(1-4). 129–143.

[66] Hamdan, MN & MHF Dado. 1997. Large amplitude free vibrations of a uniform cantilever beam carrying an intermediate lumped mass and rotary inertia. *Journal of Sound and Vibration* 206(2). 151–168.

[67] Hanert, Emmanuel. 2010. A comparison of three eulerian numerical methods for fractional-order transport models. *Environmental fluid mechanics* 10(1-2). 7–20.

[68] Hashim, I., O. Abdulaziz & S. Momani. 2009. Homotopy analysis method for fractional ivps. *Communications in Nonlinear Science and Numerical Simulation* 14(3). 674–684.

[69] Hu, X., F. Liu, I. Turner & V. Anh. 2015. An implicit numerical method of a new time distributed-order and two-sided space-fractional advection-dispersion equation. *Numerical Algorithms* 1–15.

[70] Huang, J, Y Tang & L Vazquez. 2012. Convergence analysis of a block-by-block method for fractional differential equations. *Numer. Math. Theor. Methods Appl.* 5(2). 229–241.

[71] Inc, M. 2008. The approximate and exact solutions of the space-and time-fractional Burgers equations with initial conditions by variational iteration method. *Journal of Mathematical Analysis and Applications* 345(1). 476–484.

[72] Ionescu, C, A Lopes, D Copot, JAT Machado & JHT Bates. 2017. The role of fractional calculus in modelling biological phenomena: A review. *Communications in Nonlinear Science and Numerical Simulation* .

[73] Jafari, H. & V. Daftardar-Gejji. 2006. Solving linear and nonlinear fractional diffusion and wave equations by Adomian decomposition. *Applied Mathematics and Computation* 180(2). 488–497.

[74] Jaishankar, A. & G. H. McKinley. 2013. Power-law rheology in the bulk and at the interface: quasi-properties and fractional constitutive equations. *Proceedings of the Royal Society A: Mathematical, Physical and Engineering Science* 469(2149). 20120284.

[75] Jaishankar, Aditya & Gareth H McKinley. 2013. Power-law rheology in the bulk and at the interface: quasi-properties and fractional constitutive equations. In *Proc. r. soc. a*, vol. 469 2149, 20120284. The Royal Society.

[76] Jaishankar, Aditya & Gareth H McKinley. 2014. A fractional k-bkz constitutive formulation for describing the nonlinear rheology of multiscale complex fluids. *Journal of Rheology (1978-present)* 58(6). 1751–1788.

[77] Jasra, A., K. J. Law & Y. Zhou. 2016. Forward and inverse uncertainty quantification using multilevel monte carlo algorithms for an elliptic nonlocal equation. *International Journal for Uncertainty Quantification* 6(6).

[78] Jha, R., P. K. Kaw, D. R. Kulkarni, J. C. Parikh & ADITYA Team. 2003. Evidence of lévy stable process in tokamak edge turbulence. *Physics of Plasmas (1994-present)* 10(3). 699–704.

[79] Jin, B.i, R. Lazarov, J. Pasciak & W. Rundell. 2015. Variational formulation of problems involving fractional order differential operators. *Mathematics of Computation* 84(296). 2665–2700.

[80] Jin, B.i, R. Lazarov, J. Pasciak & Z. Zhou. 2014. Error analysis of a finite element method for the space-fractional parabolic equation. *SIAM Journal on Numerical Analysis* 52(5). 2272–2294.

[81] Karniadakis, G. E. & S. J. Sherwin. 2005. *Spectral/hp element methods for cfd*. Oxford University Press (2nd edition).

[82] Kelly, J. F., D. Bolster, M. M. Meerschaert, J. D. Drummond & A. I. Packman. 2017. Fracfit: A robust parameter estimation tool for fractional calculus models. *Water Resources Research* 53(3). 2559–2567.

[83] Khader, M. M. 2011. On the numerical solutions for the fractional diffusion equation. *Communications in Nonlinear Science and Numerical Simulation* 16(6). 2535–2542.

[84] Khader, M. M. & A. S. Hendy. 2012. The approximate and exact solutions of the fractional-order delay differential equations using Legendre pseudospectral method. *International Journal of Pure and Applied Mathematics* 74(3). 287–297.

[85] Kharazmi, E. & M. Zayernouri. 2017. Fractional pseudo-spectral methods for distributed-order fractional pdes. *International Journal of Computer Mathematics* .

[86] Kharazmi, E. & M. Zayernouri. 2018. Fractional pseudo-spectral methods for distributed-order fractional pdes. *International Journal of Computer Mathematics* 1–22.

[87] Kharazmi, E., M. Zayernouri & G. E. Karniadakis. 2017. Petrov–galerkin and spectral collocation methods for distributed order differential equations. *SIAM Journal on Scientific Computing* 39(3). A1003–A1037.

[88] Kharazmi, E., M. Zayernouri & G. E. Karniadakis. 2017. A petrov–galerkin spectral element method for fractional elliptic problems. *Computer Methods in Applied Mechanics and Engineering* 324. 512–536.

[89] Kilbas, A. 2006. A., hm srivastava, jj trujillo. *Theory and applications of fractional differential equations* .

[90] Kilbass, A. A., H. M. Srivastava & J. J. Trujillo. 2006. *Theory and applications of fractional differential equations*. Amsterdam, Netherlands:Elsevier.

[91] Klages, Rainer, Günter Radons & Igor M Sokolov. 2008. *Anomalous transport: foundations and applications*. John Wiley & Sons.

[92] Knio, O. M. & O. P. Le Maitre. 2006. Uncertainty propagation in cfd using polynomial chaos decomposition. *Fluid Dynamics Research* 38(9). 616–640.

[93] Langlands, TAM & BI Henry. 2005. The accuracy and stability of an implicit solution method for the fractional diffusion equation. *Journal of Computational Physics* 205(2). 719–736.

[94] Le Maıtre, O. P., H. N. Knio, O. M. a nd Najm & R. G. Ghanem. 2004. Uncertainty propagation using wiener–haar expansions. *Journal of computational Physics* 197(1). 28–57.

[95] Le Maıtre, O. P., H. N. Najm, R. G. Ghanem & O .M. Knio. 2004. Multi-resolution analysis of wiener-type uncertainty propagation schemes. *Journal of Computational Physics* 197(2). 502–531.

[96] Li, Changpin & Fanhai Zeng. 2012. Finite difference methods for fractional differential equations. *International Journal of Bifurcation and Chaos* 22(04). 1230014.

[97] Li, Gen-guo, Zheng-you Zhu & Chang-jun Cheng. 2001. Dynamical stability of viscoelastic column with fractional derivative constitutive relation. *Applied Mathematics and Mechanics* 22(3). 294–303.

[98] Li, X. & B. Wu. 2016. A numerical method for solving distributed order diffusion equations. *Applied Mathematics Letters* 53. 92–99.

[99] Li, X. & C. Xu. 2009. A space-time spectral method for the time fractional diffusion equation. *SIAM Journal on Numerical Analysis* 47(3). 2108–2131.

[100] Li, X. & C. Xu. 2010. Existence and uniqueness of the weak solution of the space-time fractional diffusion equation and a spectral method approximation. *Communications in Computational Physics* 8(5). 1016.

[101] Li, X. & C. Xu. 2010. Existence and uniqueness of the weak solution of the space-time fractional diffusion equation and a spectral method approximation. *Communications in Computational Physics* 8(5). 1016.

[102] Lim, C. Y., M. M. Meerschaert & H. P. Scheffler. 2014. Parameter estimation for operator scaling random fields. *Journal of Multivariate Analysis* 123. 172–183.

[103] Lin, Y. & C. Xu. 2007. Finite difference/spectral approximations for the time-fractional diffusion equation. *Journal of Computational Physics* 225(2). 1533–1552.

[104] Lin, Yumin & Chuanju Xu. 2007. Finite difference/spectral approximations for the time-fractional diffusion equation. *Journal of Computational Physics* 225(2). 1533–1552.

[105] Lion, Alexander. 1997. On the thermodynamics of fractional damping elements. *Continuum Mechanics and Thermodynamics* 9(2). 83–96.

[106] Lischke, A., M. Zayernouri & G. E. Karniadakis. 2017. A petrov–galerkin spectral method of linear complexity for fractional multiterm odes on the half line. *SIAM J. Sci. Comput.* 39(3). A922–A946.

[107] Liu, S. & R. A. Canfield. 2016. Two forms of continuum shape sensitivity method for fluid–structure interaction problems. *Journal of Fluids and Structures* 62. 46–64.

[108] Liu, W. K., T. Belytschko & A. Mani. 1986. Probabilistic finite elements for nonlinear structural dynamics. *Computer Methods in Applied Mechanics and Engineering* 56(1). 61–81.

[109] Liu, W. K., T. Belytschko & A. Mani. 1986. Random field finite elements. *International journal for numerical methods in engineering* 23(10). 1831–1845.

[110] Loéve, M. 1977. *Probability theory*. New York, Springer-Verlag.

[111] Lubich, C. 1983. On the stability of linear multistep methods for volterra convolution equations. *IMA Journal of Numerical Analysis* 3(4). 439–465.

[112] Lubich, Ch. 1986. Discretized fractional calculus. *SIAM Journal on Mathematical Analysis* 17(3). 704–719.

[113] Magin, Richard L. 2006. *Fractional calculus in bioengineering*. Begell House Redding.

[114] Mainardi, F., G. Pagnini & R. Gorenflo. 2007. Some aspects of fractional diffusion equations of single and distributed order. *Applied Mathematics and Computation* 187(1). 295–305.

[115] Mainardi, Francesco & Rudolf Gorenflo. 2008. Time-fractional derivatives in relaxation processes: a tutorial survey. *arXiv preprint arXiv:0801.4914* .

[116] Mainardi, Francesco & Giorgio Spada. 2011. Creep, relaxation and viscosity properties for basic fractional models in rheology. *The European Physical Journal Special Topics* 193(1). 133–160.

[117] Martins, J., I. Kroo & J. Alonso. 2000. An automated method for sensitivity analysis using complex variables. In *Proceedings of the 38th aerospace sciences meeting*, AIAA 2000–0689. Reno, NV.

[118] Meerschaert, M. M., P. Straka, Y. Zhou & R. J. McGough. 2012. Stochastic solution to a time-fractional attenuated wave equation. *Nonlinear dynamics* 70(2). 1273–1281.

[119] Meirovitch, Leonard. 2010. *Fundamentals of vibrations*. Waveland Press.

[120] Meral, F. C., T. J. Royston & R. Magin. 2010. Fractional calculus in viscoelasticity: an experimental study. *Communications in Nonlinear Science and Numerical Simulation* 15(4). 939–945.

[121] Metzler, R. & J. Klafter. 2000. The random walk's guide to anomalous diffusion: a fractional dynamics approach. *Physics Reports* 339(1). 1–77.

[122] Miller, K. S. & B. Ross. 1993. *An introduction to the fractional calculus and fractional differential equations*. New York, NY:John Wiley and Sons, Inc.

[123] Miller, Kenneth S & Bertram Ross. 1993. An introduction to the fractional calculus and fractional differential equations .

[124] Morgado, M. & M. Rebelo. 2015. Numerical approximation of distributed order reaction–diffusion equations. *Journal of Computational and Applied Mathematics* 275. 216–227.

[125] Mullins, Joshua & Sankaran Mahadevan. 2016. Bayesian uncertainty integration for model calibration, validation, and prediction. *Journal of Verification, Validation and Uncertainty Quantification* 1(1). 011006.

[126] Naghibolhosseini, M. 2015. *Estimation of outer-middle ear transmission using DPOAEs and fractional-order modeling of human middle ear*: City University of New York, NY. dissertation.

[127] Najm, Habib N. 2009. Uncertainty quantification and polynomial chaos techniques in computational fluid dynamics. *Annual review of fluid mechanics* 41. 35–52.

[128] Nayfeh, Ali H & Dean T Mook. 2008. *Nonlinear oscillations*. John Wiley & Sons.

[129] Nobile, F., R. Tempone & C. G Webster. 2008. A sparse grid stochastic collocation method for partial differential equations with random input data. *SIAM Journal on Numerical Analysis* 46(5). 2309–2345.

[130] Novak, E. & K. Ritter. 1996. High dimensional integration of smooth functions over cubes. *Numerische Mathematik* 75(1). 79–97.

[131] Novak, E. & K. Ritter. 1999. Simple cubature formulas with high polynomial exactness. *Constructive approximation* 15(4). 499–522.

[132] Oksendal, B. 1998. *Stochastic differential equations*. Springer-Verlag.

[133] Owen, N. E., P. Challenor, P. P. Menon & S. Bennani. 2017. Comparison of surrogate-based uncertainty quantification methods for computationally expensive simulators. *SIAM/ASA Journal on Uncertainty Quantification* 5(1). 403–435.

[134] Podlubny, I. 1999. *Fractional differential equations*. San Diego, CA, USA: Academic Press.

[135] Podlubny, Igor. 1998. *Fractional differential equations: an introduction to fractional derivatives, fractional differential equations, to methods of their solution and some of their applications*, vol. 198. Academic press.

[136] Rawashdeh, E. A. 2006. Numerical solution of fractional integro-differential equations by collocation method. *Applied Mathematics and Computation* 176(1). 1–6.

[137] Rizzi, F., H. N. Najm, B. J. Debusschere, K. Sargsyan, M. Salloum, H. Adalsteinsson & O. M. Knio. 2012. Uncertainty quantification in md simulations. part I: Forward propagation. *Multiscale Modeling & Simulation* 10(4). 1428–1459.

[138] Rogosin, Sergei & Francesco Mainardi. 2014. George william scott blair–the pioneer of factional calculus in rheology. *arXiv preprint arXiv:1404.3295* .

[139] Roop, J. P. 2006. Computational aspects of fem approximation of fractional advection dispersion equations on bounded domains in r2. *Journal of Computational and Applied Mathematics* 193(1). 243–268.

[140] Rossikhin, Yuriy A & Marina V Shitikova. 1997. Applications of fractional calculus to dynamic problems of linear and nonlinear hereditary mechanics of solids. *Applied Mechanics Reviews* 50. 15–67.

[141] Rossikhin, Yuriy A & Marina V Shitikova. 2010. Application of fractional calculus for dynamic problems of solid mechanics: novel trends and recent results. *Applied Mechanics Reviews* 63(1). 010801.

[142] Roy, C. J. & W. L. Oberkampf. 2011. A comprehensive framework for verification, validation, and uncertainty quantification in scientific computing. *Computer methods in applied mechanics and engineering* 200(25). 2131–2144.

[143] Samiee, M., E. Kharazmi & M. Zayernouri. 2017. Fast spectral methods for temporally-distributed fractional PDEs. In *Spectral and high order methods for partial differential equations icosahom 2016*, 651–667. Springer.

[144] Samiee, M., E. Kharazmi, M. Zayernouri & M. M. Meerschaert. 2018. Petrov-Galerkin method for fully distributed-order fractional partial differential equations. *arXiv preprint arXiv:1805.08242* .

[145] Samiee, Mehdi, Mohsen Zayernouri & Mark M Meerschaert. 2018. A unified spectral method for fpdes with two-sided derivatives; part i: a fast solver. *Journal of Computational Physics* .

[146] Samko, S. G., A. A. Kilbas & O. I. Marichev. 1993. *Fractional integrals and derivatives: Theory and applications*. Gordon and Breach, Yverdon.

[147] Samko, Stefan G, Anatoly A Kilbas & Oleg I Marichev. 1993. Fractional integrals and derivatives: theory and applications .

[148] Sanz-Serna, J. M. 1988. A numerical method for a partial integro-differential equation. *SIAM Journal on Numerical Analysis* 25(2). 319–327.

[149] Schuss, Z. 1980. Singular perturbation methods in stochastic differential equations of mathematical physics. *Siam Review* 22(2). 119–155.

[150] Shoshani, Oriel, Steven W Shaw & Mark I Dykman. 2017. Anomalous decay of nanomechanical modes going through nonlinear resonance. *Scientific reports* 7(1). 18091.

[151] Smolyak, S. 1963. Quadrature and interpolation formulas for tensor products of certain classes of functions. *Soviet Math. Dokl.* 4. 240–243.

[152] Sobieski, J. S. 1990. Sensitivity of complex, internally coupled systems. *AIAA Journal* .

[153] Sreenivasan, K. R. & R. A. Antonia. 1997. The phenomenology of small-scale turbulence. *Annual Review of Fluid Mechanics* 29(1). 435–472.

[154] Srokowski, T. 2008. Lévy flights in nonhomogeneous media: distributed-order fractional equation approach. *Physical Review E* 78(3). 031135.

[155] Stanford, B., P. Beran & M. Kurdi. 2010. Adjoint sensitivities of time-periodic nonlinear structural dynamics via model reduction. *Computers & structures* 88(19). 1110–1123.

[156] Su, C. H. & D. Lucor. 2006. Covariance kernel representations of multidimensional second-order stochastic processes. *J. Comput. Phys.* 217(1). 82–99.

[157] Su, Y. 2015. A parallel spectral element method for fractional lorenz system. *Discrete Dynamics in Nature and Society* 2015.

[158] Sugimoto, N. 1991. Burgers equation with a fractional derivative; hereditary effects on nonlinear acoustic waves. *Journal of Fluid Mechanics* 225(631-653). 4.

[159] Sun, Z. & X. Wu. 2006. A fully discrete difference scheme for a diffusion-wave system. *Applied Numerical Mathematics* 56(2). 193–209.

[160] Suzuki, J. L., M. Zayernouri, M. L. Bittencourt & G. E. Karniadakis. 2016. Fractional-order uniaxial visco-elasto-plastic models for structural analysis. *Computer Methods in Applied Mechanics and Engineering* 308. 443–467.

[161] Svenkeson, A., B. Glaz, S. Stanton & B. J. West. 2016. Spectral decomposition of nonlinear systems with memory. *Physical Review E* 93(2). 022211.

[162] Sweilam, N. H., M. M. Khader & R. F. Al-Bar. 2007. Numerical studies for a multi-order fractional differential equation. *Physics Letters A* 371(1). 26–33.

[163] Todor, R. A. 2005. *Sparse perturbation algorithms for elliptic pde's with stochastic data*: dissertation.

[164] Torvik, Peter J & Ronald L Bagley. 1984. On the appearance of the fractional derivative in the behavior of real materials. *Journal of Applied Mechanics* 51(2). 294–298.

[165] Van Dam, Noah & Chris Rutland. 2016. Uncertainty quantification of large-eddy spray simulations. *Journal of Verification, Validation and Uncertainty Quantification* 1(2). 021006.

[166] Van Keulen, F., R. T. Haftka & N. H. Kim. 2005. Review of options for structural design sensitivity analysis. part 1: Linear systems. *Computer methods in applied mechanics and engineering* 194(30). 3213–3243.

[167] Wang, H., K. Wang & T. Sircar. 2010. A direct o (nlog 2 n) finite difference method for fractional diffusion equations. *Journal of Computational Physics* 229(21). 8095–8104.

[168] Wang, H. & D. Yang. 2013. Wellposedness of variable-coefficient conservative fractional elliptic differential equations. *SIAM Journal on Numerical Analysis* 51(2). 1088–1107.

[169] Wang, H., D. Yang & S. Zhu. 2014. Inhomogeneous dirichlet boundary-value problems of space-fractional diffusion equations and their finite element approximations. *SIAM Journal on Numerical Analysis* 52(3). 1292–1310.

[170] Wang, H. & X. Zhang. 2015. A high-accuracy preserving spectral galerkin method for the dirichlet boundary-value problem of variable-coefficient conservative fractional diffusion equations. *Journal of Computational Physics* 281. 67–81.

[171] Wang, Hong, Danping Yang & Shengfeng Zhu. 2015. A petrov–galerkin finite element method for variable-coefficient fractional diffusion equations. *Computer Methods in Applied Mechanics and Engineering* 290. 45–56.

[172] Wang, K. & H. Wang. 2011. A fast characteristic finite difference method for fractional advection–diffusion equations. *Advances in Water Resources* 34(7). 810–816.

[173] Wei, H., W. Chen, H. Sun & X. Li. 2010. A coupled method for inverse source problem of spatial fractional anomalous diffusion equations. *Inverse Problems in Science and Engineering; Formerly Inverse Problems in Engineering* 18(7). 945–956.

[174] Winter, C L. & D. M Tartakovsky. 2002. Groundwater flow in heterogeneous composite aquifers. *Water Resources Research* 38(8).

[175] Xiu, D. & J. S. Hesthaven. 2005. High-order collocation methods for differential equations with random inputs. *SIAM Journal on Scientific Computing* 27(3). 1118–1139.

[176] Xiu, D. & G. E. Karniadakis. 2002. Modeling uncertainty in steady state diffusion problems via generalized polynomial chaos. *Computer methods in applied mechanics and engineering* 191(43). 4927–4948.

[177] Xiu, D. & G. E. Karniadakis. 2002. The wiener–askey polynomial chaos for stochastic differential equations. *SIAM journal on scientific computing* 24(2). 619–644.

[178] Xu, Q. & J. Hesthaven. 2014. Discontinuous galerkin method for fractional convection-diffusion equations. *SIAM Journal on Numerical Analysis* 52(1). 405–423.

[179] Ye, H., F. Liu & V. Anh. 2015. Compact difference scheme for distributed-order time-fractional diffusion-wave equation on bounded domains. *Journal of Computational Physics* 298. 652–660.

[180] Yu, B. & X. Jiang. 2016. Numerical identification of the fractional derivatives in the two-dimensional fractional cable equation. *Journal of Scientific Computing* 68(1). 252–272.

[181] Yu, B., X. Jiang & H. Qi. 2017. Numerical method for the estimation of the fractional parameters in the fractional mobile/immobile advection–diffusion model. *International Journal of Computer Mathematics* 1–20.

[182] Zamani, Vahid, Ehsan Kharazmi & Ranjan Mukherjee. 2015. Asymmetric post-flutter oscillations of a cantilever due to a dynamic follower force. *Journal of Sound and Vibration* 340. 253–266.

[183] Zayernouri, M., M. Ainsworth & G. E. Karniadakis. 2015. Tempered fractional sturm–liouville eigenproblems. *SIAM Journal on Scientific Computing* 37(4). A1777–A1800.

[184] Zayernouri, M., M. Ainsworth & G. E. Karniadakis. 2015. A unified petrov–galerkin spectral method for fractional pdes. *Computer Methods in Applied Mechanics and Engineering* 283. 1545–1569.

[185] Zayernouri, M., W. Cao, Z. Zhang & G. E. Karniadakis. 2014. Spectral and discontinuous spectral element methods for fractional delay equations. *SIAM Journal on Scientific Computing* 36(6). B904–B929.

[186] Zayernouri, M. & G. E. Karniadakis. 2013. Fractional Sturm-Liouville eigen-problems: theory and numerical approximations. *J. Comp. Physics* 47-3. 2108–2131.

[187] Zayernouri, M. & G. E. Karniadakis. 2014. Discontinuous spectral element methods for time-and space-fractional advection equations. *SIAM Journal on Scientific Computing* 36(4). B684–B707.

[188] Zayernouri, M. & G. E. Karniadakis. 2014. Exponentially accurate spectral and spectral element methods for fractional odes. *J. Comp. Physics* 257. 460–480.

[189] Zayernouri, M. & G. E. Karniadakis. 2014. Fractional spectral collocation method. *SIAM Journal on Scientific Computing* 36(1). A40–A62.

[190] Zayernouri, M. & G. E. Karniadakis. 2015. Fractional spectral collocation methods for linear and nonlinear variable order fpdes. *Journal of Computational Physics* 293. 312–338.

[191] Zayernouri, M. & A. Matzavinos. 2016. Fractional adams–bashforth/moulton methods: An application to the fractional keller–segel chemotaxis system. *Journal of Computational Physics* 317. 1–14.

[192] Zayernouri, M. & A. Matzavinos. 2016. Fractional Adams-Bashforth/Moulton methods: An application to the fractional Keller–Segel chemotaxis system. *Journal of Computational Physics-In Press* .

[193] Zayernouri, M & M Metzger. 2011. Coherent features in the sensitivity field of a planar mixing layer. *Physics of Fluids (1994-present)* 23(2). 025105.

[194] Zayernouri, Mohsen & George Em Karniadakis. 2013. Fractional sturm–liouville eigenproblems: theory and numerical approximation. *Journal of Computational Physics* 252. 495–517.

[195] Zelenev, V Mo, SI Meshkov & Yu A Rossikhin. 1970. Damped vibrations of hereditary-elastic systems with weakly singular kernels. *Journal of Applied Mechanics and Technical Physics* 11(2). 290–293.

[196] Zeng, F., C. Li, F. Liu & I. Turner. 2015. Numerical algorithms for time-fractional subdiffusion equation with second-order accuracy. *SIAM Journal on Scientific Computing* 37(1). A55–A78.

[197] Zhang, H., F. Liu & V. Anh. 2010. Galerkin finite element approximation of symmetric space-fractional partial differential equations. *Applied Mathematics and Computation* 217(6). 2534–2545.

[198] Zhang, Y., H. Sun, H. H. Stowell, M. Zayernouri & S. E. Hansen. 2017. A review of applications of fractional calculus in earth system dynamics. *Chaos, Solitons & Fractals* .